ANALYTICAL STOCHASTIC MODELS FOR STORMWATER MANAGEMENT

Development of Analytical Stochastic Models for Hydrologic Design of Stormwater Control Measures

By

Jun Wang

B.Eng., M.Sc.

Faculty of Engineering
Department of Civil Engineering

A Thesis
Submitted to the School of Graduate Studies
in Partial Fulfillment of the Requirements
for the Degree of

Doctor of Philosophy

McMaster University
Hamilton, Ontario, Canada

DOCTOR OF PHILOSOPHY (2019) McMaster University
(Civil Engineering) Hamilton, Ontario

TITLE: Development of Analytical Stochastic Models for Hydrologic Design of Stormwater Control Measures

AUTHOR: Jun Wang

B.Eng. (Xi'an University of Technology, China)

M.Sc. (Shandong University, China)

SUPERVISOR: Professor Yiping Guo

NUMBER OF PAGES: 281 pages (I- XVI, 1-265)

Abstract

Urbanization has great impacts on hydrologic processes and can result in increased flooding, water quality deterioration, and the hazards of erosion. To deal with the challenges caused by urbanization, stormwater control measures (SCMs) have been widely advocated and utilized. SCMs consist of conventional centralized end-of-pipe control facilities and distributed source control or low-impact development practices (LIDs). Combined sewer overflow (CSO) tanks, detention ponds, wetlands are examples of end-of-pipe control facilities while representative LIDs include infiltration trenches, green roofs, permeable pavements, and rain gardens.

Methods used in the design and analysis of SCMs are generally classified into three categories: single-event design storm simulation models, continuous simulation models, and probability-based analytical models. Among them, probability-based analytical models consist of previously developed analytical probabilistic models (APMs) and recently proposed analytical stochastic models (ASMs). Probability-based analytical models have the advantages of being in the form of closed-form analytical equations and requiring no numerical solutions. APMs and ASMs can be used as the surrogate of continuous simulation models for design and analysis. APMs have the shortcoming of requiring simplifying assumptions of antecedent storage or soil moisture conditions. Single-event design storm simulation models have limitations of relying on the assumption that the frequency of occurrence of some of the runoff hydrograph characteristics is always

equal to that of some of the input rainfall hyetograph characteristics. Continuous simulation models are time-consuming to run and require large amounts of input. ASMs can overcome many of the drawbacks of other three types of models.

ASMs for stormwater management purposes treat rainfall inputs at a location of interest as a marked Poisson process and describe the temporal evolution of the probability distribution of the relative water level or the degree of soil saturation of a SCM by the Chapman-Kolmogorov equation. Both rainfall event depth and inter-arrival time are assumed to be exponentially distributed in ASMs. The concept of effective storage capacity was proposed to properly consider the effects of the instantaneous rainfall pulses represented by the Poisson process. The steady-state probability distributions of the water content or the degree of soil saturation were analytically derived and form the basis of ASMs. Relevant SCM performance statistics of interest were derived based on these probability distributions.

This thesis aims to develop a suite of ASMs for the design and analysis of SCMs which can significantly reduce the impact of some of the simplifying assumptions required in previously developed APMs and ASMs, while the newly developed ASMs are still in analytically tractable forms which simplify the calculation tasks required in engineering design. In Chapter 2, an ASM is developed for evaluating the performance of CSO tanks. In Chapter 3, instead of using constant outflow functions as in previous ASM studies, more realistic orifice outflow functions are considered in the development of ASMs for stormwater detention ponds. In Chapter 4, considering different possible operating conditions rather than simply assuming a constant bottom infiltration rate, different ASMs are proposed for different types of infiltration facilities. In Chapter 5, as an example application of the ASMs, the developed ASMs are applied for the sizing of infiltration trenches following local design standards and procedures.

Throughout the thesis, the developed ASMs were verified by comparing their analytical results with results obtained from continuous simulations considering various factors of climate conditions, land use conditions, soil conditions, and facility dimensions. The usefulness of ASMs were demonstrated through cases studies at different test locations. The developed ASMs are recommended as an efficient alternative of, or used together with, continuous simulation models in the planning, design, and analysis of SCMs.

Acknowledgements

Firstly, I would like to thank my academic supervisor, Prof. Yiping Guo, for guiding me into this interesting field of urban stormwater management. Without his ongoing support and instructive suggestions over the past years, I could never have achieved the current progress. His immense knowledge, dedicated personality and unceasing encouragement haven been an inspiration to my future career and life.

My sincere appreciation also extends to the other two members of my supervisory committee: Prof. Paulin Coulibaly and Prof. Sarah Dickson, for their insightful comments and instructional advices to improve my research.

I gratefully acknowledge the financial support I have received from the China Scholarship Council, the School of Graduate Studies and the Department of Civil Engineering at McMaster University, the National Sciences and Engineering Research Council of Canada, and Mitacs Accelerate Fellowship. Without this financial support, I could not have completed my Ph.D. program.

I wish to extend my thanks to my classmates and officemates in JHE-330 and JHE-233 at McMaster University where I stayed in the past years (Dr. Yaqian Liu, Dr. Sina Moallemi, Dr. Jingshan Shi, Ashkan Ezazi, Shasha Han, Tankian Coulibaly, Hojjat

Mohammadi, Hui Guo, Qianqian Zhang, et al.). A heartfelt thank you is also given to the other friends I met during my PhD study. It is the friendship of you who have made my life here memorable.

It has been a great pleasure to meet with the other members in Prof. Guo's research group, including Dr. Rui Guo, Pavneet Brar, Wan Miao, Zihao Zhang, Robert Rawlins, Elizabeth Rowe, Dr. Yuyin Liang, Dr. Chao Han, Cecilia Fareri, and Alessia Peluchetti. Thank you for those happy moments we have shared together.

Special gratitude spreads to those senior Ph.D. graduates from McMaster University. We still keep in touch and they shared with me about their research and job experience and provided me with some helpful advices during my Ph.D. study. They are Dr. Shouhong Zhang, Dr. Vali Gorbanian, Dr. Xing Li, and Dr. Savitri Jetoo.

Last but foremost, I would like to express my deepest gratefulness to my parents for their unstinted love. Without their encouragement and expectation, I could not have realized my PhD dream. This work is dedicated to my family, especially to my late father, Zhiqing, who taught me the perseverance and humility in the life, study and work; to my mother, Meirong, who gives me unconditional trust and support; and to my elder sister who grew up with me.

Publication List

This thesis consists of the following peer reviewed journal papers:

Paper I: Wang, J., and Guo, Y. (2018). An analytical stochastic approach for evaluating the performance of combined sewer overflow tanks. *Water Resources Research*, 54(5), 3357–3375. (Source paper for Chapter 2 with permission from the publisher)

Paper II: Wang, J., and Guo, Y. (2019). Stochastic analysis of storm water quality control detention ponds. *Journal of Hydrology*, 571, 573–584. (Source paper for Chapter 3 with permission from the publisher)

Paper III: Wang, J., and Guo, Y. (2019). Dynamic water balance of infiltration-based storm water best management practices. Submitted to *Advances in Water Resources*. (Source paper for Chapter 4)

Paper IV: Wang, J., and Guo, Y. (2019). Proper sizing of infiltration trenches using closed-from analytical equations. To be submitted to ASCE *Journal of Hydrologic Engineering*. (Source paper for Chapter 5)

Additional relevant work: Wang, J., Zhang, S., and Guo, Y. (2019). Analyzing the Impact of Impervious Area Disconnection on Urban Runoff Control Using an Analytical Probabilistic Model. *Water Resources Management*. 33(5), 1753–1768. (Source paper for Appendix A with permission from the publisher)

Co-Authorship

This thesis was prepared on the "sandwich" format in accordance with the guidelines provided by the School of Graduate Studies, McMaster University and was co-authored. A total of five peer-reviewed journal papers that have been published or submitted make up the major components in this thesis, including Chapters 2 through 5 and a related study in the Appendix. Contributions of the co-authors for each publication contained in this thesis are outlined, and the reason to include them in the thesis is described below.

Four papers presented in Chapters 2 through 5 area were co-authored by Jun Wang and Dr. Y. Guo. The literature review was conducted by J. Wang, the mathematical derivation, continuous simulations, and model verification were performed by J. Wang in consultation with Dr. Y. Guo, the papers were written by Jun Wang and edited by Dr. Y. Guo. The development of analytical stochastic models for three main types of stormwater control measures were introduced in Chapters 2 through 4. Chapter 5 is about the further application of ASMs to size infiltration type facilities. The proposed stochastic models involve the representative types of stormwater control measures.

For Appendix A, the source paper was co-authored by J. Wang, Dr. S. Zhang and Dr. Y. Guo. The idea originated from Dr. S. Zhang. The paper was written by J. Wang and Dr. Zhang and edited by Dr. Y. Guo. Data analysis, continuous simulations, derivation improvement, model modification, and major revision were conducted by J. Wang in consultation with Dr. Y. Guo and Dr. S. Zhang. The disconnection of impervious areas as one type of LID practices was studied using the analytical probabilistic approach. The theme of this paper is in line with the stormwater control measures.

Table of Contents

List of Tables

List of Figures

Chapter 1

Background and Objectives

1.1 Urban Stormwater Management

Urban growth has resulted in significant negative effects on the natural hydrological processes and drainage patterns, the associated urban flooding and water pollution problems have become a significant challenge to stormwater management in recent decades (Rodríguez-Sinobas et al., 2018; Ebrahimian et al., 2019). The increased impervious areas fasten the rainfall-runoff transformation process, along with the implementation of urban drainage systems causing a shorter time of concentration on urban catchments. As a result, the alteration of land covers due to the urbanization results in great increases in runoff volumes, peak discharges, pollutant yields and erosion hazards (Woznicki et al., 2018).

For cities with combined sewer systems, urbanization and climate change can increase the frequency and severity of combined sewer overflows (CSOs), and proper control of CSOs is an imperative task (Andrés-Doménech et al., 2012). The increased runoff volume and rate of discharge may also cause severe downstream flooding and channel erosion (CVC and TRCA, 2010). In addition, stormwater carries and transports large amounts of pollutants to receiving waters and is often regarded as the primary water pollution contributor (Lee et al, 2007). Suspended solids, nutrients, heavy metals, insecticides, and pathogenic microorganisms are examples of contaminants carried by urban runoff (Adams and Papa, 2000; Barbosa et al., 2012). Contaminants collected by receiving waters can cause degradation of water quality (USEPA, 2003). These stormwater related water quantity and quality issues necessitate sustainable and effective urban stormwater management strategies. The impacts of urbanization on water quantity and quality are not expected to be eliminated but required to be mitigated by proper stormwater control measures (Horner et al., 2002; Bradford and Gharabaghi, 2004).

1.2 Stormwater Control Measures

To effectively deal with stormwater problems, different approaches, either strategic, political decisions, or end-of-pipe and source control measures, may be utilized (German et al., 2005). Sustainable stormwater management strategies encourage the application of efficient stormwater control measures (SCMs). The term SCMs are relatively new, previously terminologies such as low-impact development (LID) practices and best management practices (BMPs) are used in North America, water sensitive urban design (WSUD) are used in Australia, sustainable urban drainage systems (SUDS) are used in the UK, green infrastructures (GIs) are used in the USA, and Sponge City (SC) practices are used in China (Fletcher, et al., 2015; Golden and Hoghooghi, 2018; Li et al., 2019).

Generally, SCMs consists of two primary categories of facilities, the conventional centralized end-of-pipe control facilities and the decentralized source control facilities (CVC and TRCA, 2010). Combined sewer overflow (CSO) detention tanks (Andrés-Doménech, et al., 2012; Wang and Guo, 2018) and detention ponds (Chen and Adams, 2006; Wang and Guo, 2019a) are two examples of end-of-pipe control SCMs. Green roofs (Berndtsson, 2010; Guo, 2016), permeable pavement systems (Imran, et al., 2013; Guo et al, 2018), rainwater harvesting systems (Pelak and Porporato, 2016; Guo and Guo, 2018a; Zhang, et al., 2019), infiltration trenches (Chahar, et al., 2011; Wang and Guo, 2019b) and rain gardens (Zhang and Guo, 2013) are representative source control practices (also denoted as LIDs). The integrated application of both categories of SCMs can effectively control the occurrence of overflow and flashy floods at a catchment scale. Example SCMs including combined sewer overflow tanks, detention ponds, infiltration trenches, and disconnection of impervious areas studied in this thesis are described below.

1.2.1 End-of-Pipe Control Facilities

An end-of-pipe control facility is defined as a centralized stormwater control facility receiving runoff from a conveyance system (i.e., pipes, roads) and discharging to a receiving water (OMOE, 2003). As a traditional practice of stormwater management, end-of-pipe control facilities are designed to collect runoff from a drainage basin; and are normally located downstream of the drainage basin where the collected runoff is stored and/or treated for the purposes of runoff volume, peak discharge and water quality control. For instance, detention/retention ponds, infiltration basins, detention tanks and wetlands are commonly used as stormwater end-of-pipe control facilities (OMOE, 2003). These facilities may be effective in reducing downstream flooding, improving water quality and reducing downstream channel erosion. However, over-reliance on stormwater management ponds or tanks will not necessarily maintain the integrity of aquatic ecosystems in receiving water bodies (Bradford and Gharabaghi, 2004).

Combined sewer systems are the prevalent urban drainage system of old downstream neighborhoods. Combined sewer flows exceeding the wastewater treatment plant (WWTP) processing capacity are discharged directly into receiving waters as CSOs (Adams and Papa, 2000; Andrés-Doménech et al., 2010; Barone et al., 2019). Studies on the implementations of CSO tanks in different cities around the world demonstrated that detention tanks can be used an effective measure for CSO control (Heitz et al., 2000; Weiss et al., 2006; Martino et al., 2011; Li et al., 2015; Llopart-Mascaró et al., 2015). The two main objectives of implementing CSO tanks are, (1) to reduce the frequency and severity of CSOs with the proper selection of tank size and its discharge capacity, and (2) to mitigate water pollution caused by overflows by allowing for the sedimentation and self-purification of stored inflows (Andrés-Doménech et al., 2010).

As one of the most commonly implemented stormwater best management practice (BMP), detention ponds often serve as effective means for both flood control and quality enhancement purposes (Behera and Teegavarapu, 2015). Stormwater ponds provide water quality control by detaining the captured runoff and providing sufficient residence time needed for the settling and decay of pollutants (Guo and Adams, 1999). Typically, stormwater detention ponds are classified as dry ponds or wet ponds according to their outflow control configurations. Orifices and weirs are two commonly used outflow control devices in detention ponds (Akan, 1992). In practice, detention ponds are designed to provide a proper storage capacity and release rate so that the desired level of performance can be achieved (Chen and Adams, 2006).

1.2.2 Low-Impact Development Practices

In recent decades, low-impact development (LID) practices have emerged as an innovative stormwater management approach (CVC and TRCA, 2010; Ahiablame et al., 2012). LIDs aim to restore or replicate the predevelopment hydrologic patterns of an urbanized area (USEPA, 2000). As an example LID, infiltration trenches are simply trenches filled with gravel aggregates or plastic lattice structures and lined with geotextile filter cloths. Infiltration trenches are usually of relatively long, narrow and shallow shapes for the purpose of convenient postconstruction maintenance (Pitt et al., 1999). An underdrain is often required when the permeability of native soils surrounding the trench is very low. The time to emptying a full trench (referred to as drain time or drawdown time) should not be too long because the trench needs to recover its full storage capacity before the occurrence of the subsequent rainfall event (DWSRT, 2007). It was found that the required drain time ranges between 24 hours and 96 hours (Burack et al., 2008; CVC and TRCA, 2010; GVSDD, 2012; AMEC, 2014). Widely accepted design standards and procedures for infiltration trenches do not exist (Chahar et al., 2011), different jurisdictions adopt different standards.

Infiltration trenches are an example type of structural LIDs. A simple modified rational method was applied to size infiltration basins or trenches by Akan (2002a). Akan (2002b) also proposed a numerical model based on the water balance equation and the Green and Ampt infiltration equation for sizing infiltration trenches. Chahar et al. (2011) derived analytical equations for sizing trapezoidal infiltration trenches but still requiring numerical solutions at the end. Creaco and Franchini (2012) came up with a dimensionless procedure for sizing infiltration trenches where the rainfall-runoff model used is based on the kinematic wave equation. Although both infiltrations from the bottom area and the sidewalls were considered, the average side infiltration area was used by Creaco and Franchini (2012) to represent the actual varying side infiltration areas. Guo and Gao (2016) developed an analytical probabilistic model for the design of infiltration trenches but it requires a simplifying assumption about the antecedent moisture condition of the trench. Guo and Guo (2018b) proposed a modified analytical probabilistic model using the Horton infiltration equation to calculate infiltration instead of the constant infiltration rate and also using the estimated average antecedent moisture level as the initial moisture of the trench. There have been many attempts of deriving analytical equations for use in the design and evaluation of infiltration trenches, numerical solutions are still required in some of the previous studies, some simplifying assumptions which may overestimate or underestimate the performance of the trenches are still needed.

Disconnection of impervious areas is one of the non-structural LID practices. Use of this practice results in non-directly connected impervious areas (NCIAs). An NCIA is an impervious area that drains to pervious grounds, for example, rooftops that drain onto lawns and parking lots that drain into bioretention systems. On the contrary, directly-connected impervious areas (DCIAs), are impervious areas from which the generated runoff is discharged to other paved surfaces, drain pipes, or other impervious conveyance and detention structures that do not effectively reduce runoff volumes (Ebrahimian et al., 2016). Therefore, NCIAs and DCIAs are the two main types of impervious areas (Alley and Veenhuis, 1983; Han and Burian, 2009; Seo et al., 2013). Whether an impervious area is a type of a DCIA or an NCIA affects runoff routing (Boyd et al., 1993). It was found that DCIA can serve as a better catchment parameter for estimating urban runoff as compared to total impervious area. Use of total impervious area may overestimate runoff volume (Ebrahimian et al., 2016; Yao et al., 2016). Since runoff generated from NCIAs will be greatly reduced after routing onto and infiltrated by the adjacent pervious areas, DCIAs contribute to the majority of the total runoff generated from the impervious areas (Brabec et al., 2002; Lee and Heaney, 2003). However, in many previous modeling studies (Adams and Papa, 2000; Bacchi et al., 2008; Zhang and Guo, 2014), the effects of NCIAs on runoff generation were not adequately considered.

1.3 Stormwater Management Models

The accuracy of numerical hydrologic models usually improves with the increase of model complexity. However, complex models require more input data, more model parameters to be validated, and longer simulation times. This is clearly demonstrated in the three types of models used for the design and analysis of stormwater control measures, i.e., single-event design storm simulation models, continuous simulation models, and probability-based analytical models. Among them, probability-based analytical models consist of the previously developed analytical probabilistic models and the recently proposed analytical stochastic models. Continuous simulation models require the input of the entire historical rainfall records, whereas probability-based analytical models need only the input of the main rainfall statistics which can be obtained from rainfall statistical analysis. Descriptions of these four types of models are presented below.

1.3.1 Single-event Design Storm Simulation Models

The design storm approach has been widely applied in the design and analysis of urban drainage systems and recommended in many of the design guidance manuals. This is because synthetic design storms can be easily constructed for locations of interest and use of them seems to guarantee that uniform design standards can be achieved. Besides, the design storm approach simplifies hydrologic and hydraulic calculations compared to continuous simulation models, and it benefits locations with scarce historical rainfall data (Balbastre-Soldevila et al., 2019). However, the basic assumption of the design storm approach is that the known frequency of occurrence of the input design storm would always result in output runoff hydrograph characteristics having the same frequency of occurrence (or return period). This assumption is not strictly rigorous, and its limitation has been discussed by some researchers (Adams and Howard, 1986; García-Bartual and Andrés-Doménech, 2017). The effects of the antecedent storage condition or soil moisture condition in a SCM is often ignored in single-event design storm simulations. Examples applying the design storm approach for urban stormwater management purposes can be found in Quader and Guo (2006), Guo and Zhuge (2008), Lucas (2009), etc.

1.3.2 Continuous Simulation Models

Long-term rainfall series are used as the input in continuous simulation models to generate long series of output variables of interest such as runoff volumes, peak discharges and overflows. Unlike single event models, effects of the catchment initial conditions on the resulting runoff series and runoff statistics in continuous simulations are negligible. Given the rainfall input of sufficient length, performance statistics of a SCM can be calculated based on the long-term continuous simulation results. Continuous simulation models have the limitations that they are time-consuming to perform and input data-intensive, especially when system designs need to be modified to achieve specific performance requirements (Adams and Papa, 2000). A large number of continuous simulation runs need to be conducted in order to evaluate different configurations of SCMs.

As a widely used continuous simulation model, the Stormwater Management Model (SWMM) (Rossman, 2015) developed by the U.S. Environmental Protection Agency (EPA) has been applied to analyze the operations of stormwater tanks (Todeschini et al., 2012), water quality control detention ponds (Chen and Adams, 2006) and LID practices (Baek et al., 2015; Rosa et al., 2015). There are some other continuous simulation models applied in the study of stormwater detention facilities, including NetSTORM (Park et al., 2013), COSMOSS (De Paola and Martino, 2013), HEC-HMS (Emerson et al., 2005), and MIKE

URBAN (Bisht et al., 2016). A variety of continuous simulation models used in LID practices were reviewed and discussed by Elliott and Trowsdale (2007).

1.3.3 Analytical Probabilistic Models

The analytical probabilistic approach was pioneered by Eagleson (1972) based on rainfall statistical analysis and derived probability distribution theory (Benjamin and Cornell, 1970). By determining a suitable minimum inter-event time (MIET) and a threshold for screening out extremely small rainfall events, a continuous rainfall series is divided into discrete rainfall events (Guo and Adams, 1998; Adams and Papa, 2000; ABL and EI, 2016; Hassini and Guo, 2016). Each rainfall event is characterized by its rainfall event depth, duration and inter-event time. It was found that the frequency histograms of these rainfall event characteristics of many different locations can be represented well by exponential distributions. The exponential distribution assumption was tested and accepted for many locations around the world including Canada (Adams and Papa, 2000), the U.S. (USEPA, 1986; Wanielista and Yousef, 1993; Hassini and Guo, 2016), South Korea (Lee and Kim, 2018), Malaysia (Shamsudin et al., 2014) and Italy (Ursino, 2015). Generalized Pareto and Weibull distributions were used to represent rainfall event characteristics together with the analytical probabilistic approach for some other locations as well (Balistrocchi et al., 2009; Zegpi and Fernandez, 2010; Andrés-Doménech et al., 2012).

Incorporating the exponentially distributed rainfall event characteristics and using the derived distribution theory, the probability density functions (PDFs) of runoff and overflow can be analytically derived based on the rainfall-runoff transformations occurring over the catchment and flow processes through channels and storage facilities. The hydrologic performance of urban drainage system and SCMs can then be calculated using closed-form analytical equations.

Although APMs employ simplified rainfall-runoff transformation relationships which can limit their accuracy, this is acceptable for planning level analysis in small urban drainage areas where time of concentration is usually very short. For a small urban catchment, its time of concentration should be less than the selected MIET to ensure the separation of resulting runoff events, or should be usually less than 6 hours. There is no specific quantitative definition of "small" in terms of the size of an urban drainage area. Since the analytical approach usually requires the estimate of runoff volume bases on the rational methods, which is applicable for small urban drainage areas with an upper bound of about 200-300 acres (Cleverland et al., 2011); the recommended upper limit of the size of urban drainage areas that suitable for the analytical probabilistic approach (as well as the analytical stochastic approach to be discussed in the following sections) in this thesis is approximately 100 hectares.

Comprehensive studies and reviews on the analytical probabilistic approach for stormwater management can be found in Li (1991), Guo (1998), Adams and Papa (2000), Chen (2004), Raimondi (2012), Quader (2007), Zhang (2014), Guo (2018), Hassini (2018), Guo et al. (2019) etc. Although APMs can provide extremely compact and closed-form mathematical equations and are computationally efficient and easy-ot-use, it is worth noting that a few limitations of APMs do exist. Firstly, the antecedent soil moisture or initial storage condition of the SCM is usually assumed to be fully saturated or full at the beginning of a random dry period-rainfall event cycle (Howard, 1976; Loganathan and Delleur, 1984; Guo and Baetz, 2007; Zhang and Guo, 2013) or to be completely dry or empty at the end of the dry period preceding a random rainfall event (Bacchi et al., 2008; Balistrocchi et al., 2009; Balistrocchi et al., 2013; Zhang and Guo, 2014). Secondly, the majority of APMs employ the assumption that rainfall event depth and rainfall event duration are statistically independent to each other for analytical tractability. Although a few studies (Zegpi and Fernandez, 2010; Balistrocchi et al., 2017) applied Copula theory to relax this assumption in APMs, numerical solutions to the final derived analytical equations are required, which increased the complexity and reduced the computational efficiency of the models. Lastly, the effects of disconnection of impervious areas on the runoff routing process and runoff estimation are not considered in previous APM studies, which may overestimate the total runoff generated from the total impervious areas because runoff generated from NCIAs will be greatly reduced after routing onto and infiltrated by adjacent pervious areas (Wang et al., 2019).

1.3.4 Analytical Stochastic Models

The analytical stochastic approach applied in developing the ASMs originate from Takács (1955) waiting time process in the queueing theory (Takács, 1962). The occurrence of the customer arrivals in a queue follows a marked Poisson process and the process of the waiting time of a customer from his/her arrival to being serviced can be treated as a Markov process with jumps and drifts (Takács, 1955). Similar findings also apply to the storage processes where the occurrence of discrete inflows follows a Poisson process and the storage content fluctuations are treated as a Markov process (Cox and Isham, 1986).

In the early ecohydrological studies (Rodriguez-Iturbe et al., 1999; Laio et al., 2001) of soil moisture dynamics, the root zone of the soil layers is treated as a storage system, rainfall events are treated as input, and evapotranspiration and leakage are regarded as the primary water losses from the storage system. The infiltration generated from daily rainfall events whose occurrence is assumed to follow a marked Poisson process can also be treated as a marked Poisson process, and the soil moisture fluctuations follow a Markov process. For this Markov process governed by the stochastic soil moisture balance equation, Chapman-Kolmogorov forward equations describing the evolution of the probability distribution of soil moisture were derived by Rodriguez-Iturbe et al. (1999). The steady-state probability distributions of soil moisture were further derived considering the long-term soil moisture dynamics. Other statistics or performance of interest regarding the soil moisture dynamics can be estimated based on the steady state probability distributions of soil moisture. More details of the basic theory of analytical stochastic approach for soil moisture dynamics can be found in Rodriguez-Iturbe and Proporato (2004). Further relevant studies in ecohydrology using similar methodologies to develop analytical stochastic models include analyses of soil moisture dynamics (Bartlett et al., 2015), biomass dynamics (Nordbotten et al., 2007), soil nitrate dynamics (Botter et al., 2008), street trees (Vico et al., 2014), and lowland water balance (Thompson et al., 2017), etc.

Analytical stochastic models for stormwater management purposes are characterized by treating rainfall inputs at a location of interest as a marked Poisson process (Restrepo-Posada and Eagleson, 1982) and describing the temporal evolution of the probability distribution of the relative water level or the degree of soil saturation of a SCM by the Chapman-Kolmogorov equation (Gardiner, 2004). Both rainfall event depth and inter-arrival time are assumed to be exponentially distributed in ASMs. Recently, studies on the development of ASMs for stormwater management purposes included those for bio-filters (Daly et al., 2012), for green roofs (Guo, 2006), for urban street trees (Revelli and Porporato, 2018), for rainfall water harvesting systems (Pelak and Porporato, 2016; Guo and Guo, 2018), for permeable pavement systems (Guo et al., 2018), and for detention basins (Parolari et al., 2018). In ASMs developed for stormwater management purposes, the runoff reduction ratio, also referred to as the runoff capture efficiency, is an important indicator of the performance of a SCM; proper sizing of SCMs is a challenging task. In this thesis, the development and application of ASMs for three representative types of SCMs including CSO tanks (Wang and Guo, 2018), water quality detention ponds (Wang and Guo, 2019a), and infiltration trenches (Wang and Guo, 2019b, 2019c) will be presented.

In summary, in the planning and design of urban drainage systems and SCMs, on one hand, probability-based analytical models can well describe and simulate the core hydrologic processes including the main rainfall-runoff transformation and routing processes; on the other hand, with the advantages of compact and closed-form analytical solutions, either APMs or ASMs can be used as the surrogate of continuous simulation models in design practices. ASMs overcome the shortcomings of APMs which require simplifying assumptions about antecedent storage or moisture conditions, the limitations of the single-event design storm simulation models which rely on the assumption that the frequency of occurrence of runoff hydrograph characteristics is equal to that of the input rainfall event, and the drawbacks of continuous simulation models which is time-consuming to perform and input data-intensive. Since so far there has been limited studies on ASMs for urban stormwater management compared to an extensive number of previous studies on the development and application of APMs, it is necessary to investigate further the development and application of ASMs.

1.4 Objectives and Organization

1.4.1 Objectives of the Research

This thesis was aimed at developing a suite of analytical stochastic models (ASMs) for different stormwater control measures (SCMs). Specifically, the primary objective was to derive a collection of closed-form analytical equations for the hydrologic design and operation of both end-of-pipe control facilities (combined sewer overflow tanks, detention ponds), and infiltration-type BMPs (infiltration trenches) using the analytical stochastic approach. In addition to developing specific SCMs by incorporating constant outflow functions similar to previous ASM studies (e.g., Guo, 2016; Pelak and Porporato, 2016; Guo and Guo, 2018a; Guo et al., 2018), the developed ASMs were also expected to consider more complex outflow functions for other types of SCMs. The newly developed ASMs will be verified by comparing their analytical results with those obtained from continuous simulations considering various climate conditions, land use conditions, soil conditions, and facility sizes. The advantages of analytical tractability, computational-efficiency and ease-to-use will be exhibited through case studies at different test locations. ASMs can therefore be recommended to be used as an efficient alternative of, or together with, continuous simulation models in the planning, design, and analysis of SCM facilities. The application of ASMs will also be investigated following the design standards and procedures specified in local stormwater management guidance manuals. Accuracy and usefulness of the proposed ASMs will be demonstrated.

1.4.2 Thesis Structure

Four papers were completed in order to achieve the overall objectives of this thesis. These papers are presented in Chapters 2 through 5 and are outlined as follows.

Chapter 2 presents the development of an analytical stochastic model for evaluating the hydrologic performance of combined sewer overflow detention tanks. The proposed model overcomes the shortcomings of the previous analytical probabilistic models which require simplifying assumptions about the initial storage conditions of the tank. A case study at Atlanta, Georgia, U.S. was conducted for model verification.

In Chapter 3, a set of closed-form analytical equations of detention ponds in which the outflow is controlled by orifices are derived using the stochastic approach. A more realistic representation of the discharge-storage relationship by power functions is applied instead of the assumed constant discharges as used in previous analytical studies. Jackson, Mississippi, U.S. is the selected location in a case study to demonstrate the accuracy and reliability of the proposed model.

Chapter 4 focuses on developing analytical stochastic models for infiltration-type BMPs considering three possible operating conditions. Considering infiltration through both the sides and the bottom, through only the sides, or through only the bottom of an infiltration trench, three ASMs are developed for all possible operating conditions of infiltration trenches. Case studies at Jackson, Mississippi and Billings, Montana, U.S. are presented for model verification.

Chapter 5 discusses the application of ASMs developed in Chapter 4 for the sizing of infiltration trenches. Following the design procedures and standards specified by the guidance manuals at two locations (Atlanta, Georgia and New Durham, New Hampshire, U.S.), case studies are presented to analyze the effects of influential factors such as trench shapes, soil infiltration capacity, drain time, and infiltration condition on runoff reduction ratios.

Chapter 6 summarizes the main conclusions of this thesis and outlines recommendations for future research. In the appendix, a study about developing an analytical probabilistic model for analyzing the effects of disconnection of impervious areas on runoff reduction ratios is presented as supplemental findings of this thesis.

References

Adams, B. J., and Howard, C. D. (1986). Design storm pathology. *Canadian Water Resources Journal*, 11(3), 49–55.

Adams, B. J., and Papa, F. (2000). *Urban Stormwater Management Planning with Analytical Probabilistic Models*, John Wiley & Sons, Inc., New York, USA.

Ahiablame, L., Engel, B., and Chaubey, I. (2012). Effectiveness of low impact development practices: literature review and suggestions for future research. *Water, Air, and Soil Pollution*, 223(7), 4253–4273.

Akan, A. O. (1992). Storm runoff detention for pollutant removal. *Journal of Environmental Engineering*, 118(3), 380–389.

Akan, A. O. (2002a). Modified rational method for sizing infiltration structures. *Canadian Journal of Civil Engineering*, 29(4), 539–542.

Akan, A. O. (2002b). Sizing stormwater infiltration structures. *Journal of Hydraulic Engineering*, 128(5), 534–537.

Alley, W.M., and Veenhuis, J.E. (1983). Effective impervious area in urban runoff modeling. *Journal of Hydraulic Engineering*, 109(2), 313–319.

AMEC Environment and Infrastructure (AMEC). (2014). *Green infrastructure stormwater management practices for small commercial development*, City of Atlanta Stormwater Guidelines, Atlanta, Georgia, U.S. https://mariettaga.gov/DocumentCenter/View/227/Small-Commercial-Green-

Infrastructure-Guidance-PDF?bidId=.pdf

Aquafor Beech Ltd. and Earthfx Inc. (ABL and EI) (2016). *Runoff volume control targets for Ontario final report*, prepared for Ministry of the Environment and Climate Change. http://www.downloads.ene.gov.on.ca/envision/env_reg/er/documents/2017/012-9080_Runoff.pdf

Andrés-Doménech, I., Montanari, A., and Marco, J. (2012). Efficiency of storm detention tanks for urban drainage systems under climate variability. *Journal of Water Resources Planning and Management*, 138(1), 36–46.

Andrés-Doménech, I., Múnera, J., Francés, F., and Marco, J. (2010). Coupling urban event-based and catchment continuous modelling for combined sewer overflow river impact assessment. *Hydrology and Earth System Science*, 14(10), 2057–2072.

Bacchi, B., Balistrocchi, M., and Grossi, G. (2008). Proposal of a semi-probabilistic approach for storage facility design. *Urban Water Journal*, 5(3), 195–208.

Baek, S. S., Choi, D. H., Jung, J. W., Lee, H. J., Lee, H., Yoon, K. S., and Cho, K. H. (2015). Optimizing low impact development (LID) for stormwater runoff treatment in urban area, Korea: Experimental and modeling approach. *Water Research*, 86, 122–131.

Balbastre-Soldevila, R., García-Bartual, R., and Andrés-Doménech, I. (2019). A Comparison of Design Storms for Urban Drainage System Applications. *Water*, 11(4), 757. https://doi.org/10.3390/w11040757

Balistrocchi, M., Grossi, G., and Bacchi, B. (2009). An analytical probabilistic model of the quality efficiency of a sewer tank. *Water Resource Research*, 45(12).

https://doi.org/10.1029/2009WR007822

Balistrocchi, M., Grossi, G., and Bacchi, B. (2013). Deriving a practical-probabilistic method to size flood routing reservoirs. *Advances in Water Resources*, 62(2013), 37–46.

Balistrocchi, M., Orlandini, S., Ranzi, R., and Bacchi, B. (2017). Copula-based modeling of flood control reservoirs. *Water Resources Research*, 53(11), 9883–9900.

Barbosa, A. E., Fernandes, J. N., and David, L. M. (2012). Key issues for sustainable urban stormwater management. *Water Research*, 46(20), 6787–6798.

Barone, L., Pilotti, M., Valerio, G., Balistrocchi, M., Milanesi, L., Chapra, S. C., and Nizzoli, D. (2019). Analysis of the residual nutrient load from a combined sewer system in a watershed of a deep Italian lake. *Journal of Hydrology*, 571, 202–213.

Bartlett, M. S., Daly, E., McDonnell, J. J., Parolari, A. J., and Porporato, A. (2015). Stochastic rainfall-runoff model with explicit soil moisture dynamics. *Proceedings of the Royal Society A: Mathematical, Physical and Engineering Sciences*, 471(2183), 20150389. https://doi.org/10.1098/rspa.2015.0389

Behera, P. K., and Teegavarapu, R. S. (2015). Optimization of a stormwater quality management pond system. *Water Resources Management*, 29(4), 1083–1095.

Benjamin, J. R., and Cornell, C. A. (1970). *Probability, statistics, and decision for civil engineers*. McGraw-Hill, New York.

Berndtsson, J. C. (2010). Green roof performance towards management of runoff water quantity and quality: A review. *Ecological Engineering*, 36(4), 351–360.

Bisht, D. S., Chatterjee, C., Kalakoti, S., Upadhyay, P., Sahoo, M., and Panda, A. (2016). Modeling urban floods and drainage using SWMM and MIKE URBAN: a case study. *Natural Hazards*, 84(2), 749–776.

Botter, G., Daly, E., Porporato, A., Rodriguez-Iturbe, I., and Rinaldo, A. (2008). Probabilistic dynamics of soil nitrate: Coupling of ecohydrological and biogeochemical processes. *Water resources research*, 44(3). https://doi.org/10.1029/2007WR006108

Boyd, M.J., Bufill, M.C., and Knee, R.M. (1993). Pervious and impervious runoff in urban catchments. *Hydrological Science Journal*, 38, 463–478.

Brabec, E., Schulte, S., and Richards, P.L. (2002). Impervious surfaces and water quality: A review of current literature and its implications for watershed planning. *Journal of Planning Literature*, 16(4), 499–514.

Bradford, A., and Gharabaghi, B. (2004). Evolution of Ontario's stormwater management planning and design guidance. *Water Quality Research Journal*, 39(4), 343–355.

Burack, T. S., Walls, M. J., and Stewart, H. (2008). *New Hampshire Stormwater Manual, Volume 2 Post-Construction Best Management Practices: Selection and Design*. Comprehensive Environmental Inc.& New Hampshire Department of Environmental Services, Concord, New Hampshire, U.S. https://www.des.nh.gov/organization/commissioner/pip/publications/wd/documents/wd-08-20b.pdf

Chahar, B. R., Graillot, D., and Gaur, S. (2011). Storm-water management through infiltration trenches. *Journal of Irrigation and Drainage Engineering*, 138(3), 274–281.

Chen, J., and Adams, B. J. (2006). Urban stormwater quality control analysis with detention ponds. *Water Environment Research*, 78(7), 744–753.

Chen, J. (2004). *Integrated urban stormwater management modeling*, Ph.D. Thesis, University of Toronto, Department of Civil Engineering, Toronto, Canada.

Cleveland, T. G., Thompson, D. B., and Fang, X. (2011). *Use of the rational and modified rational method for hydraulic design* (No. FHWA/TX–08/0–6070–1), Technical Report. https://library.ctr.utexas.edu/hostedpdfs/techmrt_0-6070-1.pdf

Cox, D. R., and Isham, V. (1986). The virtual waiting-time and related processes. *Advances in Applied Probability*, 18(2), 558–573.

Creaco, E., and Franchini, M. (2012). A dimensionless procedure for the design of infiltration trenches. *Journal-American Water Works Association*, 104(9), E501-E509. http://dx.doi.org/10.5942/jawwa.2012.104.0124

Credit Valley Conservation Authority and Toronto and Region Conservation Authority (CVC and TRCA), (2010). *Low impact development stormwater management planning and design guide*. CVC and TRCA, Toronto, Canada. https://cvc.ca/wp-content/uploads/2014/04/LID-SWM-Guide-v1.0_2010_1_no-appendices.pdf

Daly, E., Deletic, A., Hatt, B. E., and Fletcher, T. D. (2012). Modelling of stormwater biofilters under random hydrologic variability: a case study of a car park at Monash University, Victoria (Australia). *Hydrological Processes*, 26(22), 3416–3424.

Department of Water and Swan River Trust (DWSRT), 2007. *Structural controls, stormwater management manual for Western Australia*. Department of Water and Swan

River Trust, Perth, Western Australia.

De Paola, F., and Martino, F. D. (2013). Stormwater tank performance: design and management criteria for capture tanks using a continuous simulation and a semi-probabilistic analytical approach. *Water*, 5(4), 1699–1711.

Eagleson, P. S. (1972). Dynamics of flood frequency, *Water Resources Research*, 8(4), 878–898.

Ebrahimian, A., Wilson, B.N., and Gulliver, J.S. (2016). Improved methods to estimate the effective impervious area in urban catchments using rainfall-runoff data. *Journal of Hydrology*, 536, 109–118.

Ebrahimian, A., Wadzuk, B., and Traver, R. (2019). Evapotranspiration in green stormwater infrastructure systems. *Science of the Total Environment*, 688, 797–810.

Elliott, A. H., and Trowsdale, S. A. (2007). A review of models for low impact urban stormwater drainage. *Environmental Modelling and Software*, 22(3), 394–405.

Emerson, C., Welty, C., and Traver, R. (2005). Watershed-scale evaluation of a system of storm water detention basins. *Journal of Hydrologic Engineering*, 10(3), 237–242.

Fletcher, T.D., Shuster, W., Hunt, W.F., Ashley, R., Butler, D., Arthur, S., Trowsdale, S., Barraud, S., Semadeni-Davies, A., Bertrand-Krajewski, J.L. and Mikkelsen, P.S. (2015). SUDS, LID, BMPs, WSUD and more–The evolution and application of terminology surrounding urban drainage. *Urban Water Journal*, 12(7), 525–542.

García-Bartual, R., and Andrés-Doménech, I. (2017). A two-parameter design storm for

Mediterranean convective rainfall. *Hydrology and Earth System Sciences*, 21(5), 2377–2387.

Gardiner, C. (2004). *Handbook of stochastic methods: for physics, chemistry & the natural sciences* (Series in synergetics, Vol. 13).

German, J., Vikstrom, M., Svensson, G., and Gustafsson, L. G. (2005). Integrated stormwater strategies to reduce impact on receiving waters. In: *Proceedings of the 10th International Conference on Urban Drainage*, 21–26, Copenhagen, Denmark.

Golden, H. E., and Hoghooghi, N. (2018). Green infrastructure and its catchment-scale effects: an emerging science. *Wiley Interdisciplinary Reviews: Water*, 5(1), e1254. https://doi.org/10.1002/wat2.1254

Greater Vancouver Sewerage and Drainage District (GVSDD). (2012). *Stormwater source control design guidelines*. Vancouver, British Columbia, Canada. http://citeseerx.ist.psu.edu/viewdoc/download?doi=10.1.1.730.8610&rep=rep1&type=pdf

Guo, R. (2018). *Stochastic approaches for estimating the performance of low impact development practices*, Ph.D. Thesis, Department of Civil Engineering, McMaster University, Hamilton, Canada.

Guo, R., and Guo, Y. (2018a). Stochastic modelling of the hydrologic operation of rainwater harvesting systems. *Journal of Hydrology*, 562, 30–39.

Guo, R., and Guo, Y. (2018b). Analytical equations for use in the planning of infiltration facilities. *Journal of Sustainable Water in the Built Environment*, 4(2), 06018001.

Guo, R., Guo, Y., and Wang, J. (2018). Stormwater capture and antecedent moisture characteristics of permeable pavements. *Hydrological Processes*, 32(17), 2708–2720.

Guo, Y. (1998). *Development of analytical probabilistic urban stormwater models*, Ph.D. Thesis, Department of Civil Engineering, University of Toronto, Toronto, Canada.

Guo, Y. (2016). Stochastic analysis of hydrologic operation of green roofs. *Journal of Hydrologic Engineering*, 21(7). https://doi.org/10.1061/(ASCE)HE.1943-5584.0001371

Guo, Y., and Adams, B. J. (1998). Hydrologic analysis of urban catchments with event-based probabilistic models. Part I: Runoff volume, *Water Resources Research*, 34(12), 3421–3431.

Guo, Y., and Adams, B. J. (1999). Analysis of detention ponds for storm water quality control, *Water Resources Research*, 35(8), 2447–2456.

Guo, Y., and Baetz, B. W. (2007). Sizing of rainwater storage units for green building applications. *Journal of Hydrological Engineering*, 12(2), 197–205.

Guo, Y., and Gao, T. (2016). Analytical equations for estimating the total runoff reduction efficiency of infiltration trenches. *Journal of Sustainable Water Built Environment*, 2(3), 06016001. https://doi.org/10.1061/JSWBAY.0000809

Guo, Y., Park, D., Mejia, A., Gironás, J., and Roesner, L. (2019). *Probabilistic models for urban stormwater management*. In *Statistical analysis of hydrologic variables: methods and applications*, 333–380, ASCE.

Guo, Y., and Zhuge, Z. (2008). Analytical probabilistic flood routing for urban stormwater management purposes. *Canadian Journal of Civil Engineering*, 35(5), 487–499.

Han, W., and Burian, S. (2009). Determining effective impervious area for urban hydrologic modeling. *Journal of Hydrologic Engineering*, 14, 111–120.

Hassini, S. (2018). *Data analysis of rainfall event characteristics and derivation of flood frequency distribution equations for urban stormwater management purposes*, Ph.D. Thesis, McMaster University, Department of Civil Engineering, Hamilton, Canada.

Hassini, S., and Guo, Y. (2016). Exponentiality test procedures for large samples of rainfall event characteristics. *Journal of Hydrologic Engineering*, 21(4), 04016003. https://doi.org/10.1061/(ASCE)HE.1943-5584.0001352

Heitz, L. F., Khosrowpanah, S., and Nelson, J. (2000). Sizing of surface water runoff detention ponds for water quality improvement. *Journal American Water Resources Association*, 36(3), 541–548.

Horner, R., May, C., Livingston, E., Blaha, D., Scoggins, M., Tims, J., and Maxted, J. (2002). *Structural and non-structural BMPs for protecting streams*. In: Proceedings of the Seventh Biennial Stormwater Research and Watershed Management Conference, 185–203, Southwest Florida Water Management District.

Howard, C. (1976). Theory of storage and treatment-plant overflows. *Journal of Environmental Engineering Division*, ASCE, 102(4), 709–722.

Imran, H. M., Akib, S., and Karim, M. R. (2013). Permeable pavement and stormwater management systems: a review. *Environmental Technology*, 34(18), 2649–2656.

Laio, F., Porporato, A., Ridolfi, L., and Rodriguez-Iturbe, I. (2001). Plants in water-controlled ecosystems: active role in hydrologic processes and response to water stress: II. Probabilistic soil moisture dynamics. *Advances in Water Resources*, 24(7), 707-723.

Lee, E. H., and Kim, J. H. (2018). Development of new inter-event time definition technique in urban areas. *KSCE Journal of Civil Engineering*, 1–8.

Lee, H., Swamikannu, X., Radulescu, D., Kim, S. J., and Stenstrom, M. K. (2007). Design of stormwater monitoring programs. *Water Research*, 41(18), 4186–4196.

Lee, J.G., and Heaney, J.P. (2003). Estimation of urban imperviousness and its impacts on storm water systems. *Journal of Water Resources Planning and Management*, 129(5), 419–426.

Li, C., Peng, C., Chiang, P., Cai, Y., Wang, X., and Yang, Z. (2019). Mechanisms and applications of green infrastructure practices for stormwater control: A review. *Journal of Hydrology*, 568, 626–637.

Li, F., Duan, H., Yan, H., and Tao, T. (2015). Multi-objective optimal design of detention tanks in the urban stormwater drainage system: framework development and case study. *Water Resource Management*, 29(7), 2125–2137.

Li, J. (1991). *Comprehensive urban runoff control modeling*, Ph.D. Thesis, Department of Civil Engineering, University of Toronto, Toronto, Canada.

Llopart-Mascaró, A., Farreny, R., Gabarrell, X., Rieradevall, J., Gil, A., Martínez, M., Puertas, J., Suárez, J., Río, H., and Paraira, M. (2015). Storm tank against combined sewer overflow: Operation strategies to minimize discharges impact to receiving waters.

Urban Water Journal, 12(3), 219–228.

Loganathan, G.V., and Delleur, J.W. (1984). Effects of urbanization on frequencies of overflows and pollutant loadings from storm sewer overflows: A derived distribution approach. *Water Resource Research*, 20(7), 857–865.

Lucas, W. C. (2009). Design of integrated bioinfiltration-detention urban retrofits with design storm and continuous simulation methods. *Journal of Hydrologic Engineering*, 15(6), 486–498.

Ontario Ministry of the Environment (OMOE), (2003). *Stormwater management planning and design manual*, Toronto, Ontario, Canada.

Park, D., Song, Y. and Roesner, L.A. (2013). Effect of the seasonal rainfall distribution on storm-water quality capture volume estimation. *Journal of Water Resources Planning and Management*, 139(1), 45–52.

Parolari, A. J., Pelrine, S., and Bartlett, M. S. (2018). Stochastic water balance dynamics of passive and controlled stormwater basins. *Advances in Water Resources*, 122, 328–339.

Pelak, N., and Porporato, A. (2016). Sizing a rainwater harvesting cistern by minimizing costs. *Journal of Hydrology*, 541, 1340–1347.

Pitt, R., Clark, S., and Field, R. (1999). Groundwater contamination potential from stormwater infiltration practices. *Urban Water*, 1(3), 217–236.

Quader, A. (2007). *Analytical estimation of the effective discharge of small urban streams*, Ph.D. Thesis, Department of Civil Engineering, McMaster University, Hamilton, Canada.

Quader, A., and Guo, Y. (2006). Peak discharge estimation using analytical probabilistic and design storm approaches. *Journal of Hydrologic Engineering*, 11(1), 46–54.

Raimondi, A. (2012). *Analytical probabilistic modeling of storage basins for stormwater management*, Ph.D. Thesis, Dipartimento di Ingegneria Idraulica, Ambientale, Infrastrutture Viarie, Rilevamento, Politecnico di Milano, Milano, Italy.

Restrepo-Posada, P.J., and Eagleson, P.S. (1982). Identification of independent rainstorms. *Journal of Hydrology*. 55 (1), 303–319.

Revelli, R., and Porporato, A. (2018). Ecohydrological model for the quantification of ecosystem services provided by urban street trees. *Urban Ecosystems*, 21(3), 489–504.

Rodriguez-Iturbe, I., Porporato, A., Ridolfi, L., Isham, V., and Coxi, D. R. (1999). Probabilistic modelling of water balance at a point: the role of climate, soil and vegetation. *Proceedings of the Royal Society of London. Series A: Mathematical, Physical and Engineering Sciences*, 455(1990), 3789–3805.

Rodriguez-Iturbe, I., and Proporato, A. (2004). *Ecohydrology of water-controlled ecosystems*, UK: Cambridge University Press.

Rodríguez-Sinobas, L., Zubelzu, S., Perales-Momparler, S., and Canogar, S. (2018). Techniques and criteria for sustainable urban stormwater management. The case study of Valdebebas (Madrid, Spain). *Journal of Cleaner Production*, 172, 402–416.

Rosa, D. J., Clausen, J. C., and Dietz, M. E. (2015). Calibration and verification of SWMM for low impact development. *JAWRA Journal of the American Water Resources Association*, 51(3), 746–757.

Rossman, L.A. (2015). Storm water management model user's manual. Version 5.1 (EPA-600/R-14/413b). National Risk Management Research Laboratory, Office of Research and Development, US Environmental Protection Agency, Cincinnati, US. https://www.innovyze.com/products/swmm/download/ZyPDF.pdf

Martino, G. D., De Paola, F., Fontana, N., Marini, G., and Ranucci, A. (2011). Pollution reduction in receivers: storm-water tanks. *Journal of Urban Planning and Development*, 137(1), 29–38.

Nordbotten, J. M., Rodriguez-Iturbe, I., and Celia, M. A. (2007). Stochastic coupling of rainfall and biomass dynamics. *Water Resources Research*, 43(1). https://doi.org/10.1029/2006WR005068

Seo, Y., Choi, N.J., and Schmidt, A.R. (2013). Contribution of directly connected and isolated impervious areas to urban drainage network hydrographs. *Hydrology and Earth System Sciences*, 17, 3473–3483.

Shamsudin, S., Dan'azumi, S., Aris, A., and Yusop, Z. (2014). Optimum combination of pond volume and outlet capacity of a stormwater detention pond using particle swarm optimization. *Urban Water Journal*, 11(2), 127–136.

Takács, L. (1955). Investigation of waiting time problems by reduction to Markov processes. *Acta Mathematica Hungarica*, 6(1-2), 101–129.

Takács, L. (1962). *Introduction to the theory of queues*. Oxford University Press, London, U.K.

Thompson, S., MacVean, L., and Sivapalan, M. (2017). A stochastic water balance framework for lowland watersheds. *Water Resources Research*, 53(11), 9564–9579.

Todeschini, S., Papiri, S., and Ciaponi, C. (2012). Performance of stormwater detention tanks for urban drainage systems in northern Italy. *Journal of Environmental Management*, 101, 33–45.

U.S. Environmental Protection Agency (USEPA). (1986). *Methodology for analysis of detention basins for control of urban runoff quality*. Rep. EPA, 440, 5–87, Washington, DC.

U. S. Environmental Protection Agency (USEPA). (2000). *Low impact development (LID), A literature review*. Washington, D.C: Office of Water. EPA-841-B-00-005.

U. S. Environmental Protection Agency (USEPA). (2003). *Bacterial water quality standards for recreational waters (freshwater and marine waters) status report*. Rep. No. EPA-823-R-03–008, USEPA, Washington, D.C., USA.

Ursino, N. (2015). Risk analysis of sustainable urban drainage and irrigation. *Advances in Water Resources*, 83, 277–284.

Vico, G., Revelli, R., and Porporato, A. (2014). Ecohydrology of street trees: design and irrigation requirements for sustainable water use. *Ecohydrology*, 7(2), 508–523.

Wang, J., and Guo, Y. (2018). An analytical stochastic approach for evaluating the performance of combined sewer overflow tanks. *Water Resources Research*, 54(5), 3357–3375.

Wang, J., and Guo, Y. (2019a). Stochastic analysis of storm water quality control detention ponds. *Journal of Hydrology*, 571, 573–584.

Wang, J., and Guo, Y. (2019b). Dynamic water balance of infiltration-based storm water best management practices. *Advances in Water Resources*. (Under Review)

Wang, J., and Guo, Y. (2019c). Proper sizing of infiltration trenches using closed-form analytical equations. *Journal of Hydrologic Engineering* (to be submitted)

Wang, J., Zhang, S., and Guo, Y. (2019). Analyzing the Impact of Impervious Area Disconnection on Urban Runoff Control Using an Analytical Probabilistic Model. *Water Resources Management*, 33(5), 1753–1768.

Wanielista, M.P., and Yousef, Y.A. (1993). *Stormwater management*, Wiley, New York.

Weiss, J. D., Hondzo, M., and Semmens, M. (2006). Storm water detention ponds: modeling heavy metal removal by plant species and sediments. *Journal of Environmental Engineering*, 132(9), 1034–1042.

Woznicki, S. A., Hondula, K. L., and Jarnagin, S. T. (2018). Effectiveness of landscape-based green infrastructure for stormwater management in suburban catchments. *Hydrological Processes*, 32(15), 2346–2361.

Yao, L., Chen, L., and Wei, W. (2016). Assessing the effectiveness of imperviousness on stormwater runoff in micro urban catchments by model simulation. *Hydrological Processes*, 30(12), 1836–1848.

Zegpi, M., and Fernandez, B. (2010). Hydrological model for urban catchments–analytical development using copulas and numerical solution. *Hydrological Sciences Journal*, 55(7), 1123–1136.

Zhang, S. (2014). *Analytical probabilistic Models for evaluating the hydrologic performance of structural low impact development practices*, Ph.D. Thesis, Department of Civil Engineering, McMaster University, Hamilton, Canada.

Zhang, S., and Guo, Y. (2013). Explicit equation for estimating storm-water capture efficiency of rain gardens. *Journal of Hydrologic Engineering*, 18(12), 1739–1748.

Zhang, S., and Guo, Y. (2014). Stormwater capture efficiency of bioretention systems. *Water Resources Management*, 28(1), 149–168.

Zhang, S., Zhang, J., Yue, T., and Jing, X. (2019). Impacts of climate change on urban rainwater harvesting systems. *Science of the Total Environment*, 665, 262–274.

Chapter 2

An Analytical Stochastic Approach for Evaluating the Performance of Combined Sewer Overflow Tanks

Jun Wang and Yiping Guo

Abstract: Stormwater detention tanks are widely used for the control of combined sewer overflows. Conventional continuous simulation and recently developed analytical probabilistic models have been used for analyzing the hydrologic operation of stormwater detention tanks. These analyses are necessary in order to accurately estimate the runoff capture efficiency of a given control system or the required storage capacity for achieving a desired runoff capture efficiency. The analytical probabilistic models still have the shortcomings of making simplifying assumptions about the initial storage conditions of a detention tank. Developed in this study is a new stochastic analysis method which can provide similar results as provided by continuous simulations and overcome some of the shortcomings of the previously developed analytical probabilistic models. This stochastic analysis method uses closed-form analytical equations to estimate the runoff capture efficiency and required storage capacity. Results from these analytical equations are validated by comparing with continuous simulation results and close agreements are observed. These analytical equations are therefore proposed as a computationally efficient alternative for analyzing the hydrologic performance of combined sewer overflow tanks.

Key Words: Combined sewer overflow; Analytical stochastic approach; Continuous simulation; Detention tank; Runoff control; Stormwater management

2.1 Introduction

Urban stormwater runoff from downtown neighborhoods is usually conveyed through combined sewer systems and treated in a downstream wastewater treatment plant (WWTP) before being released to the natural environment (Adams and Papa, 2000; Andrés-Doménech et al., 2010). However, overflow may occur when the wet-weather flows in combined sewers exceed the treatment capacity of the downstream WWTP (Li and Adams, 2000; Andrés-Doménech et al., 2012). The combined sewer overflows (CSOs) can cause water quality problems because they may transport debris, microbial pathogens and other contaminants to receiving waters (USEPA, 2001; Barbosa et al., 2012; Mailhot et al., 2015). Increased rainfall due to climate change in regions with combined sewers can increase the frequency and severity of CSOs, and proper control of CSOs is an imperative task (Andrés-Doménech et al., 2012). Experiences gained by many countries of the world (Heitz et al., 2000; Martino et al., 2011; Li et al., 2015; Llopart-Mascaró et al., 2015) demonstrated that stormwater detention provided by tanks is an acceptable and effective measure for the proper control of CSOs (Weiss et al., 2006).

Stormwater detention tanks primarily serve two purposes in the control of CSOs (Andrés-Doménech et al., 2010). First, with the proper configuration of the tank size and its discharge capacity, the frequency and severity of CSOs can be greatly reduced. Second, storm tanks allow for the sedimentation and self-purification of stored inflow, and therefore aid in mitigating water pollution from outflows.

The hydrologic design or sizing methods used for stormwater detention tanks can be generally divided into two categories: the continuous simulation approach and the analytical probabilistic approach (Loganathan et al., 1985; Guo, 2001; Balistrocchi et al., 2013). In applying the continuous simulation approach, long series of discharge flows from the system under study is generated using a computer model. Various hydrologic and hydraulic processes can be included in this model and the observed historical rainfall data are used as the input rainfall series. The Stormwater Management Model (SWMM) developed by the U.S. Environmental Protection Agency (USEPA) is a suitable and powerful tool for continuous simulations of storm tank operations (Todeschini et al., 2012). Other continuous simulation models, such as NetSTORM (Park et al., 2013), COSMOSS (Paola and Martino, 2013), and HEC-HMS (De Emerson et al., 2005) can also be applied in the study of stormwater detention facilities. Statistics about the system operation can be obtained from the simulated outflow series and system designs can be modified based on these statistics. Continuous simulation requires large amounts of input data and is time-consuming to perform, especially when system designs need to be modified to achieve specific performance requirements (Adams and Papa, 2000).

The analytical probabilistic approach, an extremely compact, computationally efficient and easy-to-use alternative to the continuous simulation approach, was proposed and improved in the study of urban drainage systems (DiToro and Small, 1979; Guo and Adams, 1998a, 1998b; Adams and Papa, 2000; Hassini and Guo, 2017). Several analytical probabilistic models related to stormwater detention facilities were proposed by Guo and Adams (1999a, 1999b), Guo (2001) and Guo and Baetz (2007). A large number of studies on storm tanks using similar probabilistic methods by other groups of researchers can also be found in the literature (e.g., Bacchi et al., 2008; Andrés-Doménech et al., 2012; and Raimondi and Becciu, 2014).

The hydrologic analysis conducted by the analytical probabilistic approach is usually performed on an event-by-event basis, where the analyzed wet-dry cycle consists of a random rainfall event and an episode of inter-event dry time between two successive rainfall events. When assessing the hydrologic performance of a storage facility using the analytical probabilistic approach, it is necessary to take into account the initial condition (i.e., the condition of the storage facility at the beginning of a random rainfall event itself or its preceding dry period if the operation of the facility during this dry period is considered as well) of the storage facility. The storage facility may be full, partly empty or completely empty at the beginning of a random rainfall event. Theoretically, the stationary probability distribution of the available storage capacity of the facility prior to the occurrence of a random rainfall event exists, however, it was concluded that such a probability distribution is difficult to obtain in an analytical way (Chen and Adams, 2005; Zhang and Guo, 2014). That is why two types of assumptions about the initial condition of the storage facility have been tested and widely accepted in previous studies. One assumes that the storage is full at the beginning of a random dry period-rainfall event cycle which is analyzed in detail (Howard, 1976; Loganathan and Delleur, 1984; Guo and Baetz, 2007; Zhang and Guo, 2013). The other one assumes that the storage is empty at the end of the dry period preceding a random rainfall event which is analyzed in detail (Bacchi et al., 2008; Balistrocchi et al., 2009; Balistrocchi et al., 2013; Zhang and Guo, 2014). The assumed full storage condition (i.e., full storage at the beginning of a dry period) represents the most critical condition whereas the assumed empty storage condition (i.e., empty storage at the beginning of a rainfall event) represents the desired operating condition (Loganathan et al., 1985). Although these two assumptions may be justified in many cases, use of them will inevitably result in some level of underestimation or overestimation of the performance of storage facilities.

Determination of the possible initial storage conditions of stormwater control facilities at the beginning of a random rainfall event remains a challenging task. Instead of using simplifying assumptions, the long-term average storage condition of stormwater control facilities should be used as the initial conditions because it would be more representative and accurate for evaluating the performance of these facilities. In order to bridge this gap and improve the analytical probabilistic approach, the probability density function (PDF) of the storage level and the long-term average storage level will be determined in this study using a new stochastic approach. It is shown in this study that the new stochastic approach can also be used to analyze the hydrologic operation of stormwater detention tanks. Simplifying assumptions about the initial conditions are no longer needed. The new analytical stochastic model facilitates convenient evaluation of the hydrologic performance of CSO tanks or other similar types of stormwater detention tanks.

2.2 Analytical Description of Point Rainfall Series

2.2.1 Probabilistic Models of Rainfall Event Characteristics

The probabilistic features of point rainfall series can be described by two different analytical methods. In using the probabilistic method, a continuous rainfall series is viewed as consisting of individual rainfall events and dry periods between consecutive rainfall events. Individual rainfall events are treated as statistically independent of each other. For each dry period-rainfall event cycle, three important characteristics can be used to represent its main features: rainfall depth (v), duration (u) and inter-event time (b) prior to the occurrence of the event under consideration. After detailed frequency analysis for each of these characteristics, proper PDFs can be selected to fit the observed frequency distributions of each characteristic.

It has been found that exponential PDFs often fit well the histograms of rainfall event characteristics for many locations. Early in 1986, the use of exponential PDFs was recommended for the design of stormwater detention ponds by the USEPA (1986). A few researchers have also tested its applicability and presented the related PDF parameters for stations across the U.S. (Wanielista and Yousef, 1993; Hassini and Guo, 2016) and Canada (Adams and Papa, 2000). To date the exponential PDFs have been widely and successfully used for rainfall event characterization in many regions around the world (Eagleson, 1972; Howard, 1976; Adams et al., 1986; Guo and Baetz, 2007; Bacchi et al., 2008; Balistrocchi et al., 2009). These PDFs are detailed in Table 2.1 where $\langle v \rangle$, $\langle u \rangle$ and $\langle b \rangle$ are respectively, the average rainfall event depth, the average rainfall event duration, and the average inter-event time.

In using the stochastic approach, the sequential occurrence of rainfall events is viewed as a Poisson process since the Poisson process generally fits well the timing of hydrologic extremes including rainfall events (Kirby, 1969). The depth of an individual rainfall event (v) is assumed to be an independent random variable, described also by an exponential PDF. The temporal structure within rainfall events is ignored since an individual rainfall event is treated as an instantaneous pulse. The complete rainfall series can thus be treated as a marked Poisson process (Snyder and Miller, 1991). The arrival rate of the rainfall events in this marked Poisson process is denoted as μ and $\mu = 1/[\langle u \rangle + \langle b \rangle]$ with $\langle \cdot \rangle$ representing the average operator, since the inter-arrival time of each event (m) is equal to (u+b). This stochastic representation of rainfall characteristics is summarized in Table 2.1, where n denotes the total number of occurrences of rainfall events within a continuous period of time.

Table 2.1 Analytical description of local rainfall characteristics

Rainfall event characteristics	Probability distribution	Distribution parameter	Approach
Depth, v (mm)	$f_V(v) = \zeta\, \mathrm{e}^{-\zeta v}$	$\zeta = 1/\langle v \rangle$	Probabilistic /Stochastic
Duration, u (h)	$f_U(u) = \lambda\, \mathrm{e}^{-\lambda u}$	$\lambda = 1/\langle u \rangle$	Probabilistic
Inter-event time, b (h)	$f_B(b) = \psi\, \mathrm{e}^{-\psi b}$	$\psi = 1/\langle b \rangle$	Probabilistic
Number of occurrences of rainfall events from time zero to time t, $N(t)$	$P[N(t) = n] = (\mu t)^n\, \mathrm{e}^{-\mu t} / n!$ $n = 0, 1, 2, \cdots$	$\mu = 1/\langle m \rangle$	Stochastic
Inter-arrival time, m (h)	$f_M(m) = \mu\, \mathrm{e}^{-\mu m}$	$\mu = 1/\langle m \rangle$	Stochastic

The above-described two types of analytical representations of point rainfall series both consider rainfall event depth and inter-event dry period as exponentially distributed and mutually independent random variables. In the development of the analytical probabilistic model for analyzing the hydrologic performance of stormwater detention facilities, the probabilistic representation for rainfall characterization as detailed in Table 2.1 is used. In this study, instead of dealing with individual rainfall event cycles, the stochastic representation as detailed in Table 2.1 is used in the modeling of the long-term performance of CSO tanks. It is recognized that the simplified way of characterizing individual rainfall events as used in the above-described analytical probabilistic and stochastic approaches may result in inaccuracies in estimating the system responses (Knighton and Walter, 2016). That is why the analytical results obtained in this study will be compared with results from continuous simulations where no such simplification is made.

When different rainy seasons of a location need to be considered separately, different Poisson processes and exponential distributions may be fitted for different seasons. CSOs may be caused by different types of rainfall events (e.g., summer convective, tropical cyclonic, etc.) associated with different atmospheric mechanisms. The above-described probabilistic or stochastic representation of point rainfall series can also be used to describe each type of rainfall events separately. A direct linkage between CSOs and the dominant causal atmospheric mechanisms can therefore be established (see Knighton et al., 2017 for relevant methodology). In this paper, the entire rainy season will be treated as a whole, no differentiation between causal atmospheric mechanisms will be made. But the analytical results obtained in this study may serve as a foundation for more detailed studies considering seasonal differences or different causal atmospheric mechanisms.

2.3 Stochastic Analysis of CSO Tanks

2.3.1 Dynamic Water Balance of CSO Tanks

The inflow to a detention tank is primarily runoff from the contributing catchment. The outflow from the detention tank is usually the discharge or controlled outflow since evaporation and other losses from the tank are negligible. The dynamic water balance of a detention tank can thus be expressed as

$$\frac{\mathrm{d}S_s(t)}{\mathrm{d}t} = R\left[S_s(t),t\right] - Q\left[S_s(t)\right] \tag{2.1}$$

where $S_s(t)$ is the amount of water stored in the tank at time t, expressed as mm of water over the catchment area; $R[S_s(t),t]$ is the combined sewer inflow rate collected into the detention tank from the contributing catchment at time t, expressed as mm/h, this inflow rate is a function of $S_s(t)$ as well since the amount of $S_s(t)$ may affect the amount of inflow that can be collected by the tank; $Q[S_s(t)]$ is the outflow rate of the detention tank at time t, expressed as mm/h. For simplicity of notation, hereafter the indication of the time dependence is omitted when it is not necessary, i.e., $S_s(t)$, $R[S_s(t),t]$, and $Q[S_s(t)]$ may be simply represented by S_s, $R(S_s)$ and $Q(S_s)$, respectively.

2.3.2 Formulation of a Stochastic Water Balance Equation

Based on the stochastic representation described in section 2.2 and equation (2.1), the stochastic water balance equation of a detention tank can be estimated as follows.

2.3.2.1 Rainfall-runoff Transformation

When a rainfall event occurs on the contributing catchment of a CSO tank, a part of the rainwater does not contribute to surface runoff due to the initial hydrologic losses caused by interception and surface depressions. The initial losses can be lumped together and expressed as S_d for ease of analysis. Using a simple but practical runoff model (Balistrocchi et al., 2009; Li and Adams, 2000; U.S. Army Corps of Engineers, 1977), the rainfall-runoff transformation can be described by applying a factor of conversion ϕ to account for infiltration and other hydrologic losses as

$$v_r = \begin{cases} 0, & v \le S_d \\ \phi\left(v - S_d\right), & v > S_d \end{cases} \tag{2.2}$$

where v_r is the runoff (measured in depth of water over the contributing catchment area) flowing into the detention tank, mm; ϕ is the dimensionless runoff coefficient used to estimate the net rainfall; S_d is the lumped initial losses including interception and depression storage, mm.

The rainfall after deducting the initial losses can be transformed into a new censored Poisson process with an arrival rate of μ' according to

$$\mu' = \mu \int_{S_d}^{\infty} f_V(v)\,\mathrm{d}v = \mu\,\mathrm{e}^{-S_d\zeta} \tag{2.3}$$

Then the average inter-arrival time of the censored rainfall event series, $\langle m_r \rangle$, can be expressed as $1/\mu'$.

The effective rainfall $v' = (v - S_d)$ has the same PDF as v but with a new arrival rate of μ', i.e.,

$$f_{V'}(v') = \zeta\,\mathrm{e}^{-\zeta v'} \quad \text{for } v' > 0 \tag{2.4}$$

where ζ is the distribution parameter for rainfall event depth shown in Table 2.1. The part of equation (2.2) with $v \le S_d$ is taken care of by using μ' instead of μ, equation (2.2) can thus be simplified as $v_r = \phi v'$. The PDF of v_r can therefore be obtained using the derived probability distribution theory based on equation (2.4) and the relationship between v_r and v' as follows:

$$f_{V_R}(v_r) = \frac{\mathrm{d}}{\mathrm{d}v_r}\left(\int_0^{v_r/\phi} \zeta e^{-\zeta v'}\,\mathrm{d}v'\right) = (\zeta/\phi)\,\mathrm{e}^{-(\zeta/\phi)v_r} \text{ for } v_r > 0 \tag{2.5}$$

For simplicity in further analysis, dimensionless transformation and normalization are applied whenever possible. Let $r = v_r / S_m$ where S_m is the effective storage capacity of a detention tank expressed as mm of water over the catchment area, and r is the normalized runoff event volume flowing into the tank, dimensionless. The normalized runoff event volumes can also be represented as a marked Poisson process with the arrival rate of μ' and the PDF of the dimensionless individual runoff event volumes can be expressed as

$$f_R(r) = \frac{\mathrm{d}}{\mathrm{d}r}\left[\int_0^{S_m r} (\zeta/\phi) \mathrm{e}^{-(\zeta/\phi)v_r}\, \mathrm{d}v_r\right] = \gamma\, \mathrm{e}^{-\gamma r} \quad \text{for } r > 0 \tag{2.6}$$

where $\gamma = \zeta S_m / \phi$. The average inter-arrival time of the normalized runoff events is $\langle m_r \rangle$.

It should be noted that there may be a seasonality to the values of ϕ and S_d. Obvious seasonal differences in climatic and catchment conditions may exist for some locations of interest. For those locations, the annual non-winter period may be divided into several seasons and rainfall conditions may be analyzed separately for different seasons. The catchment rainfall-runoff model may be calibrated for different seasons and different ϕ and S_d values may be used to represent the catchment at different seasons. The stochastic analysis approach proposed here can still be used separately for different seasons while the required simplifying assumptions may be better satisfied on a seasonal basis.

2.3.2.2 Determination of Inflow Rate

Considering the short times of concentration for runoff generation on most urban catchments with combined sewers, runoff events are assumed to take place instantaneously subsequent to the instantaneous occurrence of rainfall events. The normalized inflow volume that can actually be stored (referred to as the inflow-event volume and denoted as y) by the storm tank is equal to the normalized runoff event volume r if no overflow occurs. But if the available storage is not enough to accommodate the total inflow, overflow occurs and y is less than r. If the relative storage occupancy s defined as S_s/S_m is no greater than 1 when a storm occurs, the maximum amount of runoff that can be stored by the tank is (1-s) as expressed in the normalized dimensionless form. Taking the possibility of overflow and the PDF of runoff event volume as shown in equation (2.6) into consideration, the PDF of the inflow-event volume (y) to the detention tank conditioned on the tank having a relative storage occupancy s when the storm occurs can be expressed as

$$P_{Y|S}\left[y|s\right]=\gamma\,\mathrm{e}^{-\gamma y}+\mathrm{e}^{-\gamma(1-s)}\,\delta\left(y+s-1\right)\quad \text{for } 0\le y\le 1-s \tag{2.7}$$

where s is the relative storage occupancy of the tank at a time when a storm occurs, s takes values from zero to unity; y is the normalized inflow-event volume to the tank, which is the actual inflow event volume that can be stored by the tank divided by S_m; and $\delta(\cdot)$ is the Dirac delta function. The probability mass of $\mathrm{e}^{-\gamma(1-s)}$ at $y=1-s$ represents the probability that a storm will fill the tank to its full extent given that the tank has a relative storage occupancy of s at the beginning of the storm.

The time series of inflow-event volumes to the detention tank can be expressed as y_i with i = 1, 2, 3, ⋯ , where i refers to the sequential number of inflow events taking place from t = 0 onward. The y_i time series can also be represented by a marked Poisson process with the arrival rate of μ' (Guo, 2016). Collectively the sequence of inflows to the tank from start to the current time t is denoted as $\varphi_t(\mu',\gamma)$, and it can be expressed as

$$\varphi_t\left(\mu';\gamma\right)=\frac{R\left(S_s,t\right)}{S_m}=\sum_{i=1}^{N(t)} y_i\delta\left(t-t_i\right) \tag{2.8}$$

where $N(t)$ is the number of inflow events from start to the current time t; t_i is occurrence times of the sequential effective inflow events, hour. It is noted that the inflow rate equals zero except when t is equal to one of the t_i's with i = 1, 2, 3, ⋯ , $N(t)$ where $t_1 < t_2 < \cdots < t_{N(t)}$, and at those t_i times the inflow would result in an instantaneous inflow volume of y_i.

2.3.2.3 Determination of Outflow Rate

Stormwater detention tanks are often constructed underground in intensively urbanized areas (Montalto et al., 2007). The outflow discharge rate $Q(S_s)$ of such tanks is mainly controlled by pumps although some gravity-controlled devices may also be in use. In this study, the pump-controlled system is of interest where $Q(S_s)$ is assumed to be a constant G whenever there is water stored in the tank. The dependence of outflow rate on storage volume $Q(S_s)$ is thus expressed as

$$Q(S_s) = \begin{cases} 0, & S_s = 0 \\ G, & 0 < S_s \le S_m \end{cases} \tag{2.9}$$

where G, expressed in mm of water over the catchment area per hour, is determined by the pumping capacity or the treatment capacity of the downstream WWTP. The normalized outflow rate of the detention tank $q(s)$ can therefore be expressed as

$$q(s) = \begin{cases} 0, & s = 0 \\ \eta, & 0 < s \le 1 \end{cases} \tag{2.10}$$

where the normalized discharge rate η is equal to G/S_m.

2.3.2.4 Normalization of the Water Balance Equation

Dividing all the terms in equation (2.1) by S_m and substituting into it the inflow rate $\varphi_t(\mu',\gamma)$ as expressed in equation (2.8) and the outflow rate $q(s)$ as expressed in equation (2.10), the normalized stochastic water balance equation of a detention tank can be expressed as

$$\frac{\mathrm{d}s}{\mathrm{d}t} = \varphi_t(\mu';\gamma) - q(s) \tag{2.11}$$

The effective storage capacity of a detention tank S_m has been used for normalization purposes but its detailed definition has not been explained yet. With the stochastic representation of rainfall characteristics, inflows into the tank are assumed to occur instantaneously. While in reality both inflows and outflows for all events may occur throughout the event durations. Outflows occurred during a rainfall event empty part of the tank so that some more inflows can be stored. Therefore if we equate S_m to S_c, where S_c is the storage size of the tank expressed in mm of water over the catchment, overflow from the tank as calculated by the stochastic model would be an overestimation of the physical reality where outflow during a rainfall event creates some additional storage volume. To reduce this discrepancy, the effective storage capacity S_m used in the stochastic model should include an additional storage capacity that is created by outflow during a rainfall event. This additional storage capacity can be calculated as the product of the constant outflow rate and the average rainfall event duration, i.e.,

$$S_m = S_c + G\langle u \rangle = S_c + G/\lambda \tag{2.12}$$

where λ is the distribution parameter for rainfall event duration shown in Table 2.1.

2.3.3 Solution of the Stochastic Water Balance Equation

Driven by the marked Poisson process $\varphi_t(\mu',\gamma)$, equation (2.11) is a stochastic differential equation requiring solution in probabilistic terms. Since $q(s)$ in equation (2.11) is a function of only the present value of s, the solution of s from this equation is therefore a Markov process (Gardiner, 2004). In a Markov process, the evolution of the state PDF at different times can be described by the Chapman-Kolmogorov forward equation (Cox and Miller, 1965; Sobczyk, 1991). Derivations based on the Chapman-Kolmogorov forward equation allow for the analytical solutions in probabilistic terms of the stochastic water balance shown in equation (2.11). According to equation (2.10), the outflow rate of the detention tank approaches zero at $s = 0$ in a discontinuous manner, as a result, the probability distribution of s at time t is a mixed distribution comprised of a discrete atom of probability $f_0(t)$ for $s = 0$ and a continuous PDF for $s > 0$ at time t as well; this continuous PDF is denoted as $f(s,t)$. Both $f_0(t)$ and $f(s,t)$ are functions of time.

Rodriguez-Iturbe et al. (1991, 1999, 2001), Proporato et al. (2004), and Rodriguez-Iturbe and Proporato (2005) developed a stochastic approach for ecohydrological studies focusing on soil moisture dynamics. More up-to-date related studies are reported by Dralle and Thompson (2016) and Thompson et al. (2017). Water balance equations very similar to equation (2.11) were used in these studies. Rodrigues-Iturbe et al. (1999) derived in detail the Chapman-Kolmogorov forward equations of a Markov process governed by an equation similar to equation (2.11) in their study of soil moisture dynamics. Adapting from their solutions, the temporal evolution of $f(s,t)$ can be expressed as

$$\frac{\partial f(s,t)}{\partial t} = \frac{\partial}{\partial s}\left[f(s,t) q(s) \right] - \mu' f(s,t) + \mu' \int_0^s f(z,t) P_{Y|S}\left[(s-z) | z \right] \mathrm{d}z + \mu' f_0(t) P_{Y|S}\left[s | 0 \right] \quad (2.13)$$

where $P_{Y|S}\left[(s-z)|z\right]$ and $P_{Y|S}\left[s|0\right]$ are both the conditional PDFs of inflows expressed in equation (2.7); z is the dummy variable of integration. The temporal evolution of the atom of probability $f_0(t)$ with $s=0$ is also governed by

$$\frac{\mathrm{d}\, f_0(t)}{\mathrm{d}t} = -\mu' f_0(t) + q(0^+)\, f(0^+,t) \quad (2.14)$$

where 0^+ is a value infinitesimally greater than zero, accounting for the case when the relative storage volume approaches zero from a positive value during a small time interval in the rain-free period; mathematically $f(0^+,t) = \lim_{s\to 0^+} f(s,t)$.

Equations (2.13) and (2.14) are the basic Chapman-Kolmogorov forward equations describing the evolution of the probability distribution of s based on the outflow function $q(s)$ and the conditional PDF of the inflows. Detailed descriptions and derivations were provided by Rodrigues-Iturbe et al. (1999) and Rodrigues-Iturbe and Porporato (2005). Replacing $P_{Y|S}\left[\cdot|\cdot\right]$ with what is expressed in equation (2.7) and $q(s)$ with what is expressed in equation (2.10), the two Chapman-Kolmogorov forward equations are transformed to

$$\frac{\partial f(s,t)}{\partial t}=\eta\frac{\partial f(s,t)}{\partial s}-\mu' f(s,t)+\mu'\int_0^s f(z,t)\left[\gamma\,\mathrm{e}^{-\gamma(s-z)}+\delta(s-1)\mathrm{e}^{-\gamma(1-z)}\right]\mathrm{d}z \qquad \text{for } 0<s\le 1 \quad (2.15)$$
$$+\mu' f_0(t)\left[\gamma\,\mathrm{e}^{-\gamma s}+\delta(s-1)\mathrm{e}^{-\gamma}\right]$$

$$\frac{\mathrm{d}\,f_0(t)}{\mathrm{d}t}=-\mu' f_0(t)+\eta f\left(0^+,t\right) \qquad \text{for } s=0 \qquad (2.16)$$

Since the forcing process $\varphi_t(\mu',\gamma)$ is a stationary process, regardless of the initial condition of the tank at the very beginning of a time period, a steady state PDF would be reached when t approaches infinity. Under such a steady state, the probability distribution of s does not change with time anymore. Although the non-stationarity of climate and other factors may cause efficiency losses of the system during its operation lifetime, for planning and design purposes, only the steady-state condition is of interest because usually the future long-term average system performance is the primary concern (Guo, 2016). By taking the limit of $t\to\infty$, the left-hand-side terms of equations (2.15) and (2.16) become zero, and $f(s,t)$, $f_0(t)$ and $f(0^+,t)$ would not change with t anymore. Because Dirac Delta functions are involved in the equation (2.14) at $s=1$, equation (2.15) can be written separately for cases with $0<s<1$ and $s=1$. By replacing $f(s,t)$, $f_0(t)$ and $f(0^+,t)$ with $f(s)$, f_0 and $f(0^+)$ to represent respectively their steady-state counterparts, equations (2.15) and (2.16) lead to equations (2.17)-(2.19). Detailed derivations can be found in Rodrigues-Iturbe et al. (1999).

$$\eta\frac{\mathrm{d}\,f(s)}{\mathrm{d}s}-\mu' f(s)+\mu'\gamma\,\mathrm{e}^{-\gamma s}\int_0^s f(z)\mathrm{e}^{\gamma z}\,\mathrm{d}z+\mu'\gamma f_0\,\mathrm{e}^{-\gamma s}=0 \qquad \text{for } 0<s<1 \qquad (2.17)$$

$$-\eta\delta(0)\,f(1)-\mu' f(1)+\mu'\gamma\int_0^1 f(z)\mathrm{e}^{-\gamma(1-z)}\,\mathrm{d}z+\mu'\delta(0)\int_0^1 f(z)\mathrm{e}^{-\gamma(1-z)}\,\mathrm{d}z + \mu'\gamma\,\mathrm{e}^{-\gamma}\,f_0+\delta(0)\mathrm{e}^{-\gamma}\,\mu' f_0=0 \quad \text{for } s=1 \tag{2.18}$$

$$-\mu' f_0+\eta f\left(0^+\right)=0 \quad \text{for } s=0 \tag{2.19}$$

where $f\left(0^+\right)=\lim_{s\to 0^+} f(s)$; $f(1)$= probability density for $s=1$.

Divided by $\delta(0)$ and neglecting the infinitesimal terms, equation (2.18) turns to be

$$-\eta f(1)+\mu'\int_0^1 f(z)\mathrm{e}^{-\gamma(1-z)}\,\mathrm{d}z+\mathrm{e}^{-\gamma}\,\mu' f_0=0 \quad \text{for } s=1 \tag{2.20}$$

The general solution to equations (2.17) and (2.20) can be expressed for two cases as

$$f(s)=\begin{cases} C_1 s+C_2, & \mu'=\eta\gamma \\ C_3\,\mathrm{e}^{(\mu'/\eta-\gamma)s}+C_4, & \mu'\neq\eta\gamma \end{cases} \quad \text{for } 0<s\le 1 \tag{2.21}$$

where C_1, C_2, C_3, and C_4 are constants of integration. Detailed solution procedures are provided in Appendix 2A. The general solution to equation (2.19) can be expressed for two cases as (see Appendix 2A for details)

$$f_0=\begin{cases} C_2/\gamma, & \mu'=\eta\gamma \\ \eta\left(C_3+C_4\right)/\mu', & \mu'\neq\eta\gamma \end{cases} \quad \text{for } s=0 \tag{2.22}$$

The overall steady-state probability distribution of the relative storage occupancy s [denoted as $h(s)$] that consists of a discrete probability mass f_0 for $s=0$ and a continuous part $f(s)$ for $0<s\le 1$ can therefore be expressed as

$$h(s) = f(s) + f_0\delta(s) \quad \text{for } 0 \le s \le 1 \tag{2.23}$$

The values of constants C_1, C_2, C_3, C_4 and f_0 in equation (2.23) have to satisfy the requirement that the total probability mass is equal to unity. The total probability mass can be found by integrating $h(s)$ from $-\infty$ to ∞, and the unity requirement can be expressed as

$$\int_{-\infty}^{\infty} h(s)\,\mathrm{d}s = \int_0^1 f(s)\,\mathrm{d}s + f_0 = 1 \quad \text{for } \; 0 \le s \le 1 \tag{2.24}$$

By carrying out the integration in equation (2.24), the constants of integration that were introduced earlier can be determined to be C_1=C_4=0, $C_2 = \gamma/(\gamma+1)$ and $C_3 = (\mu'/\eta - \gamma)\Big/\left[\mathrm{e}^{(\mu'/\eta-\gamma)} - \gamma\eta/\mu'\right]$, so the solution for f_0 is

$$f_0 = \begin{cases} 1/(\gamma+1), & \mu' = \eta\gamma \\ (\mu'/\eta - \gamma)\Big/\left[(\mu'/\eta)\mathrm{e}^{(\mu'/\eta-\gamma)} - \gamma\right], & \mu' \ne \eta\gamma \end{cases} \quad \text{for } s = 0 \tag{2.25}$$

Substituting the expressions for C_1, C_2, C_3, and C_4 into equation (2.21), the solution for $f(s)$ was found to be

$$f(s) = \begin{cases} \gamma/(\gamma+1), & \mu' = \eta\gamma \\ (\mu'/\eta - \gamma)\Big/\left[\mathrm{e}^{(\mu'/\eta-\gamma)} - \gamma\eta/\mu'\right]\mathrm{e}^{(\mu'/\eta-\gamma)s}, & \mu' \ne \eta\gamma \end{cases} \quad \text{for } 0 < s \le 1 \tag{2.26}$$

Substituting f_0 as expressed in equation (2.25) and $f(s)$ as expressed in (2.26) into equation (2.23), the complete steady-state solution of the probability distribution of the relative storage occupancy, $h(s)$, can therefore be expressed by

$$h(s)=\begin{cases}\gamma/(\gamma+1)+\delta(s)/(\gamma+1), & \mu'=\eta\gamma\\ \dfrac{\mu'/\eta-\gamma}{\left[\mathrm{e}^{(\mu'/\eta-\gamma)}-\gamma\eta/\mu'\right]\mathrm{e}^{(\mu'/\eta-\gamma)s}}+\delta(s)\dfrac{(\mu'/\eta-\gamma)}{(\mu'/\eta)\mathrm{e}^{(\mu'/\eta-\gamma)}-\gamma}, & \mu'\neq\eta\gamma\end{cases}\quad \text{for } 0\le s\le 1 \tag{2.27}$$

Although the chances of having μ' exactly equal to $\eta\gamma$ is extremely small, for the completeness of solution, this special case is included here as well. More detailed derivations are given in Appendix 2A. As will be shown later, this closed-form analytical solution can provide great convenience for the study of the hydrologic operation of CSO tanks. The cumulative probability distribution of the relative storage occupancy, $H(s)$, can be derived as

$$H(s)=\int_0^s h(s)\,\mathrm{d}s=\begin{cases}(\gamma s+1)/(\gamma+1), & \mu'=\eta\gamma\\ \left[(\mu'/\eta)\mathrm{e}^{(\mu'/\eta-\gamma)s}-\gamma\right]\Big/\left[(\mu'/\eta)\mathrm{e}^{(\mu'/\eta-\gamma)}-\gamma\right], & \mu'\neq\eta\gamma\end{cases}\quad \text{for } 0\le s\le 1 \tag{2.28}$$

2.4 Application of the Analytical Model of CSO Tanks

Based on the steady-state probability distribution of the relative storage occupancy of CSO tanks, further mathematical analyses can help provide some useful equations describing the hydrologic performance of CSO tanks. The main performance measures of interest are the long-term average relative storage occupancy, overflow volume, and runoff capture efficiency.

2.4.1 Long-term Average Amount of Water Stored in a Tank

Substituting $h(s)$ as expressed in equation (2.27), the long-term average relative storage occupancy, $\langle s\rangle$, can be calculated as

$$\langle s\rangle=\int_0^1 sh(s)\,\mathrm{d}s=\begin{cases}\gamma\big/\left[2(\gamma+1)\right], & \mu'=\eta\gamma\\ (\gamma+1)\big/\left[(\mu'/\eta)\mathrm{e}^{(\mu'/\eta-\gamma)}-\gamma\right]-1\big/(\mu'/\eta-\gamma)+1, & \mu'\neq\eta\gamma\end{cases}\tag{2.29}$$

where $\langle s\rangle$ denotes the ensemble average of s.

The variance of relative storage occupancy, Var(s), can be calculated as

$$\mathrm{Var}(s)=\int_0^1(s-\langle s\rangle)^2 h(s)\,\mathrm{d}s=\begin{cases}\gamma(\gamma+4)\big/\left[12(\gamma+1)^2\right], & \mu'=\eta\gamma\\ \dfrac{1}{(\mu'/\eta)^2}-\dfrac{1+(\gamma+2)(\mu'/\eta)\mathrm{e}^{(\mu'/\eta-\gamma)}}{\left[(\mu'/\eta)\mathrm{e}^{(\mu'/\eta)}-\gamma\right]^2}, & \mu'\neq\eta\gamma\end{cases}\tag{2.30}$$

The long-term average amount of water stored in the tank (denoted as $\langle S_s\rangle$ and measured in the unit of mm of water over the catchment) can be calculated as $\langle S_s\rangle=\langle s\rangle S_c$.

2.4.2 Long-term Average Overflow Volume

The long-term average water balance equation for the storage unit can be written as $\langle r\rangle-\langle q\rangle=\langle\omega\rangle$, where $\langle r\rangle$ is the normalized mean runoff rate from the contributing catchment; $\langle q\rangle$ is the normalized mean outflow rate from the tank; and $\langle\omega\rangle$ is the normalized mean overflow rate. The normalized mean runoff rate is the normalized runoff event volume divided by the average inter-arrival time, and it can be calculated as

$$\langle r \rangle = \int_0^\infty r f_R(r)\,\mathrm{d}r \Big/ \langle m_r \rangle = \mu' \int_0^\infty r\left(\gamma\,\mathrm{e}^{-\gamma r}\right)\mathrm{d}r = \mu'/\gamma \tag{2.31}$$

Substituting $q(s)$ as expressed in equation (2.10) and $h(s)$ as expressed into equation (2.27), the expression of the normalized mean outflow rate can be obtained as

$$\langle q \rangle = \int_0^1 q(s)h(s)\,\mathrm{d}s = \begin{cases} \eta\gamma/(\gamma+1), & \mu' = \eta\gamma \\ \mu'\left[\mathrm{e}^{(\mu'/\eta-\gamma)}-1\right] \Big/ \left[(\mu'/\eta)\mathrm{e}^{(\mu'/\eta-\gamma)}-\gamma\right], & \mu' \neq \eta\gamma \end{cases} \tag{2.32}$$

The normalized mean overflow rate $\langle \omega \rangle$ is obtained by finding the difference between $\langle r \rangle$ and $\langle q \rangle$, i.e.,

$$\langle \omega \rangle = \langle r \rangle - \langle q \rangle = \begin{cases} \mu'/\gamma - \eta\gamma/(\gamma+1), & \mu' = \eta\gamma \\ \mu'/\gamma - \mu'\left[\mathrm{e}^{(\mu'/\eta-\gamma)}-1\right] \Big/ \left[(\mu'/\eta)\mathrm{e}^{(\mu'/\eta-\gamma)}-\gamma\right], & \mu' \neq \eta\gamma \end{cases} \tag{2.33}$$

2.4.3 Long-term Average Runoff Capture Efficiency

The long-term average runoff capture efficiency E_r provided by a CSO tank is defined as the fraction of runoff volume treated by the downstream WWTP over its lifetime of operation. Overflow from the tank discharging directly into the receiving waters is considered as untreated. E_r can thus be calculated as the long-term average treatment rate divided by the long-term average runoff rate, i.e.,

$$E_r = \frac{\langle r \rangle - \langle \omega \rangle}{\langle r \rangle} = \frac{\langle q \rangle}{\langle r \rangle} \tag{2.34}$$

Substituting the expressions for $\langle r \rangle$ from equation (2.31) and $\langle q \rangle$ from equation (2.32) into equation (2.34), the general expression of E_r can be obtained as

$$E_r = \begin{cases} \gamma/(\gamma+1), & \mu' = \eta\gamma \\ \gamma\left[\mathrm{e}^{(\mu'/\eta-\gamma)}-1\right]\Big/\left[(\mu'/\eta)\mathrm{e}^{(\mu'/\eta-\gamma)}-\gamma\right], & \mu' \neq \eta\gamma \end{cases} \tag{2.35}$$

Substituting η with G/S_m and γ with $\zeta S_m/\phi$ into equation (2.35), a more direct expression of E_r can be obtained as

$$E_r = \begin{cases} \zeta/(\zeta+\phi/S_m), & \mu' = \eta\gamma \\ \dfrac{\zeta G}{\phi\mu'}\left[1-\dfrac{\mu'/G-\zeta/\phi}{(\mu'/G)\mathrm{e}^{(\mu'/G-\zeta/\phi)S_m}-\zeta/\phi}\right], & \mu' \neq \eta\gamma \end{cases} \tag{2.36}$$

Equation (2.36) shows that E_r is a monotonically increasing function of S_m. The maximum value of E_r [denoted as max (E_r)] can thus be determined as the E_r when the effective storage capacity S_m approaches infinity. For the cases where $G \geq (\phi\mu')/\zeta$, i.e., $\mu' \leq \eta\gamma$, max (E_r) reaches unity. For other cases, it can be expressed as a function of the treatment rate G. max (E_r) can therefore be expressed as

$$\max(E_r) = \begin{cases} \zeta G/(\phi\mu'), & \mu' > \eta\gamma \\ 1, & \mu' \leq \eta\gamma \end{cases} \tag{2.37}$$

2.4.4 Required Storage Capacity of a CSO Tank

The required storage capacity can be determined based on a selected runoff control target or requirement. The required storage capacity can be obtained by specifying a proper value of the runoff capture efficiency E_r as the control target, and then solving for the corresponding S_c from equations (2.12) and (2.36). The required storage capacity S_r was derived to be

$$S_r = \begin{cases} \phi E_r / [\zeta(1-E_r)] - G/\lambda, & \mu' = \eta\gamma \\ \ln[\zeta G(1-E_r)/(\zeta G - \phi\mu' E_r)] / (\mu'/G - \zeta/\phi) - G/\lambda, & \mu' \neq \eta\gamma \end{cases} \quad (2.38)$$

Equation (2.38) shows that the required storage S_r is a function of rainfall statistics ζ and μ', runoff coefficient ϕ, runoff control target E_r and treatment rate G.

The collection of equations (2.27)-(2.30), (2.32)-(2.33), and (2.36)-(2.38) are referred to as the analytical stochastic model (ASM) for CSO tanks. The key of the ASM is that the probability distribution of the relative storage occupancy [i.e., $h(s)$] was mathematically derived and expressed in a closed-form analytical equation. Based on this probability distribution, additional equations were derived for the calculation of long-term average amount of water stored in the tank, runoff capture efficiency of a given system and the required storage capacity to achieve a selected capture efficiency. Extensive numerical simulations are no longer necessary in order to obtain similar performance statistics.

2.5 Example Application of the Analytical Stochastic Model

2.5.1 Rainfall Data Analysis

An illustrative example is presented in this section in order to demonstrate better the application of the ASM for CSO tanks. A hypothetical urban test catchment is assumed to be located in Atlanta, Georgia representing humid climate conditions. Historical hourly rainfall records excluding the winter seasons from the gauge station located in the Atlanta Hartsfield Airport (COOP 090451) of Georgia in the U.S. is used for analyzing rainfall event characteristics. The rainfall record was obtained from the National Climatic Data Center (NCDC) of the United States and covers the period of 1960-2013. Non-winter months for Atlanta are from January through December as the records of daily minimum temperatures in all months are above 0 ℃.

To separate the continuous rainfall record into individual events and inter-event times, a minimum inter-event time (MIET) needs to be specified. Rainfall episodes separated by a dry period longer than the specified MIET would be considered as separate events, otherwise they would be treated as the same event. Due to perhaps malfunctions of rain gauges, some rainfall events were recorded to have very small rainfall volumes. These small rainfall events would not generate any runoff and include them in the statistical analysis may distort their probability distributions. That is why extremely small rainfall events are censored out from the original data. For Atlanta, it was found that an MIET of 8 hours is appropriate and rainfall events with volumes less than or equal to 1 mm are excluded.

Different numbers of annual rainfall events will result from the use of different MIET specifications. In order to satisfy the assumption that the occurrence of rainfall events is Poissonian, the annual number of events θ must follow a Poisson distribution. This can be examined by the Poisson test (Guo and Baetz, 2007; Hassini and Guo, 2016). Based on the fact that the mean $\langle\theta\rangle$ and variance Var(θ) of a Poisson distribution are equal, the ratio r_p = Var(θ)/$\langle\theta\rangle$ is formed as the Poisson test statistic. When the number of years of rainfall records in the analysis is N_y, (N_y-1)r_p is Chi-square distributed with (N_y -1) degrees of freedom (Cunnane, 1979). Given a selected level of significance α, the critical values of r_p including the upper and lower bounds can thus be obtained (Cruise and Arora, 1990). For the series of θ at Atlanta, N_y = 54, the critical value of r_p ranges from 0.70 to 1.34 with a level of significance $\alpha = 0.1$. The r_p of Atlanta was found to be 0.99 which lies within the interval of critical values, demonstrating that the hypothesis that θ follows a Poisson distribution cannot be rejected.

In this study, the Kolmogorov-Smirnov (K-S) test was selected for testing the goodness-of-fit of exponential distributions for rainfall event statistics. In the K-S test, the maximum deviation between the theoretical cumulative distribution function (CDF) and the observed cumulative distribution is determined. The decision to accept or reject the null hypothesis that the theoretical exponential distribution fits well the empirical distribution can thus be made at a specific significance level (Evans, 2008). The K-S test results for the exponential distributions of v, u, b and m are summarized in Table 2.2. As shown in Table 2.2, the exponential distributions fit very well the histograms of the relative frequencies of the rainfall event volume, duration, inter-event and inter-arrival time at Atlanta. The means of rainfall characteristics used to estimate the parameters of fitted exponential distributions are $\langle v \rangle = 16.06$ mm, $\langle u \rangle = 9.30$ h, $\langle b \rangle = 102.36$ h, and $\langle m \rangle = 111.66$ h; and $\langle \theta \rangle$ was found to be 78.09.

Table 2.2 Results of K-S test for v, u, b and m at Atlanta

Characteristics	Number of equal intervals	Critical value ($\alpha = 0.10$)	Observed maximum	Decision
v (mm)	56	0.163	0.057	Not rejected
u (h)	41	0.191	0.051	Not rejected
b (h)	43	0.186	0.011	Not rejected
m (h)	23	0.247	0.037	Not rejected

2.5.2 Model Comparison

To examine the accuracy of the ASM, the widely-used U.S. EPA SWMM model version 5.1 (Rossman, 2015) was used to conduct a set of continuous simulations with results compared to those obtained from ASM. SWMM can provide simulation results about the total runoff volume (*RV*) and total overflow volume (*OV*) over the period of simulation which can be used to calculate the SWMM-determined long-term average runoff capture efficiency as (*RV-OV*)/*RV*. In the ASM, the estimation of runoff volume is mainly governed by the use of the composite runoff coefficient ϕ and depression storage S_d. However, in SWMM, the catchment is divided into pervious and impervious subareas, where runoff estimation is primarily controlled by the use of the following parameters: the level of imperviousness *imp*, impervious area depression storage S_{di}, pervious area depression storage S_{dp}, and parameters describing pervious area infiltration characteristics. Nevertheless, it was found that a relationship between the runoff coefficient and the level of imperviousness can be expressed by $\phi = imp + \phi_{dp}\left(1 - imp\right)$, where ϕ_{dp} is the pervious area runoff coefficient which can be estimated from the pervious area's other parameters (Chen and Adams, 2005). The same test catchment used by Chen and Adams (2005) is used in this study. For other catchments, the method used by Chen and Adams (2005) can be adopted to determine the value of ϕ_{dp} based on the soil characteristics of the pervious area. Other studies also used similar functional relationships between ϕ and *imp* (Behera et al, 2006; Park et al, 2013). S_d in ASM represents the average depression storage for the entire catchment without dividing it into S_{di} and S_{dp}; it is therefore suggested that S_d can be estimated by the area-weighted average of S_{di} and S_{dp} which can be expressed as

$S_d = S_{di} imp + S_{dp}\left(1 - imp\right)$ (Adams and Papa, 2000). Basic SWMM input parameters describing the physical characteristics of the test catchment are listed in Table 2.3.

Table 2.3 Summary of input parameters in SWMM simulations

Input parameter	Value	Unit
Catchment area	16.8	ha
Catchment width	500	m
Slope	1	%
Impervious area Manning's roughness coefficient	0.013	time/length$^{1/3}$
Pervious area Manning's roughness coefficient	0.21	time/length$^{1/3}$
Impervious area depression storage, S_{di}	1.5	mm
Pervious area depression storage, S_{dp}	4.5	mm
Initial infiltration capacity	45	mm/h
Ultimate infiltration capacity	2.4	mm/h
Infiltration decay coefficient	4.14	h^{-1}
Evaporation rate	2.78	mm/day
Simulation time step	5	min
Pervious area runoff coefficient, ϕ_{dp}	0.25	unitless
Maximum depth of the tank	1	m

Note: The simulation time step and the maximum tank size are specified in this study; the evaporation rate of Atlanta is the same as used in Guo (2016); other parameter values are from Chen and Adams (2005).

2.5.2.1 Comparison for the Runoff Capture Efficiency

In order to evaluate the impacts of treatment rates on the capture efficiency for different tank sizes, a total of 96 cases combining 8 different treatment rates (i.e., G = 1, 2, 3, 4, 5, 6, 7 and 8 mm/d; for the sake of simplicity, G is described in the unit of mm/d, but it is calculated in the unit of mm/h.) and 12 different storage sizes (i.e., S_c = 5, 10, 15, 20, 25, 30, 35, 40, 45, 50, 55 and 60 mm) were simulated. Given a level of imperviousness imp = 0.8, equation (2.36) is used to determine the runoff capture efficiency E_r for all the simulated cases which were then compared to those determined from SWMM simulation results. It is worth noting that the 96 modeled cases represent essentially all the physically possible storage versus treatment rate combinations. For the 96 cases, the comparison of ASM and SWMM runoff capture efficiency results is presented in Fig. 2.1. The absolute relative difference of runoff capture efficiencies estimated using the ASM and SWMM simulation results for all cases are all less than 5.2%. If treating SWMM results as the observed data, the mean E_r obtained from ASM results is 0.691 compared to the observed mean of 0.694, the root mean square error (RMSE) is 0.012, the Nash-Sutcliffe model efficiency coefficient (NSE) is 0.996, and the correlation coefficient between ASM and SWMM results is 0.9998.

Detailed comparison results for 96 cases are displayed in Fig. 2.2 for demonstration purposes. In general, close agreement of the results is achieved between the two models. With the increase of storage capacity or treatment rate, the runoff capture efficiency increases and finally stabilizes at a maximum value. For the 8 pairs of the dotted and dashed curves which represent different treatment rates, the bias of E_r for each pair (i.e., the difference between the mean of ASM and the mean of SWMM results) ranges from -0.008 to 0.007, the RMSE for each pair is less than 0.015, and the NSE for each pair is larger than 0.991.

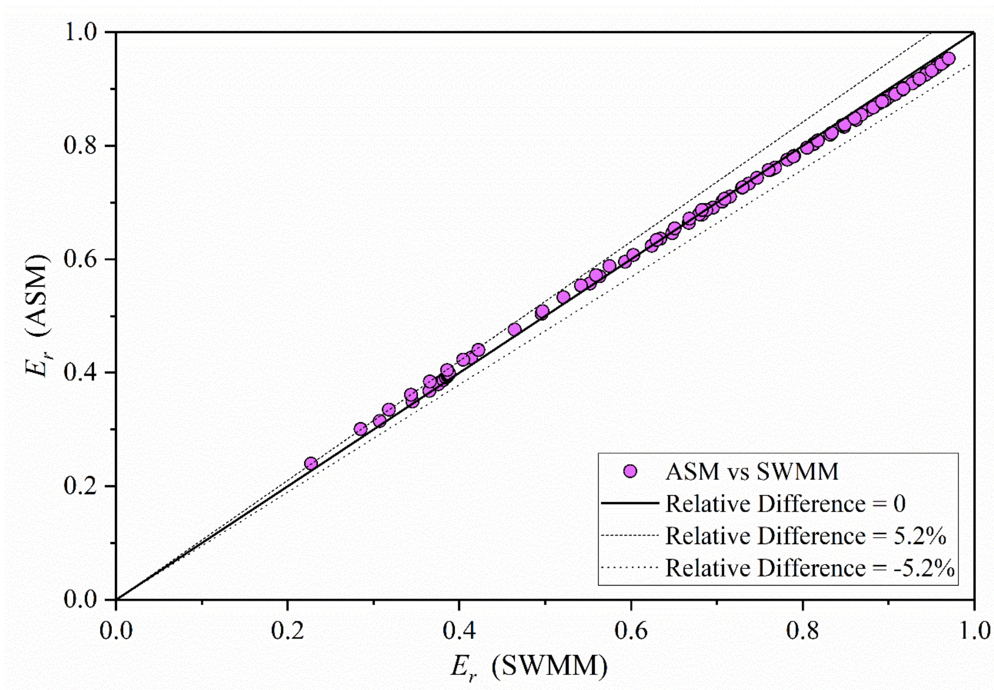

Fig. 2.1 Comparison of runoff capture efficiency determined by ASM and SWMM results

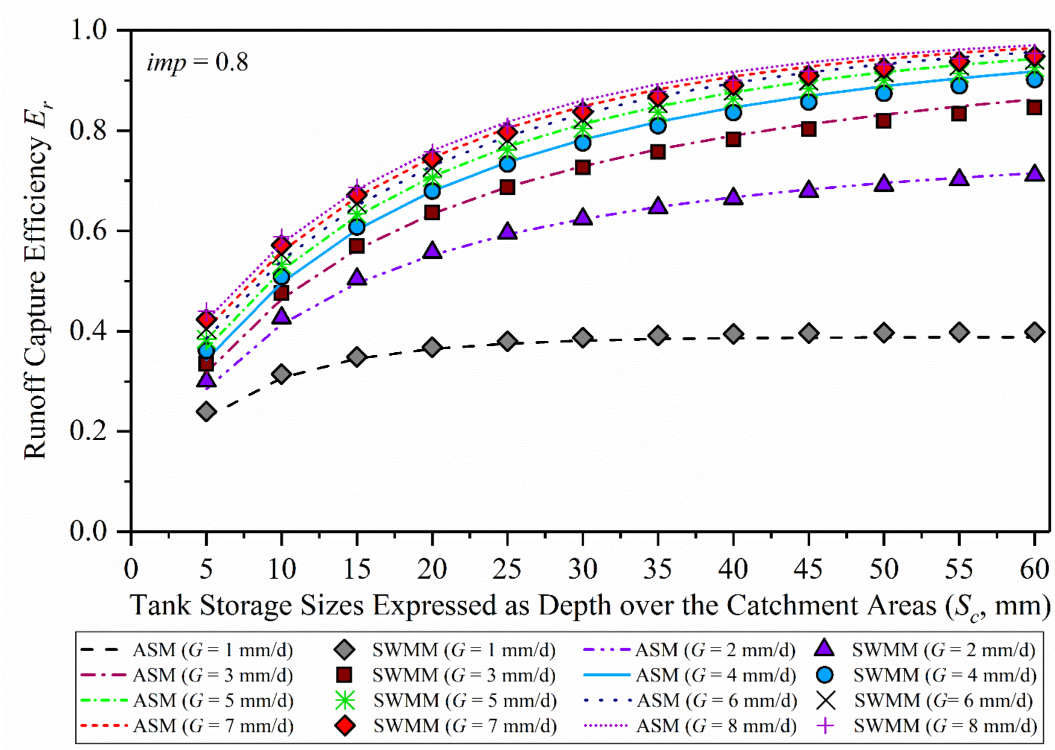

Fig. 2.2 Comparison of runoff capture efficiency curves with eight different treatment rates

2.5.2.2 Comparison for Storage Occupancy

The long-term average relative storage occupancy $\langle s \rangle$ can also be calculated from SWMM simulation results, which can be used to validate what is obtained analytically from equation (2.29). For the aforementioned 96 cases, the comparison of $\langle s \rangle$ between ASM and SWMM results is shown in Fig. 2.3. If SWMM results are treated as the observed data, ASM $\langle s \rangle$ results have a bias of 0.007, the RMSE is 0.013, the NSE is 0.996, and the correlation coefficient between ASM calculated and observed $\langle s \rangle$ values is 0.999. Generally, $\langle s \rangle$ will increase as the storage capacity increases. However, in the cases of large treatment rates (i.e., $G \geq 4$ mm/d), for example, when the treatment rate G is 8 mm/d, with the increase of the storage size of the CSO tanks, $\langle s \rangle$ rises first and then decreases when the storage size exceeds 25 mm. Beyond a certain storage size, although the additional storage space can take in some more inflow, the additional inflow is less than the amount of water needed to keep the relative water occupancy in the additional storage space the same as the rest of the tank. Fig. 2.3 also shows that larger treatment rates result in smaller average relative storage occupancies for a specific storage capacity because more water can be released on time and thus less storage needs to be used.

The derived probability distribution $h(s)$ and cumulative probability distribution $H(s)$ can be validated by comparing with SWMM results as well. For the tank with a size of S_c = 40 mm and the catchment condition with imp = 0.8, taking the two cases with G = 2 and 6 mm/d representing small and large treatment rates as examples, the $h(s)$ calculated from equation (2.27) compared with the relative frequency histogram obtained from SWMM results are shown in Figs. 2.4a, 2.4b. The plotted probability mass f_0 at $s = 0$ and the PDF $f(s)$ for $0 < s \leq 1$ both fit well the relative frequency histograms determined from SWMM simulation results. Using equation (2.28), $H(s)$ can be calculated and compared with the cumulative relative frequencies determined from SWMM results. As shown in Figs. 2.4c, 2.4d, good agreement can also be found for the two cases.

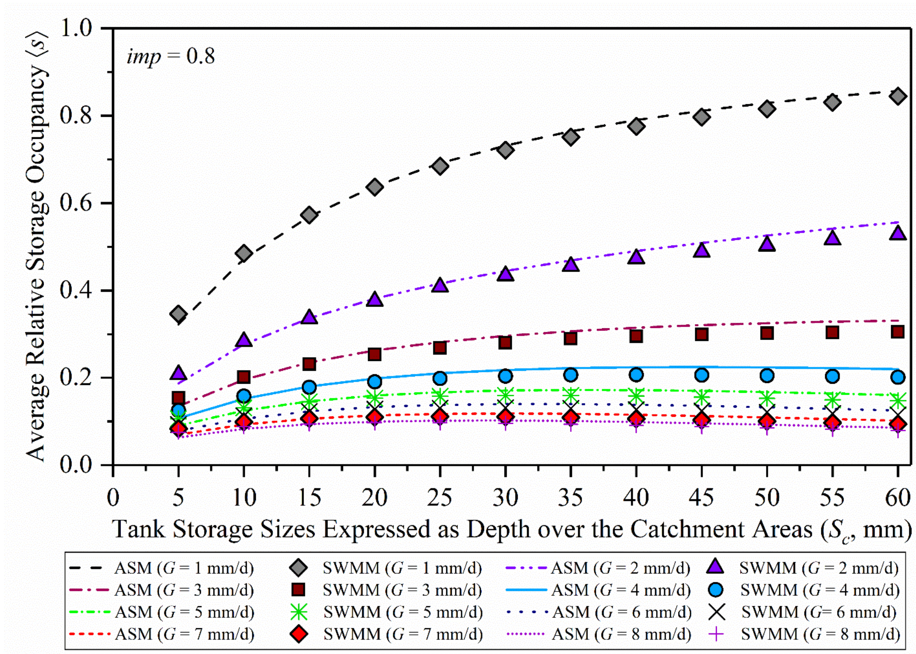

Fig. 2.3 Comparison of long-term average relative storage occupancy with eight different treatment rates

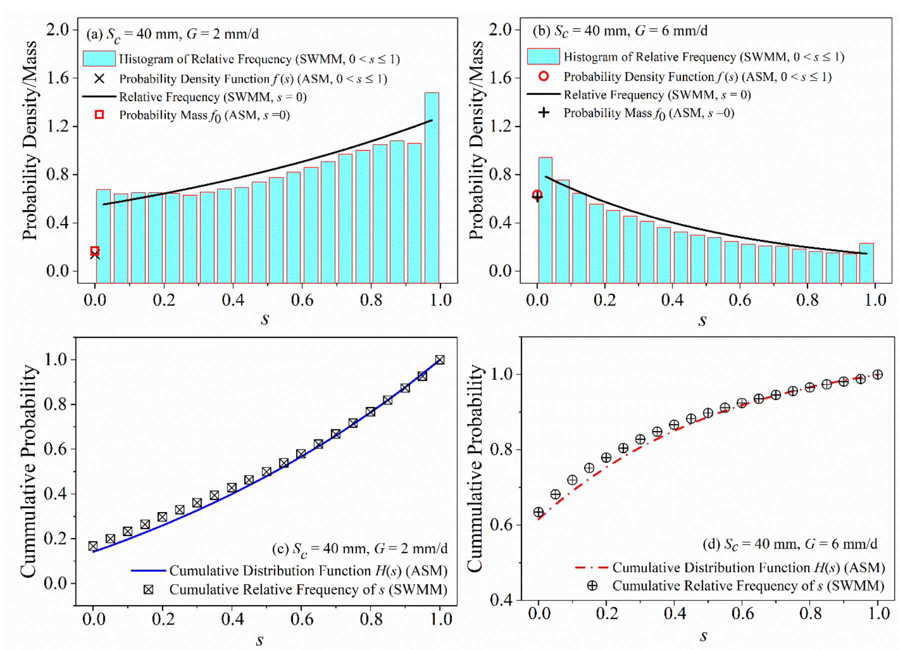

Fig. 2.4 Comparison of the probability distribution and cumulative probability distribution for two different treatment rates

2.5.2.3 Comparison on Urbanization Effects

The level of imperviousness *imp*, an important parameter to represent the catchment conditions, is a sensitive parameter of the model. A set of values (0.3, 0.6 and 0.9) are assigned to *imp*, representing low-, medium- and high-density urban catchments. In ASM, the corresponding composite runoff coefficients are estimated to be 0.475, 0.70 and 0.925 according to the aforementioned conversion method. Given an example of G = 2 mm/d, E_r from ASM and SWMM are determined and plotted. With the combination of 3 levels of imperviousness and 12 different storage capacities, a total of 36 cases are considered. The runoff capture efficiencies for these 36 cases determined from ASM and SWMM results are shown in Fig. 2.5. For the three groups of different *imp*, the largest RSME is 0.049 and the least NSE is 0.863, showing again close agreements between ASM and SWMM results. This comparison also demonstrates that the conversion from SWMM input parameters to ASM input parameters is reasonably accurate.

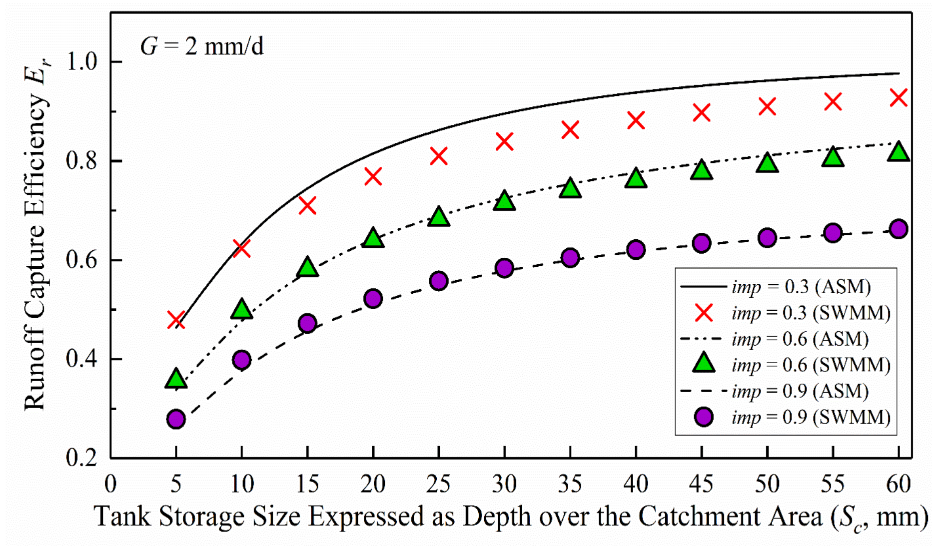

Fig. 2.5 Comparison of runoff capture efficiency curves for three different levels of imperviousness

2.5.2.4 Comparison for the Required Storage Capacity

Given that *imp* = 0.8, the storage capacity of the tank that is required to achieve five different capture efficiencies (i.e., E_r = 65%, 70%, 75%, 80% and 85%) can be determined analytically using equation (2.38). The analytically-calculated required storage capacities for achieving different target capture efficiencies are plotted in Fig. 2.6 as a function of treatment rate. The analytical results are compared with SWMM results and good agreement is observed again in Fig. 2.6. Larger storage capacity and treatment rate can reduce the occurrence of overflows. The required storage capacity would reach infinity when the treatment rate G takes relatively small values, and then decreases as the treatment rate increases. As expected, Fig. 2.6 also indicates that for a higher capture efficiency, the required storage capacity would be larger at a specific treatment rate. Using continuous simulations instead of equation (2.38), a trial and error procedure would have to be used in order to determine the required storage volume for each single treatment rate and runoff capture efficiency (i.e., each single point for each curve in Fig. 2.6). It would therefore be quite a cumbersome task to generate the required storage capacity curve for a catchment of interest using continuous simulations. The advantage of using the ASM is therefore quite clear.

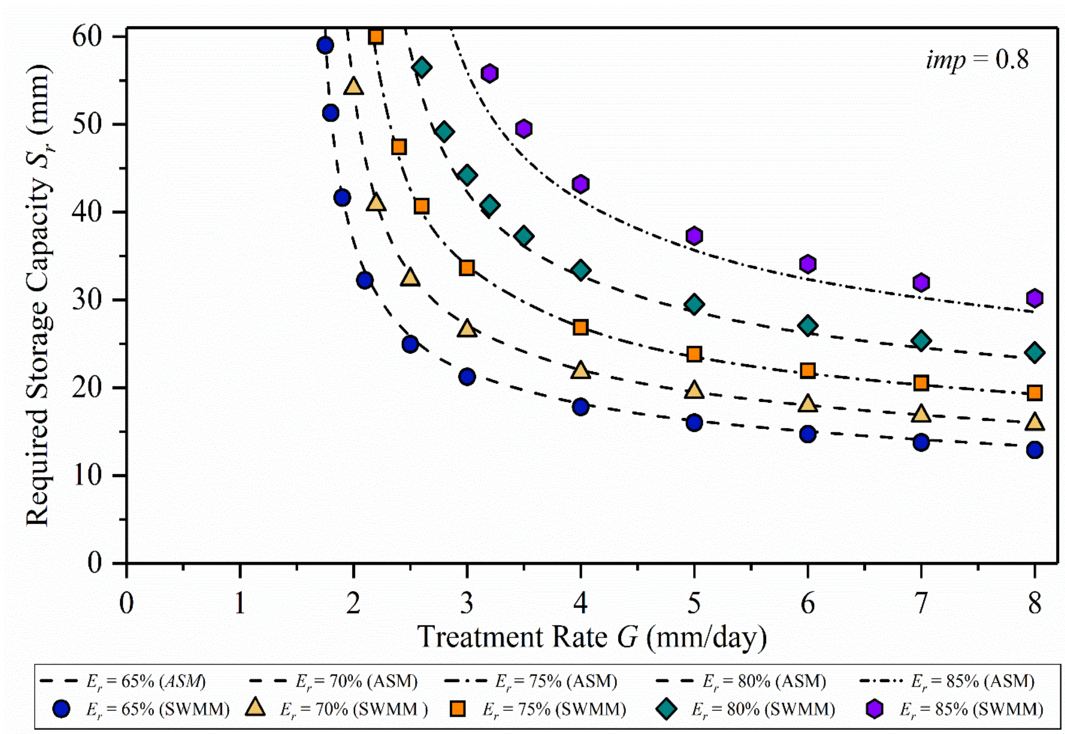

Fig. 2.6 Comparison of the required storage capacity curves for five different capture efficiencies

2.6 Concluding Remarks

This study introduces an analytical stochastic model for analyzing the hydrological performance of stormwater detention tanks. These kinds of tanks usually provide constant outflow rates and are widely used for combined sewer overflow (CSO) control. A conservative and simplifying assumption about the initial storage condition of a CSO tank is required when using the previously developed event-based analytical probabilistic approach. Without such an assumption, closed-form analytical expressions for evaluating the performance characteristics of detention tanks can still be obtained by using our new analytical stochastic approach. These analytical expressions are referred to as the analytical stochastic model (ASM) which can be used for estimating the probability distribution of the relative storage occupancy, the long-term average water volume stored in a tank, the runoff capture efficiency and the required storage capacity of CSO control systems for meeting target capture efficiencies.

For an example case study in Atlanta, the ASM was applied to assess the effects of the degree of urbanization, storage capacity and treatment rate on the long-term average relative storage occupancy and runoff capture efficiency of CSO control systems. Results from the ASM were compared with those from SWMM simulations. The analytical results were found to be very close to the continuous simulation results. Future research may focus on the validation of ASM for other locations or the same location but with different seasons and the combination of the analytical probabilistic and analytical stochastic approaches.

Acknowledgements: The authors thank the anonymous reviewers for their constructive comments and suggestions. This work was supported by the Natural Sciences and Engineering Research Council of Canada and the China Scholarship Council. The data used in this study are listed in the tables or obtained from the citied references.

Appendix 2A: Derivation of $f(s)$ and f_0

Equation (2.17) is an integro-differential equation which cannot be directly solved. However, by multiplying both sides of equation (2.17) by $e^{\gamma s}$ and differentiating both sides with respect to s, it was found that f_0 disappears and equation (2.17) can be converted to the following second-order differential equation:

$$\eta \frac{\mathrm{d}^2}{\mathrm{d}s^2} f(s) + (\eta\gamma - \mu') \frac{\mathrm{d}}{\mathrm{d}s} f(s) = 0 \quad \text{for } 0 < s < 1 \tag{2A.1}$$

2A.1. Derivation for cases with $\mu' = \eta\gamma$

For the case that $\mu' = \eta\gamma$, equation (2A.1) becomes

$$\eta \frac{\mathrm{d}^2}{\mathrm{d}s^2} f(s) = 0 \quad \text{for } 0 < s < 1 \tag{2A.2}$$

The general solution of equation (2A.2) is

$$f(s) = C_1 s + C_2 \quad \text{for } 0 < s < 1 \tag{2A.3}$$

where C_1 and C_2 are constants of integration.

By setting $s = 0^+$ in equation (2A.3), i.e., taking $f(0^+)$ as $\lim_{s \to 0^+} f(s)$, $f(0^+)$ is found to be equal to C_2. Substituting this value into equation (2.17), f_0 can be determined as

$$f_0 = C_2 / \gamma \quad \text{for } s = 0 \tag{2A.4}$$

Substituting $f(s)$ as expressed in equation (2A.3) and f_0 as expressed in equation (2A.4) into equations (2.17) and (2.20) yields

$$\left(\eta - \mu'/\gamma + \mu' \mathrm{e}^{-\gamma s}/\gamma\right) C_1 = 0 \quad \text{for } 0 < s < 1 \tag{2A.5}$$

$$-\eta f(1) + \mu' C_2/\gamma = 0 \quad \text{for } s = 1 \tag{2A.6}$$

Since $\mu' = \eta\gamma$ and $\mu' \mathrm{e}^{-\gamma s}/\gamma \neq 0$, equation (2A.5) yields $C_1 = 0$. As $\mu' = \eta\gamma$ and $\eta \neq 0$, equation (2A.6) yields $f(1) = C_2$. By substituting $C_1 = 0$ into equation (2A.3) and setting $s = 1^-$ yields $f(1^-) = \lim_{s \to 1^-} f(s) = C_2$. Therefore, $f(1^-)$ is equal to $f(1)$, that is, equation (2A.3) is valid for both the unbounded case of $0 < s < 1$ and the bounded case of $0 < s \leq 1$.

Substituting $C_1 = 0$, $f(s)$ as expressed in equation (2A.3) and f_0 as expressed in equation (2A.4) into equation (2.24), the requirement that the total probability mass is equal to unity can be expressed as

$$\int_0^1 C_2 \,\mathrm{d}s + C_2/\gamma = 1 \quad \text{for } 0 \le s \le 1 \tag{2A.7}$$

Equation (2A.7) yields $C_2 = \gamma/(\gamma+1)$. Substituting this value of C_2 and $C_1 = 0$ into equations (2A.3) and (2A.4), and f_0 for cases with $\mu' = \eta\gamma$ are found to be

$$f(s) = \gamma/(\gamma+1) \;\text{ for } 0 < s \le 1 \text{ and } \mu' = \eta\gamma \tag{2A.8}$$

$$f_0 = 1/(\gamma+1) \;\text{ for } s = 0 \text{ and } \mu' = \eta\gamma \tag{2A.9}$$

2A.2. Derivation for cases with $\mu' \neq \eta\gamma$

For cases with $\mu' \neq \eta\gamma$, equation (2A.1) becomes

$$\eta \frac{\mathrm{d}}{\mathrm{d}s} f(s) + (\eta\gamma - \mu') f(s) = \text{constant} \quad \text{for } 0 < s < 1 \tag{2A.10}$$

The general solution to equation (2A.10) is

$$f(s) = C_3 \,\mathrm{e}^{(\mu'/\eta - \gamma)s} + C_4 \;\text{ for } 0 < s < 1 \tag{2A.11}$$

where C_3 and C_4 are constants of integration.

By setting $s = 0^+$ in equation (2A.11), i.e., taking $f(0^+)$ as $\lim_{s\to 0^+} f(s)$, $f(0^+)$ is found to be equal (C_3+C_4). Substituting this value into equation (2.19), f_0 can be determined as

$$f_0 = \eta\left(C_3 + C_4\right)/\mu' \quad \text{for } s = 0 \tag{2A.12}$$

Substituting $f(s)$ as expressed in equation (2A.11) and f_0 as expressed in equation (2A.12) into equations (2.17) and (2.20) yields

$$\left(\eta\gamma - \mu'\right)C_4\,\mathrm{e}^{-\gamma s} = 0 \quad \text{for } 0 < s < 1 \tag{2A.13}$$

$$-\eta f\left(1\right) + \mathrm{e}^{\left(\mu'/\eta - \gamma\right)}\eta C_3 = 0 \quad \text{for } s = 1 \tag{2A.14}$$

Since $\mu' \neq \eta\gamma$ and $\mathrm{e}^{-\gamma s} \neq 0$, equation (2A.13) yields $C_4 = 0$. As $\eta \neq 0$, equation (2A.14) yields $f_1 = C_3\,\mathrm{e}^{\left(\mu'/\eta-\gamma\right)}$. By substituting $C_4 = 0$ into equation (2A.11) and setting $s = 1^-$ yields $f\left(1^-\right) = \lim_{s\to1^-} f\left(s\right) = C_3\,\mathrm{e}^{\left(\mu'/\eta-\gamma\right)}$. Therefore, $f\left(1^-\right)$ is equal to $f(1)$, that is, equation (2A.11) is valid for both the unbounded case of $0 < s < 1$ and the bounded case of $0 < s \le 1$.

Substituting $C_4 = 0$, $f(s)$ as expressed in equation (2A.11) and f_0 as expressed in equation (2A.12) into equation (2.24), the requirement that the total probability mass is equal to unity can be expressed as

$$\int_0^1 C_3\,\mathrm{e}^{\left(\mu'/\eta-\gamma\right)s}\,\mathrm{d}s + \eta C_3/\mu' = 1 \quad \text{for } 0 \le s \le 1 \tag{2A.15}$$

Equation (2A.15) yields $C_3 = \left(\mu'/\eta - \gamma\right)\Big/\left[\mathrm{e}^{\left(\mu'/\eta-\gamma\right)} - \gamma\eta/\mu'\right]$. Substituting this value of C_3 and $C_4 = 0$ into equations (2A.11) and (2A.12), $f(s)$ and f_0 for cases with $\mu' \neq \eta\gamma$ are found to be

$$f(s) = (\mu'/\eta - \gamma) / \left[\exp(\mu'/\eta - \gamma) - \gamma\eta/\mu'\right] \exp\left[(\mu'/\eta - \gamma)s\right] \text{ for } 0 < s \le 1 \text{ and } \mu' \ne \eta\gamma \quad (2A.16)$$

$$f_0 = (\mu'/\eta - \gamma) / \left[(\mu'/\eta)\exp(\mu'/\eta - \gamma) - \gamma\right] \text{ for } s = 0 \text{ and } \mu' \ne \eta\gamma \quad (2A.17)$$

Appendix 2B: Notation

b = rainfall inter-event time (h);

E_r = runoff capture efficiency (dimensionless);

f_0 = probability mass of s at $s = 0$;

$f(s)$ = PDF of s for $0 < s \le 1$;

G = treatment rate of WWTP (mm/h);

$h(s)$ = complete probability distribution function of s;

$H(s)$ = cumulative probability distribution function of s;

m = rainfall inter-arrival time (h);

m_r = runoff inter-arrival time (h);

N_y = number of years of rainfall record in the analysis;

$N(t)$ = the number of inflow events from start to the current time t;

r = normalized runoff event depth (dimensionless);

$R[S_s(t),t]$ Inflow rate of the tank at time t, simplified as $R(S_s)$, (mm/h);

s = relative storage volume occupancy of the detention tank (dimensionless);

S_c = storage size of the detention tank (mm);

S_d = average depression storage for the entire catchment (dimensionless);

S_{di} = impervious area depression storage (dimensionless);

S_{dp} = pervious area depression storage (dimensionless);

S_m = effective storage capacity of the detention tank (mm);

S_r = required storage capacity to achieve a specific target capture efficiency (mm);

$S_s(t)$ = water storage of a detention tank at time t, also simplified as S_s (mm);

t = time (h);

$Q[S_s(t)]$ = outflow rate of the tank at time t, also simplified as $Q(S_s)$ (mm/h);

$q(s)$ = normalized outflow rate of the detention tank (h^{-1});
u = rainfall event duration (h);
v = rainfall event depth (mm);
v' = effective rainfall depth after deducting initial losses (mm);
v_r = surface runoff event depth (mm);
y = inflow event volume to the detention tank (mm);
η = normalized discharge capacity rate (h^{-1});
ω = overflow rate (mm/h);
θ = annual number of rainfall events;
ζ = distribution parameter of rainfall event depth (mm^{-1});
λ = distribution parameter of rainfall event duration (h^{-1});
ψ = distribution parameter of rainfall inter-event time (h^{-1});
μ = Poisson process arrival rate of rainfall event series (h^{-1});
μ' = Poisson process arrival rate of runoff event series (h^{-1});
imp = level of imperviousness of the contributing catchment (dimensionless);
ϕ = composite runoff coefficient (dimensionless);
ϕ_{dp} = runoff coefficient for pervious area (dimensionless);
γ = distribution parameter of the normalized runoff event depth (dimensionless);
$\varphi_t(\mu', \gamma)$ = normalized inflow event series (h^{-1});
$\langle\cdot\rangle$ = averaging operator.

References

Adams, B. J., Fraser, H. G., Howard, C. D. D., and Hanafy, M. S. (1986). Meteorological data analysis for drainage system design. *Journal of Environmental Engineering*, 112(5), 827–848.

Adams, B. J., and Papa, F. (2000). *Urban stormwater management planning with analytical probabilistic models*. Willy, New York.

Andrés-Doménech, I., Montanari, A., and Marco, J. (2012). Efficiency of storm detention tanks for urban drainage systems under climate variability. *Journal of Water Resources Planning and Management*, 138(1), 36–46.

Andrés-Doménech, I., Múnera, J., Francés, F., and Marco, J. (2010). Coupling urban event-based and catchment continuous modelling for combined sewer overflow river impact assessment. *Hydrology and Earth System Science*, 14(10), 2057–2072.

Bacchi, B., Balistrocchi, M. and Grossi, G. (2008). Proposal of a semi-probabilistic approach for storage facility design. *Urban Water J*ournal, 5(3), 195–208.

Balistrocchi, M., Grossi, G., and Bacchi, B. (2009). An analytical probabilistic model of the quality efficiency of a sewer tank. *Water Resource Research*, 45(12). https://doi.org/10.1029/2009WR007822

Balistrocchi, M., Grossi, G., and Bacchi, B. (2013). Deriving a practical-probabilistic method to size flood routing reservoirs. *Advances in Water Res*ources, 62(2013), 37–46.

Barbosa, A., Fernandes, J., and David, L. (2012). Key issues for sustainable urban stormwater management. *Water Research*, 46(20), 6787–6798.

Behera, P.K., Adam, B.J., and Li, J.Y. (2006). Runoff quality analysis of urban catchments with analytical probabilistic models. *Journal of Water Resources Planning and Management.* 132(1), 4–14.

Chen, J., and Adams, B.J. (2005). Analysis of storage facilities for urban stormwater quantity control. *Advances in Water Resources*, 28(4), 377–392.

Cox, D.R., and Miller, D.H. (1965). *The theory of stochastic processes.* Willey, New York.

Cruise, J. F., and Arora, K. (1990). A hydroclimatic application strategy for the Poisson partial duration model. *Water Resources Bulletin*, 26(3), 431–442.

Cunane, C. (1979). A note on the Poisson assumption in partial duration series models. *Water Resource Research*, 15(2), 489–494.

De Paola, F., and Martino, F. D. (2013). Stormwater tank performance: design and management criteria for capture tanks using a continuous simulation and a semi-probabilistic analytical approach. *Water*, 5(4), 1699–1711.

DiToro, D.M., and Small, M.J. (1979). Stormwater interception and storage. *Journal of Environmental Engineering Division*, 105(1), 43–54.

Dralle, D., and Thompson, S. (2016). A minimalistic probabilistic model for soil moisture in seasonally dry climates. *Water Resources Research*, 52(2), 1507–1517.

Eagleson, P. S. (1972). Dynamics of flood frequency. *Water Resource Research*, 8(4), 878–

898.

Emerson, C., Welty, C., and Traver, R. (2005). Watershed-scale evaluation of a system of storm water detention basins. *Journal of Hydrologic Engineering*, 10(3), 237–242.

Evans, D.L., Drew, J.H., and Leemis, L.M. (2008). The distribution of the Kolmogorov–Smirnov, Cramer-von Mises, and Anderson-Darling test statistics for exponential populations with estimated parameters. *Communications in Statistics-Simulation and Computation*, 37(7), 1396–1421.

Gardiner, C. W. (2004). *Handbook of Stochastic Methods for Physics*, *Chemistry and the Natural Sciences*, 3rd Ed. Berlin Heidelberg, Germany: Springer-Verlag.

Guo, J.C.Y., and Urbonas, B. (2002). Runoff capture and delivery curves for storm-water quality control designs. *Journal of Water Resources Planning and Management*, 128(3), 208–215.

Guo, Y. (2001). Hydrologic design of urban flood control detention ponds. *Journal of Hydrologic Engineering*, 6(6), 472–479.

Guo, Y. (2016). Stochastic analysis of hydrologic operation of green roofs. *Journal of Hydrologic Engineering*, 21(7). https://doi.org/10.1061/(ASCE)HE.1943-5584.0001371

Guo, Y., and Adams, B. J. (1998a). Hydrologic analysis of urban catchments with event-based probabilistic models 1. Runoff volume. *Water Resource Research*, 34(12), 3421–3431.

Guo, Y., and Adams, B. J. (1998b). Hydrologic analysis of urban catchments with event-based probabilistic models 2. Peak discharge rate. *Water Resource Research*, 34(12), 3433–3443.

Guo, Y., and Adams, B. J. (1999a). An analytical probabilistic approach to sizing flood control detention facilities. *Water Resource Research*, 35(8), 2457–2468.

Guo, Y., and Adams, B. J. (1999b). Analysis of detention ponds for storm water quality control. *Water Resource Research*, 35(8), 2447–2456.

Guo, Y. and Baetz, B. W. (2007). Sizing of rainwater storage units for green building applications. *Journal of Hydrologic Engineering*, 12(2), 197–205.

Hassini, S. and Guo, Y. (2016). Exponentiality test procedures for large samples of rainfall event characteristics. *Journal of Hydrologic Engineering*, 21(4), 04016003. http://dx.doi.org /10.1061/(asce)he.1943-5584.0001352

Hassini, S. and Guo, Y. (2017). Derived flood frequency distributions considering individual event hydrograph shapes. *Journal of Hydrology*, 547(2017), 296–308.

Heitz, L. F., Khosrowpanah, S., and Nelson, J. (2000). Sizing of surface water runoff detention ponds for water quality improvement. *Journal American Water Resources Association*, 36(3), 541–548.

Howard, C. (1976). Theory of storage and treatment-plant overflows. *Journal of Environmental Engineering Division*, ASCE, 102(4), 709–722.

Kirby, W. (1969). On the random occurrence of major floods. *Water Resources Research*, 5(4), 778–784.

Knighton, J., Steinschneider, S., and Walter, M. T. (2017). A Vulnerability-Based, Bottom-up Assessment of Future Riverine Flood Risk Using a Modified Peaks-Over-Threshold Approach and a Physically Based Hydrologic Model. *Water Resources Research*, 53(12), 10043–10064.

Knighton, J. O., and Walter, M. T. (2016). Critical rainfall statistics for predicting watershed flood responses: rethinking the design storm concept. *Hydrological processes*, 30(21), 3788–3803.

Li, F., Duan, H., Yan, H., and Tao, T. (2015). Multi-objective optimal design of detention tanks in the urban stormwater drainage system: framework development and case study. *Water Resource Management*, 29(7), 2125–2137.

Li, J. Y., and Adams, B. J. (2000). Probabilistic Models for analysis of urban runoff control systems. *Journal of Environmental Eng*ineering, 126(3), 217–224.

Llopart-Mascaró, A., Farreny, R., Gabarrell, X., Rieradevall, J., Gil, A., Martínez, M., Puertas, J., Suárez, J., Río, H., and Paraira, M. (2015). Storm tank against combined sewer overflow: Operation strategies to minimize discharges impact to receiving waters. *Urban Water Journal*, 12(3), 219–228.

Loganathan, G.V. and Delleur, J.W. (1984). Effects of urbanization on frequencies of overflows and pollutant loadings from storm sewer overflows: A derived distribution approach. *Water Resource Research*, 20(7), 857–865.

Loganathan, V.G., Deniur, J.W., and Segarra, R.I. (1985). Planning detention storage for stormwater management. *Journal of Water Resources Planning and Management*, 111(4), 382–398.

Mailhot, A., Talbot, G., and Lavallée, B. (2015). Relationships between rainfall and combined sewer overflow (CSO) occurrences. *Journal of Hydrology*, 523(2015), 602–609.

Martino, G. D., Paola, F. D., Fontana, N., Marini, G., and Ranucci, A. (2011). Pollution reduction in receivers: storm-water tanks. *Journal of Urban Planning and Develop*ment, 137(1), 29–38.

Montalto, F., Behr, C., Alfredo, K., Wolf, M., Arye, M., and Walsh, M. (2007). Rapid assessment of the cost-effectiveness of low impact development for CSO control. *Landscape and Urban Planning*, 82(3), 117–131.

Park, D., Song, Y. and Roesner, L.A. (2013). Effect of the seasonal rainfall distribution on storm-water quality capture volume estimation. *Journal of Water Resources Planning and Management*, 139(1), 45–52.

Porporato, A., Daly, E., and Rodroguez-Iturbe, I. (2004), Soil water balance and ecosystem response to climate change. *The American Naturalist*, 164(5), 625–632.

Raimondi, A., and Becciu, G. (2014). On pre-filling probability of flood control detention facilities. *Urban Water Journal*, 12(4), 344–351.

Rodriguez-Iturbe, I., Entekhabi, D., and Bras, R. L. (1991). Nonlinear dynamics of soil moisture at climate scales: 1. stochastic analysis. *Water Resource Research*, 27(8), 1899–1906.

Rodriguez-Iturbe, I., and Proporato, A. (2005), *Ecohydrology of water-controlled ecosystems*, UK: Cambridge University Press.

Rodriguez-Iturbe, I., Porporato, A., Laio, F., and Ridolfi, L. (2001). Plants in water-controlled ecosystems: Active role in hydrologic processes and response to water stress, I. Scope and general outline. *Advances in Water Resources*, 24(7), 695–705.

Rodriguez-Iturbe, I., Porporato, A., Ridolfi, L., Isham, V., and Cox, D. (1999). Probabilistic modelling of water balance at a point: The role of climate, soil and vegetation. *Proceedings of the Royal Society of London*, *Series A*, 455, 3789–3805.

Rossman, L.A. (2015). Storm water management model user's manual. Version 5.1 (EPA-600/R-14/413b). National Risk Management Research Laboratory, Office of Research and Development, US Environmental Protection Agency, Cincinnati, US. https://www.innovyze.com/products/swmm/download/ZyPDF.pdf

Snyder, D.L., and Miller, M.I. (1991). *Random point processes in time and space*, 2nd Ed. New York: Springer.

Sobczyk, K. (1991). *Stochastic differential equations*: *with applications to physics and engineering*. Dordrecht, the Netherlands: Kluwer Academic Publishers.

Todeschini, S., Papiri, S., and Ciaponi, C. (2012). Performance of stormwater detention tanks for urban drainage systems in northern Italy. *Journal of Environmental Management*, 101, 33–45.

Thompson, S., MacVean, L., and Sivapalan, M. (2017). A stochastic water balance framework for lowland watersheds. *Water Resources Research*, 53(11), 9564–9579.

U.S. Army Corps of Engineers (1977). *Storage, Treatment, Overflow, Runoff Model*: *STORM*, 723-S8-L2250, Hydrologic Engineering Center, Davis, CA.

U.S. Environmental Protection Agency (USEPA) (1986). *Methodology for analysis of detention basins for control of urban runoff quality*. *Rep. EPA*, *440*/5-87-01 (NTIS No. PB87-116562), Washington, D.C.

U.S. Environmental Protection Agency (USEPA) (2001). *Report to congress: implementation and enforcement of the combined sewer overflow Control Policy*. *EPA 833-R-01-003*, Washington, D.C.

Wanielista, M. P., and Yousef, Y. A. (1993). *Stormwater management*. Wiley, New York.

Weiss, J. D., Hondzo, M., and Semmens, M. (2006). Storm water detention ponds: modeling heavy metal removal by plant species and sediments. *Journal of Environmental Engineering*, 132(9), 1034–1042.

Zhang, S., and Guo, Y. (2013). Explicit equation for estimating storm-water capture efficiency of rain gardens. *Journal of Hydrologic Eng*ineering, 18(12), 1739–1748.

Zhang, S., and Guo, Y. (2014). Stormwater capture efficiency of bioretention systems. *Water Resources Management*, 28(1), 149–168.

Chapter 3

Stochastic Analysis of Storm Water Quality Control Detention Ponds

Jun Wang and Yiping Guo

Abstract: Stormwater detention ponds are recognized as an effective type of treatment facility for urban stormwater management purposes. This paper presents methodologies for the development of an analytical stochastic model describing the hydrologic operation of stormwater quality control detention ponds with outflows controlled by orifices. The concept of effective storage capacity is proposed to properly represent a pond's storage in its stochastic water balance equation. The accuracy of the analytical stochastic model (ASM) is verified for many different hypothetical design cases. It is shown that the ASM for detention pond systems can provide accurate results for almost all possible design conditions. Implemented easily into a spreadsheet, the ASM provides an easy-to-use and computationally-efficient tool for analyzing the hydrologic performance of detention pond systems. The ASM can be used separately as a planning or design tool or together with continuous simulation models to help verify simulation results or reduce the number of simulation runs.

Key Words: Surface water quality control; Analytical stochastic approach; Continuous simulation; Detention pond; Stormwater management.

3.1 Introduction

Nonpoint source pollution has been recognized as the leading cause of water quality degradation (Akan, 1992; Tsihrintzis and Hamid, 1998; Wong and Kerkez, 2016). Pollutants found from nonpoint sources may include suspended solids, heavy metals, chlorides, oil and grease, bacteria and other pathogenic microorganisms (Tsihrintzis and Hamid, 1997; Barbosa et al., 2012). These pollutants are generated over urban catchments and are carried by runoff to receiving waters (Fletcher et al, 2013). As an effective stormwater management practice, detention ponds can be utilized for both flood and water quality control (Behera and Teegavarapu, 2015).

Proper control of outflow from a detention pond is required to ensure sufficient residence time needed for the settling and decay of pollutants (Guo and Adams, 1999). Outflow control is commonly achieved through the use of an orifice with a properly selected diameter. Runoff draining to the pond from the majority of rainfall events will go through the orifice and then flow downstream. Under extremely large rainfall events, part of the generated runoff may by-pass or overflow from the detention pond because the pond is totally filled before the end of the runoff event. The runoff that by-passes or overflows from the pond is considered as not receiving any treatment.

The long-term average fraction of removal of total suspended solids is commonly used as the main design criteria for water quality control purposes. Since it is difficult to directly quantify this fraction, it is often estimated as a positive linear function of the runoff capture efficiency provided by a detention pond (Guo and Adams, 1999; Chen and Adams, 2006). The runoff capture efficiency is defined as the fraction of the total volume of runoff captured by a detention pond instead of overflowing from or by-passing the detention pond. In this study, the runoff capture efficiency is selected as a representative performance measure for the evaluation of the water quality control performance of detention ponds.

Models used for evaluating the long-term average performance of detention facilities can be classified into two types: continuous simulation models and analytical probabilistic models (Guo and Adams, 1999; Wang and Guo, 2018). Continuous simulation models are appealing because they can simulate the natural sequences of the occurrence of runoff events. However, continuous simulation is data intensive and time-consuming (Adams and Papa, 2000; Chen and Adams, 2007). Analytical probabilistic models were developed by researchers employing probability distributions to represent rainfall characteristics of different locations, these models estimate pond performance statistics using analytical equations. The analytical equations used in the analytical probabilistic models were derived based on simplified representations of the event-by-event operation of detention ponds. Assumptions about how full the pond is at the beginning of an operation cycle are required in those simplified representations (Howard, 1976; Loganathan and Delleur, 1984;

Guo and Baetz, 2007; Bacchi et al., 2008; Balistrocchi et al., 2009; Zhang and Guo, 2013; Balistrocchi et al., 2013; Zhang and Guo, 2014; Ursino, 2015), they may cause an underestimation or overestimation of the performance statistics for some unusual or extreme cases. Besides, in the previously developed analytical probabilistic models of detention ponds, the pond's outflow is often assumed to be constant (Li and Adams, 2000; Chen and Adams, 2005) or the discharge-storage relationship of the pond is approximated by linear functions (Guo and Adams, 1999; Balistrocchi et al., 2013, 2017). Actually, a power function is a more realistic representation of the discharge-storage relationship when orifice is used as the outflow control device.

To overcome the shortcomings of the previously developed analytical probabilistic models, in this study, an alternative analytical stochastic approach is developed for evaluating the performance of orifice-type detention ponds for water quality control purposes. As an appealing alternative, the analytical stochastic approach describes rainfall characteristics of a location using the theories of stochastic processes. This approach was first proposed by Rodriguez-Iturbe et al. (1991) and has been widely applied in the study of soil moisture dynamics (Rodriguez-Iturbe et al., 1991; Rodriguez-Iturbe et al., 1999; Rodriguez-Iturbe and Porporato 2004; Proporato et al. 2004). Recent studies have extended the application of the stochastic approach to urban stormwater management with models developed for green roofs (Guo, 2016), rainwater harvesting systems (Pelak and Porporato, 2016; Guo and Guo, 2018), permeable pavements (Guo et al., 2018) and combined sewer overflow tanks (Wang and Guo, 2018). In the above-cited stochastic studies for urban stormwater management purposes, however, the rates of outflow from the storage components are all treated as constant. In this study, an analytical stochastic model is developed to evaluate the runoff capture efficiency of detention ponds with non-linear storage-discharge relationships. The analytical results are compared with continuous simulation results, and the developed stochastic model is tested and validated with rainfall data from Jackson, Mississippi, USA.

3.2 Methods

3.2.1 Stochastic Description of Point Rainfall Series

An observed historical rainfall series can be separated into individual rainfall events linked by inter-event dry times of different lengths. For many locations, the frequency distributions of the rainfall event depth v (i.e., the distribution of the frequency of occurrence of rainfall events with different depths), event duration u and inter-event time b, can all be fitted well by exponential probability density functions (PDFs). Exponential PDFs were therefore recommended for use in the design of stormwater management facilities at many locations in the U.S (USEPA, 1986; Wanielista and Yousef, 1993; Hassini and Guo, 2016). Exponential PDFs have also been adopted for describing rainfall event characteristics at many other locations around the world including Canada (Adams and Papa, 2000), South Korea (Lee and Kim, 2018), Malaysia (Shamsudin et al., 2014) and Italy (Ursino, 2015). The exponential PDFs of rainfall event characteristics can be described as

$$f_V(v) = \zeta\, \mathrm{e}^{-\zeta v} \qquad \text{for } v > 0 \tag{3.1}$$

$$f_U(u) = \lambda\, \mathrm{e}^{-\lambda u} \qquad \text{for } u > 0 \tag{3.2}$$

$$f_B(b) = \psi\, \mathrm{e}^{-\psi b} \qquad \text{for } b > 0 \tag{3.3}$$

where ζ, λ, and ψ are distribution parameters, which can be estimated as $\zeta = 1/\langle v \rangle$, $\lambda = 1/\langle u \rangle$, $\psi = 1/\langle b \rangle$ in which $\langle \cdot \rangle$ is the ensemble average operator. Suitable techniques for parameter estimation and procedures of goodness-of-fit tests can be found in Hassini and Guo (2016). The validity of the assumed exponential distributions of rainfall event characteristics will be examined by comparing the analytical results obtained based on the assumed distributions with those from long-term continuous simulations where no such assumptions are required.

In using the stochastic approach for describing the rainfall series of a location, the sequential occurrence of rainfall events of different depths is represented as a marked

Poisson process (Restrepo-Posada and Eagleson, 1982; Wang and Guo, 2018). The individual rainfall event is treated as occurring instantaneously rather than with a duration u (Rodriguez-Iturbe and Porporato, 2004). Therefore, the constitution of the point rainfall series is simplified as instantaneous rainfall event jumps occurring with inter-arrival times m which equals the sum of the corresponding u and b. The arrival rate of the rainfall events in this marked Poisson process is denoted as μ and is equal to $1/\langle m\rangle$, where $\langle m\rangle = \langle u\rangle + \langle b\rangle$ (Eagleson, 1978; Guo, 2016). The PDF of the inter-arrival time m is

$$f_M\left(m\right) = \mu \mathrm{e}^{-\mu m} \quad \text{for } m > 0 \tag{3.4}$$

As pointed out by Yue et al. (1999) as well as Yue and Hashino (1999, 2001), the point rainfall process may not always be Poissonian, it might instead be represented by the binomial or negative binomial distributions. In this study, only the Poisson distribution type is investigated as it is found to be applicable for many locations.

3.2.2 Dynamic Water Balance of Detention Ponds

For a detention pond, the water balance equation at an instant of time can be simply written in terms of the inflow rate, the outflow rate and the change of storage volume at that instant of time. Inflow is a result of runoff from the contributing catchment. Outflow is just the discharge from the hydraulic outlet structures such as orifices and weirs.

Overflow or by-pass flow may also occur when the pond is full. Evaporation and other water losses from the pond are usually negligible. The dynamic water balance of a detention pond can thus be expressed as

$$\frac{\mathrm{d}S_s(t)}{\mathrm{d}t} = R\left[S_s(t), t\right] - Q\left[S_s(t)\right] \tag{3.5}$$

where $S_s(t)$ is the amount of water stored in the pond at time t, expressed as depth (mm) of water over the catchment area; $R[S_s(t), t]$ is the inflow rate collected by the detention pond from the contributing catchment at time t, which is a function of the amount of water stored in the pond at time t and time t; $Q[S_s(t)]$ is the outflow rate of the detention pond at time t as a function of the amount of water stored in the pond at time t. $R[S_s(t),t]$ and $Q[S_s(t)]$ are both expressed in units of mm of water over the catchment per unit time. The inflow rate is a function of the amount of water stored in the pond (i.e., pond fullness) because inflow here equals incoming runoff minus overflow (or by-pass flow) from the pond whereas the amount of overflow (or by-pass flow) depends on both the pond fullness and the incoming runoff volume. For brevity of notation, the indication of time dependence is made implicit hereafter, i.e., $S_s(t)$, $R[S_s(t), t]$ and $Q[S_s(t)]$ are simply represented as S_s, $R(S_s, t)$ and $Q(S_s)$, respectively.

3.2.2.1 Inflow Rate

After satisfying the initial hydrologic losses including interception and depression storage, a large fraction of the remaining volume of a rainfall event occurring over the contributing catchment area may be transformed to runoff and discharged into the downstream detention pond. The rainfall-runoff transformation model (U.S. Army Corps of Engineers, 1977; Li and Adams, 2000; Behera et al., 2006; Wang and Guo, 2018) can therefore be expressed as

$$v_r = \begin{cases} 0, & v \le S_d \\ \phi\left(v - S_d\right), & v > S_d \end{cases} \tag{3.6}$$

where v_r is the runoff (measured in depth of water over the contributing catchment area) flowing towards the detention pond, mm; ϕ is the dimensionless composite runoff coefficient which is largely a function of the catchment land use conditions; S_d is the lumped initial losses including interception and depression storage losses, mm.

The derived PDF of the runoff event depth v_r (Wang and Guo, 2018) is

$$f_{V_R}\left(v_r\right) = \left(\zeta/\phi\right)\mathrm{e}^{-(\zeta/\phi)v_r} \quad \text{for } v_r > 0 \tag{3.7}$$

The series of runoff event occurrences follows a new censored Poisson process with an arrival rate of μ', where $\mu' = \mu\int_{S_d}^{\infty} f_V\left(v\right)\mathrm{d}v = \mu\,\mathrm{e}^{-S_d\zeta}$. For brevity, dimensionless normalization is applied for some variables of interest. The normalized runoff event depth that may flow into the pond is r which is equal to v_r/S_m, where S_m is the effective storage capacity of the detention pond expressed as depth of water over the catchment area. The PDF of the dimensionless individual runoff event depth r can be expressed as

$$f_R\left(r\right)=\gamma\,\mathrm{e}^{-\gamma r}\quad \text{for } r>0 \tag{3.8}$$

where $\gamma=\left(\zeta S_m\right)/\phi$. The average inter-arrival time of the normalized runoff events is $\langle m\rangle$ which is equal to the reciprocal of the arrival rate of the runoff events, i.e., $\langle m_r\rangle=\langle m\rangle\,\mathrm{e}^{S_d\zeta}$.

Given an initial pond fullness level (pond fullness is defined as the fraction of the maximum storage space of the pond occupied by water) s calculated as S_s/S_m at the beginning of a runoff event, the normalized inflow-event depth y that is actually collected and treated by the pond is not greater than the available normalized storage depth (1-s) because overflow or by-pass flow will occur if the normalized inflow-event depth exceeds (1-s). If overflow/by-pass occurs, y is equal to (1-s). The PDF of y conditioned on the pond having an initial relative storage or fullness level s, which is denoted as $P\left[y\middle|s\right]$, can therefore be expressed as

$$P_{Y|S}\left[y\middle|s\right]=\gamma\,\mathrm{e}^{-\gamma y}+\mathrm{e}^{-\gamma(1-s)}\,\delta\left(y+s-1\right)\quad \text{for } 0\le y\le 1-s \tag{3.9}$$

where y is the normalized inflow-event volume treated by the pond, which is the treated volume divided by S_m; and $\delta(\cdot)$ is the Dirac delta function. The probability mass of $\mathrm{e}^{-\gamma(1-s)}$ at $y = 1 - s$ [as expressed in equation (3.9) using the Dirac delta function] represents the probability that an inflow event will fill up the pond to its maximum capacity given that the initial pond fullness level is s at the beginning of the storm.

Represented as a marked Poisson process, the time series of inflows into the detention pond can be denoted as y_i with the sequential number of inflow events $i = 1, 2, 3, \cdots, N(t)$, where $N(t)$ is the number of inflow events from the start to the current time t (Guo, 2016). The sequence of the normalized inflow series up to time t can be expressed as

$$\varphi_t(\mu';\gamma) = \frac{R(S_s, t)}{S_m} = \sum_{i=1}^{N(t)} y_i \delta(t - t_i) \tag{3.10}$$

where $\varphi_t(\mu',\gamma)$ is the normalized inflow series which is expressed in terms of the arrival rate of the Poisson process μ' and the inverse of the mean inflow event depth γ; t_i's are the occurrence times of the sequential inflow events from time zero to time t.

3.2.2.2 Outflow Rate

The outflow rate $Q(S_s)$ of a detention pond is mainly controlled by the hydraulic devices such as orifices and weirs. In this paper, the orifice-type detention pond which is most widely used in practice for stormwater quality control is selected as the representative type. For this type of detention ponds or for cases where outflows are controlled by pumps,

$Q(S_s)$ was treated as constants for simplicity (Loganathan et al., 1994; Chen and Adams, 2005; Balistrocchi et al., 2009). A more accurate way to represent the outflow rate is to approximate it as a linear function of the storage volume (Guo and Adams, 1999; Balistrocchi et al., 2013, 2017). In this study, to be more accurate, $Q(S_s)$ is treated as functionally related to the volume of water stored in the pond S_s at time t. The dependence of the outflow rate on storage volume is expressed as $Q(D)$ where D is the depth of water in the pond at time t. $Q(D)$ in units of m^3/s can be calculated as

$$Q(D) = C_o A_o (2gD)^{0.5} \tag{3.11}$$

where C_o is the orifice discharge coefficient, dimensionless, which is usually equal to 0.67; A_o is the cross-sectional area of the orifice, m^2; for a circular orifice $A_o = \pi d^2/4$, where d is the orifice diameter, m; g is the gravitational acceleration constant (9.81 m/s^2) and D is measured in meters. The orifice is located at the bottom of the active storage portion of the pond.

In this study, the horizontal area of the pond is assumed to remain constant within the active storage portion for simplicity, this assumption was adopted in many previous studies as well (Guo and Adams, 1999; Akan, 2010; Behera and Teegavarapu, 2015). D can also be expressed as depth of water over the catchment area, i.e., $D = (A_c S_s)/A_p$, where A_c is the contributing catchment area and A_p is the bottom area of the pond. The outflow rate $Q(D)$

can thus be equivalently represented as $Q(S_s)$. Measuring $Q(S_s)$ as mm of water over the catchment area per unit time, it can be calculated as

$$Q\left(S_s\right) = kS_s^{\,0.5} \tag{3.12}$$

where $k = C_0 A_o \left[2g/\left(A_c A_p\right)\right]^{0.5}$, k is a parameter with a dimension of $mm^{0.5}$/time which is dependent on C_o, A_o, A_c and A_p.

Dividing equation (3.12) by S_m and replacing S_s/S_m with s, the normalized outflow rate of the detention pond $q(s)$ with a dimension of $time^{-1}$ can therefore be expressed as

$$q\left(s\right) = \frac{Q\left(S_s\right)}{S_m} = \eta s^{0.5} \tag{3.13}$$

where $\eta = C_o A_o \left[2g/\left(A_c A_p S_m\right)\right]^{0.5}$, and η is a parameter with a dimension of $time^{-1}$. If the horizontal area of the pond does not remain constant within the active storage portion of the pond but changes as the depth of water D changes, then usually given the relatively uniform slope of the bottom of the pond, a power function relationship similar to equation (3.13) may be obtained to describe the relationship between q and s, except that s will be raised to a power different from 0.5.

3.2.2.3 Normalized Water Balance Equation

Normalizing all the terms in equation (3.5) by dividing them by S_m and substituting the corresponding terms as expressed in equations (3.10) and (3.13) respectively, the normalized stochastic water balance equation of an orifice-type detention pond can be expressed as

$$\frac{\mathrm{d}s}{\mathrm{d}t} = \varphi_t\left(\mu';\gamma\right) - \eta s^{0.5} \tag{3.14}$$

3.2.2.4 Effective Storage Capacity

Outflows actually occur during both rainy and dry periods, the assumption of instantaneous rainfall event used in the stochastic approach would result in overestimation of overflows because outflow during a rainfall event creates some additional storage volume and this additional storage volume would accommodate more inflow which may otherwise overflow from or by-pass the pond. In order to alleviate this problem of overestimation, it is necessary to define and quantify the effective storage capacity of a pond and this has proven to be an effective technique for improving the accuracy of previously developed analytical stochastic models (Guo and Guo 2018; Wang and Guo 2018). The effective storage capacity of a detention pond (the actual storage capacity of the pond is previously denoted as S_m, but hereinafter, S_m is used to represent the effective storage capacity) can be defined as the summation of the actual storage size of the pond S_c (i.e., the maximum depth of the active storage portion of the pond expressed as mm of water over the catchment area, determined as $S_c = \left(A_p D_m\right)/A_c$ where D_m is the maximum depth of the pond measured in meters) and the additional storage capacity that is created by outflow $Q(S_s)$ during an average representative rainfall event.

The additional storage capacity can be estimated as the average outflow rate from the detention pond multiplied by the duration of an average rainfall event (i.e., $\langle u \rangle$, the ensemble average duration of rainfall events). The effective storage capacity is therefore expressed as

$$S_m = S_c + \langle Q(S_s) \rangle \langle u \rangle \tag{3.15}$$

The outflow rate $Q(S_s)$ varies with water depth in the pond. Therefore, the mean outflow rate $\langle Q(S_s) \rangle$ rather than the maximum outflow rate $Q(S_c)$ should be used in the estimation of the additional storage capacity. To obtain a simple estimate of the average outflow rate $\langle Q(S_s) \rangle$, the outflow during the average representative rainfall event is assumed to start when the pond is full. This is a reasonable assumption because portions of the runoff event volume will indeed fill up the pond and in the stochastic water balance equation, the filling of the pond as a result of a runoff event is treated as occurring instantaneously. In addition, detention ponds are usually sized to be large enough to contain runoff from an average representative rainfall event. As a result of this assumption, the initial discharge rate from the pond at the start of the average representative rainfall event is $Q_0 = Q(S_c) = kS_c^{0.5}$. After the instantaneous filling of the pond by the runoff event, the differential water balance equation governing the change of the pond storage can be expressed as

$$\mathrm{d}S_s = -Q(S_s)\mathrm{d}t \tag{3.16}$$

Substituting $S_s = Q(S_s)/k^2$ as expressed in equation (3.12) into equation (3.16) and carrying out the integration from t = 0 which is the start of the average representative rainfall event to $t = \langle u \rangle$ which is the end of the average representative rainfall event, the outflow rate at the end of the event $Q(\langle u \rangle)$ is

$$Q(\langle u \rangle) = \begin{cases} 0, & S_c \le k^2/(4\lambda^2) \\ kS_c^{0.5} - k^2\langle u \rangle/2, & S_c > k^2/(4\lambda^2) \end{cases} \tag{3.17}$$

Equation (3.17) shows that the outflow rate linearly decreases with the duration of the event. Therefore, the mean outflow rate during this event can be calculated as the average of Q_0 and $Q(\langle u \rangle)$ with $\langle u \rangle = 1/\lambda$, i.e.,

$$\langle Q(S_s) \rangle = \frac{Q_0 + Q(1/\lambda)}{2} = \begin{cases} kS_c^{0.5}/2, & S_c \le k^2/(4\lambda^2) \\ kS_c^{0.5} - k^2/(4\lambda), & S_c > k^2/(4\lambda^2) \end{cases} \tag{3.18}$$

Combining equations (3.15) and (3.18), the explicit expression of the effective storage capacity S_m is

$$S_m = \begin{cases} S_c + kS_c^{0.5}/(2\lambda), & S_c \le k^2/(4\lambda^2) \\ S_c + kS_c^{0.5}/\lambda - k^2/(4\lambda^2), & S_c > k^2/(4\lambda^2) \end{cases} \tag{3.19}$$

Equation (3.19) can be applied to detention pond systems with orifice outflow structures. This piecewise function describes how S_m is affected by related parameters including the storage size S_c, the distribution parameter of rainfall event duration λ, and the parameter k about the orifice outflow rate.

3.2.3 Solution of the Stochastic Water Balance Equation

The normalized water balance equation of detention ponds as shown in equation (3.14) is a stochastic differential equation driven by the inflow process $\varphi_t(\mu',\gamma)$ which is a marked Poisson process. Starting from a specific initial condition, the PDF of s denoted as $f(s,t)$ changes with time before the system reaches a steady state. The evolution of $f(s,t)$ in time can be described by the Chapman-Kolmogorov forward equation (Cox and Miller, 1965; Rodriguez-Iturbe and Porporato, 2004). It was shown that the probability distribution of s at time t may consist of a discrete atom of probability $f_0(t)$ for $s = 0$ and a continuous PDF, $f(s,t)$, for $s > 0$. Adapting from the solutions in previous studies involving similar stochastic water balance equations (Rodrigues-Iturbe et al., 1999; Rodriguez-Iturbe and Porporato, 2004), the temporal evolution of $f(s,t)$ and $f_0(t)$ can be shown to be

$$\frac{\partial f(s,t)}{\partial t} = \frac{\partial}{\partial s}\left[f(s,t)q(s) \right] - \mu' f(s,t) + \mu' \int_0^s f(z,t) P_{Y|S}\left[(s-z) \middle| z \right] \mathrm{d}z + \mu' f_0(t) P_{Y|S}\left[s \middle| 0 \right] \quad (3.20)$$

$$\frac{\mathrm{d} f_0(t)}{\mathrm{d}t} = -\mu' f_0(t) + q\left(0^+\right) f\left(0^+, t\right) \quad (3.21)$$

where $P_{Y|S}\left[(s-z) \middle| z \right]$ and $P_{Y|S}\left[s \middle| 0 \right]$ are both the conditional PDFs of inflows to a pond as expressed in equation (3.9); z is the dummy variable of integration; 0^+ is a value infinitesimally greater than zero; and $f\left(0^+, t\right) = \lim_{s \to 0^+} f(s,t)$.

As demonstrated in Appendix 3A, although $q(s)$ shown in equation (3.13) approaches zero in a continuous manner, the probability distribution of s still includes an atom of probability at $s = 0$. Since the stochastic process $\varphi_t(\mu',\gamma)$ which drives the pond's water balance is a stationary stochastic process, the system will eventually reach a steady state where the PDF of s will remain the same and does not change with time. Although theoretically it would take an infinitely long time to reach this steady state, in the planning and design of detention ponds, we are only interested in this steady state. This is because an approximate steady-state condition of the probability distribution of water storage in the pond would usually be reached after several months of operation. We denote the atom of probability for $s = 0$ and the continuous PDF for $s > 0$ at the steady state as f_0 and $f(s)$, respectively. f_0 and $f(s)$ are governed by the two equations which are otherwise the same as equations (3.20) and (3.21) but with their left-hand-sides both replaced with zero. By replacing $P_{Y|S}\left[\cdot|\cdot\right]$ with the expressions shown in equation (3.9), the two equations governing $f(s)$ and f_0 can then be shown to be

$$\begin{aligned}\frac{\mathrm{d}}{\mathrm{d}s}\left[f(s)q(s)\right]-\mu' f(s)+\mu'\int_0^s f(z)\left[\gamma\,\mathrm{e}^{-\gamma(s-z)}+\delta(s-1)\mathrm{e}^{-\gamma(1-z)}\right]\mathrm{d}z\\+\mu' f_0\left[\gamma\,\mathrm{e}^{-\gamma s}+\delta(s-1)\mathrm{e}^{-\gamma}\right]=0\end{aligned}\quad \text{for } 0<s\le 1 \tag{3.22}$$

$$-\mu' f_0+q\left(0^+\right)f\left(0^+\right)=0 \quad \text{for } s=0 \tag{3.23}$$

As detailed in Appendix 3B, the general solution of equation (3.22) while considering what is required by equation (3.23) was derived to be

$$f(s)=\frac{C_1 s^{-0.5}}{\eta}\exp\left(-\gamma s+\frac{2\mu'}{\eta}s^{0.5}\right) \quad \text{for } 0<s\le 1 \tag{3.24}$$

where C_1 is a normalization constant ensuring that the total probability mass for all possible values of s is equal to one. Note that $q(s)$ as shown in equation (3.22) was replaced with the expression shown in equation (3.13). Let $s = 0^+$ and carrying out the integration with z from 0 to 0^+, equation (C14) yields $f\left(0^+\right)=C_1/q\left(0^+\right)$. Substituting this expression of $f(0^+)$ into equation (3.23), we obtain $f_0 = C_1/\mu'$. Therefore, the overall steady-state probability distribution of s, denoted as $h(s)$, which comprises a discrete probability mass f_0 for $s=0$ and a continuous part $f(s)$ for $0<s\le 1$ is

$$h(s)=\begin{cases}\dfrac{C_1}{\eta}s^{-0.5}\exp\left(-\gamma s+\dfrac{2\mu'}{\eta}s^{0.5}\right), & 0<s\le 1\\ \dfrac{C_1}{\mu'}\delta(0), & s=0\end{cases} \tag{3.25}$$

where the normalization constant C_1 would ensure that

$$\int_0^\infty h(s)\,\mathrm{d}s=1 \quad \text{for } 0\le s\le 1 \tag{3.26}$$

The solution of equation (3.26) leads to

$$C_1=\frac{\mu'}{1+C_2C_3/C_4} \tag{3.27}$$

where $C_2=\mu'/(\eta\gamma)$; $C_3=\sqrt{\pi\gamma}\left\{\mathrm{erf}\left[\sqrt{\gamma}(1-C_2)\right]+\mathrm{erf}\left(\sqrt{\gamma}C_2\right)\right\}$; $C_4=\exp\left(-\gamma C_2^{\,2}\right)$ and $\mathrm{erf}(\cdot)$ represents the Gauss error function which is defined as $\mathrm{erf}(x)=\dfrac{2}{\sqrt{\pi}}\int_0^x e^{-z^2}\,\mathrm{d}z$.

The expression of f_0 can thus be determined as $f_0=\dfrac{C_1}{\mu'}=\dfrac{1}{1+C_2C_3/C_4}$. Substituting C_1 as expressed in equation (3.27) into equation (3.25), the explicit expression of $h(s)$ is

$$h(s)=\begin{cases}\dfrac{\mu' s^{-0.5}}{(1+C_2C_3/C_4)\eta}\exp\left(-\gamma s+\dfrac{2\mu'}{\eta}s^{0.5}\right), & 0<s\le 1\\ \dfrac{1}{(1+C_2C_3/C_4)}\delta(0), & s=0\end{cases} \tag{3.28}$$

The cumulative probability distribution (CDF) of s, $H(s)$, can be derived as

$$H(s)=\int_0^s h(s)\,\mathrm{d}s=\left(C_1/\mu'\right)\left\{1+\left(C_2/C_4\right)\sqrt{\pi\gamma}\left[\operatorname{erf}\left(\sqrt{\gamma}s^{0.5}-\sqrt{\gamma}C_2\right)+\operatorname{erf}\left(\sqrt{\gamma}C_2\right)\right]\right\} \quad \text{for } 0\le s\le 1 \tag{3.29}$$

3.2.4 Estimation of Average Runoff Capture Efficiency

The ensemble average of s denoted as $\langle s\rangle$ can be derived as

$$\langle s\rangle=\int_0^1 sh(s)\,\mathrm{d}s=\frac{C_1C_2}{\mu' C_4}\left[C_2\left(C_4-C_5\right)-C_5+C_3\left(C_2^{\ 2}+\frac{1}{2\gamma}\right)\right] \tag{3.30}$$

where $C_5=\exp\left[-\gamma\left(1-C_2\right)^2\right]$. $\langle s\rangle$ can be interpreted as the long-term average value of s. The long-term average amount of water stored in the pond $\langle S_s\rangle$ expressed in mm of water over its contributing catchment can thus be determined as $\langle S_s\rangle=\langle s\rangle S_c$.

Define $\langle r\rangle$ as the normalized mean runoff rate from the contributing catchment; $\langle q\rangle$ as the normalized mean outflow rate from the pond; and $\langle\omega\rangle$ as the normalized mean overflow rate. The long-term average water balance equation for the detention pond can be expressed as

$$\langle r\rangle-\langle q\rangle=\langle\omega\rangle \tag{3.31}$$

where $\langle r\rangle$ can be calculated as the normalized runoff event depth averaged over the inter-arrival time, i.e.,

$$\langle r \rangle = \int_0^\infty r f_R(r)\,\mathrm{d}r \Big/ \langle m_r \rangle = \mu' \int_0^\infty r\left(\gamma\,\mathrm{e}^{-\gamma r}\right)\mathrm{d}r = \mu'/\gamma \tag{3.32}$$

The normalized mean outflow rate $\langle q \rangle$ can be calculated as the integration of the product of $q(s)$ and $h(s)$ over all the possible ranges of s values, i.e.,

$$\langle q \rangle = \int_0^1 q(s)h(s)\,\mathrm{d}s = \frac{\mu' C_4 - C_1 C_5}{\gamma C_4} \tag{3.33}$$

The normalized mean overflow rate $\langle \omega \rangle$ is determined as the difference between $\langle r \rangle$ and $\langle q \rangle$, i.e.,

$$\langle \omega \rangle = \langle r \rangle - \langle q \rangle = \frac{C_1 C_5}{\gamma C_4} \tag{3.34}$$

The hydrologic performance, i.e., the runoff capture efficiency (E_r), provided by a detention pond is defined as the fraction of runoff generated from the catchment that is captured and treated by the pond over its lifetime of operation. E_r can thus be calculated as the normalized mean long-term average outflow rate divided by the normalized mean long-term runoff rate, i.e.,

$$E_r = \frac{\langle q \rangle}{\langle r \rangle} = 1 - \frac{C_1 C_5}{\mu' C_4} \tag{3.35}$$

Since C_1, C_3, C_4 and C_5 can all be expressed as functions of C_2, by replacing them with the corresponding functions of C_2 in equations (3.30) and (3.35), the following alternative expressions for $\langle s\rangle$ and E_r can be obtained:

$$\langle s\rangle = C_2^{\,2} + \frac{C_2\sqrt{\pi\gamma}}{\exp\left(-\gamma C_2^{\,2}\right)+C_2\sqrt{\pi\gamma}\left\{\operatorname{erf}\left[\sqrt{\gamma}\left(1-C_2\right)\right]+\operatorname{erf}\left(\sqrt{\gamma}C_2\right)\right\}} \left\{\frac{\operatorname{erf}\left[\sqrt{\gamma}\left(1-C_2\right)\right]+\operatorname{erf}\left(\sqrt{\gamma}C_2\right)}{2\gamma+C_2}+\frac{\left(1+C_2\right)\exp\left[-\gamma\left(1-C_2\right)^2\right]}{\sqrt{\pi\gamma}}\right\} \tag{3.36}$$

$$E_r = 1-\frac{\exp\left[-\gamma\left(1-C_2\right)^2\right]}{\exp\left(-\gamma C_2^{\,2}\right)+C_2\sqrt{\pi\gamma}\left\{\operatorname{erf}\left[\sqrt{\gamma}\left(1-C_2\right)\right]+\operatorname{erf}\left(\sqrt{\gamma}C_2\right)\right\}} \tag{3.37}$$

where $C_2 = 4\mu\phi A_c \exp\left(-S_d\zeta\right)\Big/\left(\zeta C_o \pi d^2\sqrt{2gD_m}\right)$; $\gamma = \zeta S_m/\phi$; and $R_a = A_c/A_p$, denoting the ratio between the catchment area and the pond bottom area. Equations (3.36) and (3.37) relate E_r and $\langle s\rangle$ directly to the primary parameters including climatic factors (ζ, μ, λ), pond dimensions (d, D_m, R_a), and catchment characteristics (A_c, ϕ, S_d).

Equations (3.28)-(3.30) and (3.33)-(3.37) are collectively referred to as the analytical stochastic model (ASM) of orifice-type detention ponds. Using this collection of closed-form analytical equations, the probability distribution of s which can be used to determine the fractions of time that water in the pond is at different levels, the long-term average amount of water stored in the pond, the runoff capture efficiency, the required orifice diameter, and the maximum water level that would be reached during the operation of the pond can all be determined in an analytical way without numerical simulations.

3.3. Model Validation

3.3.1 Study Area and Data

A hypothetical test catchment located in Jackson, Mississippi, USA with an area of 16.8 ha was created for the purpose of validating the accuracy of the ASM. Hypothetical detention ponds serving this test catchment are all assumed to be designed only for water quality control purposes. Overflows or bypass flows would occur when the incoming runoff volume exceeds the available storage capacity of the pond. These overflows or bypass flows would be routed through separate hydraulic structures (e.g., overflow weirs or spillways) rather than the water quality control orifice. Detailed routing of the overflows or bypass flows is not considered in this study but needs to be considered if the pond is also used for flood control purposes.

The U.S. EPA SWMM model was used to provide continuous simulation results as a surrogate of observed data due to the lack of actual long-term continuous measurements. The main physical characteristics of the test catchment used as SWMM input parameters are displayed in Table 3.1. The evaporation rate at Jackson, Mississippi is obtained from NOAA (1982). The level of imperviousness of the test catchment is assumed to be 80%. Details of the other SWMM input parameters of the catchment can be found in Chen and Adams (2005) and Wang and Guo (2018). Techniques used to estimate ϕ and S_d for the catchment can be found in Wang and Guo (2018). Historical hourly rainfall records from Jackson-Medgar Wiley Evers International Airport (COOP: 224472, 32.317°N, 90.083°W) in Jackson is used for analysis of rainfall event characteristics. The 50-year rainfall record obtained from the National Climatic Data Center (NCDC) of the United States covers the years of 1964-2013, and the data for each year is from January through December. A minimum inter-event time (MIET) is used to separate the continuous rainfall record into individual events and inter-event times. A rainfall event volume threshold is selected so that extremely small rainfall events with volumes less than or equal to the selected threshold are censored out from the original data. It was found that an MIET of 12 hours and a rainfall event volume threshold of 1 mm are appropriate for the statistical analysis of rainfall event characteristics at Jackson. The statistical test results of rainfall event characteristics are presented in Table 3.2.

To satisfy the assumptions of the Poissonian process of rainfall inter-arrival times and the exponential distributions of rainfall event characteristics, statistical tests such as Poisson test and Kolmogorov-Smirnov test can be conducted, detailed testing procedures can be found in Guo and Baetz (2007), Hassini and Guo (2016) and Wang and Guo (2018). The histograms and fitted exponential PDF curves of the rainfall event characteristics including v, u, b and m are displayed in Fig. 3.1. It can be observed that the exponential PDFs fit well with the histograms. The means of rainfall event characteristics for Jackson are $\langle v \rangle = 19.20$ mm, $\langle u \rangle = 10.11$ h, $\langle b \rangle = 111.58$ h, $\langle m \rangle = 121.69$ h, and $\langle \theta \rangle = 71.7$. These rainfall event characteristics are required in the application of the ASM.

Table 3.1 Summary of input parameters of the test catchment used in SWMM simulations

Input parameter	Value
Catchment area, ha	16.8
Catchment width, m	500
Slope	0.01
Level of imperviousness, %	80
Impervious area Manning's roughness coefficient, s/m$^{1/3}$	0.013
Pervious area Manning's roughness coefficient, s/m$^{1/3}$	0.21
Impervious area depression storage, mm	1.5
Pervious area depression storage, mm	4.5
Initial infiltration capacity, mm/hr	45
Ultimate infiltration capacity, mm/hr	2.4
Infiltration decay coefficient, hr^{-1}	4.14
Evaporation rate, mm/day	2.36

Table 3.2 Poisson and Kolmogorov-Smirnov goodness-of-fit tests of rainfall characteristics

Poisson tests					
Station	Years of record	Critical value ($\alpha_p = 0.10$)	MIET (hour)	r_p	Decision
Jackson	50	0.692-1.354	12	1.049	Accept
Kolmogorov-Smirnov goodness-of-fit tests					
Station	Rainfall characteristic	Mean value	Critical value ($\alpha_k = 0.10$)	Maximum difference	Decision
Jackson	v	$\langle v \rangle = 19.20$	0.163	0.071	Accept
Jackson	t	$\langle t \rangle = 10.11$	0.188	0.085	Accept
Jackson	b	$\langle b \rangle = 111.58$	0.156	0.027	Accept
Jackson	m	$\langle m \rangle = 121.69$	0.156	0.095	Accept

Note: α_p and α_k are the levels of significance of the Poisson and K-S tests, respectively; r_p is Poisson test statistic (i.e., the ratio between the mean and the variance of the annual number of rainfall events); the maximum difference refers to the maximum absolute difference between the empirical and theoretical cumulative probability distributions.

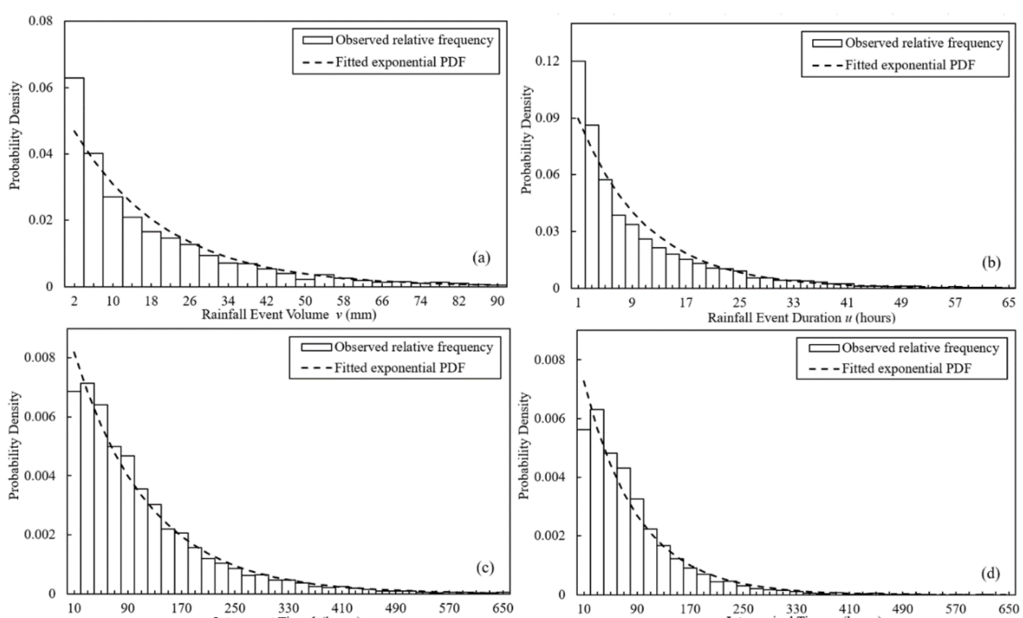

Fig. 3.1 Frequency distribution of rainfall event characteristics at Jackson, Mississippi, U.S.

The same historical hourly rainfall data are used as input of the U.S. EPA SWMM model (version 5.1) for the catchment (Rossman, 2015). The results obtained by a set of SWMM continuous simulations are used to examine the accuracy of the ASM. The total runoff volume (RV) and total overflow volume (OV) provided by SWMM simulation results are used to calculate the SWMM-determined long-term average runoff capture efficiency as

$$E_{rswmm} = \left(RV - OV\right)/RV \tag{3.38}$$

The other performance statistics such as the average pond fullness level $\langle s \rangle$ and the detailed s distributions are all directly calculated using the time step-by-time step output data from SWMM models.

3.3.2 Validation of E_r and $\langle s \rangle$

The accuracy of the proposed ASM can be verified by comparing the analytical results and SWMM continuous simulation results. Two main hydrologic performance indicators for pond systems, i.e. the runoff capture efficiency E_r and the average pond fullness level $\langle s \rangle$, are evaluated and their results from ASM and SWMM are compared. For the test catchment with an area of 16.8 ha located at Jackson and the pond with a maximum water depth of 1 m, a total of 78 cases incorporating 6 different values of storage sizes (i.e.,

S_c = 5, 10, 15, 20, 30 and 40 mm) and 13 different values of orifice diameters (i.e., d = 1, 2.5, 5, 7.5, … , 30 cm) are selected for the purpose of model validation. The combinations of selected S_c and d values are physically reasonable and representative for various pond systems. For these selected cases, equations (3.36) and (3.37) are used to determine $\langle s \rangle$ and E_r, respectively, using the ASM. The analytical results are then compared with the SWMM simulation results.

The comparison of ASM- and SWMM-determined E_r and $\langle s \rangle$ results for the 78 cases are shown in Figs. 3.2a and 3.2b, respectively. If the SWMM results are treated as the observed data, the mean values of E_r and $\langle s \rangle$ obtained from ASM are 0.663 and 0.185 compared to the observed mean values of 0.653 and 0.194, respectively. Between ASM results and the observed data (i.e., SWMM results), the root-mean-square error (RMSE) is 0.021, the Nash-Sutcliffe model efficiency coefficient (NSE) is 0.994 and the correlation coefficient is 0.9983 for runoff capture efficiency; while the RMSE of 0.012, NSE of 0.998 and correlation coefficient of 0.9997 are obtained for the average pond fullness level. This demonstrates good agreements between the ASM and SWMM results of E_r and $\langle s \rangle$ for all the 78 cases.

For further demonstration, the comparison results for the 78 cases are shown in Fig. 3.3. Detailed comparison between E_r and E_{rswmm} for 6 different pond storage sizes is shown in Figs. 3.3a and 3.3b while the comparison results of $\langle s \rangle$ are shown in Figs. 3.3c and 3.3d. As shown in Fig. 3.3, ASM-determined curves agree well with the dotted plots of SWMM results. For a specific pond size, E_r increases and $\langle s \rangle$ decreases with the increase of the orifice diameter d. For orifices with a fixed diameter, when S_c increases, both E_r and $\langle s \rangle$ increase because less overflows would occur when storage size increases.

It is noted in Figs. 3.3a and 3.3b that the runoff capture efficiency curves determined from ASM results are not very smooth at certain intervals of d (i.e., around d = 15 cm in Fig. 3.3a and d = 20 cm in Fig. 3.3b). This can be explained by the fact that E_r as determined by equation (3.37) depends on S_m, and S_m as expressed in equation (3.19) is a piecewise function of k while k is dependent on d, therefore S_m and E_r are both piecewise functions of d. The middle end points of d values in the piecewise function corresponding to the middle end points of k values as demonstrated in equation (3.19) create the relatively sharp turning points of the runoff capture efficiency curves in Figs. 3.3a and 3.3b. As shown in Figs. 3.3c and 3.3d, a sharp decrease of $\langle s \rangle$ results from the increase of the orifice diameter d at first and then $\langle s \rangle$ decreases much slowly when d is larger than about 10 cm.

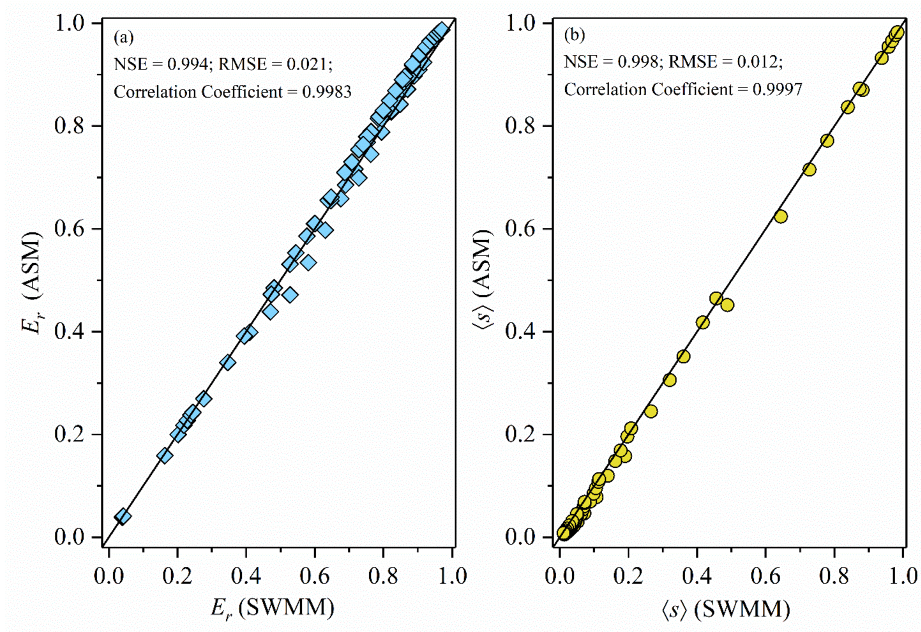

Fig. 3.2 Comparison of runoff capture efficiency and average pond fullness determined by ASM and SWMM

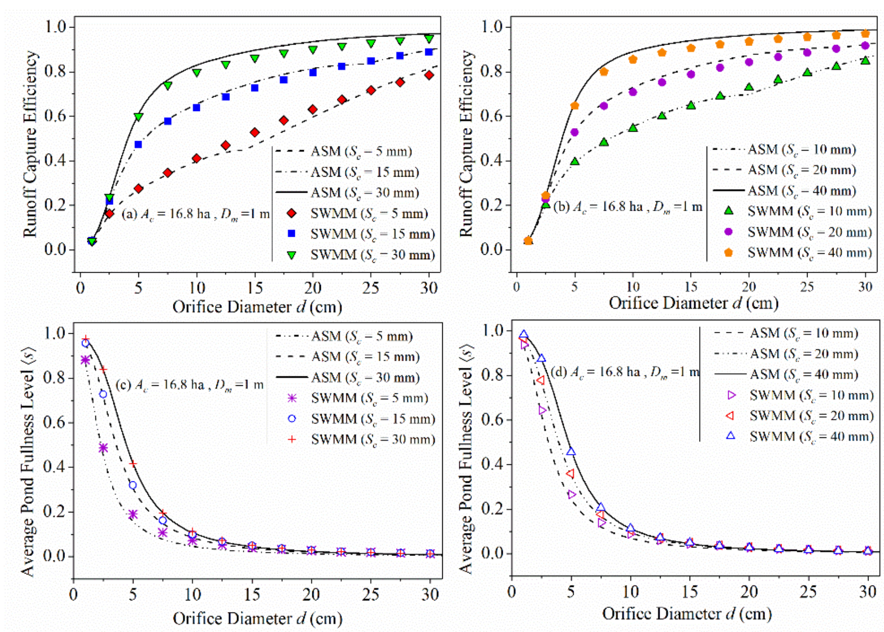

Fig. 3.3 Comparison of runoff capture efficiency and average pond fullness curves for six different ponds sizes

3.3.3 Validation for the PDF and CDF of *s*

The variation of pond fullness level as represented by the PDF and CDF of s is another useful performance characteristic for pond design and operation. The PDF and CDF of s can be analytically determined using equations (3.28) and (3.29), respectively. The long-term average pond fullness level $\langle s \rangle$ can be directly determined by equation (3.30). The comparison between the analytically determined PDF and CDF and those determined using SWMM results is shown in Fig. 3.4. For demonstration purposes, the case with a pond storage capacity of 40 mm is selected. The comparisons of PDFs for orifice diameters of 4 cm and 10 cm are shown in Figs. 3.4a and 3.4b, respectively. The relative frequency histogram for $0 < s \leq 1$ and the relative frequency of occurrence for $s = 0$ were obtained from the output of SWMM results. The analytical results including the atom of probability at $s = 0$ agree well with the SWMM results. The comparisons of CDF of s as presented in Figs. 3.4c and 3.4d also show good agreements.

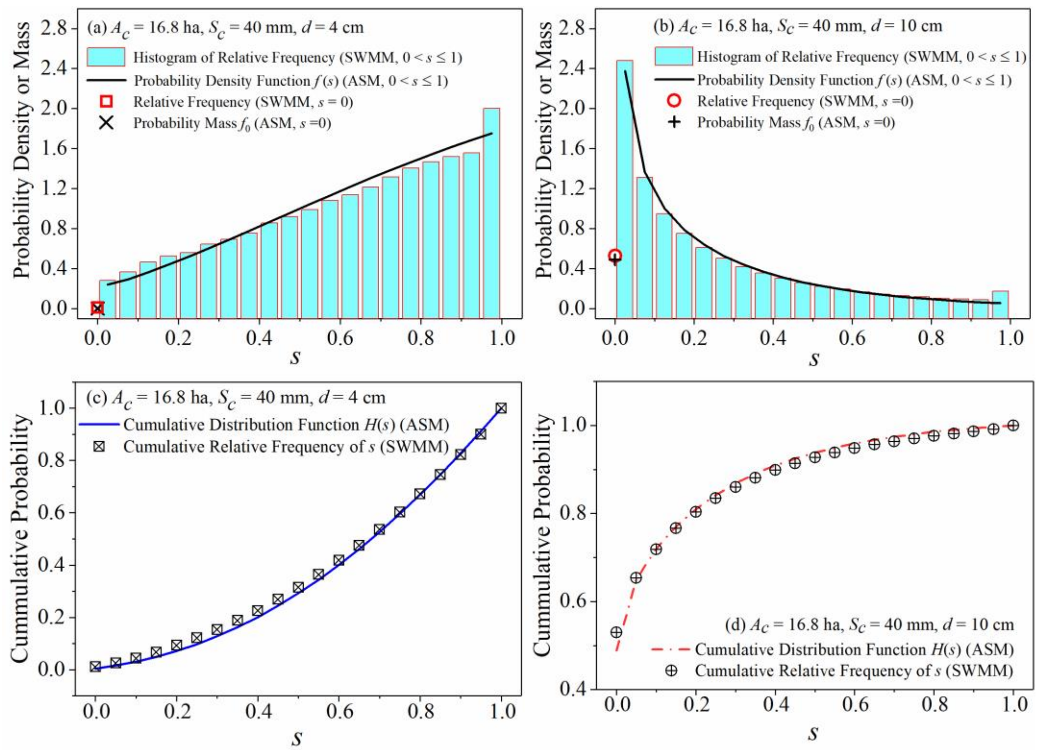

Fig. 3.4 Validation of the PDF and CDF of pond fullness level

3.3.4 Effects of D_m and R_a

For a specific catchment, the area ratio between the catchment and the pond bottom area (R_a) and the maximum water depth (D_m) of the pond are the critical design parameters in addition to the orifice diameter (d). The effects of the maximum water depth and area ratio on runoff capture efficiency and average pond fullness level are investigated to further verify the accuracy of ASM for cases including extremely large or small design parameter values. For a catchment with an area of 1 ha, four types of cases with two different D_m values (0.5 or 1.5 m) combined with two d values (2 or 5 cm) are examined. In each type of cases (i.e., each combination of D_m and d), a total of 101 continuous simulations for different area ratios (i.e., R_a = 1, 5, 10, ⋯ , 500) were conducted. The comparison results of E_r and $\langle s \rangle$ for all cases are shown in Figs. 3.5a, 3.5c, and 3.5d. For all cases with various values of D_m, d and R_a considered in Figs. 3.5a, 3.5c, and 3.5d, satisfactory agreement between ASM and SWMM results is observed.

For a specific orifice diameter, taking d = 5 cm as an example, the effects of D_m (0.5 or 2 m) and R_a (1, 5, 10, ⋯ , 500) on E_r and $\langle s \rangle$ are explored for two catchment areas (i.e., A_c = 5 or 20 ha) in Figs. 3.5b, 3.5e and 3.5f. The comparison between ASM and SWMM results still demonstrates close agreement for the total of 101 cases with different D_m, A_c and R_a values. Fig. 3.5 therefore further verifies the accuracy of the proposed ASM including the way of estimating the effective storage capacity for almost all possible design conditions. The effective storage capacity of a pond was estimated using equation (3.19) which was derived by considering an average representative rainfall event and the size of detention ponds. The verifications for the accuracy of ASM shown in Fig. 3.5 in addition to what was shown in Figs. 3.2-3.4 demonstrate that the ASM is accurate enough for almost all cases including those with extremely small and extremely large ponds or orifices.

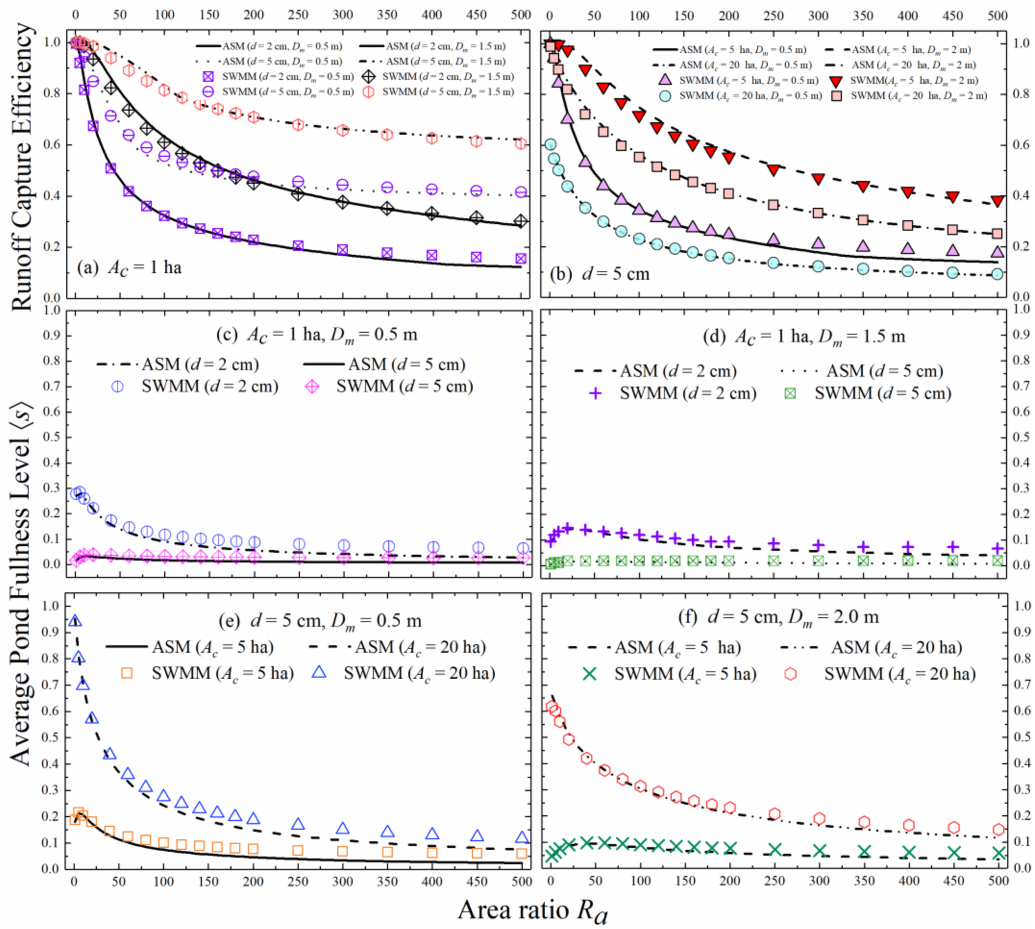

Fig. 3.5 Verification of ASM for cases of different catchment areas, orifice diameters, maximum water depth and area ratios

The relationship between pond size, orifice diameter, catchment area and the runoff capture efficiency is nonlinear and complex. Using equation (3.37), this relationship which cannot be directly obtained from continuous simulations can be obtained directly. Fig 3.6a presents an example for a test catchment with an area of 16.8 ha and a maximum water depth of 1 m. The corresponding contour plots can be found in Fig 3.6c. Another example is illustrated for a small catchment with an area of 1 ha and a maximum water depth of 0.5

m, shown in Fig. 3.6b associated with its contour results in Fig. 3.6d. The cause of break points in Fig. 3.6 is explained in section 3.3.2. The relationships between orifice diameter, runoff capture efficiency, storage size and area ratio are demonstrated well in Fig. 3.6. In addition to many other uses of the graphs as shown in Fig. 3.6, they can also be used as an efficient tool to quickly determine the required orifice diameter given a specific target of runoff capture efficiency.

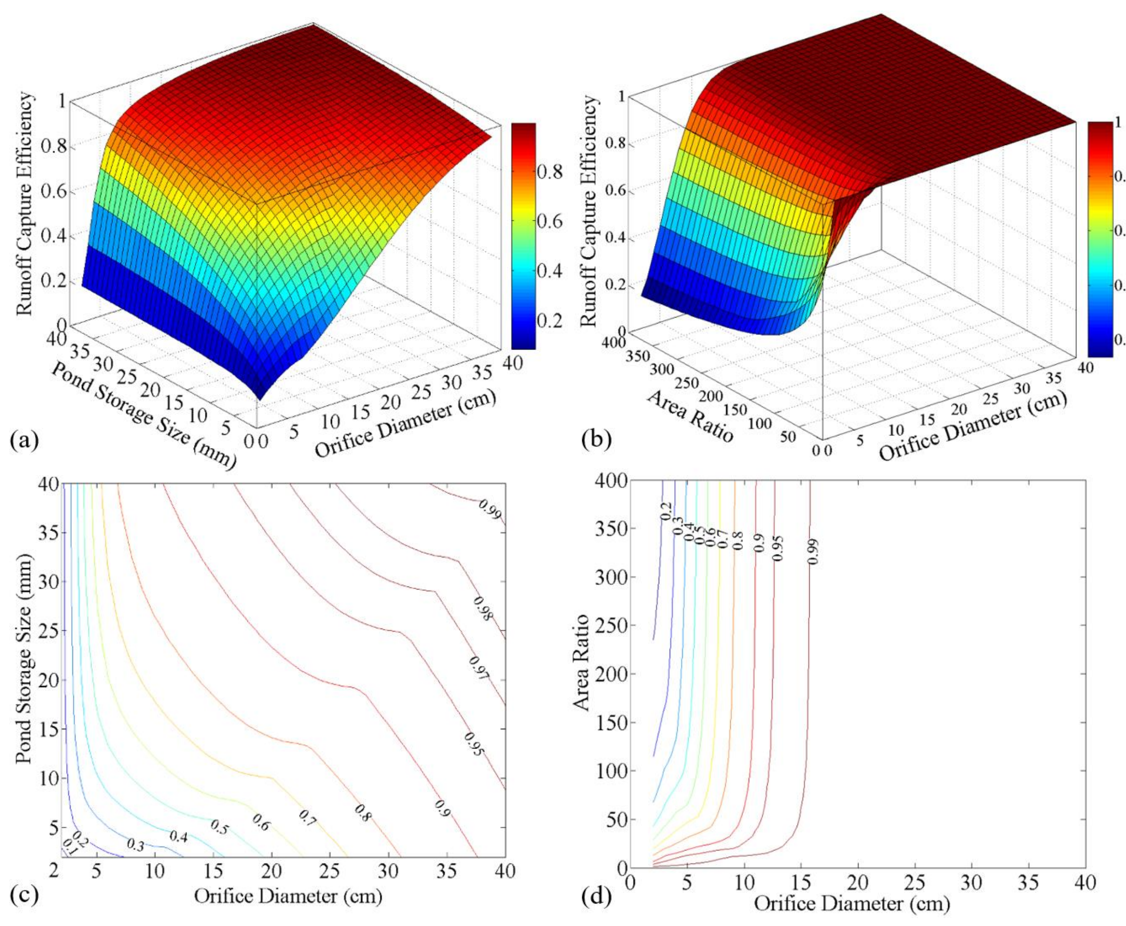

Fig. 3.6 Relationships between orifice diameter, runoff capture efficiency, area ratio and pond size

3.4 Concluding Remarks

In this paper, an analytical stochastic approach was developed to describe the hydrologic operation of stormwater quality control detention ponds with outflows controlled by orifices. In order to reduce the overestimation of overflow caused by the assumption of instantaneous rainfall inputs, the concept of effective storage capacity was proposed, an easy way of its estimation was developed considering the varying outflow rates of detention ponds. The accuracy of the resulting analytical stochastic model (ASM) was verified for many different hypothetical design cases. It was shown that the ASM for detention pond systems can provide accurate estimates of the relationships between runoff capture efficiency, pond fullness level, orifice diameter, pond size, catchment area and local climatic characteristics.

Implemented easily into a spreadsheet, the ASM provides an easy-to-use and computationally-efficient tool for analyzing the hydrologic performance of detention pond systems. The ASM can be used separately as a planning or design tool or together with continuous simulation models to help verify simulation results or reduce the number of simulation runs. Compared to the previously developed analytical probabilistic models, the ASM developed in this paper has the advantage of not requiring an independence assumption between rainfall event depth and duration. Further research may be extended to the verification of ASM for detention ponds located at more climatically different locations.

Acknowledgements: This work was supported by the Natural Sciences and Engineering Research Council of Canada and the China Scholarship Council. The data used in this study are listed in the tables or obtained from the citied references.

Appendix 3A: Demonstration of the existence of $f_0(t)$

During a dry period without inflow, the normalized differential water balance equation governing the rate of change of pond storage can be expressed as

$$\mathrm{d}s = -q(s)\,\mathrm{d}t \qquad (3A.1)$$

Substituting $q(s)$ as expressed in equation (3.13) into equation (3A.1) and carrying out the integration from time $t = 0$ to time $t = T$ with the corresponding s values from s_0 to s_T, we can obtain

$$s_T = \left(s_0^{\,0.5} - 0.5\eta T\right)^2 \qquad (3A.2)$$

where s_0 is the initial pond fullness level at $t = 0$; s_T is the pond fullness level at $t = T$.

It can be seen in equation (3A.2) that the case of $s_T = 0$ exists when $T = 2s_0^{\,0.5}/\eta$. This means that the storage of the pond would reach zero if the dry period is long enough although the outflow $q(s)$ approaches zero in a continuous manner. Since s may reach zero and may stay at zero for some dry periods that are long enough, the probability distribution of s consists of a discrete atom of probability $f_0(t)$ for $s = 0$ in addition to a continuous PDF, $f(s,t)$, for $0 < s \leq 1$. This is true for the steady-state solution of the probability distribution of s as well. Therefore, for our case of study it is worth noting that the steady-state solution of the probability distribution of s includes a discrete atom of probability at $s = 0$. The above demonstration is necessary because previous studies (Rodriguez-Iturbe and Porporato, 2004) concluded that the probability distribution of s would have no atom of probability at $s = 0$ if the outflow rate $q(s)$ approaches zero in a continuous manner. That conclusion was reached because it was believed that s would approach zero asymptotically if $q(s)$ is a continuous function and the process would only be at $s = 0$ if it starts at $s = 0$. We here actually demonstrated that this general conclusion is incorrect.

Appendix 3B: Derivation of $f(s)$ as shown in Equation (3.24)

The Dirac Delta function used in equation (3.22) is used for the special case of $s = 1$, equivalently, equation (3.22) can be written separately for cases with $0 < s < 1$ and $s = 1$ as

$$\frac{\mathrm{d}\left[f(s)q(s)\right]}{\mathrm{d}s}-\mu' f(s)+\mu'\int_0^s f(z)\gamma\,\mathrm{e}^{-\gamma(s-z)}\,\mathrm{d}z+\mu' f_0\gamma\,\mathrm{e}^{-\gamma s}=0 \quad \text{for} \quad 0<s<1 \tag{3B.1}$$

$$\begin{aligned} f(1)\left.\frac{\mathrm{d}\left[q(s)\right]}{\mathrm{d}s}\right|_{s=1} & -\delta(0)\,f(1)q(1)-\mu' f(1)+\mu'\int_0^1 f(z)\Big[\gamma\,\mathrm{e}^{-\gamma(1-z)} \\ & +\delta(0)\mathrm{e}^{-\gamma(1-z)}\Big]\mathrm{d}z+\mu' f_0\left[\gamma\,\mathrm{e}^{-\gamma}+\delta(0)\mathrm{e}^{-\gamma}\right]=0 \end{aligned} \quad \text{for} \quad s=1 \tag{3B.2}$$

where $f(1)$ is the probability density at $s = 1$.

Dividing by $\delta(0)$ and neglecting the infinitesimally small terms, equation (3B.2) turns to be

$$-f(1)q(1)+\mu'\int_0^1 f(z)\mathrm{e}^{-\gamma(1-z)}\,\mathrm{d}z+\mu' f_0\,\mathrm{e}^{-\gamma}=0 \quad \text{for} \quad s=1 \tag{3B.3}$$

Thus, equations (3.23), (3B.1) and (3B.3) are the general form of the steady-state Chapman-Kolmogorov forward equations for $0\le s\le 1$.

Multiplying both sides of equation (3B.1) by $\mathrm{e}^{\gamma s}$ yields

$$\mathrm{e}^{\gamma s}\frac{\mathrm{d}\left[f(s)q(s)\right]}{\mathrm{d}s}-\mathrm{e}^{\gamma s}\mu' f(s)+\mu'\int_0^s f(z)\gamma\,\mathrm{e}^{\gamma z}\,\mathrm{d}z+\mu' f_0\gamma=0 \quad \text{for} \quad 0<s<1 \tag{3B.4}$$

Differentiating both sides of equation (3B.4) with respect to s and dividing the resulting equation by $\mathrm{e}^{\gamma s}$, equation (3B.4) becomes

$$\gamma \frac{\mathrm{d}\left[f(s)q(s)\right]}{\mathrm{d}s}+\frac{\mathrm{d}^2\left[f(s)q(s)\right]}{\mathrm{d}s^2}-\mu'\frac{\mathrm{d}f(s)}{\mathrm{d}s}=0 \quad \text{for } 0<s<1 \tag{3B.5}$$

Carrying out an indefinite integration of the left-hand-side of equation (3B.5), a first-order linear differential equation was obtained to be

$$\frac{\mathrm{d}\left[f(s)q(s)\right]}{\mathrm{d}s}+\gamma f(s)q(s)-\mu' f(s)=\text{constant} \quad \text{for } 0<s<1 \tag{3B.6}$$

Combining equations (3B.1) and (3B.6) yields

$$\gamma f(s)q(s)-\mu'\int_0^s f(z)\gamma \mathrm{e}^{-\gamma(s-z)}\,\mathrm{d}z-\mu' f_0\gamma \mathrm{e}^{-\gamma s}=\text{constant} \quad \text{for } 0<s<1 \tag{3B.7}$$

Let $s=0^+$, equation (3B.7) becomes

$$\gamma f\left(0^+\right)q\left(0^+\right)-\mu' f_0\gamma=\text{constant} \tag{3B.8}$$

Equation (3.23) can be converted to

$$\gamma q\left(0^+\right)f\left(0^+\right)=\mu'\gamma f_0 \quad \text{for } s=0 \tag{3B.9}$$

Combining equations (3B.8) and (3B.9), the value of the constant in equations (D6)-(3B.8) is determined to be zero. Therefore, equation (3B.6) is simplified as

$$\frac{\mathrm{d}\left[f(s)q(s)\right]}{\mathrm{d}s}+\gamma f(s)q(s)-\mu' f(s)=0 \quad \text{for } 0<s<1 \tag{3B.10}$$

Let $s = 1^-$ and replacing the value of the constant with zero, equation (3B.7) leads to

$$f\left(1^-\right) = \frac{\mu' \mathrm{e}^{-\gamma} \int_0^{1^-} f\left(z\right) \mathrm{e}^{\gamma z} \,\mathrm{d}\, z + \mu' f_0 \,\mathrm{e}^{-\gamma}}{q\left(1^-\right)} = \frac{\mu' \mathrm{e}^{-\gamma} \int_0^{1} f\left(z\right) \mathrm{e}^{\gamma z} \,\mathrm{d}\, z + \mu' f_0 \,\mathrm{e}^{-\gamma}}{q\left(1\right)} \tag{3B.11}$$

According to equation (3B.3), the expression of $f(1)$ can be derived as

$$f\left(1\right) = \frac{\mu' \mathrm{e}^{-\gamma} \int_0^{1} f\left(z\right) \mathrm{e}^{\gamma z} \,\mathrm{d}\, z + \mu' f_0 \,\mathrm{e}^{-\gamma}}{q\left(1\right)} \quad \text{for } s = 1 \tag{3B.12}$$

The above procedure shows that $f\left(1\right) = f\left(1^-\right)$, therefore equation (3B.10) is applicable to not only the cases of $0 < s < 1$ but also the case of $s = 1$, i.e.,

$$\frac{\mathrm{d}\left[f\left(s\right)q\left(s\right)\right]}{\mathrm{d}\, s} + \gamma f\left(s\right)q\left(s\right) - \mu' f\left(s\right) = 0 \quad \text{for } 0 < s \leq 1 \tag{3B.13}$$

Equation (3B.13) is a first-order linear homogeneous differential equation, its general solution is

$$f\left(s\right) = \frac{C_1}{q\left(s\right)} \exp\left[-\gamma s + \mu' \int \frac{1}{q\left(z\right)} \mathrm{d}\, z\right] \quad \text{for } 0 < s \leq 1 \tag{3B.14}$$

where z is a dummy variable of integration and C_1 is a normalization constant used to ensure that the total probability mass is equal to one.

Equation (3.24) was obtained by simply substituting the expression of $q(s)$ as shown in equation (3.13) into equation (3B.14) and carrying out the integration with z values from $z = s$ to $z = 1$. Although the solution procedures presented above are very similar to what was presented in Rodriguez-Iturbe and Porporato (2004), the difference is that the solutions obtained here are for the more general case with an atom of probability at $s = 0$ whereas the solutions presented in Rodriguez-Iturbe and Porporato (2004) as well as in Rodriguez-Iturbe et al. (1999) are for the special case with no such atom of probability. For ponds with their storage-outflow relationships not accurately approximated by equation (3.13), a different functional form may be used to describe their $q(s)$ functions, and similarly the approximate $q(s)$ functions may be substituted into equation (3B.14) to obtain the solutions for those ponds.

Appendix 3C: Notation

A_c = contributing catchment area (m^2);

A_o = cross-sectional area of the orifice (m^2);

A_p = bottom area of the detention pond (m^2);

b = rainfall inter-event time (h);

C_o = orifice discharge coefficient (dimensionless);

d = orifice diameter of the detention pond (m);

D = depth of water in the pond (m);

D_m = maximum water depth for active water storage of the pond (m);

E_r = runoff capture efficiency (dimensionless);

f_0 = probability mass of s at $s = 0$;

$f(s)$ = PDF of s for $0 < s \leq 1$;

$h(s)$ = complete probability density function of s;

$H(s)$ = cumulative probability distribution function of s;

k = parameter of the outflow rate ($mm^{0.5}$/time);

m = rainfall inter-arrival time (h);

m_r = runoff inter-arrival time (h);

$N(t)$ = number of inflow events from start to the current time t;

r = normalized runoff event depth (dimensionless);

R_a = area ratio between catchment area and pond bottom area (dimensionless);

$R[S_s(t),t]$ = inflow rate of the pond at time t, simplified as $R(S_s, t)$ (mm/h);

s = initial pond fullness level (dimensionless);

S_c = pond size over the contributing catchment area (mm);

S_d = average depression storage for the entire contributing catchment (mm);

S_m = effective storage capacity of the detention pond (mm);

$S_s(t)$ = water storage of a detention pond at time t, also simplified as S_s (mm);

t = time (h);

T = duration from time $t = 0$ to the current instant (h);

Q_0 = outflow rate at time $t = 0$ (m^3/s);

$Q(T)$ = outflow rate at time $t = T$ (m^3/s);

$Q[S_s(t)]$ = outflow rate of the pond at time t, also simplified as $Q(S_s)$ (mm/time);

$q(s)$ = normalized outflow rate of the detention pond (h^{-1});

u = rainfall event duration (h);

v = rainfall event depth (mm);

v_r = surface runoff event depth (mm);

y = inflow event volume to the detention pond (mm);

η = parameter of the normalized outflow rate ($time^{-1}$);

ω = overflow rate (mm/h);

θ = annual number of rainfall events;

ζ = distribution parameter of rainfall event depth (mm^{-1});

λ = distribution parameter of rainfall event duration (h^{-1});

ψ = distribution parameter of rainfall inter-event time (h^{-1});

μ = Poisson process arrival rate of rainfall event series (h^{-1});

μ' = Poisson process arrival rate of runoff event series (h^{-1});

ϕ = composite runoff coefficient (dimensionless);

γ = distribution parameter of the normalized runoff event depth (dimensionless);

$\varphi_t(\mu'; \gamma)$ = normalized inflow event series (h^{-1});

$\langle\cdot\rangle$ = ensemble averaging operator.

References

Adams, B. J., and Papa, F. (2000). Urban stormwater management planning with analytical probabilistic models. Willy, New York.

Akan, A.O. (1992). Storm runoff detention for pollutant removal. *Journal of Environmental engineering*, 118(3), 380–389.

Akan, A.O. (2010). Design aid for water quality detention basins. *Journal of Hydrologic Engineering*, 15(1), 39–48.

Bacchi, B., Balistrocchi, M., and Grossi, G. (2008). Proposal of a semi-probabilistic approach for storage facility design. *Urban Water Journal*, 5(3), 195–208.

Balistrocchi, M., Grossi, G., and Bacchi, B. (2009). An analytical probabilistic model of the quality efficiency of a sewer tank. *Water Resource Research*, 45(12). https://doi.org/10.1029/2009WR007822

Balistrocchi, M., Grossi, G., and Bacchi, B. (2013). Deriving a practical-probabilistic method to size flood routing reservoirs. *Advances in Water Resources*, 62(2013), 37–46.

Balistrocchi, M., Orlandini, S., Ranzi, R., and Bacchi, B. (2017). Copula-based modeling of flood control reservoirs. *Water Resources Research*, 53(11), 9883–9900.

Barbosa, A., Fernandes, J., and David, L. (2012). Key issues for sustainable urban stormwater management. *Water Research*, 46(20), 6787–6798.

Behera, P.K., Adam, B.J., and Li, J.Y. (2006). Runoff quality analysis of urban catchments with analytical probabilistic models. *Journal of Water Resources Planning and Management*, 132(1), 4–14.

Behera, P. K., and Teegavarapu, R. S. (2015). Optimization of a stormwater quality management pond system. *Water Resources Management*, 29(4), 1083–1095.

Chen, J., and Adams, B.J. (2005). Analysis of storage facilities for urban stormwater quantity control. *Advances in Water Resources*, 28(4), 377–392.

Chen, J., and Adams, B. J. (2006). Urban stormwater quality control analysis with detention ponds. *Water Environment Research*, 78(7), 744–753.

Chen, J., and Adams, B. J. (2007). Development of analytical models for estimation of urban stormwater runoff. *Journal of Hydrology*, 336(3–4), 458–469.

Cox, D.R., and Miller, D.H. (1965). *The theory of stochastic processes*. Willey, New York.

Eagleson, P. S. (1978). Climate, soil, and vegetation, 2, The distribution of annual precipitation derived from observed storm sequences. *Water Resources Research*, 14(5), 712-721.

Fletcher, T. D., Andrieu, H., and Hamel, P. (2013). Understanding, management and modelling of urban hydrology and its consequences for receiving waters: A state of the art. *Advances in Water Resources*, 51, 261–279.

Guo, R., and Guo, Y. (2018). Stochastic modelling of the hydrologic operation of rainwater harvesting systems. *Journal of Hydrology*, 562, 30–39.

Guo, R., Guo, Y., and Wang, J. (2018). Stormwater capture and antecedent moisture characteristics of permeable pavements. *Hydrological Processes*, 32(17), 2708–2720.

Guo, Y. (2016). Stochastic analysis of hydrologic operation of green roofs. *Journal of Hydrologic Engineering*, 21(7), 04016016. https://doi.org/10.1061/(ASCE)HE.1943-5584.0001371

Guo, Y., and Adams, B. J. (1999). Analysis of detention ponds for storm water quality control. *Water Resource Research*, 35(8), 2447–2456.

Guo, Y., and Baetz, B. W. (2007). Sizing of rainwater storage units for green building applications. *Journal of Hydrologic Engineering*, 12(2), 197–205.

Hassini, S., and Guo, Y. (2016). Exponentiality test procedures for large samples of rainfall event characteristics. *Journal of Hydrologic Engineering*, 21(4), 04016003. http://dx.doi.org /10.1061/(asce)he.1943-5584.0001352

Howard, C. (1976). Theory of storage and treatment-plant overflows. Journal of Environmental Engineering Division, ASCE, 102(4), 709–722.

Lee, E. H., and Kim, J. H. (2018). Development of new inter-event time definition technique in urban areas. *KSCE Journal of Civil Engineering*, 1-8.

Li, J. Y., and Adams, B. J. (2000). Probabilistic Models for analysis of urban runoff control systems. *Journal of Environmental Engineering*, 126(3), 217–224.

Loganathan, G.V., and Delleur, J.W. (1984). Effects of urbanization on frequencies of overflows and pollutant loadings from storm sewer overflows: A derived distribution approach. *Water Resource Research*, 20(7), 857–865.

Loganathan, G. V., Watkins, E. W., and Kibler, D. F. (1994). Sizing storm-water detention basins for pollutant removal. *Journal of Environmental Engineering*, 120(6), 1380–1399.

NOAA (National Oceanic and Atmospheric Administration). (1982). *Mean monthly, seasonal, and annual pan evaporation for the United. States*. http://www.nws.noaa.gov/oh/hdsc/PMP_related_studies/TR34.pdf.

Pelak, N., and Porporato, A. (2016). Sizing a rainwater harvesting cistern by minimizing costs. *Journal of Hydrology*, 541, 1340–1347.

Porporato, A., Daly, E., and Rodroguez-Iturbe, I. (2004), Soil water balance and ecosystem response to climate change. *The American Naturalist*, 164(5), 625–632.

Restrepo-Posada, P.J., and Eagleson, P.S. (1982). Identification of independent rainstorms. *Journal of Hydrology*. 55 (1), 303–319.

Rodriguez-Iturbe, I., Entekhabi, D., and Bras, R. L. (1991). Nonlinear dynamics of soil moisture at climate scales: 1. stochastic analysis. *Water Resource Research*, 27(8), 1899–1906.

Rodriguez-Iturbe, I., and Porporato, A. (2004), *Ecohydrology of water-controlled ecosystems*, UK: Cambridge University Press.

Rodriguez-Iturbe, I., Porporato, A., Ridolfi, L., Isham, V., and Cox, D. (1999). Probabilistic modelling of water balance at a point: The role of climate, soil and vegetation.

Proceedings of the Royal Society of London, Series A, 455, 3789–3805.

Rossman, L. A. (2015). *Storm water management model user's manual, version 5.1*. Rep.EPA-600/R-14/413b, Office of Research and Development, Water Supply and Water Resources Division, U.S. Environmental Protection Agency, Washington DC.

Shamsudin, S., Dan'azumi, S., Aris, A., and Yusop, Z. (2014). Optimum combination of pond volume and outlet capacity of a stormwater detention pond using particle swarm optimization. *Urban Water Journal*, 11(2), 127-136.

Tsihrintzis, V. A., and Hamid, R. (1997). Modeling and management of urban stormwater runoff quality: a review. *Water Resources Management*, 11(2), 136–164.

Tsihrintzis, V. A., and Hamid, R. (1998). Runoff quality prediction from small urban catchments using SWMM. *Hydrological Processes*, 12(2), 311–329.

Ursino, N. (2015). Risk analysis of sustainable urban drainage and irrigation. *Advances in Water Resources*, 83, 277–284.

U.S. Army Corps of Engineers. (1977). *Storage, treatment, overflow, runoff model: STORM*, (Rep.723-S8-L2250). David, CA: Hydrologic Engineering Center.

U.S. Environmental Protection Agency (USEPA). (1986). *Methodology for analysis of detention basins for control of urban runoff quality*. Rep. EPA, 440, 5–87, Washington, DC.

Wanielista, M. P., Yousef, Y. A. (1993). *Stormwater management*. Wiley, New York.

Wang, J., and Guo, Y. (2018). An analytical stochastic approach for evaluating the performance of combined sewer overflow tanks. *Water Resources Research*, 54(5), 3357–3375.

Wong, B. P., and Kerkez, B. (2016). Adaptive measurements of urban runoff quality. *Water Resources Research*, 52(11), 8986–9000.

Yue, S., and Hashino, M. (1999). A stochastic model for deriving the basic statistics of J-day averaged streamflow. *Water Resources Research*, 35(10), 3127-3137.

Yue, S., Hashino, M., Bobee, B., Rasmussen, P. F., and Ouarda, T. B. M. J. (1999). Derivation of streamflow statistics based on a filtered point process. *Stochastic Environmental Research and Risk Assessment*, 13(5), 317-326.

Yue, S., and Hashino, M. (2001). The general cumulants for a filtered point process. *Applied Mathematical Modelling*, 25(3), 193-201.

Zhang, S., and Guo, Y. (2013). Explicit equation for estimating storm-water capture efficiency of rain gardens. *Journal of Hydrologic Engineering*, 18(12), 1739–1748.

Zhang, S., and Guo, Y. (2014). Stormwater capture efficiency of bioretention systems. *Water Resources Management*, 28(1), 149–168.

Chapter 4

Dynamic Water Balance of Infiltration-Based Stormwater Best Management Practices

Jun Wang and Yiping Guo

Abstract: Infiltration-based urban stormwater best management practices (BMPs) are widely used for the reduction of runoff volumes and improvement of runoff quality. In this paper, closed-form analytical equations, collectively referred to as the analytical stochastic models (ASMs), are derived for analyzing the dynamic water balance of infiltration-based BMPs. Using infiltration trench as an example, considering infiltration through both the sides and the bottom, through only the sides, or through only the bottom of an infiltration trench, three ASMs are developed for all possible operating conditions. The operating conditions of other infiltration-based BMPs can also be described by one of the three ASMs. The accuracy that these analytical models can achieve is demonstrated by comparing their results with those from continuous simulations for a total of 972 hypothetical cases considering almost all possible design configurations. Close agreements between continuous simulation and analytical results are demonstrated, and the effects of many influencing factors on a BMP's hydrologic performance are illustrated. The ASMs are therefore recommended as a computationally efficient alternative for use in the planning, design, and analysis of infiltration-based BMPs.

Key Words: Infiltration facilities; Analytical stochastic approach; Continuous simulation; Runoff capture efficiency; Stormwater management; Best management practices.

4.1 Introduction

Stormwater best management practices (BMPs) are designed to control surface runoff in urban areas by means of detention/retention, infiltration and filtration. Stormwater BMPs are also referred to as stormwater control measures (SCMs); other than the filtration/flow-through type of SCMs which do not change very much the local hydrological functions, the remaining can generally be classified into two types according to their primary hydrological functions: the storage/retention-based SCMs and the infiltration-based SCMs (Fletcher et al., 2013; Szota et al., 2019). The infiltration-based SCMs mainly include infiltration trenches, infiltration chambers, dry wells, infiltration basins, and bioretention systems (Fletcher et al., 2013; Eckart et al., 2017; D'Aniello et al., 2019).

An infiltration trench is usually comprised of a stone storage reservoir filled with gravel aggregates or plastic lattice structures and lined with geotextile filter cloths. Infiltration chambers have premanufactured modular structures serving as storage spaces which can temporarily hold stormwater (CVC and TRCA, 2010). Infiltration basins are constructed shallow impoundments lined with relatively permeable soils. Dry wells are excavated cylinder-shaped pits with perforated sides and bottoms. A Bioretention cell is generally comprised of a vegetated ponding area underlaid by a permeable media layer where plants grow (Zhang and Guo 2014).

Taking the trench as a representative infiltration facility, the other types of infiltration-based BMPs can be regarded as design variations of infiltration trenches. Since the hydrologic conditions under which all the different kinds of infiltration-based BMPs operate are very similar, in the following, for the description of the constitution, operation, and performance of infiltration-based BMPs, only infiltration trench will be included as an example. For an infiltration trench, as an option, a soil layer may be placed on the top of its stone storage reservoir. However, it was found that infiltration trenches with only stone storage layers outperform those with topsoil layers in reducing runoff volumes and peak discharges (Gironás et al., 2009). Similar to other infiltration-based BMPs, infiltration trenches are designed to capture and store an amount of stormwater while allowing the stored water to slowly percolate into the surrounding soils (Woods-Ballard et al., 2007). Suspended pollutants and sediments carried by the captured stormwater can be filtered out through the void-forming materials of the storage layers (Hatt et al., 2007). Therefore, infiltration trenches can help control both stormwater quantity by reducing surface runoff volumes and peak discharge rates and stormwater quality by removing pollutants (Warnaars et al., 1999; WEF and ASCE/EWRI, 2012).

The water level is a crucial aspect in the design of infiltration trench. Native soils surrounding the storage reservoir of an infiltration trench (i.e., soils at the bottom and sidewalls of the trench) affect the rate of infiltration of the stored water. Depletion of the stored water is also caused partly by evaporation. Overflow occurs when the storage reservoir of the trench is full, and more runoff is still filling into the trench. Overflow is usually conveyed downstream by sewer pipes. Factors affecting the infiltration rates through the sides and the bottom of an infiltration trench include the water level in the trench and the hydraulic conductivity of the native soils. A few studies have been conducted to evaluate the performance of infiltration trenches considering both the sidewall and bottom infiltrations (e.g., Duchene et al., 1994; Browne et al., 2008; Freni et al., 2009; Chahar et al., 2011; Lee et al., 2014). In design analyses, soils underneath and closely beside an infiltration trench may be assumed to be always saturated; the infiltration rate can thus be assumed to be equal to the saturated hydraulic conductivity of the soils (Chahar et al., 2011). As soils are actually not saturated all the time during a storm, assuming infiltration rate as a constant equalling the saturated hydraulic conductivity of the soils may result in a slight underestimation of the amount of infiltration (Chahar et al., 2011). In design analyses or for design purposes, however, this assumption is widely accepted by many jurisdictions and researchers (e.g., Schueler and Claytor, 2000; PDEP, 2006; CVC and TRCA, 2010; Campisano et al., 2011; Chahar et al., 2011; Creaco and Franchini, 2012).

From some monitoring studies it was found that infiltration through the bottom of some trenches may be considered negligible due to clogging (Emerson and Traver, 2008; Emerson et al., 2010). The deposition of sediments would generally result in clogging of a trench with an increase in time of operation (Siriwardene et al., 2007), as a result, the performance of infiltration trenches will gradually decrease as their service time increases (Revitt et al., 2003). To ensure the long-term satisfactory performance of infiltration trenches, routine and proper inspection and maintenance are necessary. To properly consider the effects of clogging and compaction, a safety factor may be applied in determining the design infiltration rate of the surrounding soils. Laboratory experimental approaches to estimating the safety factor for considering clogging effects on infiltration trenches can be found in Siriwardence et al. (2007) and Barraud et al. (2014).

Similar to many other infiltration-based BMPs, infiltration trenches are mainly designed to reduce runoff volume and filter out pollutants. Since measured data about pollutant concentrations are usually not available, the average runoff reduction ratio (defined as the fraction of runoff that is captured and depleted by an infiltration trench over the long term) can be used as a surrogate measure for calculating the first flush-based water quality control volume in the design of infiltration BMPs (Zhang et al., 2016). Three types of modelling techniques have been generally used for estimating the long-term average performance of infiltration trenches: the continuous simulation approach, the design storm approach, and the analytical probabilistic approach. The continuous simulation approach is widely used because it can provide an accurate estimate of the long-term average performance of trenches using long-term rainfall series as input to represent the trenches' operating conditions. However, continuous simulation is data intensive and time-consuming to perform. The conventional design storm approach is used to estimate the performance of infiltration trenches under a representative design storm event (Akan, 2002; Chahar et al., 2011). The design storm approach is not capable of directly quantifying the long-term average hydrologic performance (i.e., the fraction of runoff captured and depleted) of trenches and it may also result in over-design or under-design of trenches (Guo and Gao, 2016). Employing analytical equations, the analytical probabilistic approach provides an efficient and ease-to-use way to quantify the long-term average performance of infiltration facilities by making use of the probabilistic models of the input rainfall series (Guo and Guo, 2018).

The analytical stochastic approach was initially developed by Rodriguez-Iturbe et al. (1991) for analyzing soil moisture dynamics. Recent studies have proved that it is an appealing technique and can also be applied in stormwater management modelling (Guo, 2016; Pelak and Porporato, 2016; Bertassello et al., 2018; Guo et al., 2018; Parolari et al., 2018; Wang and Guo, 2018, 2019). Compared to the analytical probabilistic approach in which the antecedent wetness of the trench preceding the analyzed rainfall-dry period cycle needs to be assumed, the analytical stochastic approach has the advantage of not making any simplifying assumptions about the initial wetness conditions. Moreover, using the analytical stochastic approach, the outflow rate of the stored water can be described as a function of the water level in the storage facility whereas the outflow rate is simplified as a constant in the analytical probabilistic approach. The simplifying assumptions of the initial wetness conditions and outflow rates affect the accuracy of the analytical probabilistic approach. In this study, new analytical stochastic models are developed to estimate the hydrologic performance of infiltration-based BMPs considering infiltration through both their sides and bottoms, eliminating the two limitations of the previously developed analytical probabilistic models. In the following, the Poisson process representing a long-term rainfall series and the dynamic water balance of infiltration-based BMPs are described first. Then analytical expressions for estimating their runoff capture efficiencies (i.e., fractions of runoff captured and depleted) are derived. Finally, the accuracy of the derived analytical equations is systematically verified by comparing between analytical and continuous simulation results.

4.2 Methods

4.2.1 Stochastic Representation of Rainfall Series

In order to analyze the statistical rainfall characteristics of a location, the observed continuous rainfall series of the location is first separated into individual rainfall events by selecting a minimum inter-event time (MIET) (Hassini and Guo, 2016). With a suitable MIET, discrete rainfall events can be obtained and treated as statistically independent of each other (Adams and Papa, 2000; Guo et al., 2012). Each rainfall event and its preceding dry period can be characterized by three characteristics, i.e., rainfall event depth v, event duration u, and inter-event time b (or inter-arrival time m). For many locations, exponential probability density functions (PDFs) were found to fit well the observed frequency distributions of v, u, b, and m. Exponential PDFs were therefore recommended for use in the design of stormwater management facilities by the U.S. Environmental Protection Agency (USEPA, 1986). These exponential PDFs can be described as

$$f_V(v) = \zeta \, e^{-\zeta v} \qquad \text{for } v > 0 \tag{4.1}$$

$$f_U(u) = \lambda \, e^{-\lambda u} \qquad \text{for } u > 0 \tag{4.2}$$

$$f_B(b) = \psi \, e^{-\psi b} \qquad \text{for } b > 0 \tag{4.3}$$

$$f_M(m) = \mu \mathrm{e}^{-\mu m} \qquad \text{for } m > 0 \tag{4.4}$$

where $\zeta = 1/\langle v \rangle$, $\lambda = 1/\langle u \rangle$, $\psi = 1/\langle b \rangle$, and $\mu = 1/\langle m \rangle$ are the distribution parameters, in which $\langle \cdot \rangle$ is the ensemble average operator, μ is the arrival rate (events per unit time) of rainfall events, and $\langle m \rangle = \langle u \rangle + \langle b \rangle$ is the average inter-arrival time of rainfall events (Eagleson, 1978; Guo, 2016). The sequential occurrence of random rainfall events is also described stochastically as a marked Poisson process (Wang and Guo, 2018), whereas individual rainfall events are treated as occurring instantaneously (Rodriguez-Iturbe and Porporato, 2004). The point rainfall series is therefore represented as consisting of instantaneous rainfall event jumps occurring with inter-arrival times m which equals the sum of the corresponding u and b.

4.2.2 Dynamic Water Balance of Infiltration Trenches

4.2.2.1 Net Inflow Rate

An infiltration trench system includes the infiltration trench itself and its adjacent contributing catchment. The total inflow into the infiltration trench consists of the runoff generated from the adjacent catchment and the direct rainfall falling onto the trench surface, as a result of a rainfall event with rainfall depth v, the total inflow expressed in depth (mm) over the trench bottom area can be calculated as

$$v_i = \begin{cases} 0, & v \le S_d \\ (1+R_a)(v-S_d), & v > S_d \end{cases} \tag{4.5}$$

where ϕ is the runoff coefficient of the contributing catchment; $S_d = (\phi R_a S_{dc})/(\phi R_a + 1)$ is the lumped, area-weighed depression storage of the trench system, S_d is expressed in depth (mm) over the trench bottom area; R_a is the ratio between the catchment area and the trench surface area; S_{dc} is the depression storage of the catchment, it is expressed in depth (mm) over the catchment area. Equation (4.5) indicates that an inflow event would occur only when the rainfall event depth is greater than S_d. The simplified form of equation (4.5) for cases where the contributing catchment is 100% impervious and the corresponding ϕ is equal to 1 can be found in Guo et al. (2018). The justification and proof of acceptance of this simplified form is given by Guo et al. (2018).

The derived PDF of the inflow event depth v_i (Guo et al., 2018) is

$$f_{V_I}(v_i) = \left[\zeta/(1+R_a)\right] \mathrm{e}^{-\left[\zeta/(1+R_a)\right]v_i} \qquad \text{for } v_i > 0 \tag{4.6}$$

Since the input rainfall event series can be represented as a marked Poisson process, the resulting series of inflow event depths still follows a marked Poisson process with a modified arrival rate of μ' where $\mu' = \mu \int_{S_d}^{\infty} f_V(v)\,\mathrm{d}v = \mu \mathrm{e}^{-S_d \zeta}$. For simplicity of notation, dimensionless normalization of some variables of interest are used. For example, the normalized inflow event depth that may flow into the trench's storage reservoir is denoted as r which is equal to v_i/S_m, where S_m is the storage capacity of the infiltration trench expressed as depth of water (mm) over the trench surface or bottom area. Then the PDF of the dimensionless individual inflow event depth r can be expressed as

$$f_R(r) = \gamma \mathrm{e}^{-\gamma r} \quad \text{for } r > 0 \tag{4.7}$$

where $\gamma = (\zeta S_m)/(1+R_a)$ is the distribution parameter equaling the inverse of the mean value of r.

The amount of water stored in the trench at the beginning of an inflow event is denoted as S_s which is measured in the same unit as S_m. The storage fraction already occupied at the beginning of an inflow event is therefore S_s/S_m which is denoted as s and referred to as the trench's degree of saturation hereafter. Subsequent to an inflow event, the normalized inflow-event depth that can actually be retained by the trench's storage reservoir is denoted as y. When the normalized inflow event depth r exceeds the normalized storage space that is still available (i.e., $1-s$), overflow/by-pass occurs and the actual retained normalized depth from the inflow event y is equal to $(1-s)$. Otherwise, the actual retained rainfall depth from the inflow event equals the normalized inflow event depth r. The PDF of the normalized net inflow event depth y conditioned on the trench having an initial degree of saturation s, denoted as $P\left[y|s\right]$, can therefore be expressed as

$$P_{Y|S}\left[y|s\right]=\gamma\,\mathrm{e}^{-\gamma y}+\mathrm{e}^{-\gamma(1-s)}\,\delta\left(y+s-1\right)\qquad\text{for }0\le y\le 1-s\tag{4.8}$$

where $\delta(\cdot)$ is the Dirac delta function. The probability mass of $\mathrm{e}^{-\gamma(1-s)}$ for $y=1-s$ represents the probability that the trench's reservoir is filled by an inflow event given that the trench's initial degree of saturation is *s* at the start of the rainfall event.

Represented as a marked Poisson process, the sequential number of random net inflow event series from time zero to the current time *t* is denoted as *i* which may take values of 1, 2, 3,$\cdots$, *N*(*t*) where *N*(*t*) is the total number of net inflow events from time zero to time *t*. The normalized net inflow rate at time *t* can then be expressed as

$$\varphi_t\left(\mu';\gamma\right)=\frac{I\left(S_s,t\right)}{S_m}=\sum_{i=1}^{N(t)}y_i\delta\left(t-t_i\right)\tag{4.9}$$

where $\varphi_t\left(\mu';\gamma\right)$ is the normalized inflow rate expressed as a function of the arrival rate of the Poisson process μ' and the reciprocal of the mean inflow event depth *γ*; $I\left(S_s,t\right)$ is the inflow rate collected by the trench from the contributing catchment at time *t*; t_i is an individual occurrence time in the sequential inflow events from time zero to time *t*.

4.2.2.2 Outflow Rate

During the inter-arrival periods of rainfall events, inflow retained in an infiltration trench is depleted by evaporation and infiltration into the native soils underneath and surrounding the trench's storage reservoir. Infiltrations may occur through both the bottom and sidewalls of the trench (Warnaars et al., 1999; Bergman et al., 2011). Although occurring at a small rate, it was found that evaporation should also be considered in trench design (Guo and Guo, 2018). Therefore, the total outflow from a trench includes the bottom and side infiltrations and evaporation of water from its storage reservoir. When the amount of water stored in the trench is S_s, the total outflow rate $Q(S_s)$ of an infiltration trench expressed as the water depth in mm per unit time, can be calculated as

$$Q(S_s) = \begin{cases} 0, & S_s = 0 \\ E_a + \alpha_b f_b + \alpha_s f_s A_s / A_b, & 0 < S_s \le S_m \end{cases} \tag{4.10}$$

where $A_b=LW$ is the bottom area of a trench with length L and width W; $A_s = 2(L+W)S_s$ is the area of the sidewalls of the trench from which infiltration occurs when water stored in the trench is S_s; E_a is the evaporation rate; f_b is the infiltration rate from the trench bottom; f_s is the infiltration rate from the trench's sidewalls; α_b and α_s are the safety factors used to reflect the compaction and clogging effects on the rate of infiltration from, respectively, the bottom and sides of the trench.

The normalized outflow rate $q(s)$ from the infiltration trench can be expressed as

$$q(s)=\frac{Q(S_s)}{S_m}=\begin{cases} 0, & s=0 \\ C_1(s+C_2), & 0<s\le 1\ \&\ \alpha_b>0\ \&\ \alpha_s>0 \\ C_1\left[s+E_a/(C_1S_m)\right], & 0<s\le 1\ \&\ \alpha_b=0\ \&\ \alpha_s>0 \\ (E_a+\alpha_b f_b)/S_m, & 0<s\le 1\ \&\ \alpha_b>0\ \&\ \alpha_s=0 \end{cases} \tag{4.11}$$

where $C_1=2\alpha_s f_s(L+W)/(LW)$; $C_2=(E_a+\alpha_b f_b)/(C_1S_m)$. In the case where α_s equals 0, $q(s)$ turns to be a constant independent of s. Considering the impacts of soil clogging and compaction (i.e., using clogging factors α_b and α_s) on the outflow rates of infiltration trenches, their operating conditions may be classified into three possibilities: (1) infiltration through both the bottom and sides of a trench (i.e., when $\alpha_b \neq 0$ and $\alpha_s \neq 0$); (2) infiltration only through the sides of a trench (i.e., when $\alpha_b = 0$ and $\alpha_s \neq 0$); and (3) infiltration only through the bottom of a trench (i.e., when $\alpha_b \neq 0$ and $\alpha_s = 0$). For infiltration BMPs other than infiltration trenches, one of the above three operating conditions may be used to describe their outflow rates as well. The corresponding three types of stochastic models will be derived and introduced later.

4.2.2.3 Effective Storage Capacity

Rainfall events are treated as instantaneous pulses in the above stochastic analysis whereas in reality both inflow and outflow occur throughout the duration of a rainfall event. Instantaneous occurrence of inflows and outflows results in instantaneous overflows, consequently the estimated overflow volume will be larger than the actual overflow volume.

This is because the additional storage space resulting from outflows occurred during a rainfall event can actually accommodate more inflows and result in less overflows. To avoid the overestimation of overflows, an extra storage capacity created by outflows during a rainfall event may be added to the actual physical storage capacity (the actual physical storage capacity is denoted as S_c hereafter) of a trench and the sum may be regarded as the trench's effective storage capacity. This effective storage capacity should then be used as S_m in all previous calculations.

Similar to other kinds of infiltration-based BMPs, the physical storage provided by an infiltration trench is mainly contributed by its storage reservoir and the shallow depression storage created by the surface of the storage reservoir. The total physical storage capacity of a trench S_c can therefore be calculated as $S_c = S_{dt} + r_v D_m / (1 + r_v)$, where S_{dt} is the depression storage of the trench expressed in mm; r_v is the void ratio between the total void volume and the total solid volume of the storage reservoir; D_m is the depth of the storage reservoir; The schematic of the infiltration trench storage components and water balance elements is presented in Fig. 4.1.

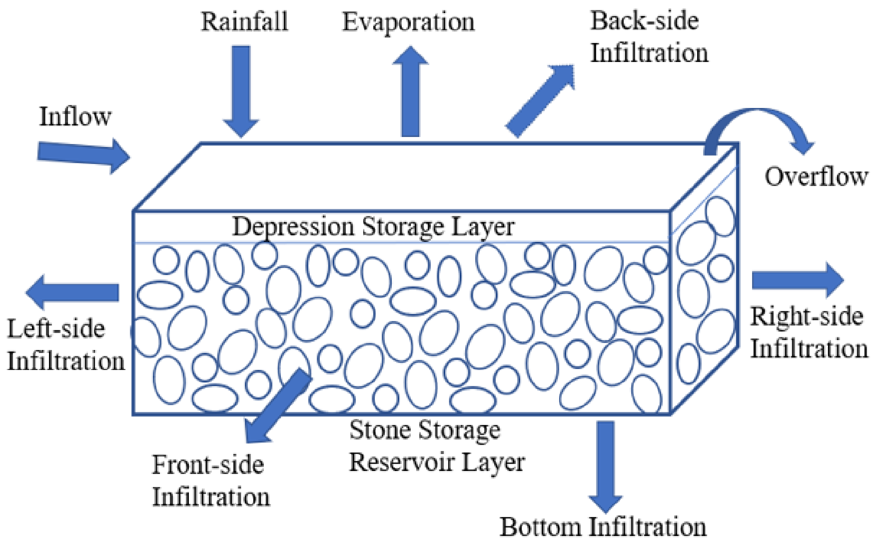

Fig. 4.1 Schematic of the storage layer and water balance components of an infiltration trench

The effective storage capacity S_m may be estimated by considering an average representative rainfall event with duration $\langle u \rangle$. For this event, S_m may be calculated as

$$S_m = S_c + \langle Q(S_s) \rangle \langle u \rangle = S_c + \langle Q(S_s) \rangle / \lambda \tag{4.12}$$

where $\lambda = 1/\langle u \rangle$ and λ is the distribution parameter for rainfall event duration; $\langle Q(S_s) \rangle$ is the average outflow rate during this representative rainfall event, it can be estimated as

$$\langle Q(S_s) \rangle = \left(Q_0 + Q_{\langle u \rangle}\right)/2 \tag{4.13}$$

where Q_0 and $Q_{\langle u \rangle}$ are the outflow rates at respectively $t = 0$ and $t = \langle u \rangle$ (i.e., the end) of the representative rainfall event.

The outflow rates during a representative rainfall event can be estimated by approximating the outflow rate calculated using equation (4.10) as a linear function of S_s, i.e., $Q(S_s) = kS_s$, where $k = Q(S_c)/S_c$. This simplification will only be used to estimate Q_0 and $Q_{\langle u \rangle}$ in equation (4.13). Infiltration rates through native soils are usually much lower than the average intensities of rainfall events; in addition, inflows into a trench includes not only rainfall falling directly onto the trench surface but also runoff from the catchment. As a result, similar to other infiltration-based BMPs, the typical operation of a trench during a rainfall event is that the trench is filled up quickly during the initial portion of the rainfall event and then outflow from the trench gradually decreases because of the decrease of water contained in the trench. If the process of the filling-up of the trench is further simplified as occurring instantaneously at the beginning of the representative rainfall event, the outflow rate as a function of time t during this event would be exponentially decreasing. Thus, the outflow rate at the beginning of a representative rainfall event Q_0 can be estimated as $Q(S_c)$, while the outflow rate at the end of the representative rainfall event can be determined to be $Q_{\langle u \rangle} = Q(S_c)\exp(-k\langle u \rangle)$. According to equation (4.13), the average outflow rate can then be estimated as $\langle Q(S_s) \rangle = \left[Q(S_c)\exp(-k/\lambda) + Q(S_c) \right] / 2$. Substituting this expression of $\langle Q(S_s) \rangle$ into equation (4.12), S_m can be estimated as

$$S_m = S_c + \left\{Q(S_c)\exp\left[-Q(S_c)/(\lambda S_c)\right] + Q(S_c)\right\}/(2\lambda) \tag{4.14}$$

4.2.2.4 Normalized Water balance Equation

The following dynamic water balance equation of an infiltration trench is used to describe the water level fluctuations in its storage reservoir:

$$\frac{\mathrm{d}S_s}{\mathrm{d}t} = I(S_s, t) - Q(S_s) \tag{4.15}$$

In equation (4.15), S_s is the amount of water held in the trench at time t, expressed in mm of water over the trench surface area; $I(S_s, t)$ and $Q(S_s)$ are the net inflow and outflow rates as determined earlier and are both expressed in the unit of mm of water over the trench surface area per unit time. Dividing all terms in equation (4.15) by S_m and incorporating equations (4.9) and (4.11), the normalized stochastic water balance equation of an infiltration trench can be described as

$$\frac{\mathrm{d}s}{\mathrm{d}t} = \varphi_t(\mu';\gamma) - q(s) \tag{4.16}$$

4.2.3 Analytical Solution of the Stochastic Water Balance Equation

Equation (4.16) is a stochastic differential equation since it is driven by a marked Poisson process, i.e., the inflow into the trench $\varphi_t(\mu';\gamma)$. The solution for the probability distribution of s from equation (4.16) can be derived by obtaining the corresponding Chapman-Kolmogorov forward equations first (Cox and Miller, 1965; Gardiner, 2004; Rodriguez-Iturbe and Porporato, 2004). From the start of operation of a trench, the probability distribution of s denoted as $h(s, t)$ changes with time t and consists of a discrete atom of probability $f_0(t)$ for $s = 0$ and a continuous PDF, $f(s,t)$, for $s > 0$ due to the discrete form of the outflow function $q(s)$ shown in equation (4.11). The general form of the temporal evolution of $f(s,t)$ and $f_0(t)$ as derived by Rodriguez-Iturbe and Porporato (2004) can be expressed as

$$\begin{aligned}\frac{\partial f(s,t)}{\partial t} = \frac{\partial}{\partial s}\left[f(s,t)q(s)\right] - \mu' f(s,t) + \mu' \int_0^s f(z,t) P_{Y|S}\left[(s-z)|z\right] \mathrm{d}z \\ + \mu' f_0(t) P_{Y|S}\left[s|0\right]\end{aligned} \quad \text{for } 0 < s \le 1 \quad (4.17)$$

$$\frac{\mathrm{d}\, f_0(t)}{\mathrm{d}t} = -\mu' f_0(t) + q\left(0^+\right) f\left(0^+, t\right) \quad \text{for } s = 0 \qquad (4.18)$$

where $P_{Y|S}\left[(s-z)|z\right]$ and $P_{Y|S}\left[s|0\right]$ are both the conditional probability distributions of inflows to a trench as expressed in equation (4.8); 0^+ is a value infinitesimally larger than zero; $f\left(0^+,t\right) = \lim_{s \to 0^+} f(s,t)$; z is the dummy variable of integration.

As the operation time continues, the infiltration trench system will eventually reach a steady state where the probability distribution of s will remain the same and does not change with time anymore. The steady-state solutions of $f(s,t)$ and $f_0(t)$ can be obtained by letting t approach infinity in equations (4.17) and (4.18). Theoretically it would take an infinitely long time for the system to reach a steady state, however, this steady state is the only interest for the planning and design of infiltration trenches. The steady-state atom of probability for $s = 0$ and the continuous PDF for $s > 0$ are denoted as f_0 and $f(s)$, respectively. By setting t to approach infinity in equations (4.17) and (4.18) while replacing $P_{Y|S}\left[\cdot|\cdot\right]$ with the expressions shown in equation (4.8), the two equations governing $f(s)$ and f_0 were obtained to be

$$\begin{aligned}\frac{\mathrm{d}}{\mathrm{d}s}\left[f(s)q(s)\right]-\mu' f(s)+\mu'\int_0^s f(z)\left[\gamma\,\mathrm{e}^{-\gamma(s-z)}+\delta(s-1)\mathrm{e}^{-\gamma(1-z)}\right]\mathrm{d}z \\ +\mu' f_0\left[\gamma\,\mathrm{e}^{-\gamma s}+\delta(s-1)\mathrm{e}^{-\gamma}\right]=0\end{aligned} \quad \text{for } 0<s\le 1 \quad (4.19)$$

$$-\mu' f_0+q\left(0^+\right)f\left(0^+\right)=0 \quad \text{for } s=0 \quad (4.20)$$

As shown in equation (4.11), the $q(s)$ function is discontinuous at $s = 0$, that is why the notation of 0^+ is necessary here. Adapting from Wang and Guo (2019), the general solutions of equations (4.19) and (4.20) are

$$f(s)=\frac{C_3}{q(s)}\exp\left[-\gamma s+\mu'\int_0^s\frac{1}{q(z)}\mathrm{d}z\right] \quad \text{for } 0<s\le 1 \quad (4.21)$$

$$f_0=C_3/\mu' \quad \text{for } s=0 \quad (4.22)$$

where C_3 is the normalization constant needed to satisfy the requirement that the total probability mass must equal one. By carrying out the integration in equation (4.21) for $q(s)$ cases with $\alpha_s > 0$, the general form of the steady-state probability distribution of s, $h(s)$, which includes a discrete probability mass f_0 for $s=0$ and a continuous part $f(s)$ for $0 < s \leq 1$ is

$$h(s) = \begin{cases} C_3 C_4 \,\mathrm{e}^{-\gamma(s+C_2)} \left(s+C_2\right)^{(\mu'/C_1 - 1)} & 0 < s \leq 1 \\ (C_3/\mu')\,\delta(0) & s = 0 \end{cases} \tag{4.23}$$

where $C_4 = C_2^{-\mu'/C_1} \mathrm{e}^{\gamma C_2} / C_1$. It is noted that equation (4.23) is valid only for $q(s)$ cases with $\alpha_s > 0$; for $q(s)$ cases with $\alpha_s = 0$, equations (4.21) and (4.22) can still be used to derive their corresponding $h(s)$ but the derivations and final results will be different. That is why the analytical solutions of the stochastic water balance equation for cases with $\alpha_s = 0$ will be presented separately in section 4.2.5.

In order to satisfy the requirement that $\int_0^1 h(s)\,\mathrm{d}s = 1$, the normalization constant C_3 was found to be equal to $\left[1/\mu' + C_4 C_5 \gamma^{(-\mu'/C_1)}\right]^{-1}$, where $C_5 = \Gamma\left[\mu'/C_1, \gamma\left(1+C_2\right)\right] - \Gamma\left(\mu'/C_1, \gamma C_2\right)$, and $\Gamma(\cdot,\cdot)$ represents the incomplete gamma function which is defined as $\Gamma(a,x) = \int_0^x z^{a-1} \mathrm{e}^{-z}\,\mathrm{d}z$. f_0 can thus be determined to be $f_0 = \dfrac{C_3}{\mu'} = \dfrac{1}{1 + C_4 C_5 \mu' \gamma^{(-\mu'/C_1)}}$.

Substituting the expression of C_3 into equation (4.23), the explicit expression of $h(s)$ was obtained to be

$$h(s)=\begin{cases}\dfrac{C_4\,\mathrm{e}^{-\gamma(s+C_2)}\left(s+C_2\right)^{(\mu'/C_1-1)}}{1/\mu'+C_4C_5\gamma^{(-\mu'/C_1)}} & 0<s\le 1\\ \dfrac{1}{1+C_4C_5\mu'\gamma^{(-\mu'/C_1)}}\delta(0) & s=0\end{cases} \tag{4.24}$$

The cumulative distribution function (CDF) of s, $H(s)$, can be derived as

$$\begin{aligned}H(s)=\int_0^s h(s)\,\mathrm{d}s &= C_3/\mu'+C_3C_4\gamma^{-\mu'/C_1}\\ &\left\{\Gamma\left[\mu'/C_1,\gamma\left(s+C_2\right)\right]-\Gamma\left(\mu'/C_1,\gamma C_2\right)\right\}\end{aligned} \quad \text{for } 0\le s\le 1 \tag{4.25}$$

4.2.4 Estimation of Average Runoff Capture Efficiency

The long-term average amount of water stored in the trench $\langle S_s\rangle$, in mm of water over the trench surface area, can be expressed as $\langle S_s\rangle = \langle s\rangle S_c$, where $\langle s\rangle$ is the ensemble average of s and can be calculated as

$$\langle s\rangle=\int_0^1 sh(s)\,\mathrm{d}s=C_3C_4C_6\left(C_7-\gamma C_2C_5\right) \tag{4.26}$$

where $C_6=\gamma^{-(1+\mu'/C_1)}$, $C_7=\Gamma\left[\mu'/C_1+1,\gamma\left(1+C_2\right)\right]-\Gamma\left(\mu'/C_1+1,\gamma C_2\right)$.

The long-term average water balance of an infiltration trench can be expressed as $\langle r\rangle-\langle q\rangle=\langle\omega\rangle$, where $\langle r\rangle$ is the normalized mean inflow rate into the trench; $\langle q\rangle$ is the normalized mean outflow rate from the trench; and $\langle\omega\rangle$ is the normalized mean overflow rate from the trench. $\langle r \rangle$ can be calculated as the normalized inflow event depth averaged over the inter-arrival time, i.e.,

$$\langle r \rangle = \mu' \int_0^\infty r f_R(r)\,\mathrm{d}\,r = \mu'/\gamma \tag{4.27}$$

$\langle q \rangle$ can be calculated as the integration of the product of $q(s)$ and $h(s)$ with s ranging from 0 to 1, i.e.,

$$\langle q \rangle = \int_0^1 q(s)h(s)\,\mathrm{d}\,s = C_1C_3C_4C_6C_7 \tag{4.28}$$

$\langle \omega \rangle$ is calculated as the difference between $\langle r \rangle$ and $\langle q \rangle$, i.e.,

$$\langle \omega \rangle = \langle r \rangle - \langle q \rangle = \mu'/\gamma - C_1C_3C_4C_6C_7 \tag{4.29}$$

The long-term average runoff capture efficiency (also referred to as the runoff reduction rate or ratio), denoted as E_r, of an infiltration trench is defined as the fraction of runoff captured and processed by the trench over its lifetime of operation. E_r can be calculated as the ratio between the normalized mean long-term average outflow rate and the normalized mean long-term inflow rate, i.e.,

$$E_r = \frac{\langle q \rangle}{\langle r \rangle} = C_1C_3C_4C_6C_7\gamma\mu'^{-1} \tag{4.30}$$

Using equation (4.30), the long-term average runoff capture efficiency provided by a trench can be easily calculated. In addition, equation (4.26) can be used to analytically determine the long-term average amount of water stored in a trench, while equations (4.24) and (4.25) can be used to quantify the chances of having different water levels in a trench. The collection of these closed-form analytical equations is referred to as the analytical stochastic model (ASM) for infiltration trenches.

4.2.5 Three Possible Operating Conditions

Equation (4.11) is used to represent three possible operating infiltration conditions, the resulting analytical stochastic models are referred to as ASM I for the case with $\alpha_b \neq 0$ and $\alpha_s \neq 0$, ASM II for the case with $\alpha_b = 0$ and $\alpha_s \neq 0$, and ASM III for the case with $\alpha_b \neq 0$ but $\alpha_s = 0$. For ASM I, equations (4.24)-(4.30) themselves with α_b and α_s both greater than zero can be collectively used in the analysis of the hydrologic performance of infiltration trenches or other types of infiltration BMPs with infiltration through both their bottoms and sides. ASM II, which considers only infiltration from the sides of a trench, is obtained by setting the bottom clogging factor $\alpha_b = 0$ in equation (4.11). Analytical equations for ASM II are the same as for ASM I except that C_2 is simplified to be equal to $\left(E_a + \alpha_b f_b\right) / \left(C_1 S_m\right)$ in ASM II as $\alpha_b = 0$. As noted earlier, analytical solutions of the stochastic water balance equation and average runoff capture efficiency presented in sections 4.2.3 and 4.2.4 are only valid for ASM I and II where $\alpha_s > 0$.

ASM III which considers infiltration only through the bottom of a trench is obtained by setting the side clogging factor $\alpha_s = 0$. The outflow rate function of ASM III is shown in equation (4.11) with $\alpha_s = 0$. The $h(s)$ for ASM III is not the same as described by equation (4.23) but it can still be derived from equations (4.21) and (4.22). Derivation of the analytical solutions for ASM III is different from that for ASMs I and II because $q(s)$ is no longer a linear increasing function of s but remains constant for $s > 0$. This constant outflow function of ASM III for an infiltration trench has mathematically the same format as that for a combined sewer detention tank with a constant outflow rate (Wang and Guo, 2018). Adapting from the solutions provided in Wang and Guo (2018), the runoff capture efficiency E_r, the normalized average water content $\langle s\rangle$, the probability mass associated with empty storage f_0, the probability density function $f(s)$ for $s > 0$, and the cumulative distribution function $H(s)$ of s for ASM III can be expressed as follows:

$$E_r = \begin{cases} \zeta / \left(\zeta + \phi / S_m \right), & \mu' = \eta\gamma \\ \dfrac{\zeta G}{\phi \mu'} \left\{ 1 - \dfrac{\mu'/G - \zeta/\phi}{\left(\mu'/G \right) \exp\left[\left(\mu'/G - \zeta/\phi \right) S_m \right] - \zeta/\phi} \right\}, & \mu' \neq \eta\gamma \end{cases} \tag{4.31}$$

$$\langle s \rangle = \begin{cases} \gamma / \left[2\left(\gamma + 1 \right) \right], & \mu' = \eta\gamma \\ \dfrac{\gamma + 1}{\left(\mu'/\eta \right) \exp\left(\mu'/\eta - \gamma \right) - \gamma} - \dfrac{1}{\mu'/\eta - \gamma} + 1, & \mu' \neq \eta\gamma \end{cases} \tag{4.32}$$

$$f_0 = \begin{cases} 1/(\gamma+1), & \mu' = \eta\gamma \\ (\mu'/\eta-\gamma)/\left[(\mu'/\eta)\exp(\mu'/\eta-\gamma)-\gamma\right], & \mu' \neq \eta\gamma \end{cases} \quad \text{for } s=0 \tag{4.33}$$

$$f(s) = \begin{cases} \gamma/(\gamma+1), & \mu' = \eta\gamma \\ \dfrac{\mu'/\eta-\gamma}{\left[\exp(\mu'/\eta-\gamma)-\gamma\eta/\mu'\right]}\exp\left[(\mu'/\eta-\gamma)s\right], & \mu' \neq \eta\gamma \end{cases} \quad \text{for } 0<s\leq 1 \tag{4.34}$$

$$H(s) = \begin{cases} (\gamma s+1)/(\gamma+1), & \mu' = \eta\gamma \\ \dfrac{(\mu'/\eta)\exp\left[(\mu'/\eta-\gamma)s\right]-\gamma}{(\mu'/\eta)\exp(\mu'/\eta-\gamma)-\gamma}, & \mu' \neq \eta\gamma \end{cases} \tag{4.35}$$

where $G = E_{a+}\ \alpha_b f_b$; $\eta = G/S_m$. Although not for the same purpose, Wang and Guo (2018) already provided detailed derivations of equations (4.31) through (4.35) and demonstrated why for systems where $\mu' = \eta\gamma$ and $\mu' \neq \eta\gamma$ the solutions are different. Although the form of analytical equations in ASM III used for infiltration trenches is the same as that in Wang and Guo (2018) used for detention tanks, the ASM III contains more design parameters than the analytical model in Wang and Guo (2018) and the explicit expressions of some design parameters between them are different. In addition to infiltration trenches, equations (4.31) through (4.35) can also be used for infiltration basins and bioretention cells where infiltration through the bottom is the most predominant.

4.3 Example Study Areas and Input Data

Clearly, with changes made to the definitions of some of the variables and parameters, the above derived ASMs can be used for many different types of infiltration-based BMPs. However, for clarity in explanation, the following example and verification studies still focus on infiltration trenches. The Storm Water Management Model (SWMM) is widely used tool for modelling the stormwater best management practices (Avellaneda et al., 2017). To demonstrate the accuracy of the proposed ASMs, a set of continuous SWMM (U.S. EPA Version 5.1, Rossman, 2015) simulations were performed for urban catchments with different types of soils (loam, sandy loam and sand), and different infiltration conditions (ASMs I, II and III). Hypothetical catchments were assumed to be located in two climatically different locations in the U.S.: Jackson, Mississippi with a humid climate, and Billings, Montana with an arid climate. In the SWMM simulations, long-term hourly rainfall records of Jackson and Billings obtained from the National Climatic Data Center (NCDC) of the U.S. are used as input rainfall series and their rainfall statistics are shown in Table 4.1. The rainfall event characteristics in Table 4.1 are required for the use of ASMs.

Table 4.1 Climatic statistics of two test locations

Station	Record Length	Non-winter Months	MIET (h)	$\langle v \rangle$ (mm)	$\langle u \rangle$ (hr)	$\langle b \rangle$ (hr)	E_a (mm/d)	Annual Precipitation (mm)	Climate Condition
Jackson	1964-2013	Jan.-Dec.	12	19.20	10.11	111.58	2.37	1375	Humid
Billings	1967-2013	Apr.-Oct.	12	7.57	10.43	135.26	3.38	347	Arid

Notes: The evaporation rates are obtained from NOAA (1982). Annual precipitation data are obtained from NOAA (2011). Humid climate usually has an annual precipitation greater than 750 mm while arid climate usually has an annual precipitation less than 400 mm (Raghunath, 2006). Rainfall event statistics of Jackson and Billings are obtained from Wang et al. (2019).

The accuracy of the ASMs are examined by comparing their results with those from SWMM continuous simulations. The long-term average runoff capture efficiency determined by SWMM simulations is calculated as $\left(V_{SWMM} - O_{SWMM}\right)/V_{SWMM}$, where V_{SWMM} and O_{SWMM} are respectively the total runoff volume and total overflow volume determined from SWMM continuous simulation results. The values of parameters used in the SWMM simulations are listed in Table 4.2. ϕ is assumed to be 1 for the contributing catchments of infiltration trenches in case studies. To simplify the illustration of the application and verification of ASMs, f_b and f_s are treated as equal to the saturated hydraulic conductivity of soils, which are 6, 13, and 30 mm/h for loam, sandy loam and sandy soils, respectively (Guo and Gao, 2016). Both α_b and α_s are assumed to be 0.8. It should be noted that the SWMM LID module of infiltration trenches is not capable of simulating infiltration from the sides of trenches. As an alternative, we used a storage unit representing the trench with a total storage capacity of S_c. The outflow is controlled by an orifice with a specified rating curve, the same as what is described by equation (4.10). This way, outflows from this storage unit are equivalent to the outflows from infiltration trenches. The inflows collected by the storage unit are from two subcatchments in the SWMM model, one representing the adjacent contributing catchment area and the other representing the trench surface area where rainfall falls directly.

Table 4.2 Input parameters used in ASM and SWMM simulations

Parameter	SWMM simulations	ASM
Trench Width, W (m)	1	1
Trench Length, L (m)	2	2
Storage Reservoir Depth, D_m (mm)	50-1500	50-1500
Area Ratio, R_a	1-50	1-50
Void Ratio, R_v	0.4	0.4
Depression Storage of Catchment, S_{dc} (mm)	2	2
Depression storage of trench surface, S_{dt} (mm)	1	1
Catchment Slope, S_l (%)	1	N/N[a]
Simulation time step (min)	5	N/N[a]

[a]The parameter is not needed.

4.4 Verification of the Analytical Stochastic Models

4.4.1 Overall Accuracy of the Analytical Stochastic Models

Using equation (4.14) to estimate S_m, three different ASMs were developed for infiltration trenches with different infiltration conditions. To verify the accuracy of ASMs for all possible field conditions, a comprehensive set of hypothetical cases with different characteristics are simulated by SWMM and calculated using ASMs. For a specific soil type and location, 32 cases representing a combination of two different values of R_a (10 and 50) and 16 different values of D_m (50, 100, 200, …, 1500 mm) were simulated. In addition, 24 cases formed by a combination of two different values of D_m (500 and 1000 mm) and 12 different values of R_a (1, 2.5, 5, 10, …, 50) for one specific soil type and location were also simulated. Two locations (Jackson and Billings) and three different soil types (loam, sandy loam and sand) are considered for all the above described combinations, resulting in a total of 324 cases for each ASM models. Therefore, for the verification of the three ASM models, a total of 972 cases were simulated by SWMM and compared with ASM results. For each of these three ASMs, their overall performance for 324 cases are presented in Fig. 4.2.

Treating the continuous simulation results of SWMM as the observed data, root mean square error (RMSE), Nash-Sutcliffe model efficiency coefficient (NSE) and correlation coefficient (CC) between observed and ASM model results can all be calculated. In reality, SWMM models themselves would only provide accurate results when they are properly calibrated against observed data. In this study, since SWMM models do not require the simplifications needed by the ASMs, given enough data for calibration, it is assumed that the SWMM models can be properly calibrated and can provide results that are very close to observed data. The SWMM models that were set up here for hypothetical cases are treated as based on calibrated parameter values and therefore provide results close to observed data. As shown in Fig. 4.2, the values of NSE and CC are very close to 1 and the values for RMSE are close to 0 for all the three models. These statistical indices demonstrate that ASM results resemble well SWMM continuous simulation results for a wide range of possible operating conditions. Some of the modeled extreme operating conditions may not be recommended for infiltration trenches, but they are possible or recommended for other type of infiltration-based BMPs. Including a wide range of cases in this verification study helps in illustrating that the developed ASMs are reliable for estimating the runoff capture efficiencies of all types of infiltration-based BMPs.

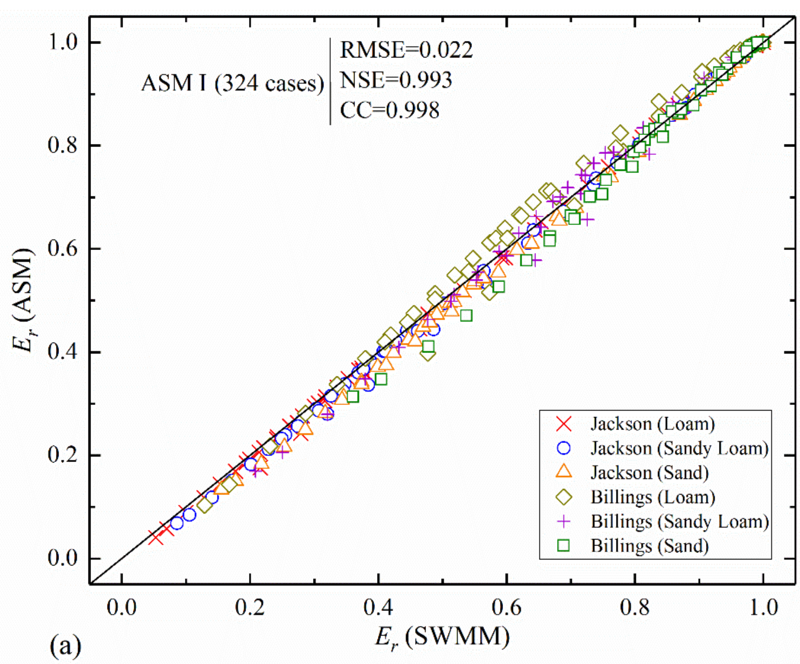

(a)

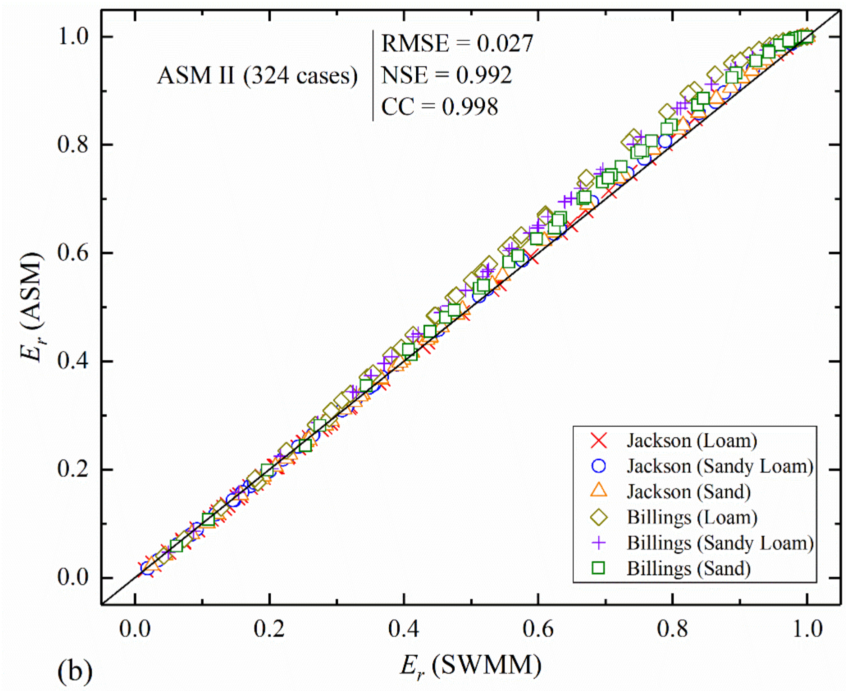

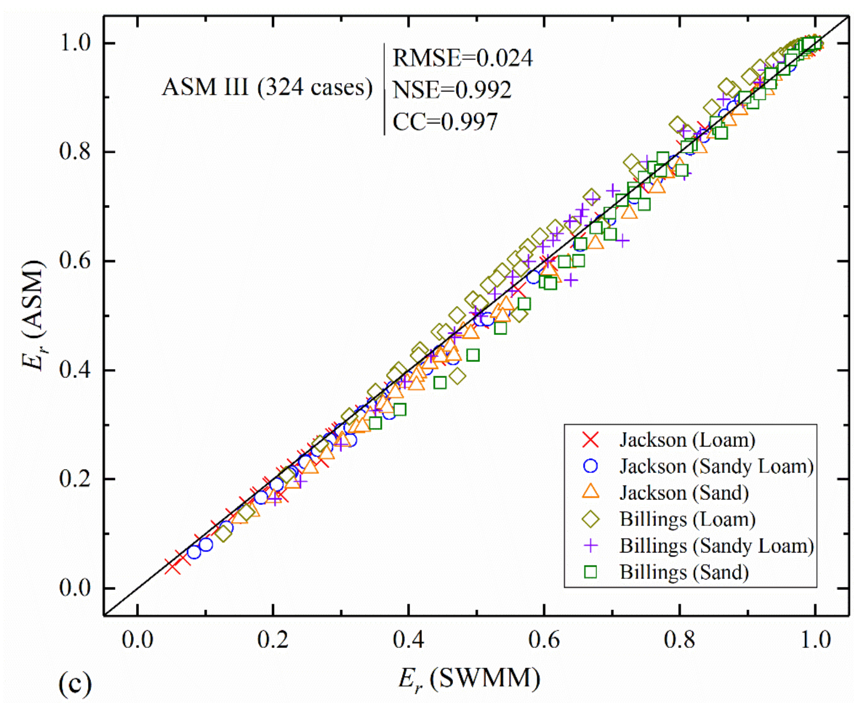

Fig. 4.2 Overall accuracy of runoff capture efficiencies estimated by the analytical stochastic models

4.4.2 Effects of Storage Reservoir Depth, Soil Types and Area Ratios

The depth of the storage reservoir D_m determines the storage capacity of a trench, which affects directly the overflow volumes. The effects of D_m on runoff capture efficiencies were investigated. Given an area ratio R_a=10, a total of 48 cases for three soil types (loam, sandy loam and sand) using ASM I at Jackson were simulated. Comparison between ASM and SWMM results is presented in Fig. 4.3. The runoff capture efficiency increases when D_m increases. Higher runoff capture efficiencies were achieved for soil types with greater infiltration capacities. The largest absolute relative difference between ASM and SWMM results is 17.7% which is from the case with loam soil when D_m is equal to 50 mm. Close agreement between the two models can be observed from Fig. 4.3.

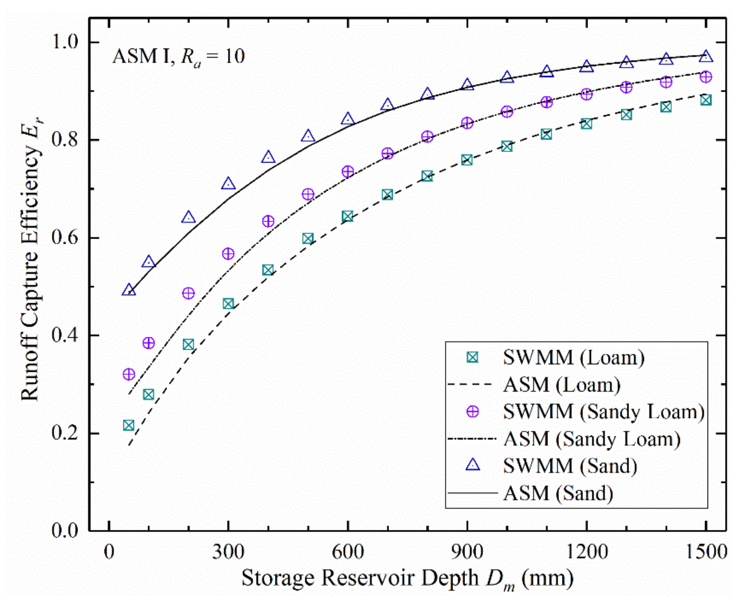

Fig. 4.3 Comparison of runoff capture efficiencies with different storage reservoir depths at Jackson

For an infiltration trench with a specific size, the area ratio R_a determines the contributing catchment area and therefore the inflow volume. ASM II and simulation results are presented for two values of D_m (i.e., 500 and 1000 mm) for demonstration purposes. For each value of D_m, a total of 24 cases for a combination of two soil types (loam and sand) and 12 area ratios (R_a = 1, 2.5, 5, 10, …, 50) at Billings were simulated and plotted in Fig. 4.4. Runoff capture efficiency increases with a decrease of the area ratio or an increase of the infiltration capacity of soils. The largest absolute relative difference between ASM and SWMM is 10.0% which is from the case with loam soil when D_m is equal to 1000 mm and R_a approaches 30. Overall, the ASM results agree well with SWMM results for all 48 cases as shown in Fig. 4.4. Soils with larger infiltration capacities result in less overflows and provide larger runoff capture efficiencies.

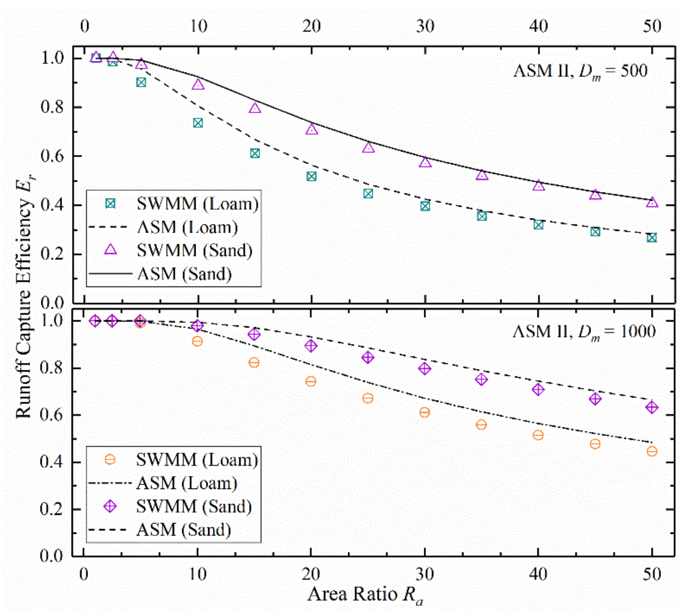

Fig. 1.4 Comparison of runoff capture efficiencies with different area ratios at Billings

4.4.3 Effects of Climate Conditions

Two representative climatic conditions, i.e., humid Jackson and arid Billings, were simulated. Effects of climate conditions on runoff capture efficiency can be analyzed from the plotted E_r versus D_m and R_a curves in Fig. 4.5. For sandy loam soils with a D_m of 500 mm, 24 cases with different values of R_a obtained from ASM III at the two locations were simulated. For the same D_m and R_a, the runoff capture efficiency obtained at Billings is generally larger than that at Jackson. When R_a is small, taking $R_a \leq 2.5$ at Jackson and $R_a \leq 10$ at Billings as examples, the runoff capture efficiencies are very close to 1 ($E_r > 0.9$), indicating that runoff contributed from catchments with such area ratios will be almost completely captured by the infiltration trenches. As R_a increases, E_r decreases and finally stabilizes at about 0.21 at Jackson and 0.43 at Billings, respectively, when R_a approaches 50.

In addition, when the soil type is sand and R_a equals 10, ASM II results for 32 cases with various D_m values were compared with SWMM results and also shown in Fig. 4.5. Similar conclusions of the effects of climatic conditions can also be reached. The arid climate conditions of Billings result in larger runoff capture efficiencies. The runoff capture efficiency of Billings increases sharply from 0.25 to 0.92 as D_m increases from 50 to 600 mm, therefore it rises slowly to 0.99 and stays at 0.99 when D_m exceeds 1200 mm. For

Jackson, a smooth increasing trend of the runoff capture efficiency from 0.10 to 0.93 as D_m goes up from 50 to 1500 mm is clear. Good agreements can also be observed in Fig. 4.5, which demonstrates again the accuracy of ASMs II and III.

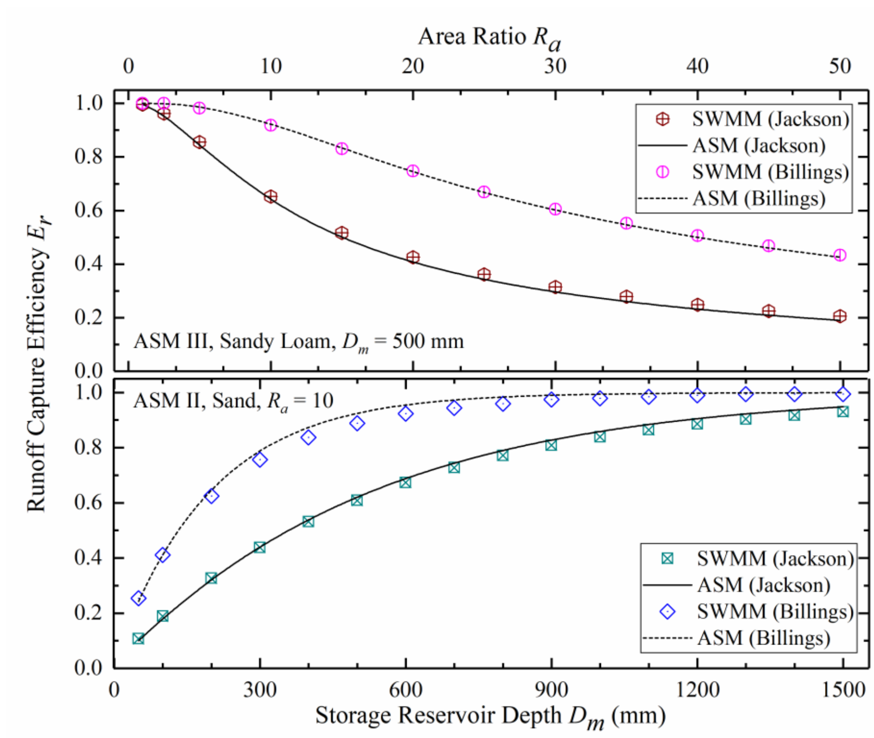

Fig. 4.5 Comparison of runoff capture efficiency curves between two locations

4.4.4 Additional Analysis

In addition to runoff capture efficiency, ASMs can provide many other useful performance indicators which cannot be directly provided by continuous simulation models. Example indicators may include the chance of having an empty trench and the long-term average water level inside a trench. The chance of having an empty trench, or equivalently the fraction of time when the trench is empty is equal to the probability of having s = 0, which is denoted as f_0 and can be directly calculated using equation (4.33). The long-term average water level inside a trench is simply the average degree of saturation $\langle s \rangle$ multiplied by D_m. In fact, the PDF of s, f(s), and the cumulative distribution function H(s) provide even more detailed information about the wetness that a trench experiences in its operation. Together they help designers gain a better understanding of the wetness characteristics varying with soil types, climate conditions, land use conditions and storage capacity. Using equations (4.24)-(4.26) and (4.32)-(4.35), ASMs can easily provide this kind of useful information, example results are presented in Fig. 4.6.

Using ASM I for Jackson with D_m = 1000 mm and R_a =10, probability distributions of s and the average degree of saturation $\langle s \rangle$ varying with three soil types were obtained and plotted in Figs. 5a and 5b. For sandy loam soils at Jackson and Billings, taking D_m = 500 mm as an example, Figs. 5c and 5d show the analytical results of the probability distributions of s and $\langle s \rangle$ obtained by using ASM II. An increase in area ratio results in an increase in $\langle s \rangle$ for all soil types and locations. It is worth noting that $\langle s \rangle$ are very small and f_0 are quite high for all cases. This demonstrates that infiltration trenches as usually designed at these two locations are indeed capable of infiltrating captured runoff and are usually in a state of being almost empty when a rainfall event randomly occurs. Fig. 4.6

also shows that sandy soils and Billings' climate result in higher chances of having empty trenches (i.e., higher f_0 values). As area ratio increases, the chance of having empty trenches decreases and gradually stabilizes when R_a approaches 50. These additional analysis results may not seem to be that useful for infiltration trenches, but for infiltration basins and bioretention systems where the growing conditions of plants inside the facilities are also a major concern, these additional results will be very helpful.

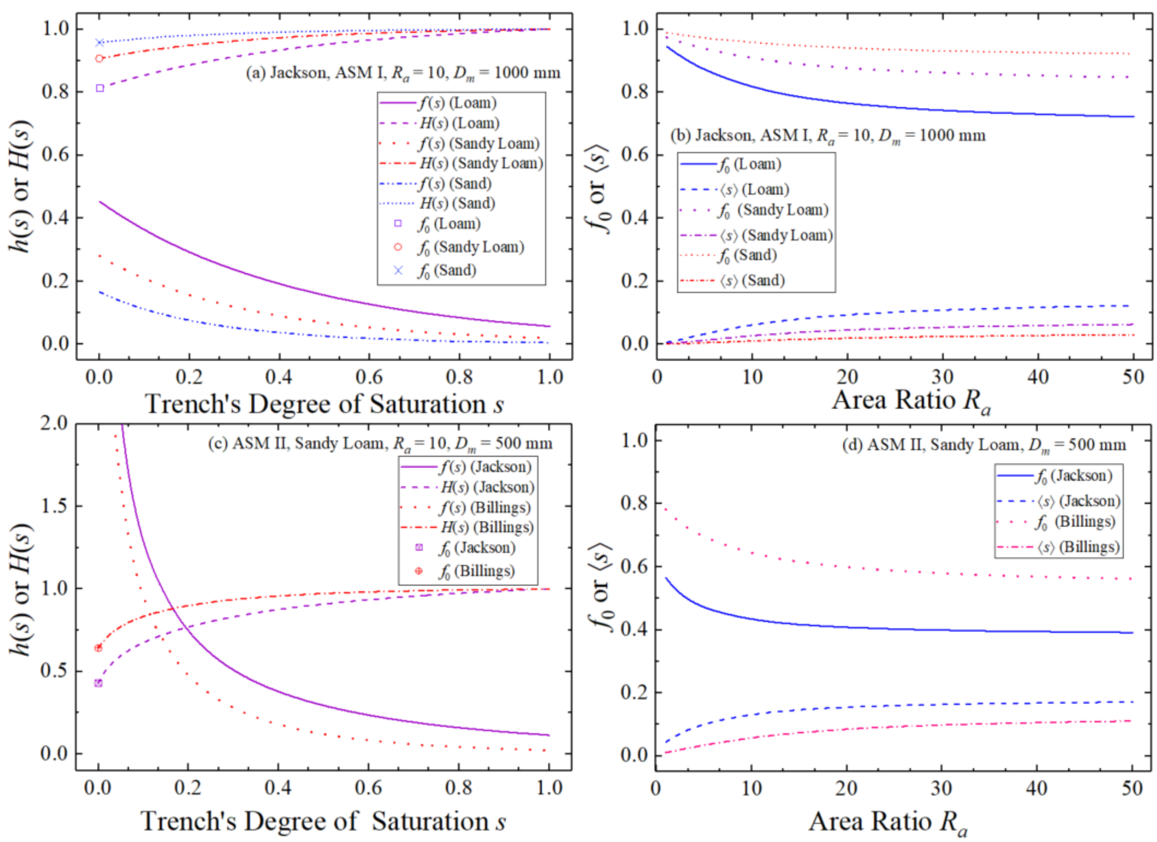

Fig. 4.6 Probability distributions of infiltration trenches' degree of saturation

4.5 Concluding Remarks

In this paper, three analytical stochastic models (ASMs) considering different operating conditions of infiltration-based stormwater best management practices (BMPs) were developed. Runoff capture efficiency, chance of having empty facilities and the average water content inside a facility can all be analytically determined using the closed-form equations comprising the ASMs. Effects of soil types, area ratios, sizes of storage reservoirs, and climate conditions on the performance of infiltration facilities can all be easily and systematically investigated using these ASMs. The accuracy of ASMs were verified by comparing their results with SWMM continuous simulation results. The comparisons demonstrate that the ASMs can provide reliable and accurate results for almost all possible design configurations. The ASMs are therefore recommended for use in the planning, design, and evaluation of the infiltration-based BMPs with any of the three possible operating conditions.

Acknowledgements: This work was supported by the Natural Sciences and Engineering Research Council of Canada and the Canadian Mitacs Accelerate Program. The data used in this study are listed in the tables or obtained from the citied references.

References

Adams, B. J., and Papa, F. (2000). *Urban stormwater management planning with analytical probabilistic models*. New York: Willy.

Akan, A. O. (2002). Sizing stormwater infiltration structures. *Journal of Hydraulic Engineering*, 128(5), 534-537.

Avellaneda, P. M., Jefferson, A. J., Grieser, J. M., and Bush, S. A. (2017). Simulation of the cumulative hydrological response to green infrastructure. *Water Resources Research*, *53*(4), 3087–3101.

Barraud, S., Gonzalez-Merchan, C., Nascimento, N., Moura, P., and Silva, A. (2014). A method for evaluating the evolution of clogging: Application to the Pampulha Campus infiltration system (Brazil). *Water Science and Technology*, *69*(6), 1241–1248.

Bergman, M., Hedegaard, M. R., Petersen, M. F., Binning, P., Mark, O., and Mikkelsen, P. S. (2011). Evaluation of two stormwater infiltration trenches in central Copenhagen after 15 years of operation. *Water Science and Technology*, 63(10), 2279–2286.

Bertassello, L. E., Rao, P. S. C., Park, J., Jawitz, J. W., and Botter, G. (2018). Stochastic modeling of wetland-groundwater systems. *Advances in Water Resources*, 112, 214–223.

Browne, D., Deletic, A., Mudd, G. M., and Fletcher, T. D. (2008). A new saturated/unsaturated model for stormwater infiltration systems. *Hydrological Processes*, 22(25), 4838–4849.

Campisano, A., Creaco, E., and Modica, C. (2011). A simplified approach for the design of infiltration trenches. *Water Science and Technology*, 64(6), 1362. https://doi.org/10.2166/wst.2011.170

Chahar, B. R., Graillot, D., and Gaur, S. (2011). Storm-water management through infiltration trenches. *Journal of Irrigation and Drainage Engineering*, 138(3), 274–281.

Cox, D.R., and Miller, D.H. (1965). *The Theory of Stochastic Processes.* New York, Willey.

Creaco, E., and Franchini, M. (2012). A dimensionless procedure for the design of infiltration trenches. *Journal-American Water Works Association*, 104(9), E501-E509. https://doi.org/10.5942/jawwa.2012.104.0124

D'Aniello, A., Cimorelli, L., and Cozzolino, L. et al. (2019). The Effect of Geological Heterogeneity and Groundwater Table Depth on the Hydraulic Performance of Stormwater Infiltration Facilities. *Water Resource Management* 33: 1147. https://doi.org/10.1007/s11269-018-2172-5

Duchene, M., McBean, E. A., and Thomson, N. R. (1994). Modeling of infiltration from trenches for storm-water control. *Journal of Water Resources Planning and Management*, 120(3), 276–293.

Eagleson, P. S. (1978). Climate, soil, and vegetation: 2. The distribution of annual precipitation derived from observed storm sequences. *Water Resources Research*, 14(5), 713–721.

Eckart, K., McPhee, Z., and Bolisetti, T. (2017). Performance and implementation of low impact development–a review. *Science of the Total Environment*, *607*, 413–432.

Emerson, C. H., and Traver, R. G. (2008). Multiyear and seasonal variation of infiltration from storm-water best management practices. *Journal of Irrigation and Drainage Engineering*, 134(5), 598–605.

Emerson, C. H., Wadzuk, B. M., and Traver, R. G. (2010). Hydraulic evolution and total suspended solids capture of an infiltration trench. *Hydrological Processes*, 24(8), 1008–

1014.

Fletcher, T. D., Andrieu, H., and Hamel, P. (2013). Understanding, management and modelling of urban hydrology and its consequences for receiving waters: A state of the art. *Advances in water resources*, 51, 261–279.

Freni, G., Mannina, G., and Viviani, G. (2009). Assessment of data availability influence on integrated urban drainage modelling uncertainty. *Environmental Modelling and Software,* 24(10), 1171–1181.

Gardiner, C. (2004). Handbook of stochastic methods: for physics, chemistry & the natural sciences (Series in synergetics, Vol. 13).

Gironás, J., Niemann, J. D., Roesner, L. A., Rodriguez, F., and Andrieu, H. (2009). Evaluation of methods for representing urban terrain in stormwater modeling. *Journal of Hydrologic Engineering*, 15(1), 1–14.

Guo, R., and Guo, Y. (2018). Analytical Equations for Use in the Planning of Infiltration Facilities. *Journal of Sustainable Water in the Built Environment*, *4*(2), 06018001. https://doi.org/10.1061/JSWBAY.0000849

Guo, R., Guo, Y., and Wang, J. (2018). Stormwater capture and antecedent moisture characteristics of permeable pavements. *Hydrological Processes*. 32(17), 2708–2720.

Guo, Y. (2016). Stochastic analysis of hydrologic operation of green roofs. *Journal of Hydrologic Engineering*, *21*(7), 04016016. https://doi.org/10.1061/(ASCE)HE.1943-5584.0001371

Guo, Y., and Gao, T. (2016). Analytical equations for estimating the total runoff reduction efficiency of infiltration trenches. *Journal of Sustainable Water Built Environment*, 2(3), 06016001. https://doi.org/10.1061/JSWBAY.0000809

Guo, Y., Liu, S., and Baetz, B. W. (2012). Probabilistic rainfall-runoff transformation considering both infiltration and saturation excess runoff generation processes. *Water Resources Research*, 48(6). https://doi.org/10.1029/2011WR011613

Hassini, S. and Guo, Y. (2016). Exponentiality test procedures for large samples of rainfall event characteristics. *Journal of Hydrologic Engineering*, 21(4), 04016003. http://dx.doi.org /10.1061/(asce)he.1943-5584.0001352

Hatt, B., Deletic, A., and Fletcher, T. (2007). Stormwater reuse: Designing biofiltration systems for reliable treatment. *Water Science and Technology*, 55(4), 201–209.

Lee, J. G., Borst, M., Brown, R. A., Rossman, L., and Simon, M. A. (2014). Modeling the hydrologic processes of a permeable pavement system. *Journal of Hydrologic Engineering*, 20(5), 04014070. https://doi.org/10.1061/(ASCE)HE.1943-5584.0001088

NOAA (National Oceanic and Atmospheric Administration). (1982). Mean monthly, seasonal, and annual pan evaporation for the United. States. http://www.nws.noaa.gov/oh/hdsc/PMP_related_studies/TR34.pdf.

NOAA (National Oceanic and Atmospheric Administration). (2011). 1981-2010 United States Climate Normals, National Climatic Data Center. https://www.ncdc.noaa.gov/cdo-web/datatools/normals.

Parolari, A. J., Pelrine, S., and Bartlett, M. S. (2018). Stochastic water balance dynamics of passive and controlled stormwater basins. *Advances in Water Resources*, 122, 328–339.

PDEP (Pennsylvania Department of Environmental Protection). (2006). Pennsylvania stormwater best management practices manual. Bureau of Watershed Management, Harrisburg, PA.

Pelak, N., and Porporato, A. (2016). Sizing a rainwater harvesting cistern by minimizing costs. *Journal of Hydrology*, 541, 1340–1347.

Raghunath, H.M. (2006). Hydrology: principles, analysis and design. New Age International.

Revitt, M., Ellis, B., and Scholes, L. (2003). Report 5.1 Review of the use of stormwater BMPs in Europe. Project under EU RTD 5th Framework Programme. WP5, 5.

Rodriguez-Iturbe, I., Entekhabi, D., and Bras, R. L. (1991). Nonlinear dynamics of soil moisture at climate scales: 1. Stochastic analysis. *Water Resources Research*, 27(8), 1899–1906.

Rodriguez-Iturbe, I., and Proporato, A. (2004), *Ecohydrology of water-controlled ecosystems*, UK: Cambridge University Press.

Rossman, L.A. (2015). Storm water management model user's manual. Version 5.1 (EPA-600/R-14/413b). National Risk Management Research Laboratory, Office of Research and Development, US Environmental Protection Agency, Cincinnati, US. https://www.innovyze.com/products/swmm/download/ZyPDF.pdf

Schueler, T. R., and Claytor, R. A. (2000). Maryland stormwater design manual. Maryland Department of the Environment. Baltimore, MD.

Siriwardene, N. R., Deletic, A., and Fletcher, T. D. (2007). Clogging of stormwater gravel infiltration systems and filters: Insights from a laboratory study. *Water Research*, 41(7), 1433–1440.

Szota, C., Coutts, A. M., Thom, J. K., Virahsawmy, H. K., Fletcher, T. D., & Livesley, S. J. (2019). Street tree stormwater control measures can reduce runoff but may not benefit established trees. *Landscape and Urban Planning*, 182, 144–155.

Credit Valley Conservation Authority and Toronto and Region Conservation Authority

(CVC and TRCA). (2010). Low impact development stormwater management planning and design guide, Ontario, Canada. https://cvc.ca/wp-content/uploads/2014/04/LID-SWM-Guide-v1.0_2010_1_no-appendices.pdf

U.S. Environmental Protection Agency (USEPA). (1986). *Methodology for analysis of detention basins for control of urban runoff quality*. *Rep. EPA*, *440*/5-87-01 (NTIS No. PB87-116562), Washington, D.C.

Wang, J., and Guo, Y (2018). An analytical stochastic approach for evaluating the performance of combined sewer overflow tanks. *Water Resources Research*, 54(5), 3357–3375.

Wang, J., and Guo, Y (2019). Stochastic analysis of storm water quality control detention ponds. *Journal of Hydrology*, 571, 573–584.

Wang, J., Zhang, S., and Guo, Y. (2019). Analyzing the impact of impervious area disconnection on urban runoff control using an analytical probabilistic model. *Water Resources Management*, 33(5), 1753–1768.

Warnaars, E., Larsen, A. V., Jacobsen, P., and Mikkelsen, P. S. (1999). Hydrologic behaviour of stormwater infiltration trenches in a central urban area during 2¾ years of operation. *Water Science and Technology*, 39(2), 217. https://doi.org/10.1016/S0273-1223(99)00026-8

WEF and ASCE/EWRI (Water Environment Federation and Environmental and American Society of Civil Engineers/Environmental & Water Resources Institute). (2012). Design of Urban Stormwater Controls, McGraw-Hill, New York.

Woods-Ballard, B., Kellagher, R., Martin, P., Jefferies, C., Bray, R., and Shaffer, P. (2007). The DUDS Manual (Vol. 697). London: Ciria.

Zhang, K., Che, W., Zhang, W., and Zhao, Y. (2016). Discussion about initial runoff and volume capture ratio of annual rainfall. *Water Science and Technology*, 74(8), 1764–1772.

Zhang, S., and Guo, Y. (2014). Stormwater capture efficiency of bioretention systems. *Water Resources Management*, 28(1), 149–168.

Chapter 5

Proper Sizing of Infiltration Trenches Using Closed-form Analytical Equations

Jun Wang and Yiping Guo

Abstract: Infiltration trenches in urban areas are mainly used for the purposes of water balance maintenance and water quality improvement. To ensure that a high enough fraction of runoff from a contributing catchment would be infiltrated through an infiltration trench, the trench is usually sized to provide enough storage capacity so that runoff from a storm of certain depth can be temporarily contained inside the trench. Since it is difficult to verify the actual long-term average runoff control performance of individual trenches, their exact long-term average performance is often unknown. In this study, previously derived analytical equations are used to verify the actual performance of infiltration trenches. Locations of Atlanta, Georgia and New Durham, New Hampshire, U.S., infiltrations through both the sides and bottom of a trench, restrictions on the ratio between catchment area and trench bottom area, and restrictions on the trench depth are all considered. The effects of soil infiltration rate, trench width, drain time, operating conditions on the long-term average performance of infiltration trenches are investigated. The analytical equations are recommended as a useful tool that can be used for the proper sizing of infiltration trenches so that a uniform and consistent long-term average performance can be achieved for all individual cases.

Key Words: Analytical stochastic model; Infiltration trench; Side infiltration; Water quality volume; Stormwater management.

5.1 Introduction

Urban stormwater best management practices (BMPs) for water quality control and low impact development (LID) techniques are used to capture and treat runoff generated under small and frequently occurring rainfall events (USEPA, 2011). The concept of first flush for water quality control was originally introduced in the 1970s (Sartor and Boyd, 1972). First flush runoff occurring in the early stages of a rainfall event carries with it relatively high concentrations of pollutants (Baek et al., 2015). Properly sized BMPs and LIDs can effectively reduce pollutants carried by first flushes through retention, detention or flow-through treatment processes. Water quality capture volume (WQCV) was proposed as a sizing criterion for BMPs and LIDs to reduce the majority of pollutants resulting from all storm events (WEF and ASCE, 1998; Guo and Urbonas, 2002; Park et al., 2013). WQCV is usually defined as the amount of stormwater runoff from a rainfall event that should be captured and treated over a prescribed period of time (Burack et al., 2008). Other terminologies equivalent or similar to WQCV are also used in different jurisdictions, e.g., water quality volume is used in New Hampshire, U.S. (Burack et al., 2008) and Minnesota, U.S. (MPCA, 2005), runoff reduction volume is used in Georgia, U.S. (AMEC, 2014), and runoff volume control target is used in Ontario, Canada (ABL and EI, 2016). The WQCV concept and the sizing procedure based on it have been widely adopted in practices and are described in the BMP/LID (simply referred to as LID hereafter) design guidance manuals of many jurisdictions across North America (WEF and ASCE, 1998; Clar et al., 2004; CVC and TRCA, 2010).

Two types of methods can be used to determine the required WQCV. The first type is based on a specific initial runoff depth and the second type is based on a required runoff reduction ratio (USEPA, 2011; ABL and EI, 2016; Zhang et al., 2016). Since LIDs are mainly used in highly impervious areas, runoff depth is often treated as approximately equal to the input rainfall depth by some jurisdictions. The initial runoff depth that should be captured by an LID is generally determined based on the observation that a certain amount of initial runoff from a rainfall event actually contains the vast majority of pollutants that will result from that rainfall event. The runoff reduction ratio is defined as the average ratio between the annual runoff volume captured by the LID and the total annual runoff volume. A summary of WQCV targets or similar design standards for a large number of jurisdictions in the U.S., Canada, England, France, Netherland, New Zealand and China can be found in ABL (2016), ABL and EI (2016), MOECC (2017), USEPA (2011) and Zhang et al. (2016). The "specific initial runoff depth rule" is the preferred standard used in the majority of these jurisdictions. As an example of the second type of methods for the determination of WQCV, the approach using the volume capture ratio of annual rainfall as the control target for sizing LIDs in China was described in Zhang et al. (2016).

Examples of the "specific initial runoff depth rule" mainly includes "1-inch rule" and "0.5-inch rule" depending on the site-specific conditions in different jurisdictions. The "1-inch rule" (i.e., the WQCV should be equal to the volume of runoff generated from the first 1-inch of rainfall) was widely accepted because it was found that, for many locations, about 90% of all rainfall events have depths less than or equal to 1 inch (MPCA, 2005). LIDs should be properly sized so that they have capacity to capture a 1-inch storm and can treat, on average, about 90% of runoff volumes generated from the contributing catchment (Claytor and Schueler, 1996). The 1-inch rainfall event is referred to as the 90th percentile rainfall event (Claytor and Schueler, 1996; ABL and EI, 2016). The required WQCV can then be calculated as runoff generated from the contributing catchment under this 90th percentile rainfall event. After conducting more detailed rainfall frequency analysis, different jurisdictions may set rainfall event depth different from 1 inch as their local 90th percentile or different percentile storm event.

The "0.5-inch rule" is also used in some jurisdictions of the U.S. (Sharifi et al., 2011; USEPA, 2011; Daly et al., 2014), similarly it assumes that 90% of a runoff event's total pollutant load is transported in the first half inch of runoff (Bach et al., 2010). Other "specific initial runoff depth rules" are followed in other jurisdictions such as 0.52 inches for Alaska, 0.75 inches for Ohio, 1.2 inches for Georgia, 1.25 inches for Iowa, a range between 0.8 and 1.2 inches for New York, U.S. (USEPA, 2011), a range between 4 and 8 mm for China (Zhang et al., 2016), and a range between 16.7 to 43 mm for New Zealand (ABL, 2016). It is noted that the 90th or other percentile rainfall events are used for sizing LIDs at a location of interest, these rainfall events are sometimes referred to as the water quality control design storms or simply water quality storms. For example, Georgia, U.S., sets the control target as 1.2 inches which is equivalent to the 85th percentile storm event depth (Haubner, 2001), the 91st percentile storm is set by Washington as its water quality storm, and the 80th percentile storm is set for Kentucky (USEPA, 2011).

Converting the water quality design storm depth to WQCV based on the "specific initial runoff depth rule" for sizing LIDs follows essentially the design storm approach. This design storm approach is valid and acceptable based on the assumption that LIDs sized to capture runoff from the water quality design storm would indeed capture and treat the required percentage of total runoff from the contributing catchment regardless of differences in individual design cases. Only when the required fraction of total runoff is treated, the majority of pollutants from the site may be removed. However, when using the design storm approach for sizing LIDs, the actual fraction of total runoff that will be treated by the individual LIDs is usually not verified. It is worth noting that the relationship between the specific initial runoff depth captured and the corresponding fraction of total runoff reduced/treated is not clear and is not determined in many design manuals. This is because this relationship is site-specific and influenced by climate, soil and land use conditions. Although the "specific initial runoff depth rule" is widely used in LID design for its simplicity (Sharif et al., 2011), some researchers (e.g., Chang et al., 1999; Bach et al., 2010; Daly et al., 2014; Zhang et al., 2016) have found that the "specific initial runoff depth rule" has its limitations. The ambiguous definition of first flush and arbitrary selection of the initial runoff depth can lead to different designs of LIDs (Daly et al., 2014).

On the other hand, the "runoff reduction ratio rule" can be more easily and clearly specified compared to the "specific initial runoff depth rule." Different reduction ratios of mean annual storm volumes are required by different jurisdictions, for example, 80% is required by Oregon, U.S. (USEPA, 2011), 90% is required by Vermont, U.S. (USEPA, 2011) and British Columbia, Canada (MOECC, 2017). For infiltration or other retention type LIDs, the fraction of total runoff that is treated by these facilities is the same as the fraction of total runoff reduced, i.e., infiltrated by these facilities. The fraction of total runoff reduced is also referred to as the long-term runoff reduction ratio or simply runoff reduction ratio. The runoff reduction ratio may not be equal to the percentile of the design storm event for all cases because of the differences in rainfall-runoff transformations over different catchments and different runoff routings through different LID facilities.

Continuous simulations take the entire observed long-term rainfall record (including both rainfall and dry periods) as input to the hydrologic model of the catchment and its LID, the inflows into and outflows from the LID over the period of record are all numerically determined, the long-term average runoff reduction ratio can then be calculated from the inflow and overflow statistics over the long term. Compared to the design storm approach, continuous simulation can provide more reliable and accurate estimates of the performance statistics of LIDs. That is why Guo et al. (2014) proposed a continuous simulation model (WQ-COSM) to calculate long-term runoff reduction ratios for LID facilities. Continuous simulation models such as QUALHYMO or SWMM are recommended for the proper sizing of LIDs in British Columbia, Canada (GVSDD, 2012). Recognizing the difficulties and time-consuming nature of continuous simulations, two simpler sizing approaches were also accepted in British Columbia (GVSDD, 2012): sizing for a specific runoff capture depth from a 24-hour rainfall event and sizing for a percentage of capture of average annual rainfall. The latter approach requires the use of charts plotting the relationship between the annual rainfall capture percentage and the trench depth, these charts are prepared based on continuous simulation results.

In addition to design storm and continuous simulation approaches, the analytical stochastic models (ASMs) (Guo, 2016; Pelak and Porporato, 2016; Guo et al., 2018; Parolari et al, 2018; Wang and Guo, 2018, 2019a, 2019b) provide a new appealing approach to estimating the long-term average performance of LIDs. ASMs are comprised of closed-form analytical equations and using those equations the long-term average runoff duction ratio of a specific design case can be easily determined and therefore the "runoff reduction ratio rule" can be more easily enforced. Application of ASMs is more time-saving and less data-demanding compared to the continuous simulation approach yet provides results as accurate as continuous simulations. In the application of ASMs, continuous rainfall inputs are represented as a marked Poisson process, long-term average inflows, outflows and runoff reduction ratios are analytically derived based on the stochastic water balance equation of the LID.

Infiltration trench is an example type of LIDs used to receive, store and infiltrate stormwater runoff generated from adjacent impervious areas such as roofs, driveways and parking lots (Chahar, et al., 2011; Guo and Gao, 2016). Wang and Guo (2019b) developed a set of ASMs for analyzing infiltration trenches which consider infiltration through the bottom and the sides of a trench. The accuracy of these ASMs were verified by comparing the analytical results with continuous simulation results. The aim of this paper is to demonstrate the application of these ASMs and its usefulness for sizing infiltration trenches. Following the design requirements and procedures specified in guidance manuals of two example jurisdictions, ASMs are applied to test the accuracy of the conventional design-storm based sizing approach. Recommendations are made for the improvement on the sizing of infiltration trenches.

5.2 Methods

5.2.1 Stochastic Characterization of Rainfall Event Series

In the statistical analysis of rainfall characteristics, historical rainfall records are discretized into event-by-event series by specifying a proper minimum inter-event time (MIET) and minimum rainfall event depth (Adams and Papa, 2000; Hassini and Guo, 2016). The separated rainfall event and inter-event dry period series is then represented as a marked Poisson process, this process is comprised of the point rainfall event pulses occurring at different inter-arrival times (i.e., the actual rainfall event duration is shortened as pulses and the inter-event time between this rainfall event and the subsequent rainfall event plus the rainfall event duration is the corresponding inter-arrival time). The two major characteristics used for ASMs are rainfall event depth (v) and the inter-arrival time (m); their probability distributions can be approximated by the following exponential probability density functions (Eagleson, 1978; Rodriguez-Iturbe and Proporato, 2004; Wang and Guo, 2019 a, 2019b):

$$f_V(v) = \zeta \, \mathrm{e}^{-\zeta v} \qquad v > 0 \tag{5.1}$$

$$f_M(m) = \mu \, \mathrm{e}^{-\mu m} \qquad m > 0 \tag{5.2}$$

where $\zeta = 1/\langle v \rangle$ and $\mu = 1/\langle m \rangle$ are the distribution parameters, $\langle v \rangle$ and $\langle m \rangle$ are the mean rainfall event depth and the mean inter-arrival time, respectively.

5.2.2 Stochastic Water Balance of Infiltration Trenches

The inflows into an infiltration trench include both the runoff generated from the contributing catchment and the rainfall directly fallen on the surface of the trench. The general form of the inflow event depth v_i of an infiltration trench can be expressed as (Wang and Guo, 2019b)

$$v_i = \begin{cases} 0, & v \le S_d \\ (1+\phi R_a)(v - S_d), & v > S_d \end{cases} \tag{5.3}$$

where ϕ is the composite runoff coefficient of the catchment, $S_d = (R_a S_{dc})/(R_a + 1)$ is the lumped area-weighed depression storage of the trench system expressed in depth (mm) over the trench bottom area; R_a is the ratio between the catchment area and the trench bottom area; S_{dc} is the depression storage of the catchment, mm. For simplicity of derivations, the normalized inflow event depth r which is equal to v_i/S_m is used, the resulting r series can also be described by a Poisson process with the arrival rate of μ' with $\mu' = \mu\,\mathrm{e}^{-S_d \zeta}$. The derived probability density function (PDF) of r, $f_R(r)$, can be expressed as $f_R(r) = [\zeta S_m/(1+R_a)]\mathrm{e}^{-[\zeta S_m/(1+R_a)]r}$ for $r > 0$ (Wang and Guo, 2019b). Let y be the normalized net inflow event depth into a trench resulting from a rainfall event, this y will be bounded by s, i.e., $0 \le y \le 1 - s$, where s is the fraction of the trench storage that is still occupied by water at the beginning of the rainfall event, s is referred to as the initial degree of saturation of the trench (Wang and Guo, 2019b). It is noted that only part of r is converted to y stored in the trench since overflows may occur. The PDF of y, $P_{Y|S}\left[y|s\right]$, is equal to $\gamma e^{-\gamma y} + e^{-\gamma(1-s)}\delta(y+s-1)$, where $\delta(\cdot)$ is the Dirac delta function. Detailed explanations and derivations can be found in Wang and Guo (2019b).

The water retained in the infiltration trench is usually depleted by evaporation and infiltration. Infiltrations may occur through the bottom and sidewalls of a trench into the native soils beneath and surrounding the trench. The total outflow rate [denoted as $Q(S_s)$] from a trench which is the sum of the evaporation and infiltration rates at a specific time is a function of the amount of water stored in the trench (denoted as S_s, mm). $Q(S_s)$ can be described as (Wang and Guo, 2019b)

$$Q(S_s) = \begin{cases} 0, & S_s = 0 \\ E_a + \alpha_b f_b + \alpha_s f_s A_s / A_b, & 0 < S_s \le S_m \end{cases} \tag{5.4}$$

where $A_b = LW$ is the bottom area (i.e., the footprint area) of the trench, in which L and W are, respectively, the length and width of the trench; $A_s = 2(L+W)S_s$ is the wetted area of the sidewalls of the trench when water stored in the trench is S_s; E_a is the evaporation rate; f_b and f_s are infiltration rates from the bottom and sidewalls of the trench, respectively, which are usually treated to be equal to the saturated hydraulic conductivity of soils f_c; α_b and α_s

are the safety factors used to consider the effects of compaction and clogging on the rates of infiltration from the trench's bottom and sides. There are three possible infiltration conditions during the operation of an infiltration trench: Condition 1, infiltration occurs through both the bottom and sides of the trench (i.e., $\alpha_b \neq 0$ & $\alpha_b \neq 0$), Condition 2, infiltration occurs only through sides of the trench (i.e., $\alpha_b = 0$ & $\alpha_s \neq 0$), and Condition 3, infiltration occurs only through the bottom of the trench (i.e., $\alpha_b \neq 0$ & $\alpha_s = 0$). Depending on these three infiltration conditions (Conditions 1, 2 and 3), three corresponding analytical stochastic models (ASMs I, II and III) were developed (Wang and Guo, 2019b).

In the ASMs, considering the additional storage capacity created by the outflows during an average representative rainfall event, the effective storage capacity S_m of the infiltration trench can be estimated as (Wang and Guo, 2019b)

$$S_m = S_c + \left\{Q(S_c)\exp\left[-Q(S_c)/(\lambda S_c)\right] + Q(S_c)\right\}/(2\lambda) \tag{5.5}$$

where λ is the exponential distribution parameter for rainfall event duration [the exact exponential PDF for rainfall event duration u is the same as expressed by equation (5.1), simply replacing v with u and ζ with λ]; $S_c = S_{dt} + \beta D_m$ is the total physical storage capacity of an infiltration trench, where S_{dt} is the depression storage depth of the trench, mm; D_m is the depth of the storage reservoir, mm; $\beta = r_v/(r_v+1)$ is the porosity of the storage reservoir, in which r_v is the ratio between the total volume of voids and the total volume of solid (i.e., sand and gravel) particles of the trench.

The normalized stochastic water balance equation of infiltration trenches is expressed as $\frac{\mathrm{d}s}{\mathrm{d}t}=\sum_{i=1}^{N(t)} y_i\delta(t-t_i)-q(s)$, where $\sum_{i=1}^{N(t)} y_i\delta(t-t_i)$ is the normalized net inflow rate, in which y_i is an event from the net inflow event series from time zero to the current time t; the sequential number of the inflow event is i which takes values from 1 to the total number of net inflow events [denoted as $N(t)$] from time zero to time t; t_i is the individual occurrence time in the sequential inflow event series from time zero to time t; $q(s)=Q(S_s)/S_m$ is the normalized outflow rate.

5.2.3 Analytical Expressions of the Variables of Interest

Using the Chapman-Kolmogorov forward equations (Gardiner, 2004), the temporal evolution of the probability distribution of s can be derived from the above-described normalized stochastic water balance equation of infiltration trenches (Wang and Guo, 2019b). Moreover, closed-form analytical equations of some useful performance statistics can be derived. The detailed derivations can be found in Wang and Guo (2019b). The analytical expressions for some of the main variables of interest in these ASMs are listed in Table 5.1. In Table 5.1, f_0 is the fraction of time when the trench is empty; $f(s)$ is the probability density function of s; $H(s)$ is the cumulative distribution function of s; $\langle s\rangle$ is the average degree of saturation of the trench; E_r is the long-term average runoff reduction ratio provided by the infiltration trench; $\gamma = \zeta S_m / \phi'$ is the inverse of the mean inflow event depth; $\eta = Q(S_m)/S_m$, $C_1 = 2\alpha_s f_s (L+W)/(LW)$, $C_2 = (E + \alpha_b f_b)/(C_1 S_m)$, $C_3 = \mu'/\eta - \gamma$; $C_4 = (\mu'/\eta)\mathrm{e}^{C_3} - \gamma$; $C_5 = C_2^{-\mu'/C_1} \mathrm{e}^{\gamma C_2} / C_1$, $C_6 = \Gamma[\mu'/C_1, \gamma(1+C_2)] - \Gamma(\mu'/C_1, \gamma C_2)$, $C_7 = \gamma^{-(1+\mu'/C_1)}$, $C_8 = \Gamma[\mu'/C_1 + 1, \gamma(1+C_2)] - \Gamma(\mu'/C_1 + 1, \gamma C_2)$, and $\Gamma(\cdot,\cdot)$ represents the incomplete gamma function defined as $\Gamma(a,x) = \int_0^x z^{a-1} \mathrm{e}^{-z}\, \mathrm{d}z$.

Table 5.1 Analytical expressions of the main variables of ASMs

Variable	Infiltration Conditions 1 and 2	Infiltration Condition 3
$q(s)$	$\begin{cases} 0, & s=0 \\ C_1(s+C_2), & 0<s\le 1 \end{cases}$	$\begin{cases} 0, & s=0 \\ \eta, & 0<s\le 1 \end{cases}$
f_0	$\left[C_5 C_6 \mu' \gamma^{(-\mu'/C_1)} + 1\right]^{-1}$	$\begin{cases} (\gamma+1)^{-1}, & C_3 = 0 \\ C_3/C_4, & C_3 \ne 0 \end{cases}$
$f(s)$	$\dfrac{\mu' C_5 e^{-\gamma(s+C_2)} (s+C_2)^{\mu'/C_1 - 1}}{C_5 C_6 \mu' \gamma^{-\mu'/C_1} + 1}$	$\begin{cases} \gamma f_0, & C_3 = 0 \\ \dfrac{\mu' f_0}{\eta} \mathrm{e}^{C_3 s}, & C_3 \ne 0 \end{cases}$
$H(s)$	$f_0 + \mu' f_0 C_5 \gamma^{-\mu'/C_1} \left\{\Gamma\left[\dfrac{\mu'}{C_1}, \gamma(s+C_2)\right] - \Gamma\left(\dfrac{\mu'}{C_1}, \gamma C_2\right)\right\}$	$\begin{cases} \dfrac{\gamma(s+1)}{\gamma+1}, & C_3 = 0 \\ \dfrac{\mu'}{\eta C_4} \mathrm{e}^{C_3 s}, & C_3 \ne 0 \end{cases}$
$\langle s \rangle$	$\mu' f_0 C_5 C_7 (C_8 - \gamma C_2 C_6)$	$\begin{cases} \dfrac{\gamma}{2(\gamma+1)}, & C_3 = 0 \\ \dfrac{\gamma+1}{C_4} - \dfrac{1}{C_3} + 1, & C_3 \ne 0 \end{cases}$
E_r	$\gamma f_0 C_1 C_5 C_7 C_8$	$\begin{cases} \dfrac{\gamma}{\gamma+1}, & C_3 = 0 \\ \dfrac{\gamma}{C_4}(\mathrm{e}^{C_3} - 1), & C_3 \ne 0 \end{cases}$

5.3 Model Applications

5.3.1 Study Areas and Data

In developing the ASMs for infiltration trenches (Wang and Guo, 2019b), the reliability and accuracies of these models were verified by comparing their results with those from continuous simulations. The focus of this paper is to demonstrate the flexibility and usefulness of these ASMs for sizing infiltration trenches. Hypothetical catchments at two locations, Atlanta, Georgia and New Durham, New Hampshire, U.S., were used, local stormwater management design guidelines and standards were followed. The climatic statistics of the two locations are detailed in Table 5.2.

Table 5.2 Climatic statistics of two case study locations

Station	Years Covered	Month Included	MIET (hr)	$\langle v \rangle$ (hr)	$\langle m \rangle$ (hr)	$\langle u \rangle$ (hr)	E_a (hr)
Atlanta	1964-2013	Jan.-Dec.	12	16.06	111.66	9.30	0.116
New Durham	1945-2000	Apr.-Oct.	6	11.03	91.60	6.10	0.110

Notes: Climatic statistics of Atlanta and New Durham were obtained from Wang and Guo (2018), and Guo et al. (2018), respectively; $\langle u \rangle$ is the mean rainfall event duration.

5.3.2 Design Standards and Procedures

In our previous study (Wang and Guo, 2019b), after the development of ASMs, the main task was to investigate effects of different parameters (e.g., soil types, area ratios, trench depth, etc.), with values changing over wide ranges, on runoff reduction ratio and thus verify the reliability and accuracy of ASMs. In this paper, the restricted range of some of these design parameters in specific jurisdictions needs to be considered for actual design purposes. The general procedures for sizing infiltration trenches followed by many jurisdictions are very similar although there are some minor differences. The first step is to calculate the WQCV according to the target design rainfall event depth v_t (i.e., the water quality storm depth) using the following equation (Haubner, 2001; AMEC, 2014):

$$\mathrm{WQCV} = \phi v_t A_c \tag{5.6}$$

where the volumetric runoff coefficient $\phi = 0.05 + 0.9imp$, in which *imp* is the level of imperviousness of the contributing catchment. The *imp* is set to be 1 in this study. Equation (5.6) is applicable when the area ratio R_a is very large and the rainfall directly falling on the trench surface area is negligible. This simplifying assumption is often accepted by many jurisdictions. For design cases where R_a is small, the WQCV can be underestimated when using equation (5.6) because rainfall falling directly on the trench surface is neglected. In the ASMs, both the rainfall falling on the trench surface and runoff generated from the contributing catchment area are considered as the total inflow into an infiltration trench. Therefore, it is suggested that a more accurate way [equation (5.7)] is used to estimate WQCV considering cases where R_a is small.

$$\text{WQCV} = (R_a\phi + 1)v_t A_t / (R_a + 1) \tag{5.7}$$

In equation (5.7), A_t is the total area of the site including the drainage area A_c and the planned infiltration trench footprint area (i.e., bottom area) A_b; generally, A_t is fixed, i.e., given for a site and A_b is a design variable depending on the water quality control target and soil condition of the site.

In the design of infiltration trenches, the maximum allowable trench depth D_m can be determined based on the maximum allowable drain time T_d of the water stored in the trench and the infiltration capacity f_c of the soils underneath the trench bottom. The maximum allowable T_d is usually specified to ensure the complete drainage of water before the occurrence of the next rainfall event, the soil type associated with different values of f_c is an important impact factor to D_m. It is also noted that D_m should not exceed the maximum trench depth [denoted as max (D_m)] which is usually specified considering the required convenience of post-construction maintenance. Therefore, the maximum allowable trench depth can be expressed as

$$D_m = \min\left[f_c T_d / \beta, \max\left(D_m\right)\right] \tag{5.8}$$

The design drain time can be calculated as $T_d = \beta D_m / f_c$ which should not be greater than the maximum allowable T_d. Normally the design drain time T_d should also be long enough, e.g., at least 24 hours, to ensure the trench's performance for water quality control (i.e., providing enough contact time for pollutant removal) (OMOE 2003; CDOT, 2004). Therefore, some jurisdictions also specify a minimum drain time.

Usually the maximum allowable trench depth is selected as the trench depth in order to minimize the trench's footprint area, the bottom area of the trench A_b can then be calculated by

$$A_b = \mathrm{WQCV} / (\beta D_m) \tag{5.9}$$

where WQCV can be estimated using equation (5.7). Substituting WQCV expressed in equation (5.7) and $A_t = (R_a + 1) A_b$ into equation (5.9), R_a can be solved as

$$R_a = (\beta D_m - v_t) / (\phi v_t) \tag{5.10}$$

In many design standards, the depression storage depths of the catchment (S_{dc}) and the trench surface (S_{dt}) are usually not considered since they are in reality very small as compared to rainfall depths and trench depths. To keep parameters used in ASMs and design standards the same, S_{dc} and S_{dt} are treated as zero in the following case studies. The length and width of a trench may still vary given a selected bottom area, the selected values of L and W affect the rate of infiltration as shown in equation (5.4), and as a result, they will affect E_r as well. The soil infiltration capacity f_c affects E_r as well.

The detailed requirements for sizing infiltration trenches at Atlanta and New Durham are summarized in Table 5.3. In Table 5.3, some design parameters for which requirements are not specified by the guidance manuals are taken from the general requirements for sizing infiltration trenches. For example, the minimum T_d should usually be 24 hours (OMOE, 2003), although it is not specified in some guidance manuals. The minimum infiltration rate is usually specified to ensure that the drain time satisfies the required maximum allowable T_d. The maximum R_a for New Durham is 50 as recommended in GVSDD (2012). The required ranges of drain time, depth of stone reservoir and area ratio can all be used as the criteria to verify whether the soil infiltration rate is appropriate or not for a particular site.

Table 5.3 Design requirements for sizing infiltration trenches

Jurisdiction	Requirements	R_a	T_d (h)	D_m (mm)	W (m)	f_c (mm/h)	v_t (mm)	β
Atlanta	minimum	-	-	457	-	1.27	-	-
	maximum	20	48	1520	-	-	-	-
	recommended	-	-	-	0.9 or 1.5	-	25.4	0.4
New Durham	minimum	-	-	1219	-	0.8	-	-
	maximum	-	72	3048	-	-	-	-
	recommended	-	-	-	-	-	25.4	0.4

Notes: Design requirements and specifications of Atlanta and New Durham can be found in AEMEC (2014) and Burack, et al. (2008), respectively; “-” indicates that the corresponding requirement is not specified.

5.3.3 Calculation Results

This section will examine the effects of three different operating conditions on the performance of infiltration trenches. Three infiltration conditions and two locations are analyzed based on the design requirements shown in Table 5.3.

5.3.3.1 Analysis of Three Infiltration Conditions

Given an Atlanta site with an area A_t of 100 m^2, three infiltration conditions are analyzed in which two alternative widths of the bottom area (W = 0.91 or 1.52 m) and two levels of infiltration rates (f_c = 5.08 or 10.16 mm/h) are examined. The design water quality storm depth v_t is set to be 25.4 mm (i.e., 1 inch) for all cases. Runoff reduction ratios of three infiltration conditions obtained using the analytical equations listed in Table 5.1 are shown in Table 5.4. Infiltration through sidewalls is not considered in Condition 3 which is consistent with the design procedures described in the guidance manuals of the two test locations. The selected two levels of infiltration rates and the corresponding R_a both satisfy the requirements as shown in Table 5.3. As shown in Table 5.4, the calculated D_m and R_a are the same for a specific f_c under three infiltration conditions because they are dependent on f_c but not on W as shown in equations (5.8) and (5.10). D_m increases but A_b decreases when the infiltration rate increases, whereas the required storage capacity S_c stays nearly unchanged. It is shown that both f_c and W do not affect E_r (stay around 80%) under

Condition 3, while they greatly affect E_r (between 62.7% and 79.1%) under Condition 2, and cause some difference in E_r (between 82.6% and 86.2%, or a relative difference of 4.2%) under Condition 1. The highest percentage of E_r change caused by f_c and W variations occurs in Condition 2 which is 20.7%.

Table 5.4 Trench dimensions and runoff reduction ratios at Atlanta under three infiltration conditions (A_t = 100 m^2)

Infiltration Condition	f_c mm/h	D_m m	L^a m	L^b m	R_a unitless	S_c m^3	E_r^{a} %	E_r^{b} %
1	5.08	0.61	10.93	6.54	9	6.06	83.5	82.6
	10.16	1.22	5.45	3.26	19	6.05	86.2	85.1
2	5.08	0.61	10.93	6.54	9	6.06	69.2	62.7
	10.16	1.22	5.45	3.26	19	6.05	79.1	75.6
3	5.08	0.61	10.93	6.54	9	6.06	80.0	80.0
	10.16	1.22	5.45	3.26	19	6.05	79.9	79.9

Note: [a] For cases with W=0.91 m; [b] for cases with W=1.52 m.

5.3.3.2 Effects of W under Infiltration Condition 2

Condition 2 should be used as the design condition if clogging of the bottom needs to be taken into consideration. The effects of W on E_r is much more significant in Condition 2 than in the other two conditions because in Condition 2 infiltration occurs only through the sidewalls of a trench, therefore larger D_m would result in higher infiltration. Satisfying the requirements of D_m and R_a, two different widths (W = 0.5 or 2 m) and three different infiltration rates (f_c = 5, 15 or 25 mm/h) are tested for infiltration trenches serving a site area with A_t = 200 m^2 at New Durham. The resulting performance statistics including E_r,

f_0 and $\langle s \rangle$ calculated by ASMs are displayed in Fig. 5.1. E_r increases by 12% and 36% when f_c increases from 5 to 25 mm/h for W = 0.5 m and 2 m, respectively. The average degree of saturation $\langle s \rangle$ decreases the most from 0.43 to 0.07 for W = 2 m with the increase of f_c, while the fraction of time the trench remains empty (f_0) increases the most from 0.18 to 0.55 for W = 0.5 m with the increase of f_c.

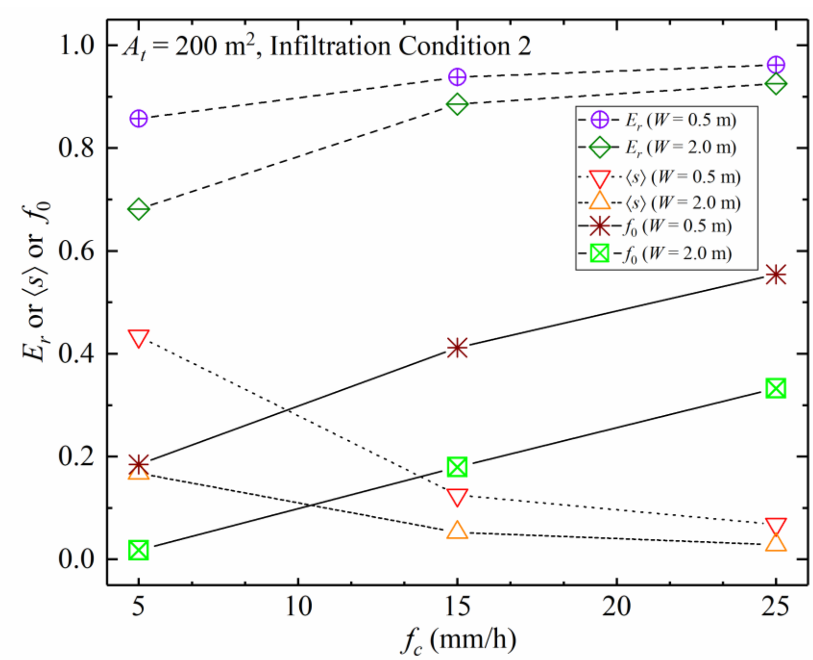

Fig. 5.1 Performance statistics of infiltration trenches at New Durham affected by soil infiltration capacities and trench widths under infiltration condition 2

5.3.3.3 Effects of W and T_d under Infiltration Condition 1

Condition 1 may be used to simulate the actual operating condition of a trench since it considers infiltration through both the bottom and sides of the trench. The maximum allowable drain time, denoted as max (T_d), at New Durham is 3 days, but the actual design drain time T_d can also be set to be 2 days. Therefore, the effects of T_d together with W were investigated at New Durham and results are shown in Table 5.5. The insignificant differences of E_r resulting from different T_d values and different A_t values show that T_d and A_t are not the influential factors for E_r, as long as the actual T_d is long enough. For cases with A_t =1000 m^2 and T_d =3 d, the largest difference of E_r is 4.0% when W changes from 0.5 to 2 m and f_c is 16.5 mm/h. But considering all the possible combinations of f_c, T_d, and W values, the maximum difference of E_r shown in Table 5.5 is 6.3%. The ASM for infiltration condition 1 is highly recommended for use in the sizing of infiltration trenches because it considers the actual operating conditions of trenches.

Table 5.5 Effects of drain time and trench width on runoff reduction ratios at New Durham under infiltration condition 1

f_c (mm/hr)	E_r (%) A_t = 1000 m^2 T_d = 3 d W = 0.5 m	E_r (%) A_t = 1000 m^2 T_d = 3 d W = 2 m	E_r (%) A_t = 200 m^2 T_d = 3 d W = 0.5 m	E_r (%) A_t = 1000 m^2 T_d = 2 d W = 2 m
7	92.3	88.9	92.4	90.6
12	94.1	90.2	94.2	91.5
16.5	95.2	91.2	95.4	92.2

5.3.3.4 Effects of v_t

Following the design procedures as specified in many guidance manuals, the selected target storm event depth v_t (i.e., water quality storm depth) is used to determine the WQCV and subsequently the required trench depth and bottom area. It is assumed that trenches sized following this procedure will provide a reasonably fixed and satisfactory (about 80%) runoff reduction ratio. But whether this procedure would indeed provide a satisfactory runoff reduction ratio for every design case is not verified because it requires tedious continuous simulations. The ASMs provide the advantage of analytically relating E_r to v_t and can be used to easily verify if the desired E_r is achieved. Taking Atlanta as an example, six different values of v_t (i.e., 20, 22, 24, 25.4, 28, 30 mm) were selected to calculate the runoff reduction ratios corresponding to three infiltration conditions where the site area is 100 m^2, the soil infiltration capacity is 7.62 mm/h and the width of the trench is 1.52 m. The analytical results E_r for 18 different v_t and infiltration condition combinations are shown in Fig. 5.2. As expected, the values of E_r calculated using ASM for infiltration condition 1 are the largest whereas those for infiltration condition 2 are the smallest.

Previously v_t is set equal to 25.4 mm and the resulting E_r for three infiltration conditions obtained using ASMs I, II and III are 83.8%, 70.5% and 79.9%, respectively. Depending on the operating conditions of a trench, the calculated E_r may not meet the water quality control target that 80 to 90% of the total runoff be captured and treated. As shown previously, for a specific jurisdiction, soil infiltration properties affect E_r the most, the width of the trench can also make a difference. Therefore, with a specified v_t at a location, one may choose a number of alternative dimensions of the trench following the specified design procedure. As a result, E_r from some of these alternatives actually do not meet the 80-90%

control requirement. It is thus recommended that ASMs be used to accurately verify if the trench design can indeed achieve the target runoff reduction ratio.

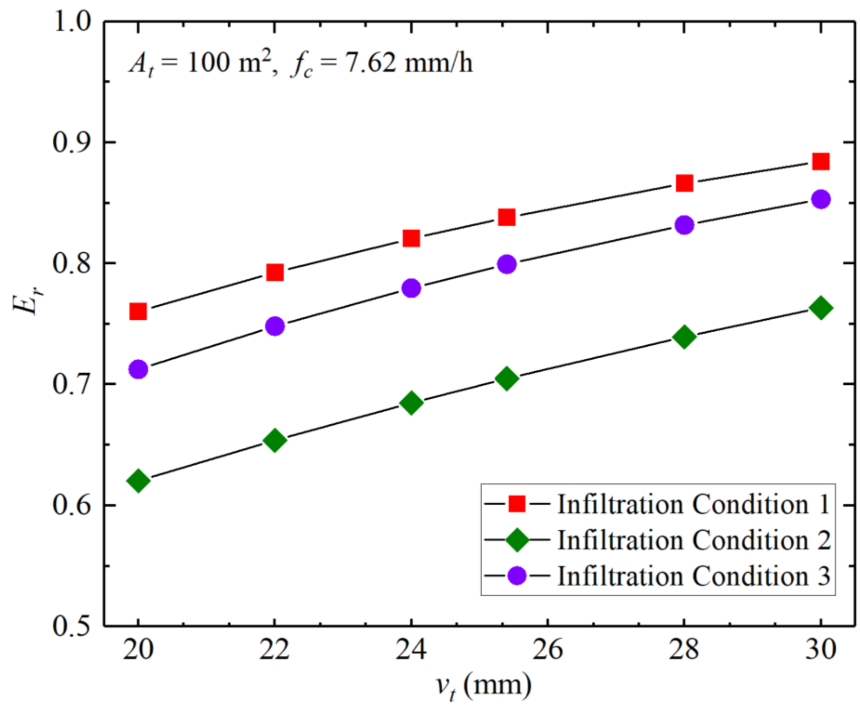

Fig. 5.2 Relationship between E_r and v_t at Atlanta

5.4 Summary and Conclusions

In this paper, the previously developed analytical stochastic models (ASMs) (Wang and Guo, 2019b) are used to verify the appropriateness of the current infiltration trench sizing practice. Following the design standards and procedures of two jurisdictions, trenches for a large number of hypothetical design cases were sized according to the same water quality design storm. For each design case, alternative but satisfactory trench dimensions were identified. ASMs for three different infiltration conditions were then applied to each of the appropriately sized infiltration trenches to determine the resulting runoff reduction ratios. Trenches sized according to the same design standards are expected to give roughly the same level of runoff reduction ratios under the same operating infiltration conditions. However, it was shown that, at the same location and assume the same type of infiltration conditions, trenches sized according to the same water quality storm depth but for different underlying soils and with different combinations of depth, length and width would result in different runoff reduction ratios. The largest difference in runoff reduction ratios can be more than 20% under infiltration condition 2 (i.e., infiltration occurs only through trench sides). Under infiltration condition 1, i.e., infiltration through both the bottom and the sides of a trench which is usually the actual operating condition of trenches, the largest difference in runoff reduction ratios can be more than 6% between different design cases. These levels of differences serve as a warning of the non-uniform performance that may be achieved by different design cases although the same design standard is enforced.

The exact level of performance differences among various design cases will also be influenced by local climate conditions. Therefore, the above-cited percentage differences may not apply to other locations, however, at least, this study verified that the design storm-based "specific initial runoff depth rule" design procedure cannot result in a fixed runoff reduction ratio because of different site soil conditions and trench dimensions. It was also found that changes in soil type and trench footprint dimensions affect the runoff reduction ratio the most even though the same requirement of WQCV is met. ASMs can facilitate more accurate and consistent design of infiltration trenches compared to the designs obtained following the "specific initial runoff depth rule." Using ASMs, the side infiltration can also be considered; more accurate sizes of infiltration trenches satisfying the required runoff reduction ratio target can be more easily obtained.

Acknowledgement: This work was supported by the Natural Sciences and Engineering Research Council of Canada and the Canadian Mitacs Accelerate Program. The data used in this study are listed in the tables or obtained from the citied references.

References

Adams, B. J. and Papa, F. (2000). *Urban stormwater management planning with analytical probabilistic models*. Wiley, New York.

AMEC Environment and Infrastructure (AMEC). (2014). *Green infrastructure stormwater management practices for small commercial development*, City of Atlanta Stormwater Guidelines. https://mariettaga.gov/DocumentCenter/View/227/Small-Commercial-Green-Infrastructure-Guidance-PDF?bidId=.pdf

Aquafor Beech Ltd (ABL). (2016). *Jurisdictional Scan of Canadian, US and International Stormwater Management Volume Control Criteria*. Prepared for Ministry of the Environment and Climate Change. Guelph, Ontario, Canada. http://www.downloads.ene.gov.on.ca/envision/env_reg/er/documents/2017/012-9080_Scan.pdf

Aquafor Beech Ltd. and Earthfx Inc. (ABL and EI) (2016). Runoff volume control targets for Ontario final report, prepared for Ministry of the Environment and Climate Change. Guelph, Ontario, Canada. http://www.downloads.ene.gov.on.ca/envision/env_reg/er/documents/2017/012-9080_Runoff.pdf

Bach, P. M., McCarthy, D. T., and Deletic, A. (2010). Redefining the stormwater first flush phenomenon. *Water Research*, 44(8), 2487–2498.

Baek, S. S., Choi, D. H., Jung, J. W., Lee, H. J., Lee, H., Yoon, K. S., and Cho, K. H. (2015). Optimizing low impact development (LID) for stormwater runoff treatment in urban area, Korea: Experimental and modeling approach. *Water Research*, 86, 122–131.

Burack, T. S., Walls, M. J., and Stewart, H. (2008). New Hampshire Stormwater Manual, *Volume 2 Post-Construction Best Management Practices: Selection and Design*. Comprehensive Environmental Inc.& New Hampshire Department of Environmental Services. https://www.des.nh.gov/organization/commissioner/pip/publications/wd/documents/wd-08-20b.pdf

Chang, G., Parrish, J., Souer, C. (1990). The first flush of runoff and its effects on control structure design. Environmental and Conservation Service Department, Environmental Resources Management Division, Austin, Texas, U.S.

Chahar, B. R., Graillot, D., and Gaur, S. (2011). Storm-water management through infiltration trenches. *Journal of Irrigation and Drainage Engineering*, 138(3), 274–281.

Clar, M. L., Barfield, B. J., and O'Connor, T. P. (2004). *Stormwater best management practice design guide: Volume 1 general considerations*. Rep. No. EPA/600/R-04, 121.

Claytor, R. A., and Schueler, T. R. (1996). *Design of stormwater filtering systems*. Chesapeake Research Consortium.

Colorado Department of Transportation (CDOT) (2004). *Drainage design manual*. Colorado, U.S.

Credit Valley Conservation Authority and Toronto and Region Conservation Authority (CVC and TRCA). (2010). *Low impact development stormwater management planning and design guide*, Ontario, Canada.

Daly, E., Bach, P. M., and Deletic, A. (2014). Stormwater pollutant runoff: A stochastic approach. *Advances in Water Resources*, 74, 148–155.

Eagleson, P. S. (1978). Climate, soil, and vegetation: 2. The distribution of annual precipitation derived from observed storm sequences. *Water Resources Research*, 14(5), 713–721.

Gardiner, C. (2004). Handbook of stochastic methods: for physics, chemistry & the natural sciences (Series in synergetics, Vol. 13).

Greater Vancouver Sewerage and Drainage District (GVSDD). (2012). *Stormwater Source Control Design Guidelines*, Vancouver, Canada. http://citeseerx.ist.psu.edu/viewdoc/download?doi=10.1.1.730.8610&rep=rep1&type=pdf

Guo, J.C.Y., and Urbonas, B. (2002). Runoff capture and delivery curves for storm-water quality control designs. *Journal of Water Resources Planning and Management*. 128 (3), 208–215.

Guo, J. C., Urbonas, B., and MacKenzie, K. (2014). Water quality capture volume for storm water BMP and LID designs. *Journal of Hydrologic Engineering*, 19(4), 682–686.

Guo, R., Guo, Y., and Wang, J. (2018). Stormwater capture and antecedent moisture characteristics of permeable pavements. *Hydrological Processes*, 32(17), 2708–2720.

Guo, Y. (2016). Stochastic analysis of hydrologic operation of green roofs. *Journal of Hydrologic Engineering*, 21(7). https://doi.org/10.1061/(ASCE)HE.1943-5584.0001371

Guo, Y., and Gao, T. (2016). Analytical equations for estimating the total runoff reduction efficiency of infiltration trenches. *Journal of Sustainable Water Built Environment*, 2(3), 06016001. https://doi.org/10.1061/JSWBAY.0000809

Hassini, S., and Guo, Y. (2016). Exponentiality test procedures for large samples of rainfall event characteristics. *Journal of Hydrologic Engineering*, 21(4), 04016003. https://doi.org/10.1061/(ASCE)HE.1943-5584.0001352

Haubner, S. M. (2001). *Georgia stormwater management manual*. Georgia Institute of Technology.

Ministry of the Environment and Climate Change (MOECC). (2017). *Low impact development* (*LID*) *stormwater management guidance manual*, Draft version, Toronto, Canada. https://www.municipalclassea.ca/files/7_DRAFT_MOECC_LID%20SWM%20Manual.pdf

Minnesota Pollution Control Agency (MPCA). (2005). *The Minnesota stormwater manual*, Version 1, St. Paul, Minnesota, U.S.

Ontario Ministry of the Environment (OMOE), (2003). *Stormwater management planning and design manual*, Toronto, Ontario, Canada.

Parolari, A. J., Pelrine, S., and Bartlett, M. S. (2018). Stochastic water balance dynamics of passive and controlled stormwater basins. *Advances in Water Resources*, 122, 328–339.

Pelak, N., and Porporato, A. (2016). Sizing a rainwater harvesting cistern by minimizing costs. *Journal of Hydrology*, 541, 1340–1347.

Park, D., Song, Y. I., and Roesner, L. A. (2011). Effect of the seasonal rainfall distribution on storm-water quality capture volume estimation. *Journal of Water Resources Planning and Management*, 139(1), 45–52.

Rodriguez-Iturbe, I., and Proporato, A. (2004). *Ecohydrology of water-controlled ecosystems*, UK: Cambridge University Press.

Sartor, J. D., and Boyd, G. B. (1972). *Water pollution aspects of street surface contaminant*, EPA-R2/72-081, U.S. Environmental Protection Agency, Washington, D.C., U.S.

Sharifi, S., Massoudieh, A., and Kayhanian, M. (2011). A stochastic stormwater quality volume-sizing method with first flush emphasis. *Water Environment Research*, 83(11), 2025–2035.

U.S. Environmental Protection Agency (USEPA). (1979). *A statistical method for the assessment of urban storm water*.

U.S. Environmental Protection Agency (USEPA). (2011). *EPA national menu of stormwater best management practices*, Washington, DC.

Wang, J., and Guo, Y. (2018). An analytical stochastic approach for evaluating the performance of combined sewer overflow tanks. *Water Resources Research*, 54(5), 3357–3375.

Wang, J., and Guo, Y. (2019a). Stochastic analysis of storm water quality control detention ponds. *Journal of Hydrology*, 571, 573–584.

Wang, J., and Guo, Y. (2019b). Dynamic water balance of infiltration-based storm water best management practices. *Advances in Water Resources Research*. (Under Review)

Water Environment Federation (WEF), ASCE, 1998. *Urban runoff quality management*.

WEF Manual of Practice No. 23 and ASCE Manual and Rep on engineering practice no. 87, Alexandria, VA.

Zhang, K., Che, W., Zhang, W., and Zhao, Y. (2016). Discussion about initial runoff and volume capture ratio of annual rainfall. *Water Science and Technology*, 74(8), 1764–1772.

Chapter 6

Summary and Future Research

6.1 Summary

This thesis focuses on the development of analytical stochastic models (ASMs) for three different types of stormwater control measures (SCMs) [i.e., combined sewer overflow (CSO) tanks, detention ponds and infiltration best management practices (BMPs)]. In addition to differences in inflows and storage forms, these SCMs have different outflow functions such as pumped constant outflows, orifice-controlled outflows and side infiltration-driven outflow functions. All the ASMs represent he series of rainfall events as a marked Poisson process where both the rainfall event depth and inter-arrival time are exponentially distributed. The effective storage capacity proposed for use in place of the physical storage capacity overcomes the shortcomings associated with the Poissonian process assumption. Compared to the previously proposed analytical probabilistic models (APMs), simplifying assumptions about the initial storage conditions are no longer needed in ASMs. The ASMs also have the advantage of not requiring an independence assumption between rainfall event depth and duration which is required in APMs.

The accuracy of the analytical stochastic models for different types of stormwater control measures is verified by comparing the results from ASMs with SWMM continuous simulation results. In the planning and design of a SCM facility, long-term observed flow data are usually not available. As a representative continuous simulation model, SWMM can provide reliable simulation results for the verification of ASMs. Therefore, SWMM simulation results were used to verify the overall accuracy of ASMs developed for CSO tanks, detention ponds and infiltration BMPs for a wide variety of cases with varying design parameter values, climate conditions, soil conditions, and land use conditions. Close agreement observed between ASM and SWMM results demonstrated the accuracy of ASMs. An application study of ASMs for infiltration trenches were also carried out to demonstrate the usefulness of the developed ASMs and identify the shortcomings of the current design standards. Overall, these ASMs, with the merits of analytical tractability and computational-efficiency, are highly recommended as alternatives to continuous simulation models for the planning, design and analysis of SCM facilities.

It is worth noting that observed flow data in a real catchment is usually insufficient for the verification of the accuracy of the ASMs. If long-term observed flow data becomes available in the future, it is possible to further verify the accuracy of the ASMs. ASMs developed in this thesis were only verified by comparing with continuous simulation results.

6.2 Recommendations for Future Research

6.2.1 Detention Ponds with Weir-Controlled Outflows

Detention ponds with orifice-controlled outflow structure were studied in Wang and Guo (2019). Another widely-used outflow control structures for detention ponds is weir, rectangular and triangular weirs with different outflow rates are often used. Therefore, development of ASMs for detention ponds with outflows predominantly controlled by weirs or a combination of orifices and weirs may be pursued in the future.

6.2.2 Modified Analytical Stochastic Models Considering Horton Infiltration Model-determined Infiltrations

The assumption that the infiltration rate is equal to the constant saturated hydraulic conductivity was widely used in previous studies on the design of LID practices. Horton infiltration model was applied in the development of APMs (Guo and Adams, 1998; Guo and Guo, 2018; Zhang and Guo, 2014). However, all the recently proposed ASMs adopted the constant infiltrate rate assumption. The effect of applying the Horton infiltration model for developing ASMs on the model accuracy has not been investigated yet. Therefore, a study of modifying the derivation of ASMs to incorporate the Horton infiltration model can be conducted in the future.

6.2.3 Establishment of a Unified Framework of Analytical Models

To date, a number of analytical models have been developed for the analysis of catchments, end-of-pipe control facilities and low impact development practices. However, a comprehensive literature review on the progress of the development and application of these models in urban stormwater management has not been conducted. It is therefore necessary to carry out an extensive literature review of the previously developed analytical probabilistic models and the recently developed analytical stochastic models. A systematic review of the similarities and differences between the two types of models will provide a better understanding of their applications and requirements for further improvement. It will be helpful to summarize and comment on the assumptions and limitations associated with these analytical models. A unified framework comprising the same or similar analytical expressions describing the inflow processes and the routing flows through storage facilities may be established to more uniformly and systematically represent all the APMs and ASMs developed for different types of stormwater control measures.

Meanwhile, the previously developed analytical probabilistic models may be modified by replacing the originally assumed initial storage condition with the average antecedent water content or soil moisture that is derived in the development of analytical stochastic models. This is a way to relate the new stochastic models with and improve the accuracy of the previously developed probabilistic models. An example of this type of study can be found in Guo et al. (2018). Furthermore, the modified APMs can be used to more accurately estimate the required size of a storage facility for flood control purposes, which is not possible by using APMs or ASMs alone.

6.2.4 Cost-effectiveness Analysis and Optimization of SCM Design

The cost-effectiveness analysis is another important factor in sizing SCM facilities. Both the runoff reduction ratio and the estimated costs should be considered in individual design cases. Cost-effectiveness analysis of SCM facilities may be treated as optimization problems, optimization example studies can be found in the sizing of rainwater harvesting system using ASM (Pelak and Porporato, 2016), as well as the sizing of detention basins (Li and Adams, 1990) and detention ponds using APM (Shamsudin et al., 2014). In future studies, the cost-effectiveness of different SCMs can be analyzed based on the ASM-estimated runoff reduction ratios. The optimal sizes of the facilities can then be determined.

6.2.5 Other Considerations

The effect of non-stationarity in rainfall series due to climate change was not considered in this thesis. The effect of spatial variability of rainfall series across a catchment was also not taken into account in this thesis where rainfall data collected at single rain gauge station were used for analyzing the entire drainage area. In future studies, effects of both factors may be investigated.

References

Guo, Y., and Adams, B. J. (1998). Hydrologic analysis of urban catchments with event-based probabilistic models: 1. Runoff volume. *Water Resources Research*, 34(12), 3421–3431.

Guo, R., and Guo, Y. (2018). Analytical equations for use in the planning of infiltration Facilities. *Journal of Sustainable Water in the Built Environment*, 4(2), 06018001.

Guo, R., Guo, Y., and Wang, J. (2018). Stormwater capture and antecedent moisture characteristics of permeable pavements. *Hydrological Processes*, 32(17), 2708–2720.

Li, J., and Adams, B. J. (1990). Optimization of urban runoff quantity/quality management. *Environmetrics*, 1(4), 321–336.

Pelak, N., and Porporato, A. (2016). Sizing a rainwater harvesting cistern by minimizing costs. *Journal of Hydrology*, 541, 1340–1347.

Shamsudin, S., Dan'azumi, S., Aris, A., and Yusop, Z. (2014). Optimum combination of pond volume and outlet capacity of a stormwater detention pond using particle swarm optimization. *Urban Water Journal*, 11(2), 127–136.

Wang, J., and Guo, Y. (2019). Stochastic analysis of storm water quality control detention ponds. *Journal of Hydrology*, 571, 573–584.

Zhang, S., and Guo, Y. (2014). Stormwater capture efficiency of bioretention systems. *Water Resources Management*, 28(1), 149–168.

Appendix A (Thesis Related Paper)

Analyzing the Impact of Impervious Area Disconnection on Urban Runoff Control Using an Analytical Probabilistic Model

Jun Wang, Shouhong Zhang and Yiping Guo

Abstract: The rapid spreading of impervious areas has been a growing concern in urban stormwater management. Runoff originating from impervious areas directly connected to or disconnected from drainage systems contributes differently to the outflow at the downstream outlet. Extensive implementations of best management practices (BMPs) and low impact development (LID) practices necessitate more accurate quantifications of the runoff control effects of disconnecting the impervious areas from drainage networks. An analytical probabilistic model was developed in this study that considers the differences between directly-connected and disconnected impervious areas. The novel feature of this model is that it can not only explicitly consider the effect of impervious area disconnection but also analytically calculate the runoff reduction effects contributed by impervious area disconnection. Model validity is demonstrated by comparing its outcomes with the results of a series of continuous simulations for cases with different types of soils and various land use parameters in Jackson, Mississippi and Billings, Montana, USA. Example applications of the proposed analytical model also demonstrate its usefulness in the planning and design of impervious area disconnections.

Key Words: Impervious area disconnection; Runoff reduction; Analytical probabilistic model; SWMM; Urban catchment.

A.1 Introduction

Rapid growth of urbanized areas brings about a range of environmental challenges (Alley and Veenhuis, 1983; Boyd et al., 1993; Pielke, 2005; Jefferson et al., 2017). A distinct characteristic of urbanization is the use of impervious areas such as roads, rooftops, parking lots and other paved surfaces to replace naturally pervious soils (Boulos, 2017). Impervious areas prevent infiltration of precipitation into soils and evaporation of soil moisture back to the atmosphere. Impervious areas also accelerate surface runoff concentration into downstream areas and may result in significant physical and biochemical changes in downstream hydrological systems (Miller and Hess, 2017).

Traditionally, the total impervious area (TIA) of a catchment has been used in many studies as an integrated indicator of the extent of urban development (Klein, 1979; Arnold and Gibbons, 1996; Liu et al., 2012). From a hydrological perspective, however, it is important to recognize that “not all impervious areas are created equal” (Jones et al., 2005). Urban areas are usually comprised of impervious and pervious subareas which are interspersed and/or connected to each other. In general, two types of impervious areas have been identified (Alley and Veenhuis, 1983; Han and Burian, 2009; Seo et al., 2013): the directly-connected impervious area (DCIA) and non-directly connected impervious area (NCIA). DCIA includes impervious area from which the generated runoff is discharged to receiving waters after only travelling over paved surfaces, drain pipes, or other impervious conveyance and detention structures that do not effectively reduce runoff volumes (Ebrahimian et al., 2016). NCIA represents impervious area that drains to pervious grounds, for example, rooftops that drain onto lawns and parking lots that drain into bioretention systems.

Runoff generated from DCIA and NCIA goes through different hydrologic processes (Boyd et al., 1993). Some studies have demonstrated that using TIA as a design parameter may overestimate runoff volume, whereas DCIA can serve as a better catchment parameter for estimating urban runoff (Yao et al., 2016; Ebrahimian et al., 2016). Moreover, the majority of the hydrologic alterations resulting from urbanization may be directly attributed to DCIA not TIA (Brabec et al., 2002; Lee and Heaney, 2003).

To reduce discharges into urban drainage systems and improve the water quality of receiving waters, proper control of impervious surfaces is necessary in urban stormwater management (Mueller and Thompson, 2009; Seo et al., 2013; Jefferson et al., 2017). Stormwater control measures [often collectively referred to as best management practices (BMP) and low impact development (LID) practices] include structural and non-structural measures (National Research Council, 2008). Structural BMPs and LID practices such as detention tanks (Wang and Guo, 2018), rainwater harvesting systems (Jing et al., 2017;

Zhang et al. 2018), green roofs (Guo et al., 2014), rain gardens (Zhang and Guo, 2013), bioretention systems (Zhang and Guo, 2014), and permeable pavements (Guo et al., 2018) are adopted to reduce urban runoff and/or improve runoff quality. Non-structural BMP and LID practices such as disconnection of impervious areas by routing runoff from impervious surfaces onto pervious surfaces can also help mitigate some adverse hydrologic impacts of urbanization (Mueller and Thompson, 2009).

Extensive implementations of the aforementioned structural and non-structural BMPs and LID practices necessitate the quantification of the effects of the spatial distribution and connectivity of impervious surfaces on the generation and routing of surface runoff (Roy and Shuster, 2009; Cano and Barkdoll, 2016). An attractive approach for quantifying these effects is the use of deterministic continuous simulation models (Yao et al., 2016). For instance, the U.S. EPA SWMM has been updated to simulate complicated overland flow processes (Rossman, 2015). With that update, flows can be routed from an impervious area to a pervious area within a single catchment. However, it is time-consuming and data-intensive to conduct process-based continuous simulations.

The derived probability distribution approach (Eagleson, 1972) has been applied to develop analytical probabilistic models (APMs) for stormwater management planning and design purposes (Adams and Papa, 2000). The APMs are computationally-efficient and can be used to directly calculate performance indices of stormwater management facilities (Bacchi et al., 2008; Balistrocchi et al., 2009; Zhang and Guo, 2014). However, the difference between the flow paths followed by runoff from DCIA and NCIA is not adequately considered in the previously developed APMs, which may negatively affect the accuracy of these model. Therefore, the previously proposed APMs need to be improved in order to properly consider the more complicated routing of runoff from NCIA.

The objective of this study is to develop an analytical probabilistic model which considers the different flow paths followed by runoff from both the DCIA and NCIA of an urban catchment. This analytical model can be used as a convenient and efficient tool for analyzing the impact of impervious area disconnection on urban runoff. Analytical equations are derived to calculate the average annual runoff from urban catchments and the effects of impervious area disconnection on runoff reduction. The validity of this analytical model is demonstrated by comparing its outcomes with the results of continuous SWMM simulations using long-term rainfall data from both Jackson, Mississippi and Billings, Montana, USA. Example applications of the analytical model are also demonstrated.

A.2 Methods

A.2.1 Statistical Representation of Rainfall Series

The analytical probabilistic stormwater runoff model is derived based on the probability density functions (PDFs) of local rainfall event characteristics. Each rainfall event-dry period cycle isolated from a continuous rainfall series is characterized by its rainfall event volume (v), rainfall event duration (t), and inter-event dry period (b). For a specific location, histograms of v, t and b can be analyzed and PDFs can be fitted to these histograms. In order to obtain these PDFs, a continuous rainfall series is separated into individual rainfall events by applying two discretization thresholds: a minimum interevent time (MIET) and a minimum rainfall event volume (Guo and Adams, 1998; Adams and Papa, 2000; Balistrocchi and Bacchi, 2011). The Poisson test can be used to test the statistical independence of successive rainfall events that are separated by properly selected MIET and minimum rainfall event volume (referred to as rainfall threshold hereafter) (Guo and Baetz, 2007). Detailed techniques that can be applied to determine the most appropriate MIET and rainfall threshold for locations of interest can be found in Hassini and Guo (2016).

Exponential PDFs have been found to provide good fits to the histograms of v, t and b for many locations in North America (e.g., Wanielista and Yousef, 1993; Adams and Papa, 2000; Hassini and Guo, 2016). For each pair of the selected MIET and rainfall threshold, the Poisson test (Guo and Baetz, 2007) and the Kolmogorov–Smirnov (K-S) test (Justel et al., 1997) can be used to evaluate the goodness-of-fit of the exponential distributions. The exponential PDFs of rainfall event characteristics used in this study are expressed as

$$f(v) = \zeta \exp(-\zeta v) \quad \text{for} \;\; v \geq 0 \tag{A.1}$$

$$f(t) = \lambda \exp(-\lambda t) \quad \text{for} \;\; t \geq 0 \tag{A.2}$$

$$f(b) = \psi \exp(-\psi b) \quad \text{for} \;\; b \geq 0 \tag{A.3}$$

where ζ, λ and ψ are distribution parameters, their values for a specific location are estimated as the inverses of the means of rainfall event volume $\langle v \rangle$, duration $\langle t \rangle$, and inter-event dry period $\langle b \rangle$, respectively.

In the following derivation, v and t are assumed to be independent random variables. This assumption has been adopted and tested in many previous studies and for many locations in Canada and the US (Guo and Adams, 1998; Adams and Papa, 2000; Hassini and Guo 2016; Wang and Guo, 2018; Zhang and Guo, 2014). Detailed discussions of the feasibility of this independence assumption can be found in Adams and Papa (2000) and Zhang and Guo (2013).

A.2.2 Derivation of the Analytical Equations

Fig. A.1 shows three subarea-routing options for the impervious areas of an urban catchment. In option (1), every impervious area drains directly to the outlet (i.e., every impervious area is DCIA, shown in Fig. 1a). In option (2), every impervious area drains over pervious areas and then to the outlet (i.e., every impervious area is NCIA, shown in

Fig. 1b). In option (3), a portion of the impervious areas drains to some of the pervious areas and the rest of the impervious areas are directly connected to the outlet (Fig. 1c). As illustrated in Fig. 1, the subarea-routing option (3) can be viewed as a combination of options (1) and (2). With the increased implementation of BMPs and LID practices in recent years, subarea-routing option (3) has become much more common than before. In the following, the expected values of the annual runoff volumes from urban catchments with all the above-described subarea-routing options are derived.

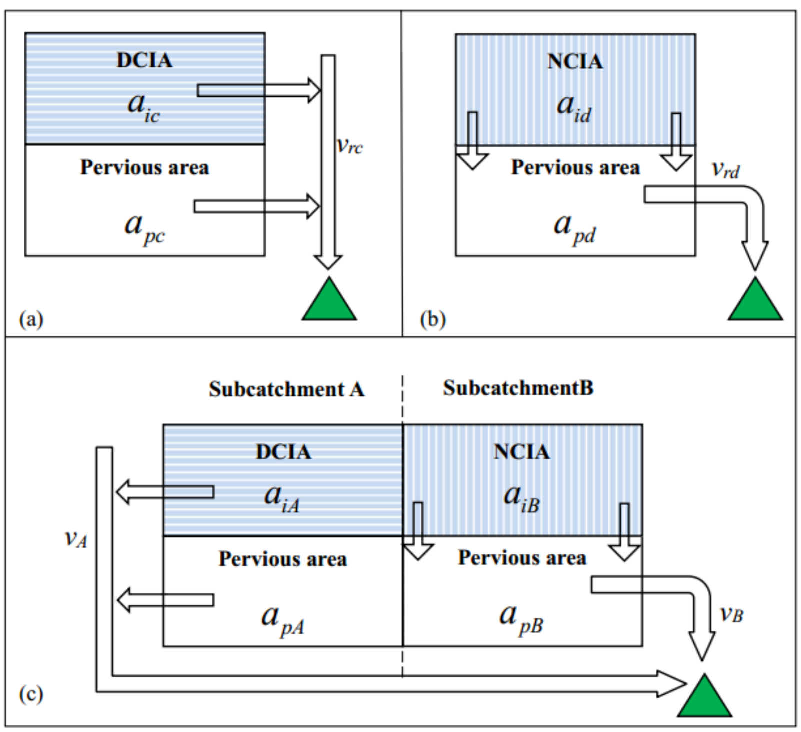

Fig. A.1 Three subarea-routing options for impervious subareas of urban catchments (DCIA: directly connected impervious area; NCIA: non-directly connected impervious area)

A.2.2.1 Catchments with All Impervious Areas Directly Connected to Outlets

When runoff from impervious and pervious areas of an urban catchment drains through two separate flow paths to the same outlet (Fig. A.1a), the volume of runoff from the impervious area (v_{ipc} expressed as mm of water over the impervious area) generated during a random rainfall event can be estimated as

$$v_{ipc} = \begin{cases} 0, & v \le S_{di} \\ v - S_{di}, & v > S_{di} \end{cases} \tag{A.4}$$

where S_{di} is the surface depression of the impervious area, expressed as mm of water over the impervious area.

The volume of runoff from the pervious area (v_{pc}, expressed as mm of water over the pervious area) can be estimated as

$$v_{pc} = \begin{cases} 0, & v \le S_{dp} + S_{iw} + f_c t \\ v - S_{dp} - S_{iw} - f_c t, & v > S_{dp} + S_{iw} + f_c t \end{cases} \tag{A.5}$$

where S_{dp} is the surface depression of the pervious area, expressed as mm of water over the pervious area; S_{iw} is the initial soil wetting infiltration volume, in mm; f_c is the ultimate infiltration rate or the hydraulic conductivity of the soils of the pervious area, in mm/h.

As derived in Guo and Adams (1998), the expected value of S_{iw} is

$$E\left(S_{iw}\right)=\frac{\left(f_m-f_c\right)k_d}{\left(k+\lambda\right)\left(k_d+\psi\right)} \tag{A.6}$$

In equation (A.6), f_m is the maximum infiltration capacity used in the Horton infiltration model, in mm/h; k in the unit of 1/h is the infiltration capacity decay coefficient; k_d is the decay coefficient of the infiltration capacity recovery curve which can be estimated from D, where D is the drying time of the fully saturated soil (Zhang and Guo, 2014).

For the purpose of simplification, the sum of S_{dp} and the expected value of S_{iw} is denoted as S_{il}, representing the initial losses of the pervious area, in mm. Denoting the fraction of impervious area of the urban catchment as h_c (dimensionless) and combining equations (A.4) and (A.5), the total volume of runoff from the catchment can be calculated as

$$v_{rc}=\begin{cases}0, & v\le S_{di}\\ h_c\left(v-S_{di}\right), & S_{di}<v\le S_{il}+f_c t\\ v-S_{dc}-\left(1-h_c\right)f_c t, & v>S_{il}+f_c t\end{cases} \tag{A.7}$$

where $h_c=a_{ic}\big/\left(a_{ic}+a_{pc}\right)$; a_{ic} and a_{pc} (in m^2) are the areas of the impervious and pervious portions of the catchment, respectively; S_{dc} is the area-weighted surface depression of the impervious portion and initial losses of the pervious portion of the catchment, it can be calculated as $h_c S_{di}+\left(1-h_c\right)S_{il}$, measured in mm of water over the catchment.

The expected value of runoff from the catchment per rainfall event, denoted as $E\left(v_{rc}\right)$, can be derived as

$$\begin{aligned} E(v_{rc}) &= \int_0^\infty \int_0^\infty v_{rc} \zeta \exp\left(-\zeta v\right) \lambda \exp(-\lambda t) \,\mathrm{d}v \,\mathrm{d}t \\ &= \frac{h_c}{\zeta} \exp\left(-\zeta S_{di}\right) + \frac{\lambda\left(1-h_c\right)}{\zeta\left(\zeta f_c + \lambda\right)} \exp\left(-\zeta S_{il}\right) \end{aligned} \tag{A.8}$$

Denoting the average number of rainfall events per year at a location of interest as θ, the average annual runoff generated from the catchment ($v_{rc\text{-}annual}$) can be calculated as

$$v_{rc-annual} = \theta E(v_{rc}) = \frac{\theta h_c}{\zeta} \exp(-\zeta S_{di}) + \frac{\theta\lambda(1-h_c)}{\zeta(\zeta f_c + \lambda)} \exp(-\zeta S_{il}) \tag{A.9}$$

A.2.2.2 Catchments with All Impervious Areas' Runoff Draining onto Pervious Areas

When 100% of runoff from impervious area of an urban catchment travels over pervious area (Fig. A.1b), the total inflow to the pervious area would include the rainwater falling directly on the pervious area (v) and the surface runoff generated from the contributing impervious area (v_{ipd}), where v_{ipd} can be calculated using equation (A.4).

Denoting the areas of the impervious and pervious portions of the catchment as a_{id} and a_{pd} (in m^2), respectively, the total volume of inflow to the pervious area (v_{id} , in mm of water over the pervious area) can be expressed as:

$$v_{id} = v + \frac{a_{id}}{a_{pd}} v_{ipd} = \begin{cases} v, & v \le S_{di} \\ (1+\frac{a_{id}}{a_{pd}})v - \frac{a_{id}}{a_{pd}} S_{di}, & v > S_{di} \end{cases} \quad \text{(A.10)}$$

Infiltration would occur at the same time when v_{id} flows onto the pervious portion of an urban catchment. The volume of runoff generated from this pervious portion (v_{pd}, in mm of water over the pervious area) can therefore be expressed as

$$v_{pd} = \begin{cases} 0, & v_{id} \le S_{il} + f_c t \\ v_{id} - S_{il} - f_c t, & v_{id} > S_{il} + f_c t \end{cases} \quad \text{(A.11)}$$

Substituting equation (A.10) into equation (A.11) while assuming that $S_{di} \le S_{il} + f_c t$ (this is reasonable since rainfall losses of impervious area are usually much less than those of pervious area), v_{pd} can be expressed as

$$v_{pd} = \begin{cases} 0, & v \le S_{dd} + (1-h_d) f_c t \\ \frac{v - S_{dd}}{1-h_d} - f_c t, & v > S_{dd} + (1-h_d) f_c t \end{cases} \quad \text{(A.12)}$$

where $h_d = a_{id} \big/ \left(a_{id} + a_{pd}\right)$, which is the fraction of impervious area of the catchment; $S_{dd} = h_d S_{di} + \left(1-h_d\right) S_{il}$, which is the area-weighted surface depression and initial losses of the catchment, expressed as mm of water over the catchment.

Taking into account the fact that pervious area occupies (1-h_d) fraction of the catchment, the volume of runoff from the catchment, v_{rd} (in mm of water over the catchment), can be calculated on the basis of equation (A.12) as

$$v_{rd} = (1-h_d)v_{pd} = \begin{cases} 0, & v \le S_{dd} + (1-h_d) f_c t \\ v - S_{dd} - (1-h_d) f_c t, & v > S_{dd} + (1-h_d) f_c t \end{cases} \tag{A.13}$$

The expected value of runoff from the catchment, denoted as $E(v_{rd})$, can therefore be derived as

$$\begin{aligned} E(v_{rd}) &= \int_0^\infty \int_0^\infty v_{rd} \zeta \exp(-\zeta v) \lambda \exp(-\lambda t)\, \mathrm{d}v\, \mathrm{d}t \\ &= \frac{\lambda}{\zeta \left[\zeta f_c (1-h_d) + \lambda \right]} \exp(-\zeta S_{dd}) \end{aligned} \tag{A.14}$$

The average annual runoff generated from this catchment $\left(v_{r-annual}\right)$ can be determined as

$$v_{rd-annual} = \theta E\left(v_{rd}\right) = \frac{\theta \lambda}{\zeta \left[\zeta f_c (1-h_d) + \lambda \right]} \exp(-\zeta S_{dd}) \tag{A.15}$$

A.2.2.3 Catchments with Part of the Impervious Areas Disconnected from the Outlet

An urban catchment with part of its impervious areas disconnected from the outlet (Fig. 1c) can be viewed as a combination of two subcatchments. One is Subcatchment A with an impervious area of a_{iA} (m^2) and a pervious area of a_{pA} (m^2) both draining directly to the outlet of the catchment. The other is Subcatchment B with an impervious area of a_{iB} (m^2) draining to its pervious area of a_{pB} (m^2) and the pervious area of this subcatchment also eventually drains to the catchment outlet. Subcatchment B represents the part of the urban catchment where impervious area disconnection (referred to as IAD for simplicity) is applied. The total volume of runoff from the catchment (v_r, in mm of water over the catchment) can be calculated as the area-weighted combination of the volumes of runoff from Subcatchments A and B and can be expressed as

$$v_r = (1-\gamma)v_A + \gamma v_B \tag{A.16}$$

where $\gamma = (a_{iB} + a_{PB})/(a_{iA} + a_{PA} + a_{iB} + a_{PB})$ which is the area ratio between Subcatchment B and the overall catchment, i.e., the ratio between the area of the subcatchment where IAD is implemented and the total area of the catchment, v_A and v_B are the volumes of runoff from Subcatchments A and B, respectively, they are measured in mm of water over their respective surface areas. for simplicity, γ is the fraction of the catchment implemented with IAD.

The runoff generation processes occurring in Subcatchments A and B are presented in Figs. A.1a and A.1b, respectively. equations (A.7) and (A.13) can be used to determine v_A and v_B, respectively. The expected values of v_A and v_B, denoted as $E(v_A)$ and $E(v_B)$, can thus be calculated using equations (A.8) and (A.14), respectively. That is

$$E(v_A) = \frac{h_A}{\zeta}\exp(-\zeta S_{di}) + \frac{\lambda(1-h_A)}{\zeta(\zeta f_c + \lambda)}\exp(-\zeta S_{il}) \tag{A.17}$$

$$E(v_B) = \frac{\lambda}{\zeta\left[\zeta f_c\left(1-h_B\right)+\lambda\right]}\exp\left(-\zeta S_{dB}\right) \tag{A.18}$$

In equations (A.17) and (A.18), $h_A = a_{iA}\big/\left(a_{iA}+a_{pA}\right)$ and $h_B = a_{iB}\big/\left(a_{iB}+a_{pB}\right)$ are the fractions of impervious areas of Subcatchments A and B, respectively; $S_{dB} = h_B S_{di} + (1-h_B)S_{il}$ is the area-weighted surface depression of the impervious area and initial losses of the pervious area of Subcatchment B, expressed as mm of water over the subcatchment. The average annual runoff generated from this catchment $\left(v_{r-annual}\right)$ can be determined as

$$v_{r-annual} = \theta E\left[\left(1-\gamma\right)v_A + \gamma v_B\right] = \theta\left[\left(1-\gamma\right)E\left(v_A\right)+\gamma E\left(v_B\right)\right] \tag{A.19}$$

A.2.2.4 Runoff Reduction Ratios Contributed by Impervious Area Disconnection

Having derived the average annual runoff volumes from a catchment with firstly part of its impervious area disconnected from the drainage system (i.e., $v_{r-annual}$) and secondly, all its impervious area directly connected to the drainage system (i.e., $v_{rc-annual}$), the long-term average runoff volume reduction ratio contributed by IAD can be determined further as

$$R_r = \frac{v_{rc-annual} - v_{r-annual}}{v_{rc-annual}} \tag{A.20}$$

Substituting equations (A.9) and (A.19) into equation (A.20) and recognizing that h_c

is defined as $a_{ic}/\left(a_{ic}+a_{pc}\right)$ and is also equal to $\left(1-\gamma\right)h_A+\gamma h_B$, R_r can be expressed as

$$R_r=1-\frac{(1-\gamma)\left[h_A\left(\zeta f_c+\lambda\right)\exp(-\zeta S_{di})+\lambda(1-h_A)\exp(-\zeta S_{il})\right]+\dfrac{\gamma\lambda\left(\zeta f_c+\lambda\right)}{\left[\zeta f_c(1-h_B)+\lambda\right]}\exp(-\zeta S_{dB})}{\left[(1-\gamma)h_A+\gamma h_B\right]\left(\zeta f_c+\lambda\right)\exp(-\zeta S_{di})+\lambda\left[1-(1-\gamma)h_A-\gamma h_B\right]\exp(-\zeta S_{il})} \quad \text{(A.21)}$$

As shown in equation (A.21), R_r is a function of a set of variables including local rainfall characteristics (i.e., ζ, λ and ψ), surface depression and infiltration loss parameters (i.e., S_{di}, S_{dp}, f_m, f_c, k and k_d), and land use parameters (i.e., γ, h_A and h_B). Three other alternative land use design parameters including the overall imperviousness of the catchment (denoted as h), the ratio between the NCIA and the total impervious area (denoted as α), and the ratio between the pervious area receiving runoff from the adjacent NCIA and the total available pervious area (denoted as β), may be used for the calculation of R_r. The relationships between h, α and β and the previously defined parameters γ, h_A and h_B are as follows:

$$h_A=a_{iA}/\left(a_{iA}+a_{pA}\right)=\left(1-\alpha\right)h/\left[\left(\beta-\alpha\right)h-\beta+1\right] \quad \text{(A.22)}$$

$$h_B=a_{iB}/\left(a_{iB}+a_{pB}\right)=\alpha h/\left[\left(\alpha-\beta\right)h+\beta\right] \quad \text{(A.23)}$$

$$\gamma=\left(a_{iB}+a_{pB}\right)/\left(a_{iA}+a_{pA}+a_{iB}+a_{pB}\right)=\left(\alpha-\beta\right)h+\beta \quad \text{(A.24)}$$

The runoff reduction rate R_r can be used to quantitatively evaluate the runoff control effects of IADs. As examples of IADs, lawns, rain gardens, or bioretention systems can be used to intercept, retain and infiltrate runoff generated from rooftops, parking lots and driveways.

A.2.3 Comparative Indices

To illustrate the accuracy of the above-derived equations, a set of continuous SWMM (Version 5.1, Rossman, 2015) simulations were performed for urban catchments with different types of soils (sand and loam), different land use parameters (γ, h_A and h_B) and located in two cities in the USA with different climate conditions: Jackson, Mississippi with a humid climate, and Billings, Montana with an arid climate. In the SWMM simulations, the Horton infiltration method was selected and the 50-year and 47-year hourly rainfall records of Jackson and Billings, respectively, were used as input rainfall series. The hypothetical test catchments were assumed to be rectangular, have a total area of 1 ha, a width of 100 m and a slope of 1%. The values of the catchment parameters required by both the analytical equations (referred to as the analytical probabilistic model or ASM) and the SWMM simulations are listed in Table A.1. In this section, two comparative indices determined from the APM and SWMM results, i.e., the average annual runoff volume and the runoff reduction ratio, are compared to verify the accuracy of the analytical expressions.

A.2.3.1 Average Annual Runoff Volume

From the SWMM simulations, the total volumes of runoff from urban catchments with all impervious areas directly connected to the outlet and with part of the impervious areas disconnected from the outlet (i.e., implemented with IAD) over the 50- or 47-year simulation periods can be obtained. Average annual runoff volumes of catchments implemented with or without IAD can be determined by dividing the total runoff volume by the number of years of simulations. These average annual runoff volumes determined from SWMM simulations were then compared with results calculated using equations (A.9) and (A.19), respectively, to demonstrate the accuracy of APM for calculating average annual runoff volume of urban catchments with or without IAD.

Table A.1 Input parameter values for SWMM and the analytical probabilistic model (APM)

Parameters	SWMM	APM
ζ (mm^{-1})	N/N*	0.0521^J or 0.1321^B
λ (h^{-1})	N/N*	0.0989^J or 0.0959^B
ψ (h^{-1})	N/N*	0.00896^J or 0.00739^B
S_{dp} (mm)	4.5	4.5
S_{di} (mm)	1.5	1.5
f_m (mm/h)	127.0^S or 76.2^L	127.0^S or 76.2^L
f_c (mm/h)	36.0^S or 3.6^L	36.0^S or 3.6^L
k (1/h)	3.0^S or 4.5^L	3.0^S or 4.5^L
D (day)	4.0^Sor 8.0^L	4.0^Sor 8.0^L

Notes: Superscript J stands for Jackson, B for Billings, S for sand and L for loam. N/N* indicates something that is not needed when using SWMM. The values of S_{dp}, S_{di}, f_m, and

f_c are the same as used in Guo and Adams (1998). The values of k and d are the same as used in Zhang and Guo (2014).

A.2.3.2 Runoff Reduction Ratio

The SWMM simulated runoff reduction ratio resulting from the implementation of IAD (denoted as R_{rSWMM}) can be calculated as

$$R_{rSWMM} = \frac{v_{rcSWMM} - v_{rSWMM}}{v_{rcSWMM}} \tag{A.25}$$

where v_{rcSWMM} is the total volume of surface runoff generated from the catchment with its entire impervious area directly connected to the outlet; v_{rSWMM} is the total volume of surface runoff generated from the same catchment but with part of its impervious area not directly connected to the outlet; both v_{rcSWMM} and v_{rSWMM} are obtained from the SWMM simulation outputs and measured in mm of water over the area of the catchment. The SWMM simulated runoff reduction ratio (R_{rSWMM}) is compared with the APM calculated runoff reduction ratio (R_r) to demonstrate the validity of the APM for the evaluation of runoff reduction effects contributed by IAD.

A.3 Study Areas and Data

For illustration purposes, Jackson, Mississippi and Billings, Montana of USA are selected as the test locations, representing typical humid and arid climates. Rainfall data were sourced from the Jackson International Airport (32.32˚ N, 90.08˚ W) and the Billings International Airport (45.80˚ N, 108.53˚ W), and cover the years of 1964-2013 and 1967-2013, respectively. In each year, the non-winter period rainfall data from April through October was analyzed for Billings, while for Jackson, the whole-year rainfall data was analyzed. The non-winter period was selected because winter activities such as snow removal may alter the intended operation of the stormwater management systems and the performance of stormwater management facilities during winter months is usually not the main interest.

The MIET of 12 hours and rainfall threshold of 1 mm were selected to separate rainfall events from the continuous rainfall records of the two locations. Results of rainfall event characteristics, the Poisson tests and K-S goodness-of-fit tests are presented in Table A.2, where r is the Poisson test statistic (i.e., the ratio between the mean and the variance of the annual number of rainfall events); α_p and α_k are the levels of significance of the Poisson test and K-S test, respectively. As demonstrated by the histograms of v, t and b at Jackson in Fig. A.2 and the K-S goodness-of-fit test results in Table A.2, the exponential PDFs fit all the histograms well.

Table A.2 Poisson tests and Kolmogorov-Smirnov goodness-of-fit tests of rainfall statistics

Poisson tests					
Station	Years of record	Critical value range of r ($\alpha_p = 0.10$)	IETD (hour)	r	Decision
Jackson	50	0.692-1.354	12	1.049	Accept
Billings	47	0.683-1.366	12	0.811	Accept

Kolmogorov-Smirnov goodness-of-fit tests					
Station	Rainfall Characteristic	Mean value	Critical value ($\alpha_k = 0.10$)	Maximum difference	Decision
Jackson	v	$\langle v \rangle = 19.20$	0.163	0.071	Accept
Jackson	t	$\langle t \rangle = 10.11$	0.188	0.085	Accept
Jackson	b	$\langle b \rangle = 111.58$	0.156	0.027	Accept
Billings	v	$\langle v \rangle = 7.57$	0.233	0.098	Accept
Billings	t	$\langle t \rangle = 10.43$	0.163	0.099	Accept
Billings	b	$\langle b \rangle = 135.26$	0.150	0.033	Accept

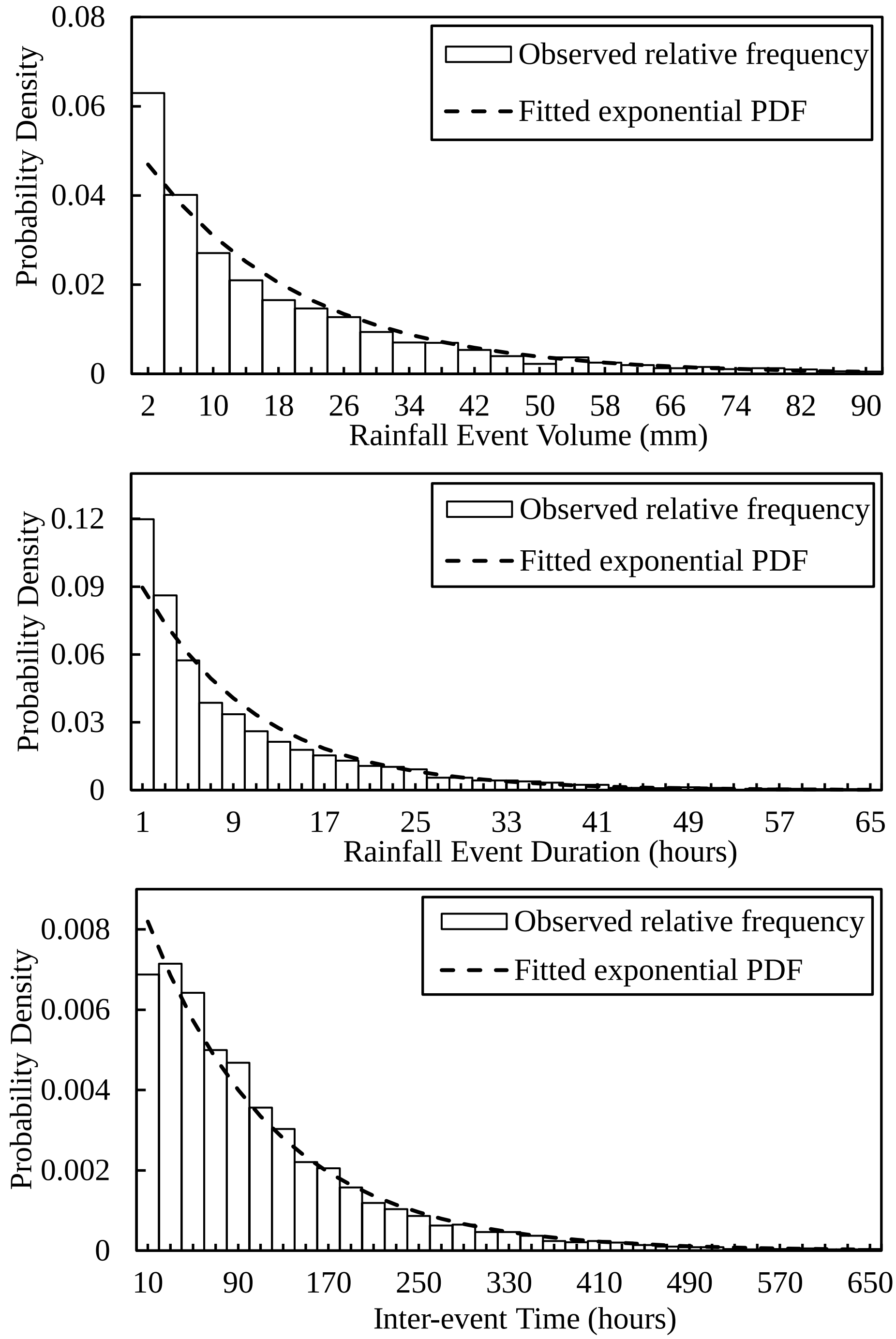

Fig. A.2 Frequency distributions of the rainfall event volume, duration and inter-event time in Jackson, Mississippi

A.4 Results and Discussion

A.4.1 Comparison of Average Annual Runoff Volume

The effects of γ (i.e., the areal fraction of an urban catchment implemented with IAD) on the average annual runoff volume from an urban catchment are investigated by comparing results obtained from both the APM and SWMM models. In Fig. A.3a, given a specified value of 0.5 for both h_A and h_B, the average annual runoff volumes of catchments with two types of soil (i.e., sand and loam) both decreases with the increase of γ in both Jackson and Billings. This is because the larger γ values, the more runoff from impervious area would be drained over the pervious area, resulting in more infiltration losses of runoff. Close agreement between the APM and SWMM results is shown in Fig. A.3a where the Nash-Sutcliffe model efficiency coefficients (NSEs) were calculated to be 0.976 and 0.923 for cases at Jackson (sand) and Billings (loam), respectively. For different values of h_B, the average annual runoff volume results obtained from both the APM and SWMM models are also compared. In Fig. A.3b, for cases with h_A and γ both equal to 0.5, when h_B changes from 0 to 1, the comparative results also show close agreement between the APM and SWMM models with NSEs calculated as 0.995 and 0.945 for cases at Jackson (loam) and Billings (sand), respectively.

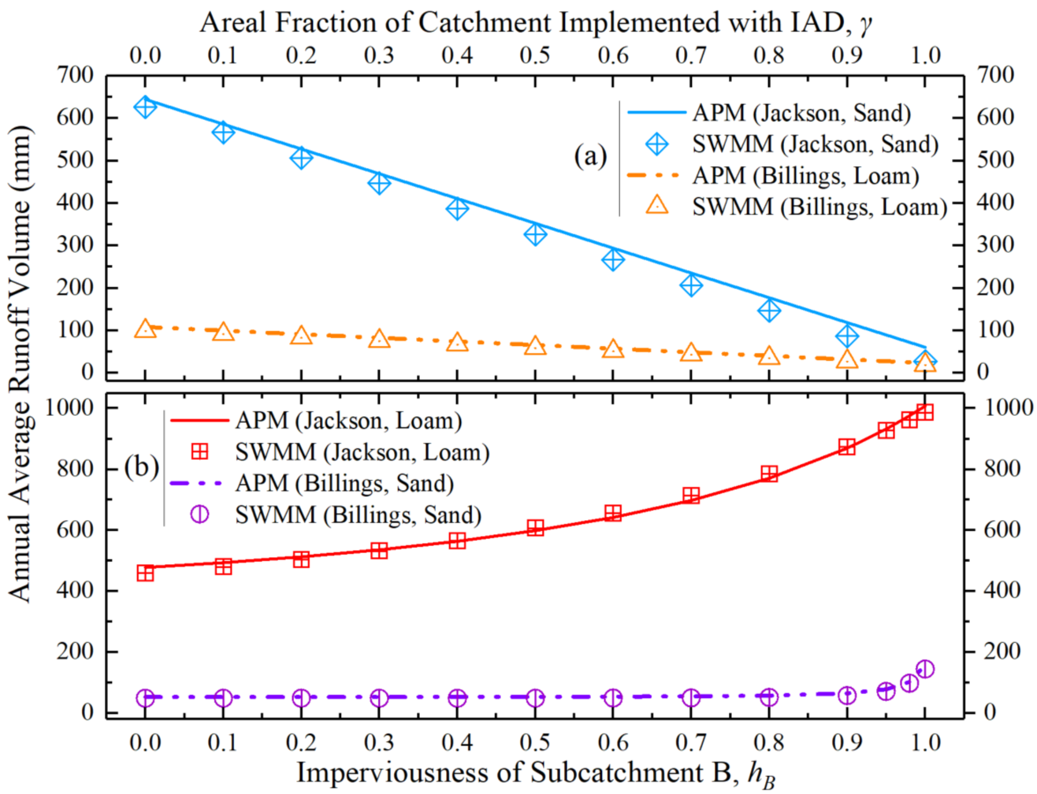

Fig. A.3 Comparison of average annual runoff volume obtained from APM and SWMM for different areal fractions of catchment implemented with IAD where $h_A = h_B = 0.5$ and for different levels of imperviousness of Subcatchment B where $h_A = \gamma = 0.5$

A.4.2 Comparison of Runoff Reduction Ratio

Runoff reduction ratios determined by the SWMM simulations (R_{rSWMM}) and APM (R_r) are also compared as shown in Fig. A.4. The relationships between the runoff reduction ratio and γ are shown in Figs A.4a and A.4b, given specified values of 0.5 for h_A and h_B at Jackson and Billings, respectively. In both locations, the runoff reduction ratio increases as γ increases, and the runoff reduction ratio for the cases of sand soils is obviously higher than that for the corresponding cases of loam soils. The largest differences between the runoff reduction ratios determined by the APM and SWMM simulations for both locations are 5.0% and 5.4% for, respectively, the soil types of sand and loam. It can be found that the runoff reduction ratios for soil types of both sand and loam at Billings are larger than those at Jackson for a specific value of γ. This can be explained by the different climate conditions of Jackson and Billings. Billings is located in an arid zone with less average annual rainfall as compared with Jackson, therefore less runoff is generated at Billings than at Jackson under same catchment conditions.

The effects of h_B on the runoff reduction ratio are explored in Figs. A.4c and A.4d given that h_A and γ are both equal to 0.5. At both locations, as h_B increases from 0 to 1, the runoff reduction ratio initially increases from 0 to a maximum value, and then drops to 0. The maximum values of the reduction ratio are dependent on local rainfall characteristics and soil types. The initial increasing and subsequent decreasing trend of the runoff reduction ratio with the increase of h_B can be explained as follows. As h_B increases, runoff generated from more impervious area can be directed to the pervious area, however at the same time, less pervious area is available to receive runoff generated from the impervious area. Therefore, there exists a critical point of h_B at which runoff generated from the non-directly connected impervious area matches optimally with the infiltration capacities of the pervious area, and this critical point of h_B results in the maximum runoff reduction ratio.

The largest differences between the runoff reduction ratios determined by APM and SWMM simulations for both locations are 6.4% and 3.5% for, respectively, the soil types of sand and loam. Fig. A.4 reveals that runoff reduction ratios calculated using the APM are very close to those determined from the continuous SWMM simulation results.

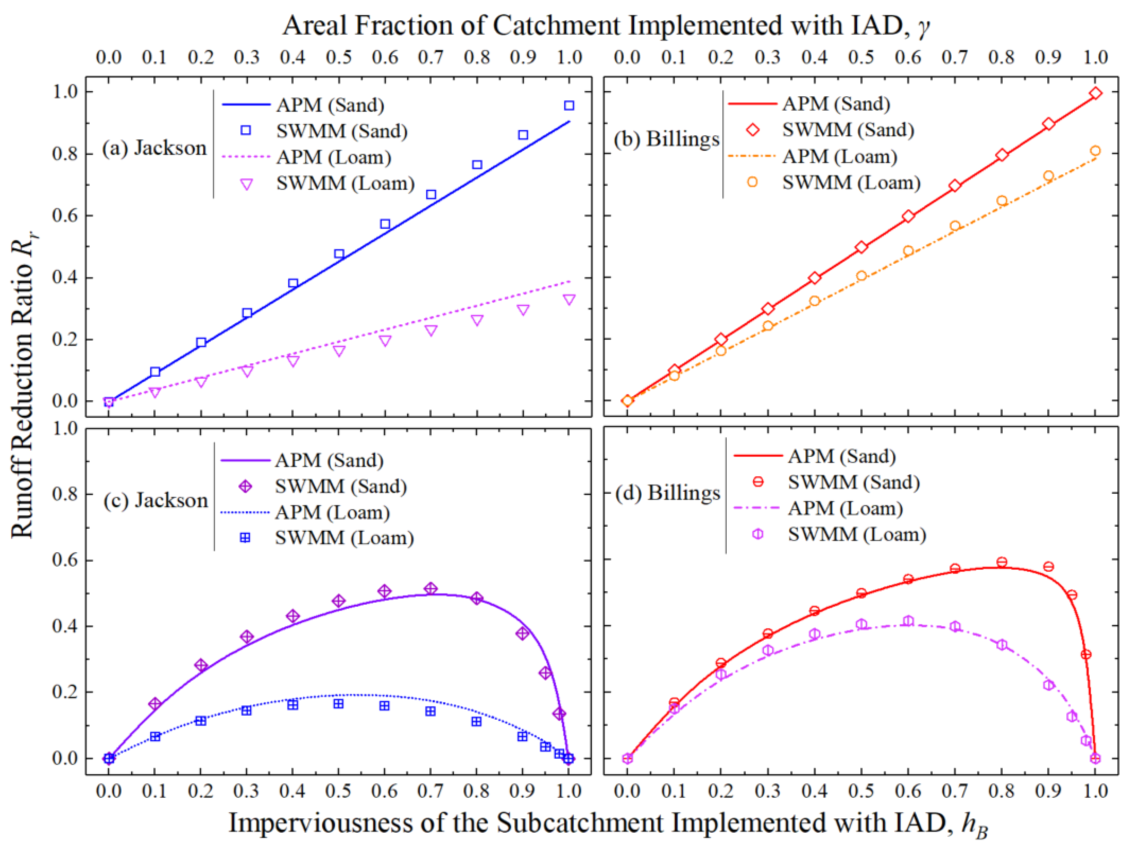

Fig. A.4 Impacts of the fraction of catchment implemented with IAD where $h_A = h_B = 0.5$ and the imperviousness of the subcatchment implemented with IAD where $h_A = \gamma = 0.5$ on runoff reduction ratios

A.4.3 Example Applications of the APM

For typical urban catchments, one primary planning or design task is to determine the appropriate total area of pervious surfaces which should be used to receive and detain runoff generated from disconnected impervious surfaces. The surface depression depth S_{dp} of the pervious surfaces receiving runoff from the impervious area may be increased by locally lowering the elevations of these pervious surfaces. S_{dp} therefore becomes an important design variable. For all these cases, figures similar to Fig. A.5 can be easily obtained using the APM for the planning or design of IAD for urban runoff control.

In Fig. A.5, the test catchment has an overall imperviousness (i.e., h) of 0.5 and the ratio (i.e., α) between the NCIA and the total impervious area is 0.6. The soil types of the pervious surfaces are loam for Billings and sand for Jackson, respectively. The ratio (i.e., β) between the pervious area receiving runoff from the adjacent NCIA and the total available pervious area (which is represented by the horizontal axis of Fig. A.5) can range from 0 to 1. These three parameters are used to better demonstrate the runoff reduction impacts of the fraction of total pervious area receiving runoff from NCIA (i.e., β).

With the given values of h and α, the corresponding h_A, h_B and γ can be determined from equations (A.22)-(A.24). Then the runoff reduction ratios can be calculated using equation (A.21). Fig. A.5a shows the impacts of both the fraction (i.e., β) and surface depression (i.e., S_{dp}) of the pervious surfaces receiving and retaining runoff from NCIA at Billings. As shown in Fig. A.5a, the runoff reduction ratio increases with both the fraction and S_{dp} of pervious surfaces receiving runoff from NCIA. It indicates that the runoff volume control effects of IAD can be enhanced by increasing the fraction or the surface depression of pervious surfaces receiving runoff from NCIA. Runoff reduction ratio rises quickly when S_{dp} increases from 3 mm to about 100 mm. Further increases in S_{dp} do not result in significant increases in runoff reduction ratio when β is greater than about 0.1. Fig. A.5b shows the same relationship for Jackson but with the only change of soil types.

Fig. A.5 is just one way of showing the relationships between runoff reduction ratios and possible design variables. Depending on a specific local design protocol or procedure, equations (A.9), (A.15), (A.19) and (A.21) may be used directly for planning or design calculations or for the generation of design-aid figures that are applicable for a specific local climate and suitable for local design requirements. In this way, more accurate results may be achieved in routine design calculations.

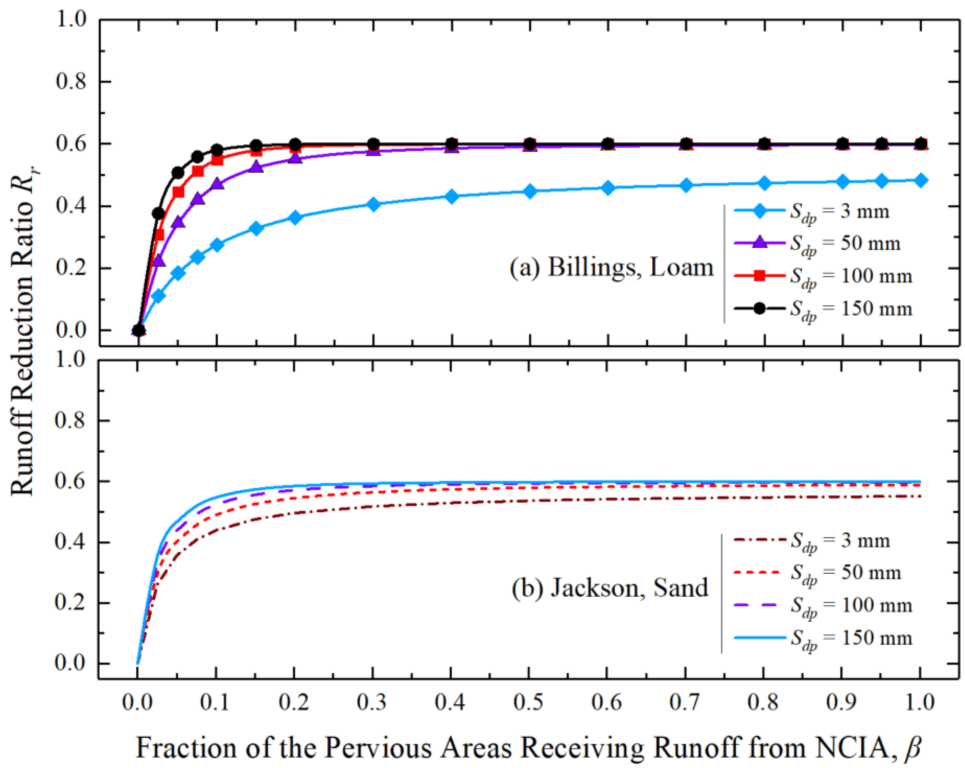

Fig. A.5 Runoff reduction impacts of the fraction and surface depression storage of pervious areas receiving runoff from NCIA where h = 0.5 and α = 0.6

A.5 Summary and Conclusions

In this paper, an analytical probabilistic model (APM) considering the different flow paths of runoff generated from both directly connected impervious area (DCIA) and non-directly connected impervious area (NCIA) of urban catchments is developed following the principle of derived probability distribution theory. The exponential probability density functions (PDFs) of local rainfall event characteristics and the event-based representations of the catchment rainfall-runoff transformation are introduced as the foundations for the derivation of the APM. The derived analytical equations can be used to calculate the average annual runoff from urban catchments with both DCIA and NCIA as well as the runoff reduction ratios contributed by different degrees of impervious area disconnection. The validity of the APM is demonstrated by comparing its outcomes with those obtained from a series of continuous SWMM simulations using hourly long-term rainfall data from Jackson, Mississippi and Billings, Montana, USA. Example planning and design applications of the APM are also demonstrated. The proposed analytical model can be used as a computationally-efficient tool to more accurately evaluate the runoff reduction ratio by taking into account the impact of the NCIA.

Acknowledgements: This work has been supported by the Fundamental Research Funds for the Central Universities, the National Natural Science Foundation of China, the Major Science and Technology Program for Water Pollution Control and Treatment, and the China Scholarship Council.

References

Adams, B.J., and Papa, F. (2000). *Urban Stormwater Management Planning with Analytical Probabilistic Models*. Wiley, New York.

Alley, W.M., and Veenhuis, J.E. (1983). Effective impervious area in urban runoff modeling. *Journal of Hydraulic Engineering*, 109(2), 313–319.

Arnold, C.L., and Gibbons, C.J. (1996). Impervious surface coverage: The emergence of a key environmental indicator. *Journal of the American Planning Association*, 62(2), 243–258.

Bacchi, B., Balistrocchi, M., and Grossi, G. (2008). Proposal of a semi-probabilistic approach for storage facility design. *Urban Water Journal*, 5(3), 195–208.

Balistrocchi, M., and Bacchi, B. (2011). Modelling the statistical dependence of rainfall event variables through copula functions. *Hydrology and Earth System Sciences*. 15, 1959–1977.

Balistrocchi, M., Grossi, G., and Bacchi, B. (2009). An analytical probabilistic model of the quality efficiency of a sewer tank. *Water Resources Research*, 45(12). https://doi.org/10.1029/2009WR007822

Boulos, P.F. (2017). Smart water network modeling for sustainable and resilient infrastructure. *Water Resources Management*, 31(10), 3177–3188.

Boyd, M.J., Bufill, M.C., and Knee, R.M. (1993). Pervious and impervious runoff in urban catchments. *Hydrological Science Journal*, 38, 463–478.

Brabec, E., Schulte, S., and Richards, P.L. (2002). Impervious surfaces and water quality: A review of current literature and its implications for watershed planning. *Journal of Planning Literature*, 16(4), 499–514.

Cano, O.M., and Barkdoll, B.D. (2016). Multi-objective, socioeconomic, boundary-emanating, nearest distance algorithm for stormwater Low-Impact BMP selection and placement. *Journal of Water Resources Planning and Management*, 143(1):05016013. https://doi.org/10.1061/(ASCE)WR.1943-5452.0000726

Eagleson, P.S. (1972). Dynamics of flood frequency. *Water Resources Research*, 8(4), 878–898.

Ebrahimian, A., Wilson, B.N., and Gulliver, J.S. (2016). Improved methods to estimate the effective impervious area in urban catchments using rainfall-runoff data. *Journal of Hydrology*, 536, 109–118.

Guo, R., Guo, Y., and Wang, J. (2018). Stormwater capture and antecedent moisture characteristics of permeable pavements. *Hydrological Process*, 32(17), 2708–2720.

Guo, Y., and Adams, B.J. (1998). Hydrologic analysis of urban catchments with event-based probabilistic models. Part I: Runoff volume. *Water Resources Research*, 34(12), 3421–3431.

Guo, Y., and Baetz, B.W. (2007). Sizing of rainwater storage units for green building applications. *Journal of Hydrologic Engineering*, 12(2), 197–205.

Guo, Y., Zhang, S., and Liu, S. (2014). Runoff reduction capabilities and irrigation requirements of green roofs. *Water Resources Management*, 28(5), 1363–1378.

Han, W., and Burian, S. (2009). Determining effective impervious area for urban hydrologic modeling. *Journal of Hydrologic Engineering*, 14, 111–120.

Hassini, S., and Guo, Y. (2016). Exponentiality test procedures for large samples of rainfall event characteristics. *Journal of Hydrologic Engineering*, 21(4), 04016003. https://doi.org/10.1061/(ASCE)HE.1943-5584.0001352

Jefferson, A.J., Bhaskar, A.S., Hopkins, K.G., Fanelli, R., Avellaneda, P.M., and McMillan, S.K. (2017). Stormwater management network effectiveness and implications for urban watershed function: A critical review. *Hydrological Processes*, 31(23), 4056–4080.

Jing, X., Zhang, S., Zhang, J., Wang, Y., and Wang, Y. (2017). Assessing efficiency and economic viability of rainwater harvesting systems for meeting non-potable water demands in four climatic zones of China. *Resources Conservation and Recycling*, 126, 74–85.

Jones, J.E., Earles, T.A., Fassman, E.A., Herricks, E.E., Urbonas, B., and Clary, J.K. (2005). Urban storm-water regulations—are impervious area limits a good idea? *Journal of Environmental Engineering*, 131, 176–179.

Justel, A., Peña, D., and Zamar, R. (1997). A multivariate Kolmogorov–Smirnov test of goodness of fit. *Statistics and Probability Letters*, 35(3), 251–259.

Klein, R. (1979). Urbanization and stream quality impairment. *Water Resources Bulletin*, 15(4), 948–963.

Lee, J.G., and Heaney, J.P. (2003). Estimation of urban imperviousness and its impacts on storm water systems. *Journal of Water Resources Planning and Management*, 129(5), 419–426.

Liu, A., Goonetilleke, A., and Egodawatta, P. (2012). Inadequacy of land use and impervious area fraction for determining urban stormwater quality. *Water Resources Management*, 26, 2259–2265.

Miller, J.D., and Hess, T. (2017). Urbanisation impacts on storm runoff along a rural-urban gradient. *Journal of Hydrology*, 552, 474–489.

Mueller, G.D., and Thompson, A.M. (2009). The ability of urban residential lawns to disconnect impervious area from municipal sewer systems. *Journal of American Water Resources Association*, 45(5), 1116–1126.

National Research Council, 2008. *Urban stormwater in the United States*. National Academies Press, Washington, DC. https://www3.epa.gov/npdes/pubs/nrc_stormwaterreport.pdf

Pielke, R.A. (2005). Land use and climate change. *Science*, 310(5754), 1625–1626.

Rossman, L.A. (2015). *Storm Water Management Model User's Manual Version 5.1*. Cincinnati OH. Environmental Protection Agency, USA.

Roy, A.H., and Shuster, W.D. (2009). Assessing impervious surface connectivity and applications for watershed management. *Journal of American Water Resources Association*, 45(1), 198–209.

Seo, Y., Choi, N.J., and Schmidt, A.R. (2013). Contribution of directly connected and isolated impervious areas to urban drainage network hydrographs. *Hydrology and Earth System Sciences*, 17, 3473–3483.

Shuster, W.D., Bonta, J., Thurston, H., Warnemuende, E., and Smith, D.R. (2005). Impacts of impervious surface on watershed hydrology: a review. *Urban Water Journal*, 2, 263–275.

Wang, J., and Guo, Y. (2018). An analytical stochastic approach for evaluating the performance of combined sewer overflow tanks. *Water Resources Research*, 54(5), 3357–3375.

Wanielista, M.P., and Yousef, Y.A. (1993). *Stormwater management*, Wiley, New York.

Yao, L., Chen, L., and Wei, W. (2016). Assessing the effectiveness of imperviousness on stormwater runoff in micro urban catchments by model simulation. *Hydrological Processes*, 30(12), 1836–1848.

Zhang, S., and Guo, Y. (2013). Explicit equation for estimating the stormwater capture efficiency of rain gardens. *Journal of Hydrologic Engineering*, 18(12), 1739–1748.

Zhang, S., and Guo, Y. (2014). Stormwater capture efficiency of bioretention systems. *Water Resources Management*, 28(1), 149–168.

Zhang, S., Zhang, J., Jing, X., Wang, Y., Wang, Y., and Yue, T. (2018). Water saving efficiency and reliability of rainwater harvesting systems in the context of climate change. *Journal of Cleaner Production*, 196, 1341–1355.